Effects of Creep in Slender Concrete Structures.

Constantinescu, D. R

Volume 2 of 2.

PhD - 1976 - D.R. CONSTANTINESCU - VOL. 2.

Chapter 5

INSTABILITY AND CREEP OF AN ARCH-MODEL

5.1 INTRODUCTION

Problems more complex than those presented in chapter 4 arise when the structural behaviour of slender arches is analysed. The increased complexity is chiefly due to the fact that the shape of the deformed state changes as the load increases and that an unstiffening postcritical behaviour can occur.

The first phenomenon means that the deformed states which correspond to different load intensities differ not only in the magnitude of displacements but in their geometric shape too. Consequently the analysis becomes mathematically complex.. The difficulties are increased when the structure displays large displacements.

The unstiffening postcritical behaviour yields information on the imperfection - sensitivity of the structure and on the significance of distabilising effects.

All these aspects are even more significant and complex when a reinforced concrete shell is considered. Since shells frequently display an overall behaviour in which a significant arch-like component is involved, some of the results arising from arch-analysis can also provide a better understanding of the complex phenomena associated with the stability of shells.

A great deal of research work, mainly theoretical, has been carried out in the last three decades on the phenomena associated with the elastic stability and postcritical behaviour of arches and shells and important achievements have contributed to a better understanding

of these phenomena and their practical implications. Hutchinson and Koiter (1971) have thoroughly surveyed the most significant of these achievements. However, many aspects are still to be clarified and, in particular, approaches suitable for practical use have to be developed. Difficulties, partially phenomenological and partially mathematical, are still to be overcome and even the implications of some of the simplifying assumptions used are not yet fully mastered.

University College London has established itself over the years as a centre for stability research. Fundamental aspects of this phenomenon has been studied such as the branching configurations (see Thompson (1965 and 1969), Supple (1967 and 1969)), the coupled modes of buckling (see Chilver and Johns (1969)) and the effects of imperfections (see Roorda (1965)). In order to analyse the stability phenomena associated with arches when large displacements are involved, some elastic mechanical models have been developed.

Croll and Walker (1972) have presented in detail the aspects connected with the behaviour of such arch-models having one or two degrees of freedom (see Fig.5.1) and made from an elastic material. The devices B oppose elastically the relative rotation of the non-deformable members L, whereas the device A opposes elastically the horizontal displacement of H_2. For both models large displacements are considered.

These arch-models concentrate the deformations of the

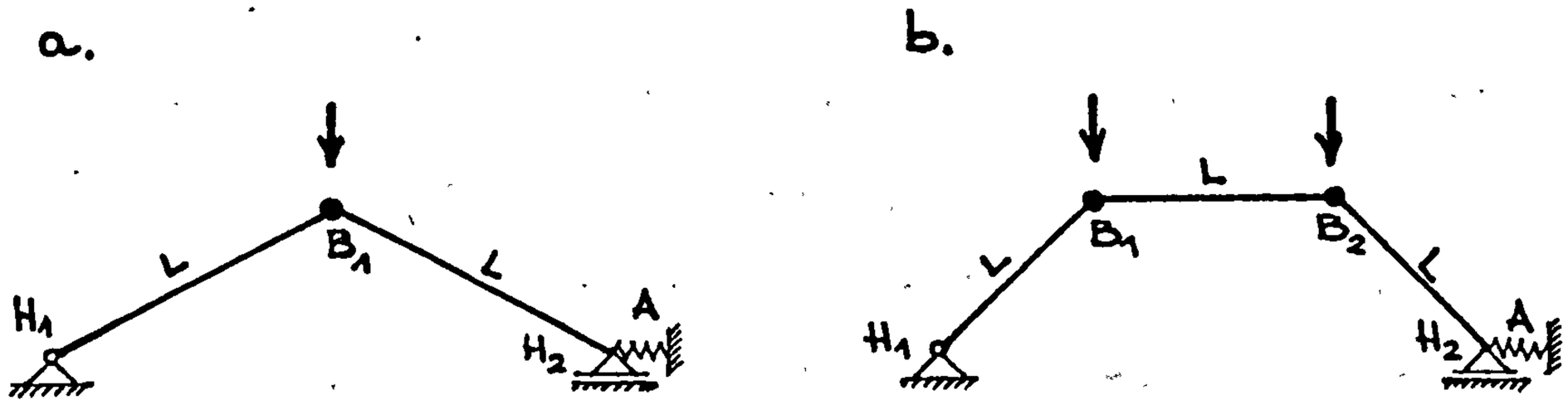

Fig. 5.1

actual arches in the devices B and A and constitute in fact a generalisation of the similar models used previously to analyse the stability of columns (see Section 4.2).

In fact the mechanical model is similar to the elastic model commonly used to analyse the dymanic response of structures, since the former concentrates stiffness in a manner similar to that in which masses are concentrated in the latter.

The models from Fig.5.1, however simple, enables some major features of the arch stability to be emphasised and provide a useful instrument for the analysis of stability with large displacements. Due to their simplicity no mathematical difficulty arises in finding the solution. Croll and Walker (1972) present a closed-form solution for the one degree of freedom model, whereas for the two degree of freedom model an approximate

solution is developed based on the truncation of Taylor's expansion of the potential functional and on the use of the perturbation technique.

Nevertheless the models from Fig.5.1 are too simplified to be able to model the complex behaviour of actual structures with curved axis and continously distributed stiffness. The more degrees of freedom are considered, the closer the arch-model is to an actual arch, but, at the same time, the more difficult it is to find the mathematical solution.

In the present chapter the elastic and visco-elastic instability of slender arches are analysed by means of a three degree of freedom arch-model (see Fig.5.2). This model generalises the mechanical arches in Fig.5.1 and has the advantage over them in that it is capable of modelling the snap-instability at the apex of the arch when this becomes the relevant mode of buckling.*)

5.2 THE ARCH-MODEL. DISCUSSION.

A symmetric arch-model as shown in Fig.5.2 is considered. The devices B_i, i=1...3, restrain partially the angular deformation in the corresponding joints and bending moments occur consequently. These devices are also assumed to restrain fully the axial and shear deformations in the joints B_i.

Footnote

*) The 'Snap-buckling' is detailed later (see Fig.5.10)

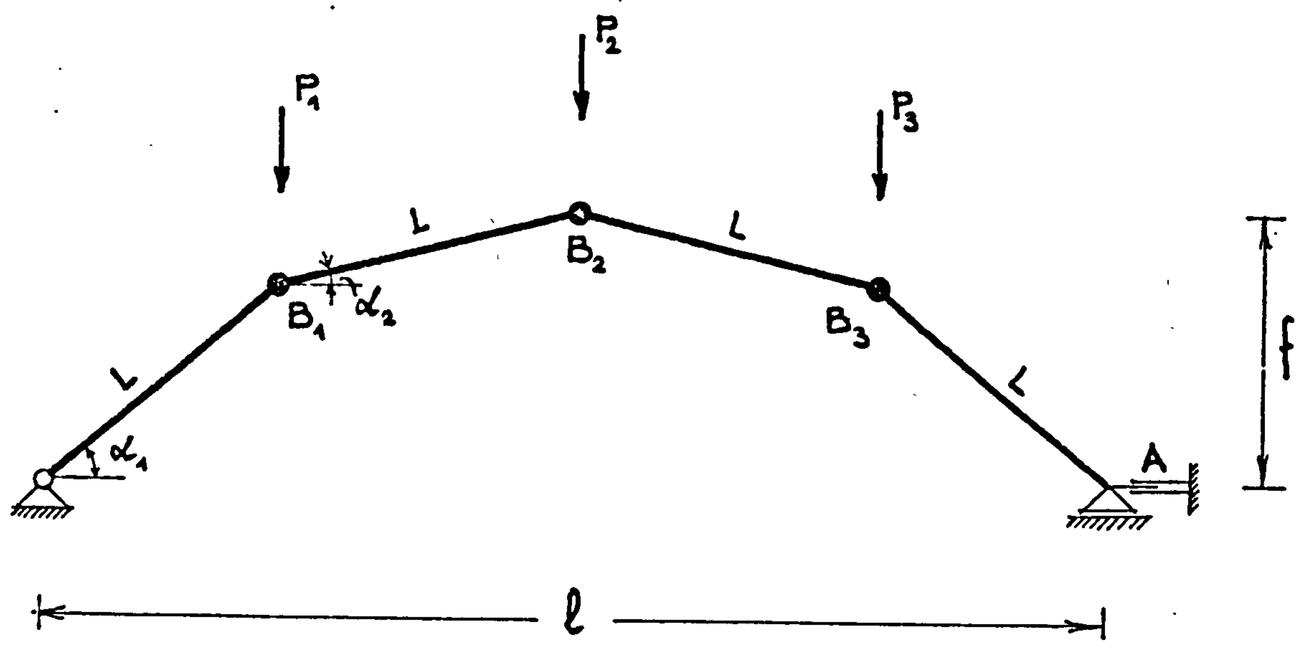
P1
P2
P3
L
L
L
L
L
B1
B2
B3
α1
α2
A
f
ℓ

Fig. 5.2

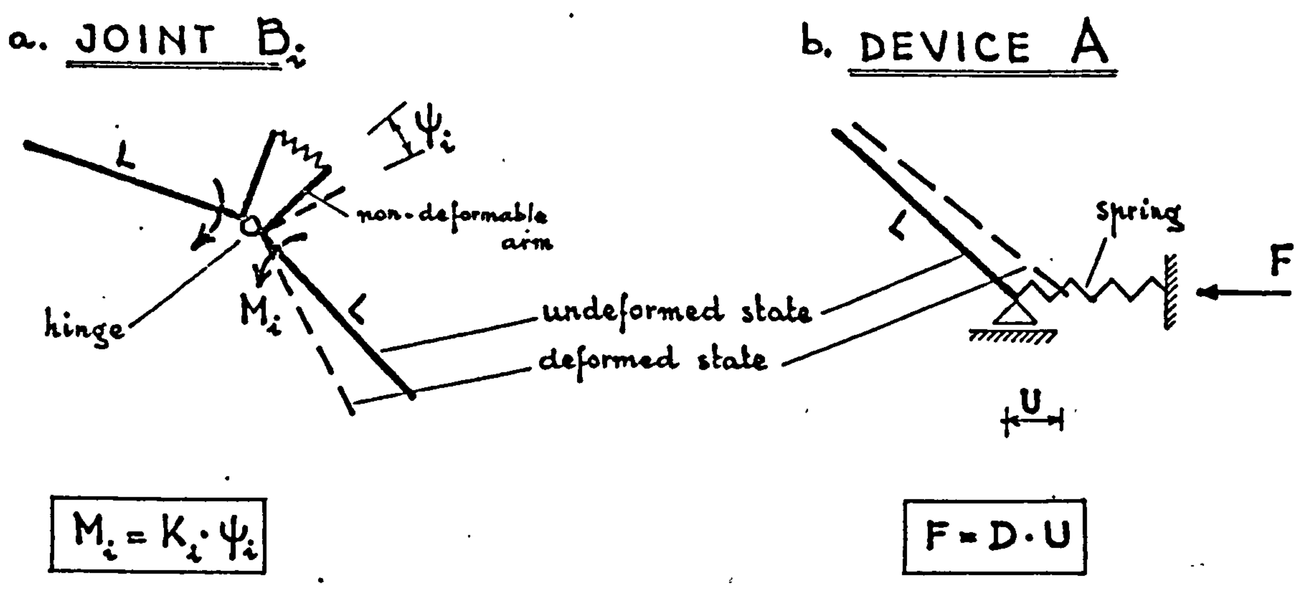
a. JOINT Bi
b. DEVICE A
L
Ψi
non-deformable arm
hinge
Mi
undeformed state
deformed state
spring
F
U
Mi = Ki · Ψi
F = D · U

Fig. 5.3

The device A restrains partially the horizontal displacement of the simple support H_2 and consequently an axial force occurs in it.

The arch-model is hinged at H_1 and the members L are assumed non-deformable.

When the elastic behaviour of the arch-model is considered the devices B_i and the device A are assumed to be as presented in Fig.5.3a and b, respectively, that is including perfect Hooke springs. Consequently a linear relationship between the generalised force and the corresponding displacement will govern their behaviour.

When the visco-elastic behaviour of the arch-model is analysed the devices B_i and A are assumed to behave according to one of the methods from Table 2.2, that is the Hooke's springs from Fig.5.3 are replaced by an appropriate rheologic model.

In comparison with the one-and two-drgree-of-freedom models the arch-model from Fig.5.2 represents a better compromise between the simplicity of the mathematical approach and the ability to model the structural behaviour of an actual arch. Thus, whereas the instability of the model from Fig.5.1a may be due only to a snap-buckling and that of the model from Fig.5.1 mainly to an anti-symmetric mode of buckling, the arch-model from Fig.5.2 may attain a critical state associated either with a snap-buckling at any joint B_i or with antisymmetric or symmetric bifurcation of equlibrium.*) Which of these

---

Footnote

*) These modes of buckling will be defined later in Section 5.3.5d and Figs.5.10 and 5.18.

models of buckling is to be critical depends on factors such as the geometry of the arch, the position of the funicular polygon relative to this geometry, the slenderness of the arch etc. The same factors are also chiefly responsible for the postcritical behaviour and the three degree-of-freedom model has been proved able to model the complexity of the phenomena involved.

The model from Fig.5.2 is analysed theoretically in the next section. Later in Section 5.5 a set of numerical applications based on this theoretical analysis are presented and their results are discussed. In Section 5.4 the correspondence is set up between the arch-model and an actual arch (i.e. an arch with deformability continuously distributed along its length) and a comparison with some known closed-form solutions is presented. A discussion of the limitations arising from the use of the arch-model and from the idealisation of the material behaviour is also presented in Section 5.4, and some possibilities of further improvements are indicated.

5.3. THEORETICAL ANALYSIS

5.3.1. INTRODUCTION

Approaches to the analysis of the elastic pre- and post-buckling behaviour of the arch-model from Fig.5.2 are presented and discussed. The analysis is extended to include the examination of the creep effects on the prebuckling behaviour and stability. These approaches are based on the assumptions listed in Section 5.3.2.

The elastic equilibrium states and their stability are analysed using the total potential strain energy and the dynamic criterion of stability.

The creep-dependent equilibrium and stability are analysed employing an incremental procedure based on the principle of virtual work.

For both instantaneous and creep-dependent behaviour the vertical displacements of joints B_i (i=1...3) from Fig.5.2 are considered as unknowns in the final equations.

The equations which analyse either the instantaneous or the creep-dependent deformed states are written in two forms:

i) a form which employs solely the assumptions presented in Section 5.3.2,

ii) a form which employs other approximations additional to those associated with the assumptions from Section 5.3.2 in order to simplify the mathematical solution.

The first form and its solution will be denominated throughout the present chapter as the 'exact' form and solution, whereas the latter ones will be referred to as 'approximate' form and solution.

No closed-form solution of the 'exact' equations can be found when either the elastic or the creep-dependent behaviour is analysed. Nevertheless solutions with a high degree of accuracy can be found for discrete values of load and creep using an algorithm due to Powell (1970).

On account of the mathematical simularities existing

between the final equations of the elastic prebuckling behaviour, of the elastic postbuckling behaviour and of the creep effects, a set of computer programs and subroutines has been built up to deal with all the matters involved. The use of the computer allows a wide range of numerical applications to be studied and facilitates the use of Powell's algorithm since this technique is programmed and available as a library routine.

No details about the computer programs and subroutines are given in this section but a general presentation of them is given in Appendix V.11.

5.3.2 ASSUMPTIONS

The assumptions on which the 'exact' solution of the arch-model from Fig.5.2 is based are presented in this section. The assumptions regarding the instantaneous response to loading are similar to those used by Croll and Walker (1972). Additional assumptions idealising the time-dependent behaviour of the arch-model are taken into consideration. The implications of all these assumptions when a reinforced concrete arch is analysed and possibilities of improving them in order to account for the actual behaviour of concrete are discussed later in Section 5.4.3.

Relative to the material

i) the response to the instantaneous loading is perfectly linearly elastic. In other words the bending and axial stiffnesses (i.e. K_i and D in Fig.5.3) are considered constant and the same at loading and unloading.

ii) the response to a sustained load is linearly viscous and according to the 'rate of creep' method (see Table 2.2)

iii) the same viscoelastic characteristics (i.e. modulus of elasticity E and creep coefficient φ) are assumed both in compression and tension.

iv) these viscoelastic characteristics are also assumed to be the same in each bending joint B_i and in the axial device A from Fig.5.2.

v) no cracking of concrete is considered

vi) the concrete shrinkage is neglected

vii) no consideration is given to the intervention of material failure.

Relative to the structure

viii) the arch-model is assumed symmetric about a vertical axis through B_2 from mechanical, geometrical and loading points of view. In other words, in Fig.5.4, $K_1=K_3$, the undeformed state is symmetric about B_2 and $P_1=P_3$.

ix) different stiffnesses and loads are allowed at joint B_1 and joint B_2. In other words it is possible to have $K_1 \neq K_2$ and/or $P_1 \neq P_2$ in Fig.5.4

x) a perfect structure is assumed, i.e. no consideration is given to the effects of geometric imperfections

xi) large displacements are concidered (non-linear geometry)

xii) the loading is assumed to increase proportionally. Thus each load has the form

$$P_i = p.\ \bar{P}_i \qquad (5.1)$$

a.

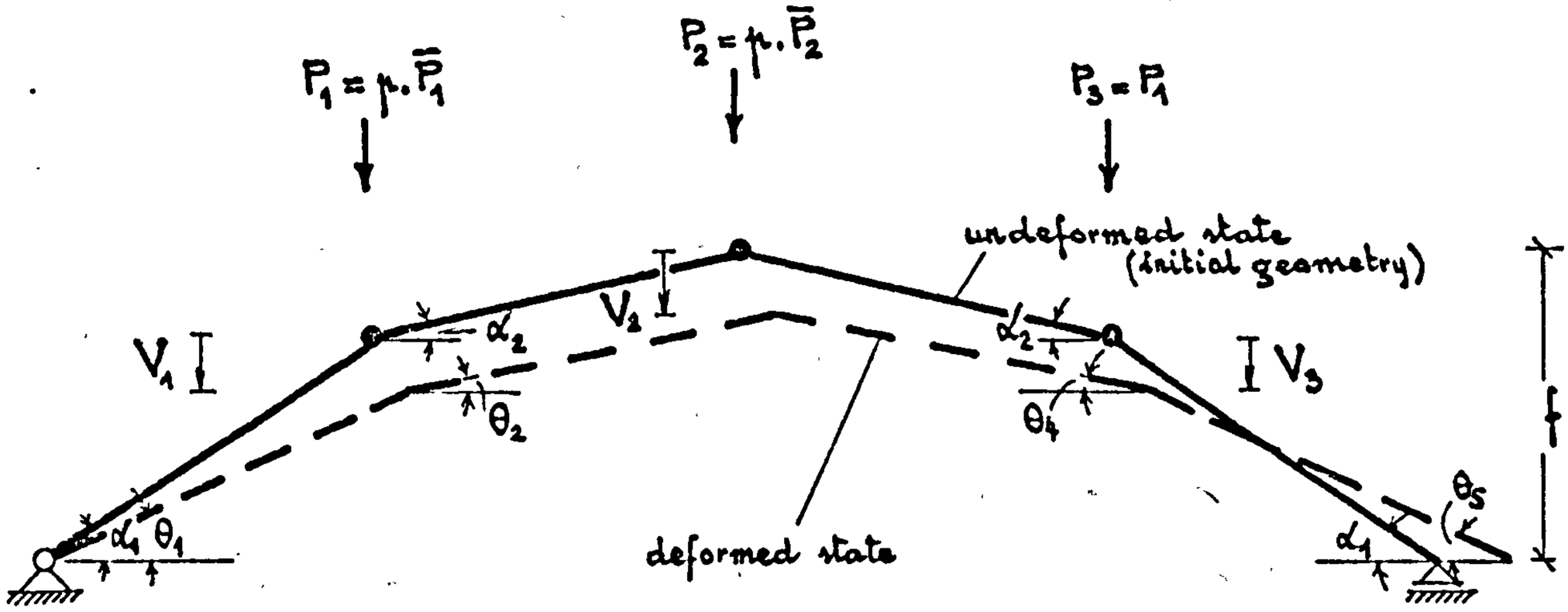
P1 = μ.P̄1
P2 = μ.P̄2
P3 = P1
undeformed state
(initial geometry)
V1
V2
V3
α2
θ2
α2
θ4
α1
θ1
α1
θ5
deformed state
f
U
l

b.

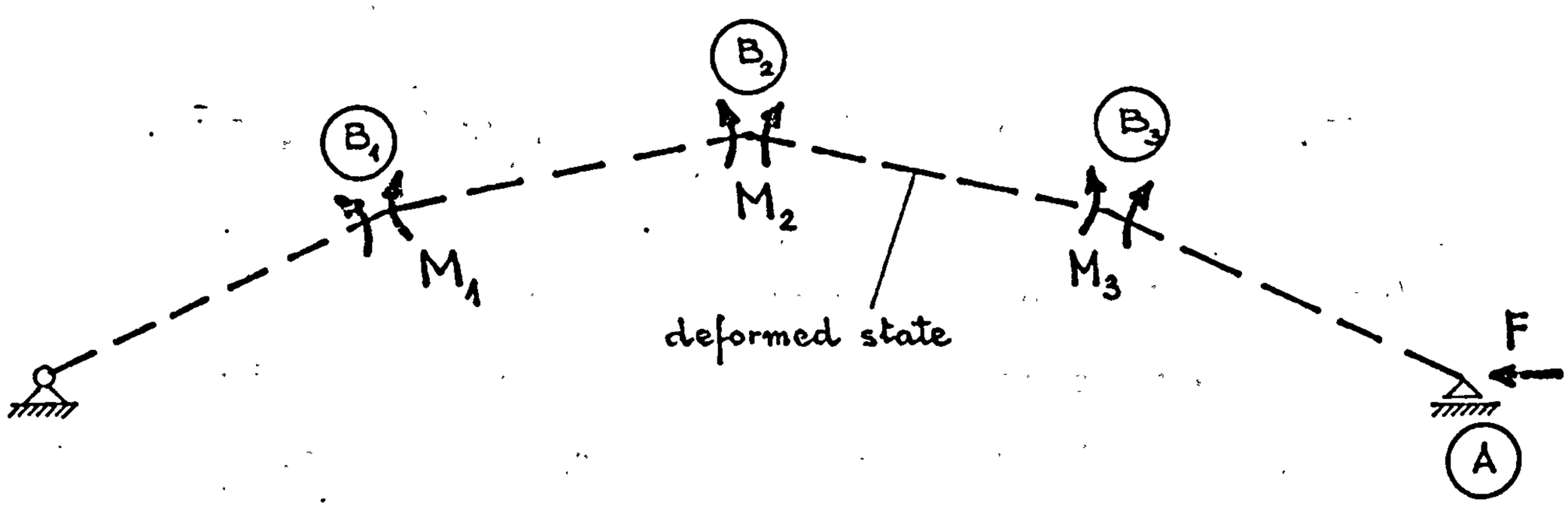
B1
B2
B3
M1
M2
M3
deformed state
F
A

Fig.5.4

where p is a non-dimensional factor of proportionality and $\bar{P}_i$ is a dimensional constant which marks the intensity of P_i relative to the others P_j ($j \neq i$). When the loading is uniform then $\bar{P}_i=1$.

xiii) no consideration is given to a possible restraining effect on creep in any device A or B_i

xiv) when the concrete creep is considered a step variation will be used to approximate the actual continuous variation of creep.

5.3.3. ELASTIC PREBUCKLING BEHAVIOUR

The minimum of the total potential is used to analyse the elastic prebuckling response of the arch-model under load. Account will be taken of the large displacements by writting the equilibrium and compatibility equations for the deformed state of the arch-model while the compatibility equations are considered nonlinear.

The change in total potential energy when the arch-model is instantaneously loaded is

$$\Delta\bar{\Pi} = \frac{1}{2}\sum_{i=1}^{3} M_i \cdot \psi_i + \frac{1}{2} F \cdot U - \sum_{i=1}^{3} P_i \cdot V_i \qquad (5.2)$$

where (see Fig.5.4) M_i and F denote the elastic bending moment and axial force occuring in the bending-carrying device B_i and in the axial force-carrying device A, respectively, when the model deforms from the initial non-loaded state to the deformed state,

ψ is the angular deformation corresponding to M_i

U is the linear deformation corresponding to F

V_i is the vertical displacement of the joint B_i

P_i is the load at the joint B_i and has the form given by eq.(5.1)

On account of the elastic behaviour,

$$\begin{aligned} M_i &= K_i . \psi_i \qquad i = 1,2,3 \\ F &= D.U \end{aligned} \tag{5.3}$$

where K_i and D denote the elastic bending stiffness of the device B_i and the elastic stiffness of the device A, respectively. (see Fig.5.3)

Introducing the non-dimensional notation

$$u = \frac{U}{L}$$

$$v_i = \frac{V_i}{L}$$

$$p_i = \frac{\bar{P}_i . L}{K_1} \tag{5.4}$$

$$c_i = \frac{K_i}{K_1} \qquad (c_1 = c_3 = 1 \text{ and } c_2 = c)$$

$$k = \frac{DL^2}{K_1}$$

and using eqs.(5.1) and (5,3), eq.(5.2) can be recast as

$$\Delta\Pi = \frac{\Delta\bar{\Pi}}{K_1} = \frac{1}{2}\sum_{i=1}^{3} c_i \psi_i^2 + \frac{1}{2} k u^2 - p \sum_{i=1}^{3} p_i v_i \tag{5.5}$$

and this dimensionless form of the potential energy will henceforth be used.

From the notation (5.4) it can be seen that $\underline{c}$ and $\underline{k}$ characterise the distribution of stiffness in the arch-model. The parameter $\underline{c}$ represents the ratio between the bending stiffnesses of the devices B_2 and B_1. When all the devices B_1 have the same bending stiffness then c=1, whereas a value $c < 1$ will arise for an arch-model having a less stiff device at the apex. The parameter $\underline{k}$ is associated with the ratio between the axial stiffness D and the bending stiffness K_1. The larger is k, the more significant is the axial stiffness of the arch-model relative to its bending stiffness when the load is applied.

It is convenient to consider the deformed state from Fig.5.4 as being characterised by the vertical displacements V_i so that, from the compatibility of deformations,

$$\begin{aligned} \sin\theta_1 &= \sin\alpha_1 - v_1 \\ \sin\theta_2 &= \sin\alpha_2 - v_2 + v_1 \\ \sin\theta_4 &= \sin\alpha_2 - v_2 + v_3 \\ \sin\theta_5 &= \sin\alpha_1 - v_3 \end{aligned} \qquad (5.6)$$

and

$$\begin{aligned} \psi_1 &= \theta_1 - \theta_2 - (\alpha_1 - \alpha_2) \\ \psi_2 &= \theta_2 + \theta_4 - 2\alpha_2 \\ \psi_3 &= \theta_5 - \theta_4 - (\alpha_1 - \alpha_2) \\ u &= \sum_j \cos\theta_j - 2\cdot(\cos\alpha_1 + \cos\alpha_2) \qquad j = 1,2,4,5 \end{aligned} \qquad (5.7)$$

The equilibrium of the deformed state is expressed by the stationary conditions (principle of minimum strain energy).

$$\frac{\partial \Delta\Pi}{\partial v_j} = 0 \qquad j = 1,2,3$$

or using eq.(5.5)

$$\boxed{\sum_i c_i \psi_i \frac{\partial \psi_i}{\partial v_j} + k u \frac{\partial u}{\partial v_j} - p p_j = 0} \qquad i,j = 1 \ldots 3 \qquad (5.8)$$

where $\partial \psi_i / \partial v_j$ and $\partial u / \partial v_j$ follow from eqs.(5.6) and (5.7) as shown in Appendix V.1.

Eqs.(5.6) ...(5.8) can be reduced to a set of three coupled equations which supply the relationships between the displacements v_i and the load p.

For each value of p the set of eqs.(5.8) provides the corresponding displacements v_i and their relationship is described by a spatial curve in the system of four coordinates (v_i, p). In the theory of elastic stability this curve is commonly called the primary path (or fundamental path or the prebuckling equilibrium path) and it fully characterises the elastic prebuckling behaviour of the arch-model so long as the load does not exceed the lowest critical value.

It can be seen from eqs(5.8) that the primary path is emanating from the unloaded and undeformed state, that is from the origin of the system of coordinates (v_1, v_2, v_3, p), and that v_1 is always equal to v_3 due to the symmetry. Thanks to this the primary path can be plotted as a curve in the triaxial space (v_1, v_2, p), as shown in Fig.5.5.

'Exact' and 'approximate' primary paths can be found.

When the accurate roots of eqs.(5.8) are used the corresponding primary path is called 'exact'. In fact,

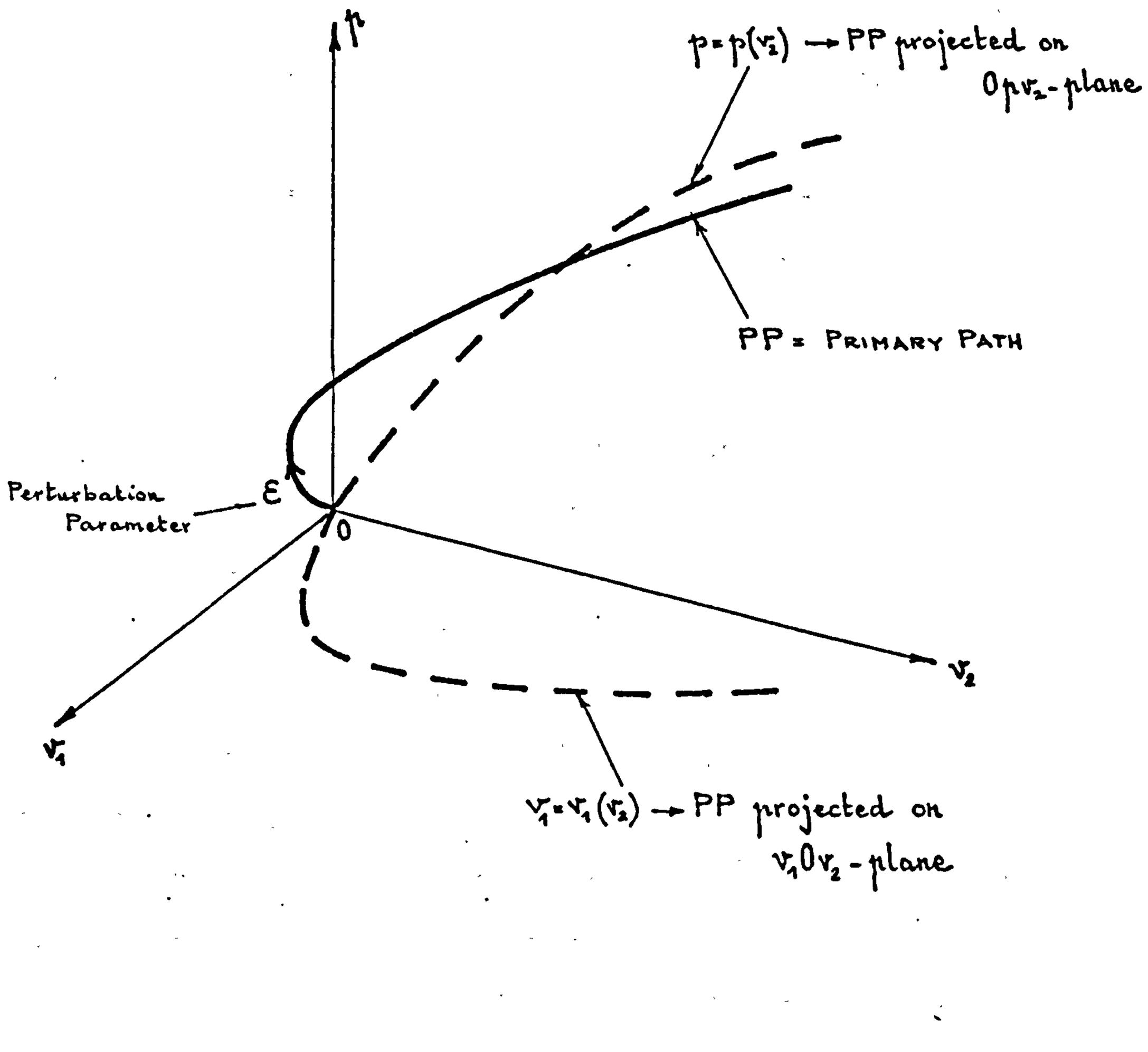
p
p = p(v₂) → PP projected on
0pv₂-plane
PP = PRIMARY PATH
Perturbation
Parameter
ε
0
v₂
v₁
v₁ = v₁(v₂) → PP projected on
v₁0v₂-plane

Fig. 5.5

as already mentioned, this primary path includes the approximations associated with the assumptions from Section 5.3.2.

When further approximations are used in order to simplify mathematically the solution of eqs.(5.8) the corresponding primary path is called 'approximate'.

These solutions will be presented in the next two sections. Later in Section 5.3.3c a comparison between the 'exact' and 'approximate' primary paths will be presented and discussed. Finally in Section 5.3.3d a decision will be made on which of these primary paths is to be further used.

a. Exact' primary path

Eqs.(5.8) represent the 'exact' analysis of the elastic prebuckling behaviour of the three degree-of-freedom arch-model.

Due to the assumption of large displacements these coupled equations are non-linear and hence no closed-form solution of them can be obtained. Nevertheless various methods can be used to find the coordinates of any arbitrary point of the primary path and thus allow the path to be built point-by-point.

An algorithm given by Powell (1970) is used to find the 'exact' solution of eqs.(5.8). This algorithm combines the Newton and steepest descent methods in such a way as to give steady progress and a fast rate of ultimate convergence to the final solution for a preset accuracy. A computer routine available with the NAG

library (1972) can yield the accurate roots of eqs(5.8), provided that a user-supplied routine calculating the left-hand sides of eqs.(5.8) is attached and that an initial estimate of the roots is given. The efficiency of this subroutine and even its success in finding the roots to a predetermined accuracy depend crucially on how close the initial estimate is to the final solution. An approximate solution of the problem can well be used for this purpose.

b. 'Approximate' primary path

An approach identical to that used by Croll and Walker (1972) is used here to yield the initial estimate of the 'exact' solution. According to it eqs.(5.8) can be linearised by combining two approximate steps. Firstly the potential functional (5.5) is transcribed in a polynomial form by replacing the transcendental functions ψ_i and u with polynomial expansions. Thus the stationary conditions (5.8) will arise in a non-linear polynomial form rather than a transcendental one.

Secondly the perturbation technique is used to replace these latter coupled equations by a set of linear coupled equations which are amenable to solution.

These two steps are detailed below for the three degree-of-freedom arch-model:

i) At first eq.(5.5) is approximated by an algebraic polynomial by replacing eqs.(5.7) with their trigonometric series.

The polynomial can be written as

$$\Delta\Pi = \sum_{i=1}^{3} \Pi_i v_i + \frac{1}{2!}\sum_{i=1}^{3}\sum_{j=1}^{3} \Pi_{ij} v_i v_j + \frac{1}{3!}\sum_{i=1}^{3}\sum_{j=1}^{3}\sum_{k=1}^{3} \Pi_{ijk} v_i v_j v_k + \frac{1}{4!}\sum_{i=1}^{3}\sum_{j=1}^{3}\sum_{k=1}^{3}\sum_{l=1}^{3} \Pi_{ijkl} v_i v_j v_k v_l + \cdots \quad (5.9)$$

A quartic polynom is chosen to approximate the exact form (5.5), that is, terms of higher order than four will be neglected. In doing so a balance is sought between the reality (necessity of dealing accurately with the large displacements) and simplicity (necessity of avoiding too complex mathematical developments).

With respect to the 'reality', the more terms there are considered beyond the quadratic term, which corresponds to the linearised model (equalibrium written on the undeformed state), the more accurate the non-linear effects of the large displacements can be analysed.

On the other hand with respect to the 'simplicity', the use of higher order polynomials would lead to mathematical formulations which are difficult to process, even if a computer is employed.

With reference to eqs.(5.6) the following trigonometric series are used in eqs. (5.7)

$$\psi_i = \sin\psi_i + \frac{1}{6}\sin^3\psi_i + \frac{3}{40}\sin^5\psi_i + \cdots \qquad , i=1,2,3 \quad (5.10)$$

$$\cos\theta_j = 1 - \frac{1}{2}\sin^2\theta_j - \frac{1}{8}\sin^4\theta_j - \cdots \qquad , j=1,2,4,5$$

The truncation of eqs.(5.10) is consistent with the degree of approximation introduced with the quartic polynomial (5.9).

Introducing eqs.(5.10) in eq.(5.5), using eqs.(5.6)

and (5.7) and accounting for the symmetry of the arch-model, the coefficients $\pi_{ij}, \pi_{ijk}, \pi_{ijkl}$ of eq.(5.9) are as listed in Table 5.1, where (m=1,2)

$$A_{1m} = 1 + \frac{1}{2}\sin^2\alpha_m + \frac{3}{8}\sin^4\alpha_m$$

$$A_{2m} = \frac{1}{2!}\left(\sin\alpha_m + \frac{3}{2}\sin^3\alpha_m\right)$$

$$A_{3m} = \frac{1}{3!}\left(1 + \frac{9}{2}\sin^2\alpha_m\right) \qquad (5.11)$$

$$B_{1m} = \sin\alpha_m + \frac{1}{2}\sin^3\alpha_m$$

$$B_{2m} = \frac{1}{2!}\left(1 + \frac{3}{2}\sin^2\alpha_m\right)$$

$$B_{3m} = \frac{1}{3!}\sin\alpha_m$$

In eq.(5.9) the π_i-coefficients are given by the 'exact' formula

$$\pi_i = -p \cdot p_i \qquad , i = 1...3 \qquad (5.12)$$

in accordance with eq.(5.5).

In setting up the coefficients from Table 5.1 it has been assumed that the maximum displacements v_i are of the same order as $\sin\alpha_1$ and that hence terms $v_1^j v_2^k v_3^l (\sin\alpha_m)^n$ with $j+k+l+n > 4$ and $m=1,2$ can be neglected (in order to be consistent with the approximation of eq.(5.9)).

Table 5.1

	①	②	③	④
$\Pi_{11}=\Pi_{33}$	2	$(A_{11}+A_{12})^2$	A_{12}^2	$(B_{11}-B_{12})^2$
Π_{22}	4	A_{12}^2	$2A_{12}^2$	$2B_{12}^2$
$\Pi_{12}=\Pi_{23}$	2	$-A_{12}(A_{11}+A_{12})$	$-2A_{12}^2$	$2B_{12}(B_{11}-B_{12})$
Π_{13}	2		A_{12}^2	$(B_{11}-B_{12})^2$
$\Pi_{111}=\Pi_{333}$	-12	$(A_{11}+A_{12})(A_{21}-A_{22})$	$-A_{12}A_{22}$	$(B_{11}-B_{12})(B_{21}+B_{22})$
Π_{222}	-24	$A_{12}A_{22}$	$2A_{12}A_{22}$	$2B_{12}B_{22}$
$\Pi_{112}=\Pi_{233}$	4	$A_{12}(A_{21}-3A_{22})-2A_{11}A_{22}$	$-4A_{12}A_{22}$	$2\left[B_{22}(B_{11}-B_{12})-B_{12}(B_{21}+B_{22})\right]$
$\Pi_{113}=\Pi_{133}$	4		$A_{12}A_{22}$	$-(B_{11}-B_{12})(B_{21}+B_{22})$
$\Pi_{122}=\Pi_{233}$	4	$A_{22}(A_{11}+3A_{12})$	$6A_{12}A_{22}$	$2B_{22}(-B_{11}+3B_{12})$
Π_{123}	8		$-A_{12}A_{22}$	$B_{22}(B_{11}-B_{12})$
$\Pi_{1111}=\Pi_{3333}$	24	$(A_{21}-A_{22})^2+2(A_{11}+A_{12})(A_{31}+A_{32})$	$A_{22}^2+2A_{12}A_{32}$	$(B_{21}+B_{22})^2+6(B_{11}-B_{12})(B_{31}-B_{32})$
Π_{2222}	48	$A_{22}^2+2A_{12}A_{32}$	$2(A_{22}^2+2A_{12}A_{32})$	$2(B_{22}^2+6B_{12}B_{32})$
$\Pi_{1113}=\Pi_{1333}$	12		$A_{12}A_{32}$	$3(B_{31}-B_{32})(B_{11}-B_{12})$
$\Pi_{1112}=\Pi_{2333}$	12	$2(A_{21}-A_{22})A_{22}-4A_{12}A_{32}-3A_{11}A_{32}-A_{12}A_{31}$	$-5A_{12}A_{32}-2A_{22}^2$	$6B_{12}(B_{31}-B_{32})-2B_{22}\cdot(B_{21}+B_{22})+9B_{32}\cdot(B_{11}-B_{12})$
$\Pi_{1222}=\Pi_{2223}$	-12	$2A_{22}^2+4A_{12}A_{32}+A_{11}A_{32}$	$8A_{12}A_{32}+4A_{22}^2$	$4B_{22}^2+6B_{32}(4B_{12}-B_{11})$
$\Pi_{1122}=\Pi_{2233}$	24	$3A_{22}^2-A_{22}A_{21}+3A_{32}(A_{11}+2A_{12})$	$4A_{22}^2+9A_{12}A_{32}$	$2B_{22}(B_{21}+2B_{22})-9B_{32}(B_{11}-3B_{12})$
Π_{1133}	8		A_{22}^2	$(B_{21}+B_{22})^2$
Π_{1223}	8		$2A_{22}^2+3A_{12}A_{32}$	$2B_{22}^2-9B_{32}(B_{11}-B_{12})$
$\Pi_{1123}=\Pi_{1233}$	-4		$2A_{22}^2+3A_{12}A_{32}$	$2B_{22}(B_{21}+B_{22})-9B_{32}(B_{11}-B_{12})$

N.B. Each Π-coefficient in Table 5.1 is given by

$$\Pi = ① \cdot \left[② + c.③ + k.④ \right]$$

where ①, ②, ③, ④ denote the values from the appropriate column and row while c and k are given by eqs.(5.4)

Using the conditions of stationary total potential energy and the approximate form (5.9) the equilibrium of the approximate deformed state is expressed by the set of equations (i=1...3)

$$\frac{\partial \Delta\Pi}{\partial v_i} = \Pi_i + \frac{1}{1!}\sum_{j=1}^{3}\Pi_{ij}v_j + \frac{1}{2!}\sum_{j=1}^{3}\sum_{k=1}^{3}\Pi_{ijk}v_jv_k + \frac{1}{3!}\sum_{j=1}^{3}\sum_{k=1}^{3}\sum_{l=1}^{3}\Pi_{ijkl}v_jv_kv_l = 0 \qquad (5.13)$$

Yet no closed-form solution of the non-linear eqs. (5.13) can be found and, therefore, other techniques must be further used to overcome this difficulty.

ii) In what follows the perturbation method is used to solve approximately eqs.(5.13). Sewell (1965) has emphasised the effectiveness of this technique in pre- and postbuckling analysis of structures with a finite number of degrees of freedom.

Using the perturbation technique the set of non-linear eqs.(5.13) is reduced to a sequence of sets of linear equations which can be readily solved. It arises that (see Appendix V.2)

$$\frac{\partial \Pi_i}{\partial p}\cdot p' + \sum_j \Pi_{ij}v_j' = 0 \qquad (5.14a)$$

$$\frac{\partial \Pi_i}{\partial p}\cdot p'' + \sum_j \Pi_{ij}v_j'' = -\sum_j\sum_k \Pi_{ijk}v_j'v_k' \qquad (5.14b)$$

$$\frac{\partial \Pi_i}{\partial p}\cdot p''' + \sum_j \Pi_{ij}v_j''' = -3\sum_j\sum_k \Pi_{ijk}v_j''v_k' - \sum_j\sum_k\sum_l \Pi_{ijkl}v_j'v_k'v_l'' \qquad (5.14c)$$

$$i,j,k,l = 1,2,3$$

where the suffices denote the first, second,....order derivatives with respect to the perturbation parameter ε.

This ordered set of linear equilibrium equations can be used to determine sequentially each of the r order derivatives of v_j and p in terms of their already known derivatives of order s where $s < r$. When moving from one set of linear perturbation equations to the next only the known right-hand vector changes and thanks to this feature the use of matrix formulation within the computer program is very effective.

Either the load p or one of the displacements v_j can be used as perturbation parameter. When $\varepsilon=p$, for instance, then

$$p' = 1 \quad \text{and} \quad p'' = p''' = \ldots = 0 \qquad (5.15)$$

and v_j', v_j'', v_j''' ($j=1,2,3$) follow from the sequence (5.14). Then the 'approximate' primary path is found by using eqs. (5.2.1) from Appendix V.2.

Whilst for the mathematical approach it makes no relevant difference which coordinate from Fig.5.5 is associated with ε, the choice of the perturbation parameter can yield significantly different shapes for the primary path with further effects on the critical load and on the branching paths.

This aspect is discussed in the next section.

c. Discussion

The 'approximate' primary path is used in this chapter solely to provide the initial estimate of the

'exact' primary path but it can be also used as an independent alternative of the 'exact' primary path (see Croll and Walker (1972)).

In order to find out the significance of the approximations, a comparison between the 'exact' primary path PP and some 'approximate' primary paths is presented and discussed herein. (PP is the accurate solution of eqs.(5.8) - see Section 5.3.3a)

Three 'approximate' primary paths are considered:

i) $\overline{PP}$ (p) is the 'approximate' primary path arising from eqs.(5.14a...c) when the load p is used as perturbation parameter - see Section 5.3.3b).

ii) $\overline{PP}$ (v_i) is similar to $\overline{PP}$ (p) but the displacement v_i is used as perturbation parameter. As mentioned different primary paths follow from choosing different perturbation parameters.

iii) PP^* is a primary path arising from the accurate solution of the approximate eqs.(5.13). This solution is found from eqs.(5.13) following the same approach as that when PP is found from eqs.(5.8).

Whereas the primary paths $\overline{PP}$ include the approximations associated with both steps from Section 5.3.3b (i.e. the use of eqs.(5.13) instead of eqs.(5.8) and the use of the perturbation technique), the primary path PP^* comprises solely the approximations due to the first step (i.e. it does not include those related to the perturbation technique). Thanks to PP^* the significance of the approximations introduced by either step in

Section 5.3.3b can be outlined. Thus, while the comparison between PP and PP^* provides information on how approximate eqs.(5.13) are relative to the 'exact' eqs.(5.8), the comparison between PP^* and $\overline{PP}$ outlines the significance of the approximations introduced by the perturbation technique. When the 'approximate' paths $\overline{PP}$ are compared to the 'exact' path PP the significance of both the above approximations is emphasised.

An initial estimate of solution is required when the Powell's procedure is used to provide both PP and PP^* and either $\overline{PP}(p)$ or $\overline{PP}(v_i)$ can be used for this aim. However, neither PP nor PP^* depend on this initial estimate, that is, the same PP and PP^* arise no matter whether the starting point of computation is on $\overline{PP}(p)$ or on $\overline{PP}(v_i)$.

The four primary paths are plotted for four representative sets of paramenters $\alpha_1, \alpha_2, c, k, p_1$ and p_2 (see Fig.5.4 and eqs.(5.4))

The arch-model from Fig.5.6 has the initial axis coincident with the funicular polygon of loading. It has a normal shallowness $\left(i.e.\ \frac{f}{\ell} = \frac{\sin\alpha_1 + \sin\alpha_2}{2(\cos\alpha_1 + \cos\alpha_2)} = \frac{1}{10}\right)$, an uniform bending stiffness and loading ($c=1$ and $p_1=p_2=1$, respectively) and an axial stiffness significantly larger than its bending stiffness ($k=100c$).

The arch-model from Fig.5.7 is similar to that from Fig.5.6 but it is more flexible at the apex ($c=0\cdot5$).

The arch-model from Fig.5.8 is identical to that from Fig.5.7 but $p_1=0\cdot7$ so that the funicular polygon of loads is no longer coincident with the initial axis of the

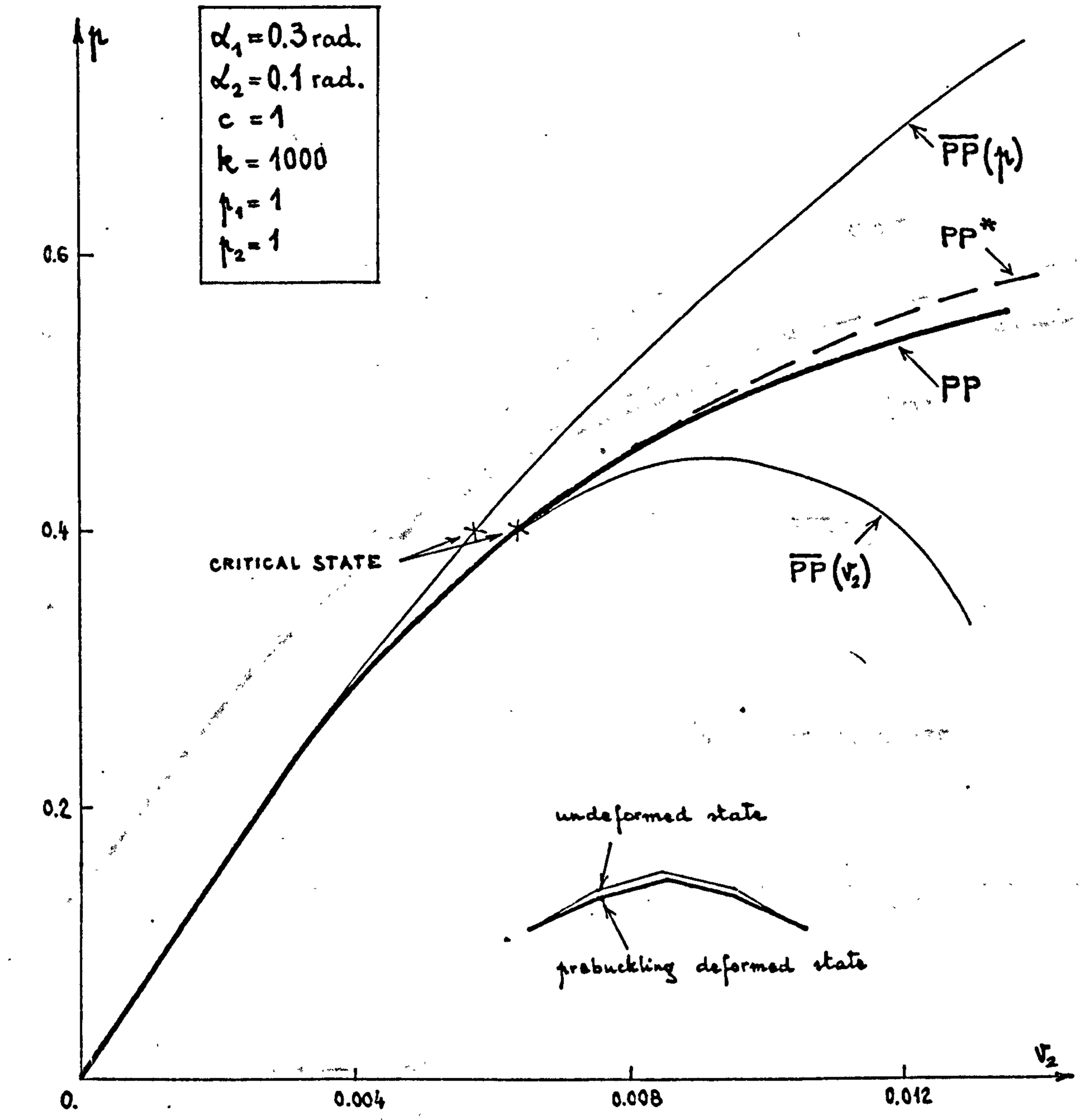
$\alpha_1 = 0.3$ rad.
$\alpha_2 = 0.1$ rad.
c = 1
k = 1000
$\mu_1 = 1$
$\mu_2 = 1$
μ
0.6
0.4
0.2
0.
0.004
0.008
0.012
V_2
$\overline{PP}(\mu)$
PP^*
PP
CRITICAL STATE
$\overline{PP}(V_2)$
undeformed state
prebuckling deformed state

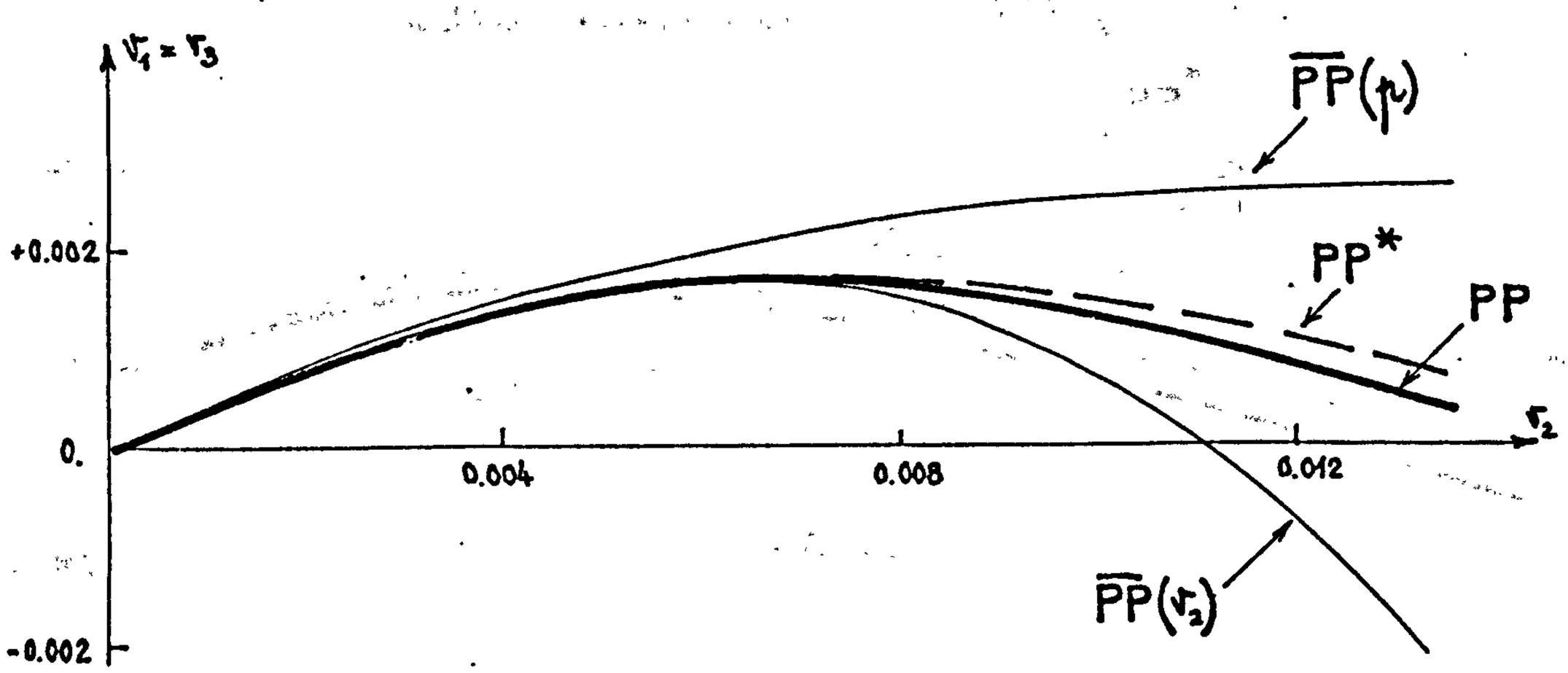
$V_1 = V_3$
+0.002
0.
-0.002
0.004
0.008
0.012
V_2
$\overline{PP}(\mu)$
PP^*
PP
$\overline{PP}(V_2)$

Fig. 5.6

$\alpha_1 = 0.3$ rad.
$\alpha_2 = 0.1$ rad.
$c = 0.5$
$k = 1000$
$\gamma_1 = 1$
$\gamma_2 = 1$

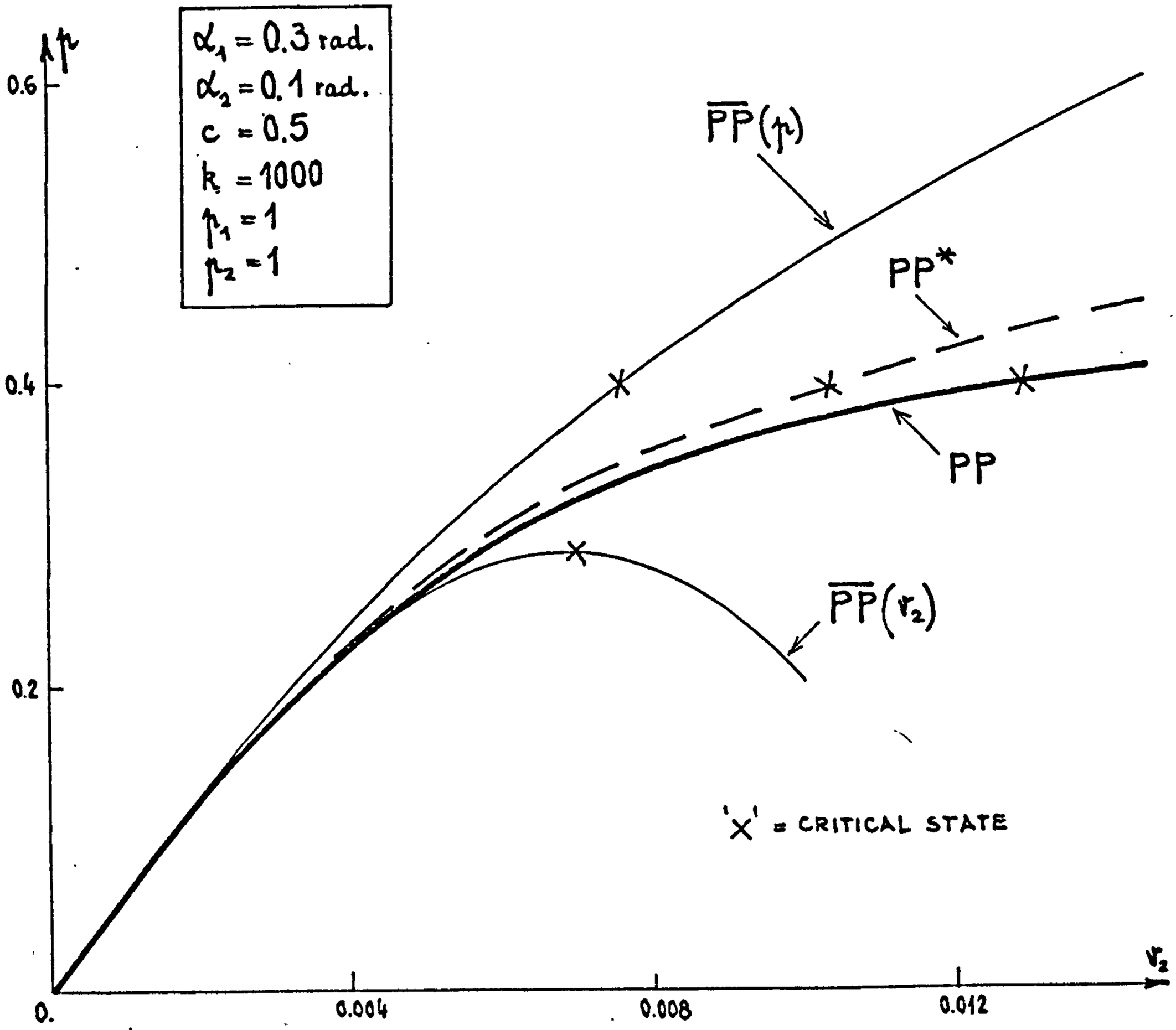

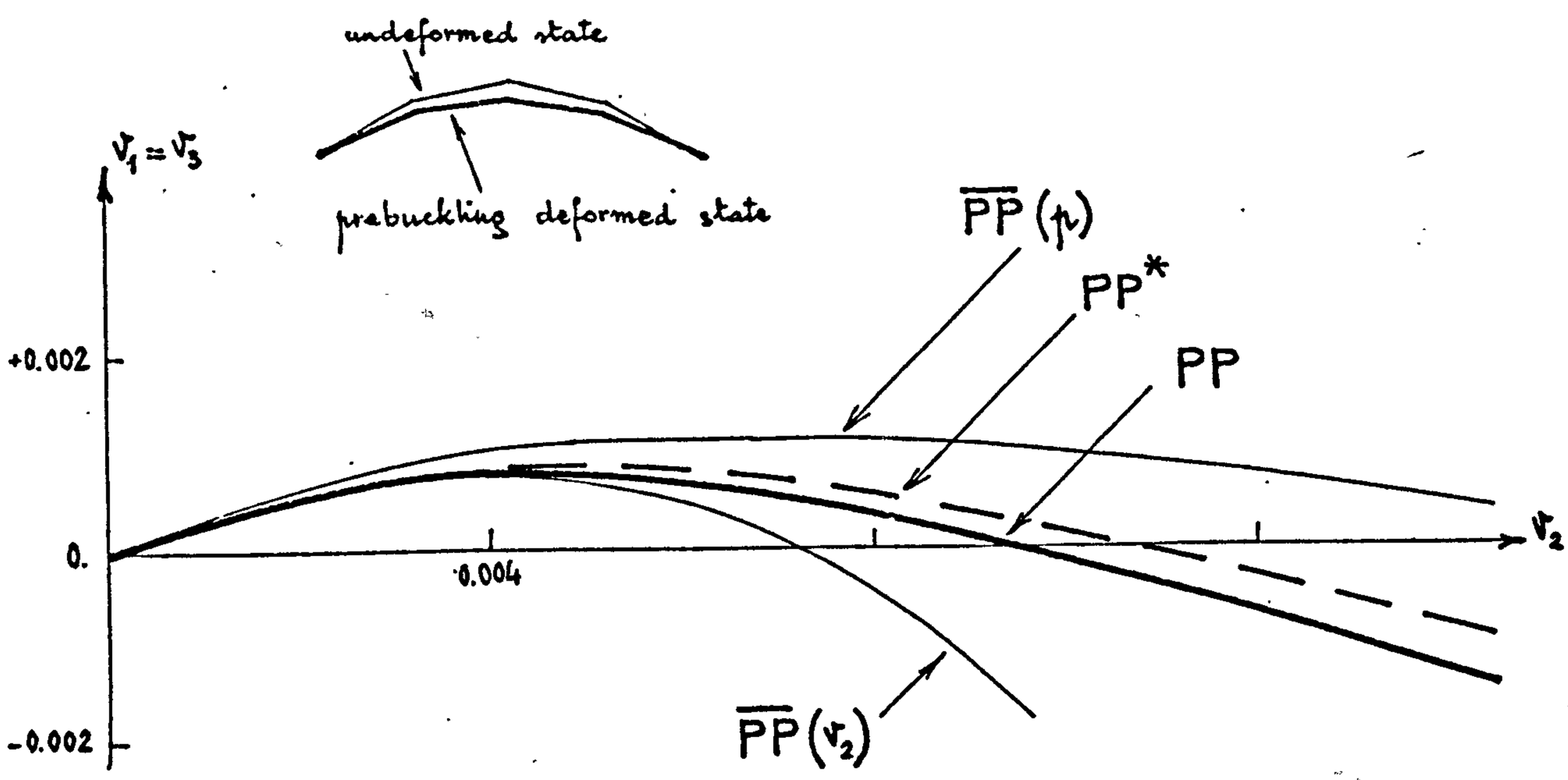

Fig. 5.7

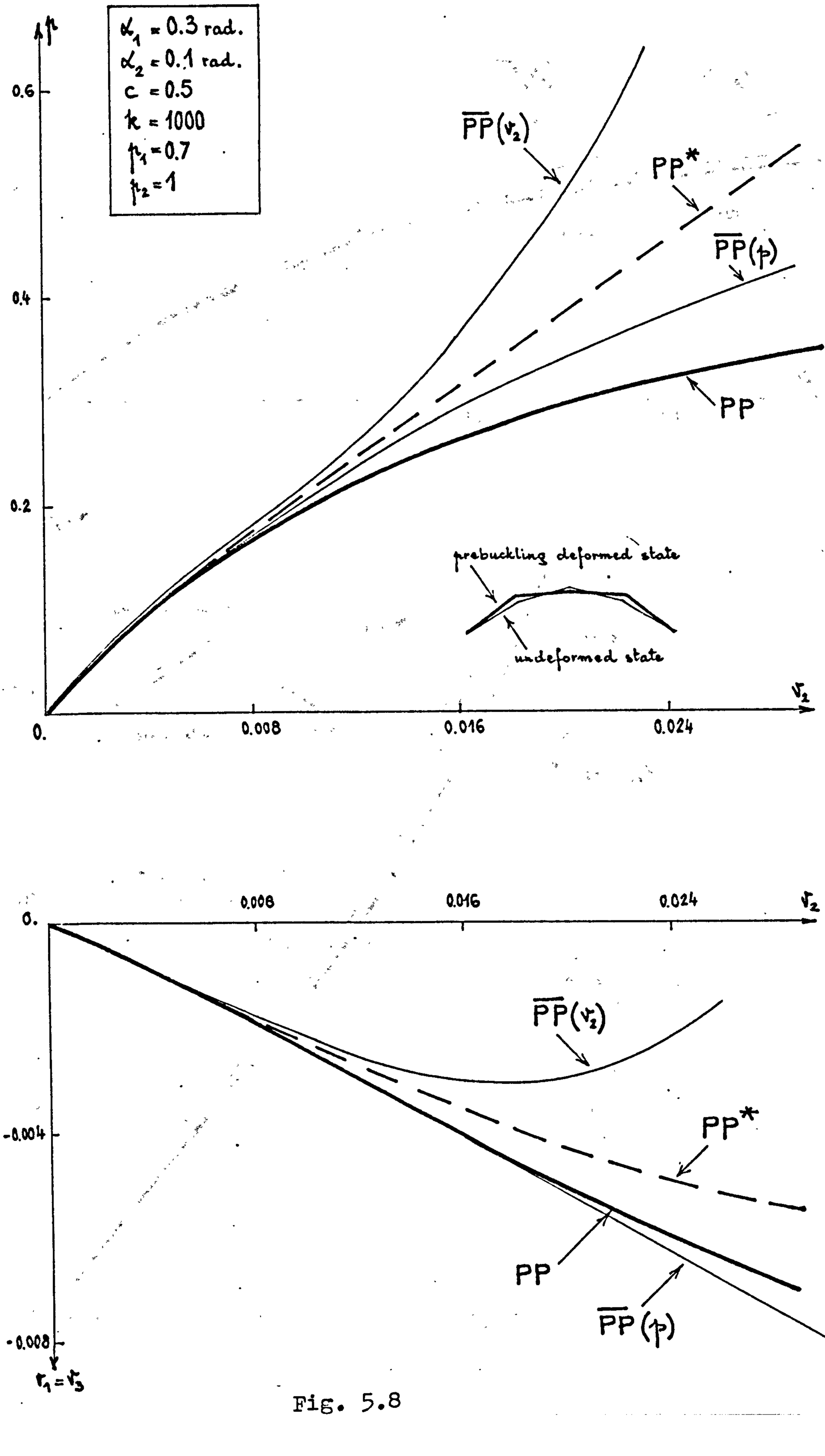
$\alpha_1 = 0.3$ rad.
$\alpha_2 = 0.1$ rad.
$c = 0.5$
$k = 1000$
$\gamma_1 = 0.7$
$\gamma_2 = 1$
γ
0.6
0.4
0.2
0.
0.008
0.016
0.024
γ_2
$\overline{PP}(\gamma_2)$
PP^*
$\overline{PP}(\gamma)$
PP
prebuckling deformed state
undeformed state
-0.004
-0.008
$\gamma_1 = \gamma_3$

Fig. 5.8

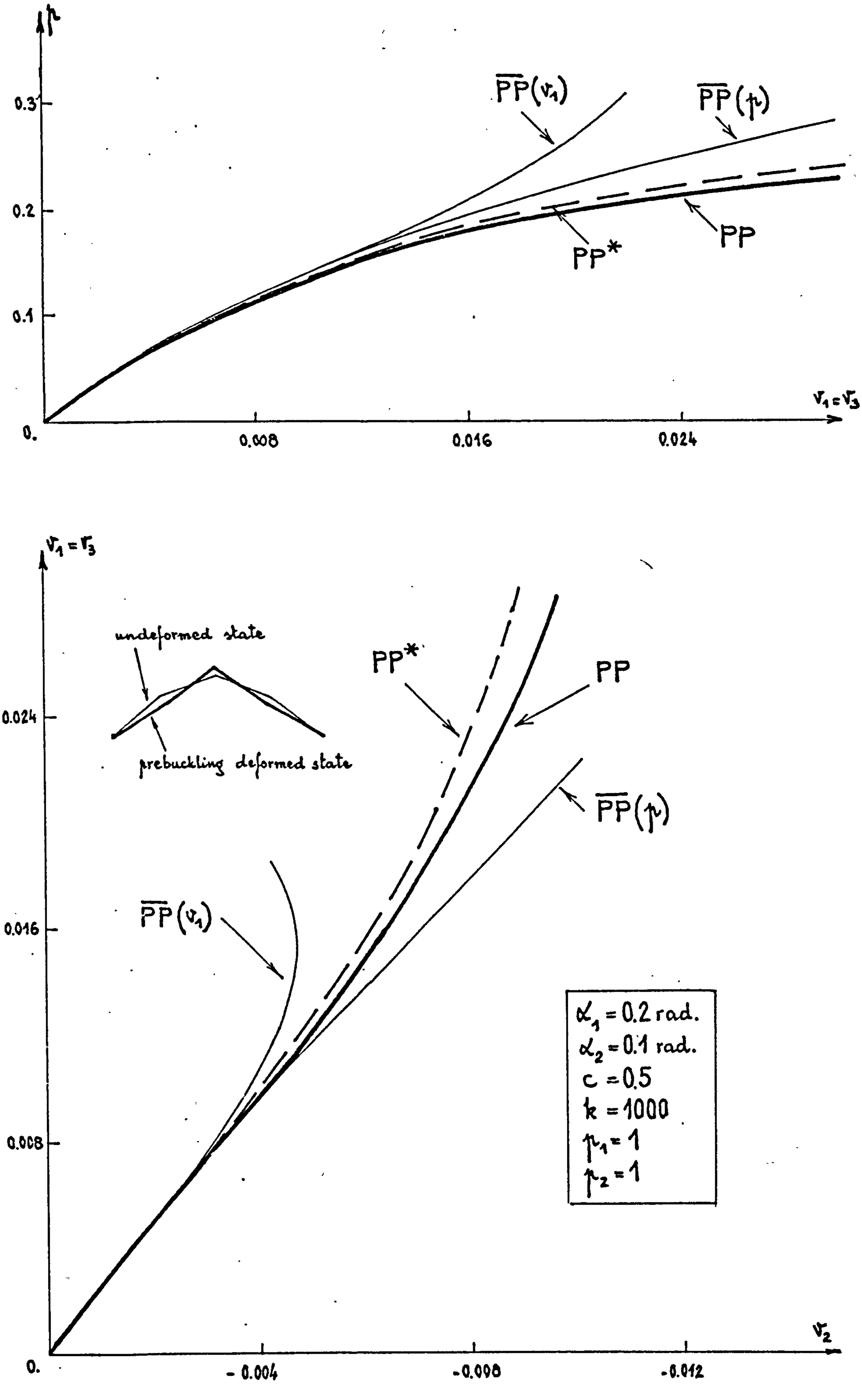
0.3
0.2
0.1
0.
0.008
0.016
0.024
$\overline{PP}(\nu_1)$
$\overline{PP}(\mu)$
PP*
PP
$\nu_1 = \nu_3$
$\nu_1 = \nu_3$
0.024
0.016
0.008
0.
undeformed state
prebuckling deformed state
PP*
PP
$\overline{PP}(\mu)$
$\overline{PP}(\nu_1)$
$\alpha_1 = 0.2$ rad.
$\alpha_2 = 0.1$ rad.
$c = 0.5$
$k = 1000$
$\mu_1 = 1$
$\mu_2 = 1$
ν_2
- 0.004
-0.008
-0.012

Fig. 5.9

arch-model.

The arch-model from Fig.5.9 has the same mechanical parameters $\underline{c}$ and $\underline{k}$ and the same loading as that from Fig.5.7 but it is more shallow $\left(\frac{f}{t} \simeq \frac{1}{13.3}\right)$ and the funicular polygon and the initial axis are no longer coincident.

In each of the Figs.5.6...5.9 the primary paths are plotted using their projections on the reference planes pOv_2 and v_1Ov_2 (see Fig.5.5).

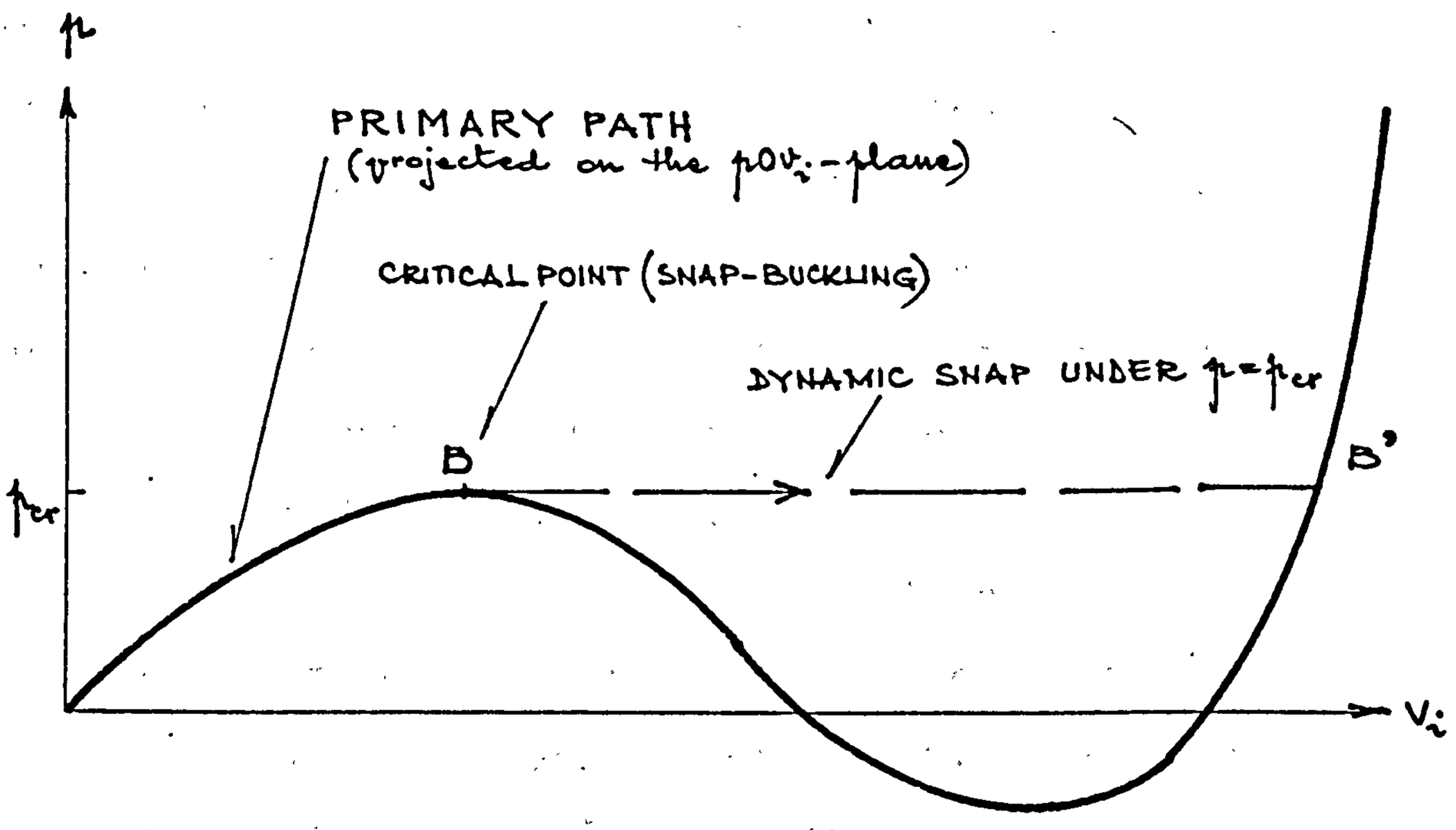

Fig. 5.10

Figs.5.6 ...5.9 give rise to the following conclusions:

i) Significant differences can occur with respect to the choice of the perturbation parameter. The larger the load p is (or the larger the displacement v_i is),

the more significant are the truncations operated in eqs.(5.2.1)*) and thus the more different $\overline{PP}(p)$ and $\overline{PP}(v_i)$ are.

ii) $\overline{PP}(p)$ is not able to predict correctly the snap behaviour of an arch-model since the displacements v_i have been assumed to be single-valued functions of p in eqs.(5.2.1).

The snap-buckling is the instability associated with a primary path as in Fig.5.10. As the load p increases from 0 to p_{cr} the structure becomes less stiff (i.e. at least a deflection increases with a faster rate for a given increase in load). At B the stiffness is zero and a new stable equilibrium state is sought by the structure. If p is held constant or increased the first new equilibrium state is B' and the move towards B' involves a noticeably large change in deformation accompanied by dynamic effects. If the displacements v_i are controlled rather than p, the equilibrium states beyond the snap point B correspond to the primary path from Fig.5.10, that is to a lower load p. The range of the primary path between B and B' can be outlined solely by choosing the displacement v_i as perturbation parameter. This conclusion is emphasised by Croll and Walker (1972).

iii) $\overline{PP}(p)$ projected on the reference plane pOv_1 (or pOv_2) is always above PP or, in other words, the choice

---

Footnote

*) see Appendix V.2.

of p as perturbation parameter yield smaller displacements than the actual ones for the same load p. This stiffening effect is a consequence of the truncation of eqs.(5.2.1) *) which is virually equivalent to imposing constraints on the displacements. When such constraints are applied reduced displacements of a body under a given set of forces arise (see Argyris and Kelsey (1960) p.8).

iv) When $\varepsilon=v_i$, the effect of the truncation of eqs.(5.2.1) *) cannot be predicted as it is equivalent to superimposing of extra loads and extra displacements v_j $(j\neq i)$. Their combined effect can yield either reduction (see $\overline{PP}(v_i)$ in Figs.5.6 and 5.7) or increase (see $\overline{PP}(v_i)$ in Fig.5.9) of the model stiffness.

v) Although less approximate than the paths $\overline{PP}$, PP^* is not always closer to PP and this means that the combined effects of the approximations associated with eqs.(5.13) and with the perturbation technique do not necessarily lead to a worse final solution. In Fig.5.8, for instance, $\overline{PP}(p)$ represents a better approximation of PP than PP^* does.

iv) Although significant, the differences between the 'exact' path PP and the 'approximate' primary paths $\overline{PP}(p)$, $\overline{PP}(v_i)$ and PP^* can be irrelevant when they depict about the same behaviour up to the critical point (the lowest load under which instability occurs). As it will be shown in Section 5.3.4, the primary path is associated with an unstable eqilibrium beyond this critical state and it is therefore of no practical importance in that range. For instance, for both cases from Figs.5.6 and 5.7

Footnote

*) see Appendix V.2

$p_{cr} \simeq 0{\cdot}4$ but only for the model from Fig.5.7 the four primary paths will yield different results when the postbuckling behaviour will be analysed.

d. Conclusion

It is apparent from the above discussion that, at this stage, it is not possible to predict the difference between the 'approximate' solutions and the 'exact' solution and whether an 'approximate' solution is on the conservative side or not.

On this account and taking into consideration that no major mathematical difficulty arises, the 'exact' primary path PP will be further used to analyse the prebuckling response of the arch-model from Fig.5.2. The 'approximate' $\overline{PP}(p)$ will be used to provide the initial estimate of the 'exact' solution.

It is worth remembering that by 'exact' primary path is meant the accurate solution of eqs.(5.8), whereas $\overline{PP}(p)$ is the solution of the approximate eqs.(5.14a..c) with the load p as perturbation parameter.*)

5.3.4. ELASTIC STABILITY

The elastic primary path provides the equilibrium position of the arch-model for a certain load p but gives no information whether the equilibrium is stable or not, and whether that position is the only possible

---

Footnote

*) see Appendix V.2.

one or not.

In order to answer the first question stability criteria are used.

Regarding the second question further information is provided later when the postbuckling behaviour will be analysed.

Within the present section stability criteria will be developed in a general form for a three degree-of-freedom model. A comparison of the stability criteria based on 'exact' and 'approximate' primary paths is also presented and it is shown that it endorses the conclusion from Section 5.3.3d.

a. Stability criteria

The dynamic criterion of stability can be employed to analyse the stability of the equilibrium position given by the primary path. Then an equilibrium position is stable if the dynamic response to any external disturbance remains small or, in other words, a damping of the vibrations occurs. That is so when the natural vibration frequencies $\bar{\omega}$ of the structure are positive.

Using this approach it is shown in Appendix V.3 that the necessary and sufficient conditions for the natural frequencies $\bar{\omega}$ of the three degree-of-freedom arch-model to be positive are:

$$\left| \begin{array}{l} \pi_{ii} > 0 \\ \\ M_{ii} > 0 \\ \\ \Delta > 0 \end{array} \right. \quad , i = 1,2,3 \tag{5.16}$$

where

$-\Pi_{ij}$ is the second partial derivative of the potential functional with respect to displacements v_i (at the point S on the primary path for which the stability of equilibrium is checked), that is

$$\Pi_{ij} = \left.\frac{\partial^2 \Delta\Pi}{\partial v_i \partial v_j}\right|_S \qquad (5.17)$$

$-M_{ij}$ is the minor of Π_{ij} in the determinant Δ

$-\Delta$ is given by

$$\Delta = |\Pi_{ij}| \qquad i,j = 1\ldots3 \qquad (5.18)$$

When one or more of the conditions (5.16) are violated the equilibrium state corresponding to S is unstable.

The elastic critical load is the lowest load under which at least one of the conditions (5.16) is no longer satisfied or, in other words, the corresponding left-hand side becomes zero. Beyond the critical load the primary path does not correspond any longer to the stable equilibrium position and only a postcritical analysis can provide information about that range.

The values Π_{ij} according to eq.(5.17) can be computed using either the exact form of $\Delta\Pi$, i.e. eq.(5.5), or the approximate one, eq.(5.9).

When eq.(5.5) is used it follows from eqs.(5.8) that

$$\Pi_{ij} = \sum_{l=1}^{3} c_l \cdot \left(\psi_l \frac{\partial^2 \psi_l}{\partial v_i \partial v_j} + \frac{\partial \psi_l}{\partial v_i} \cdot \frac{\partial \psi_l}{\partial v_j}\right) + k \cdot \left(u \frac{\partial^2 u}{\partial v_i \partial v_j} + \frac{\partial u}{\partial v_i} \cdot \frac{\partial u}{\partial v_j}\right) \qquad (5.19)$$

where Ψ_ℓ and u are given by eqs.(5.6) and (5.7), while the first and second order deviatives are given in Appendix V.1.

When eq.(5.9) is used, it follows from eqs.(5.13) that

$$\Pi_{ij} = \pi_{ij} + \frac{1}{2!}\sum_{k=1}^{3} \pi_{ijk} v_k + \frac{1}{3!}\sum_{k=1}^{3}\sum_{\ell=1}^{3} \pi_{ijk\ell} v_k v_\ell \qquad (5.20)$$

where thecoefficients π are given by Table 5.1.

In both eqs.(5.19) and (5.20) v_k are the displacements of the equilibrium state S about the undeformed and unloaded position.

Due to the symmetry of the arch-model from Fig.5.2 the primary path is always symmetric, and thus the determinent Δ given by eq.(5.18) is symmetric about both diagonals, that is

$$\begin{aligned} \Pi_{11} &= \Pi_{33} \\ \Pi_{12} &= \Pi_{21} = \Pi_{23} = \Pi_{32} \\ \Pi_{13} &= \Pi_{31} \end{aligned} \qquad (5.21)$$

so that only four coefficients Π_{ij} (i.e. $\Pi_{11}, \Pi_{12}, \Pi_{13}, \Pi_{22}$) are distinct.

On account of eqs.(5.21) the seven conditions (5.16) reduce to the following five distinct ones:

$$\left\| \begin{array}{ll} \Pi_{ii} > 0 & \\ M_{ii} > 0 & i = 1,2 \\ \Delta > 0 & \end{array} \right. \qquad (5.16a)$$

where

$$\Delta = \begin{vmatrix} \varpi_{11} & \varpi_{12} & \varpi_{13} \\ \varpi_{12} & \varpi_{22} & \varpi_{12} \\ \varpi_{13} & \varpi_{12} & \varpi_{11} \end{vmatrix} = (\varpi_{11} - \varpi_{13}) \cdot (M_{11} - M_{13}) \qquad (5.22)$$

In Appendix V.4 it is shown that none of the conditions $\varpi_{ii} > 0$ and $M_{ii} > 0$ can be violated at a lower critical load than that corresponding to $\Delta = 0$. This means that, among the criteria (5.16a), the last criterion

$$\Delta > 0 \qquad (5.23)$$

is sufficient to ensure that the equilibrium associated with the primary path is stable.

Henceforth the condition (5.23) will be used as <u>stability criterion</u> for the arch-model from Fig.5.2.

However, the analysis of the conditions $\varpi_{ii} > 0$ and $M_{ii} > 0$ will still be of interest. In Appendix V.4 it is shown that the stability criterion (5.23) is violated simultaneously with one or a group of the first two conditions (5.16a). Moreover it is shown that the violation of these latter is mathematically responsible for the violation of the stability criterion (5.23). This conclusion is of great significance and later in Section 5.3.5c a physical meaning will be associated to it.

That one or a group of the conditions $\varpi_{ii} > 0$ and $M_{ii} > 0$ is violated simultaneously with the stability criterion (5.23) arises from Figs.5.11..5.13 too. In these figures the variation of the parameters included in the conditions (5.16a) is depicted for three numerical

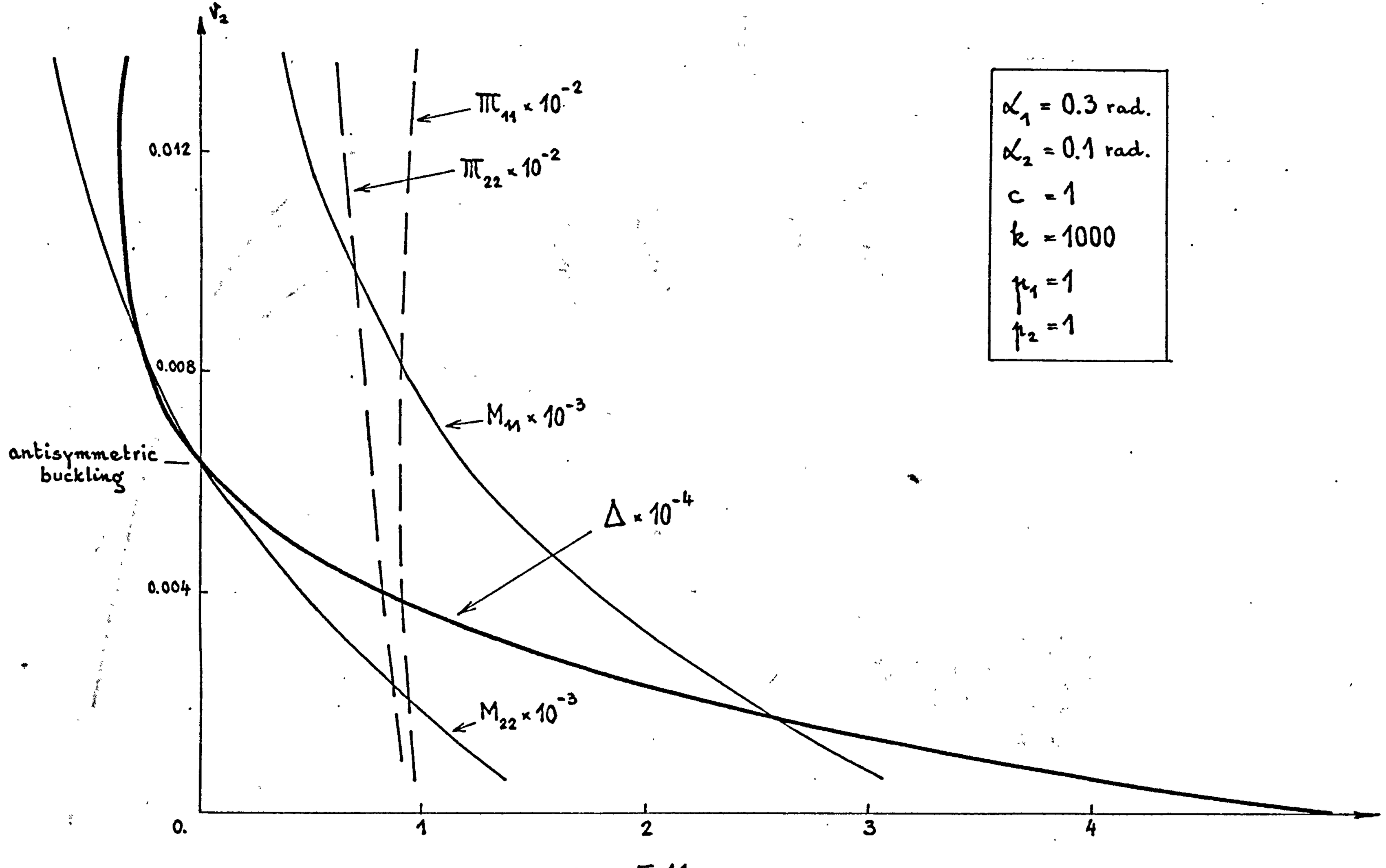

$\alpha_1 = 0.3$ rad.
$\alpha_2 = 0.1$ rad.
$c = 1$
$k = 1000$
$\mu_1 = 1$
$\mu_2 = 1$

Fig. 5.11

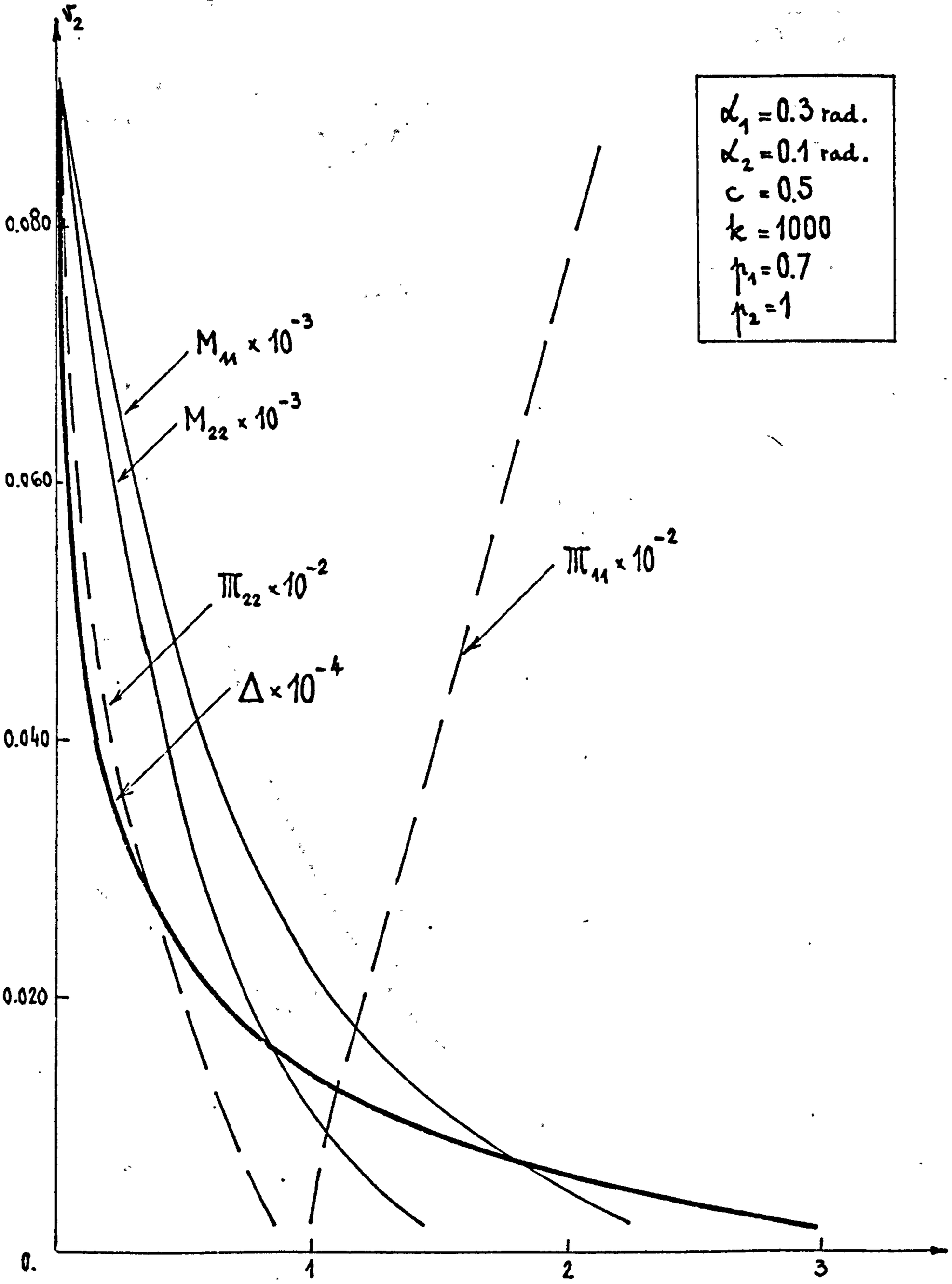
ν_2
$\alpha_1 = 0.3$ rad.
$\alpha_2 = 0.1$ rad.
$c = 0.5$
$k = 1000$
$\gamma_1 = 0.7$
$\gamma_2 = 1$
0.080
0.060
0.040
0.020
0.
1
2
3
$M_{11} \times 10^{-3}$
$M_{22} \times 10^{-3}$
$\pi_{22} \times 10^{-2}$
$\Delta \times 10^{-4}$
$\pi_{11} \times 10^{-2}$

Fig. 5.12

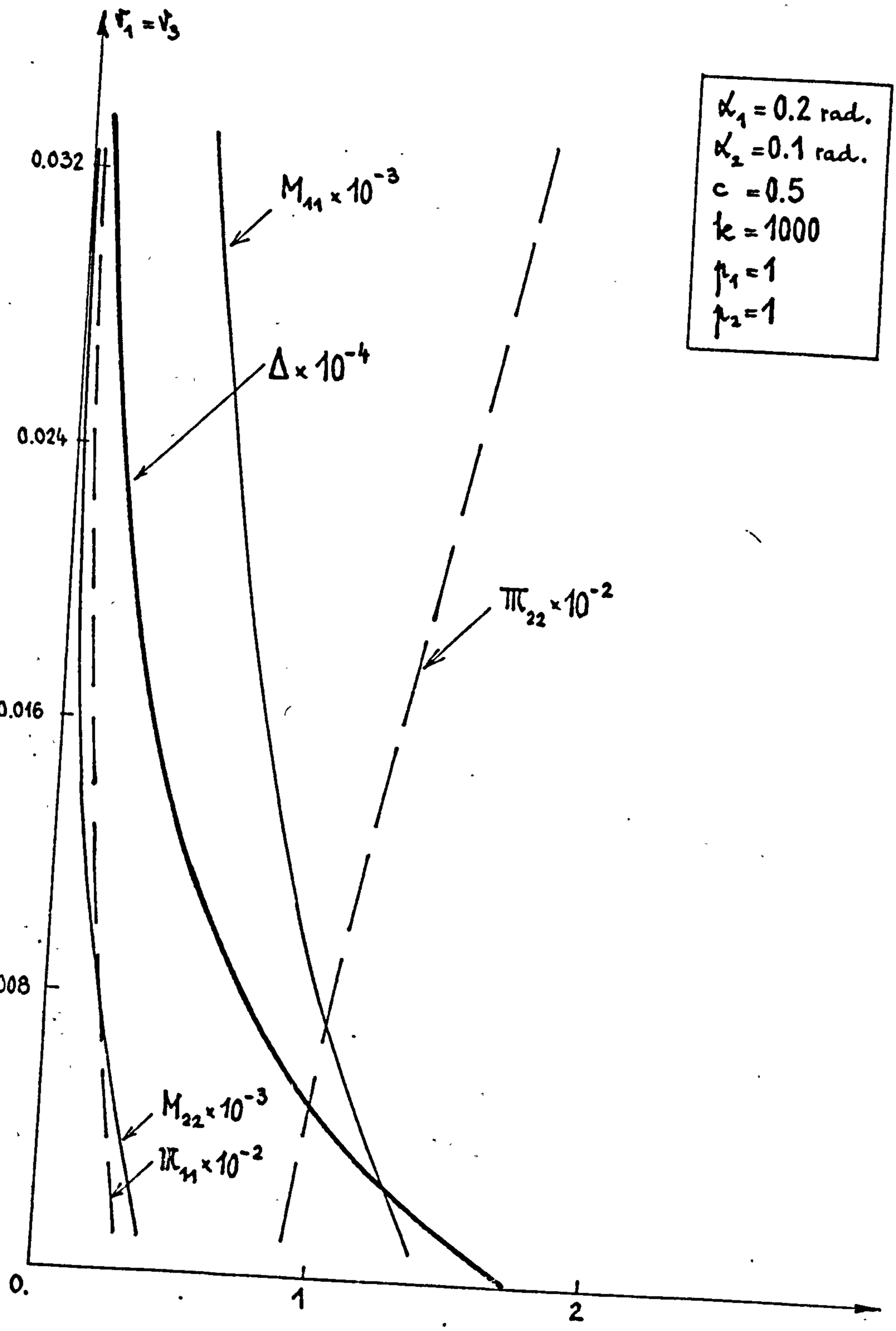
$r_1 = r_3$
0.032
0.024
0.016
0.008
0.
1
2
$M_{11} \times 10^{-3}$
$\Delta \times 10^{-4}$
$\pi_{22} \times 10^{-2}$
$M_{22} \times 10^{-3}$
$\pi_{11} \times 10^{-2}$
$\alpha_1 = 0.2$ rad.
$\alpha_2 = 0.1$ rad.
$c = 0.5$
$k = 1000$
$f_1 = 1$
$f_2 = 1$

Fig. 5.13

applications. The numerical data of the arch-model in Figs.5.11...5.13 are identical to those from Figs.5.6, 5.8 and 5.9 respectively. The 'exact' π_{ij}-coefficients according to eqs.(5.19) and to the 'exact' primary path are considered. The variation along the primary path is plotted with respect to one of the displacements v_1 or v_2. The corelation with the load p can be derived from the corresponding primary paths plotted in Figs.5.6, 5.8 and 5.9, respectively.

It can be seen that:

i) for the arch-model associated with Fig.5.11 the stability criterion (5.23) is violated simultaneously with $M_{22} = 0$

ii) for the arch-model associated with Fig.5.12 the stability criterion (5.23) is violated simultaneously with

$$\pi_{22} = 0, \quad M_{22} = 0 \text{ and } M_{11} = 0$$

iii) for the arch-model associated with Fig.5.13 the stability criterion (5.23) is violated simultaneously with

$$\pi_{11} = 0 \text{ and } M_{22} = 0$$

b. Discussion

'Exact' or 'approximate' forms of the stability criterion (5.23) arise as the π_{ij}- coefficients in eq. (5.18) are computed according to eqs.(5.19) or (5.20), respectively.

In order to establish how significantly different the 'exact' and the 'approximate' forms of the stability

criterion are, a comparison is carried out in Figs 5.14.. 5.16 where the 'exact' and 'approximate' values of Δ are depicted by unbroken and broken lines, respectively. In both eqs.(5.19) and (5.20) the displacements v_i are supposed to be given by the 'exact' primary path PP and by the 'approximate' paths PP^* and $\overline{PP}(p)$.

However, in order to simplify the graphs, the Δ-curves corresponding to PP^* are not plotted in Figs5.14 and 5.15, as they are very close to those corresponding to PP.

In Figs.5.14 and 5.15 the same models as in Figs. 5.6 and 5.7 respectively are studied. In Fig.5.16 a similar model as that in Fig.5.8 is considered, but the loading parameters are $p_1=1\cdot0$ and $p_2=0\cdot7$ instead of $p_1=0\cdot7$ and $p_2=1\cdot0$.

Figs.5.14..5.16 emphasise the following remarks which add to those already pointed out by Figs.5.6...5.9:

i) Although the 'exact' and the 'approximate' Δ-curves are in a fairly good agreement both in Rig.5.14 and in Fig.5.15, the coordinates of the critical points (i.e. load and displacements corresponding to $\Delta=0$) are affected rather differently in these two cases. While almost identical critical points arise in Fig.5.14 from using the 'exact' and/or the 'approximate' forms, different coordinates for the critical points arise in Fig.5.15. This is so because the Δ-curves reach their zeros in the same range where they diverge as a consequence of approximations.

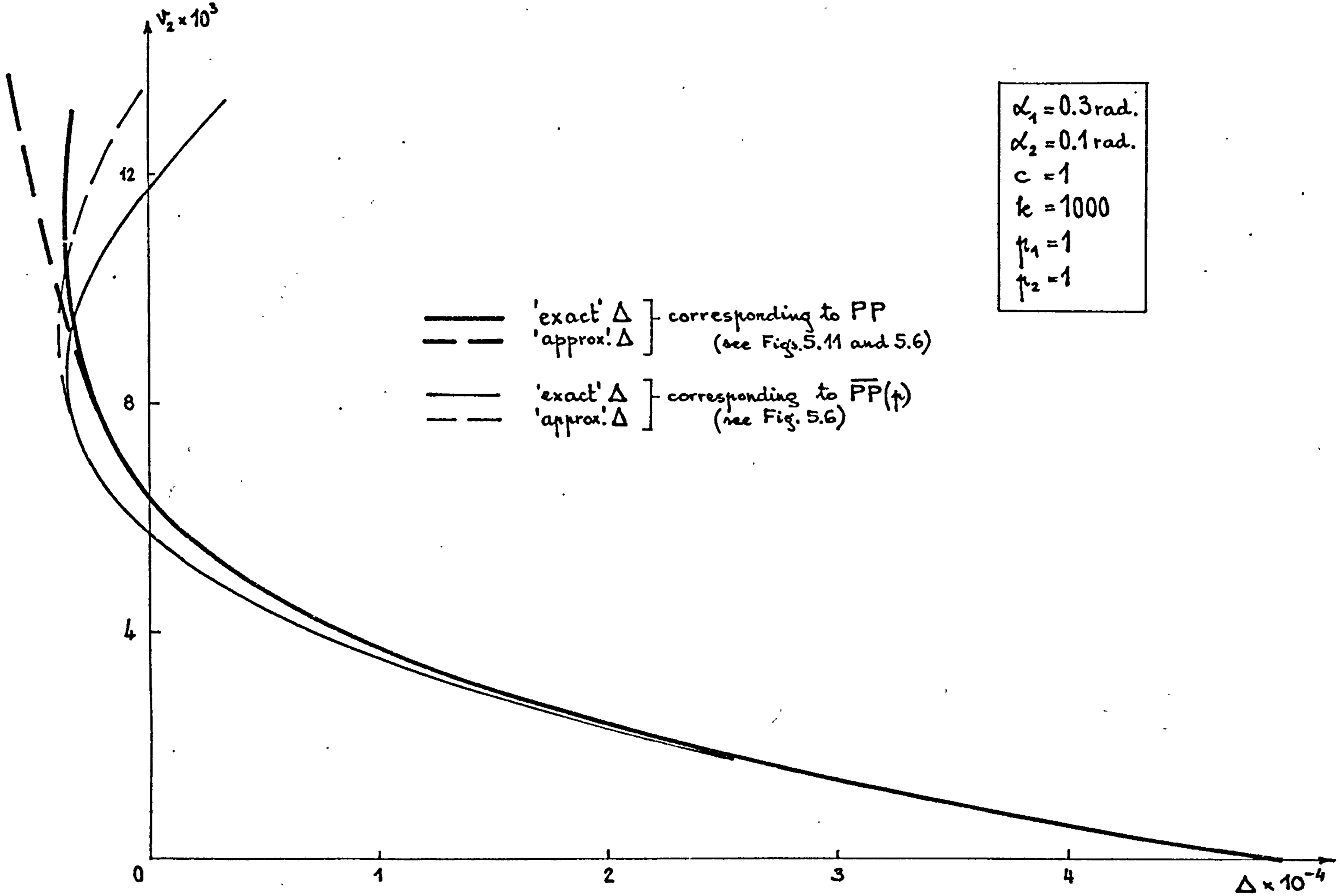
$V_2 \times 10^3$
12
8
4
0
1
2
3
4
$\Delta \times 10^{-4}$
'exact' Δ
'approx.' Δ
corresponding to PP
(see Figs. 5.11 and 5.6)
'exact' Δ
'approx.' Δ
corresponding to $\overline{PP}(f)$
(see Fig. 5.6)
$\alpha_1 = 0.3$ rad.
$\alpha_2 = 0.1$ rad.
$c = 1$
$k = 1000$
$f_1 = 1$
$f_2 = 1$

Fig. 5.14

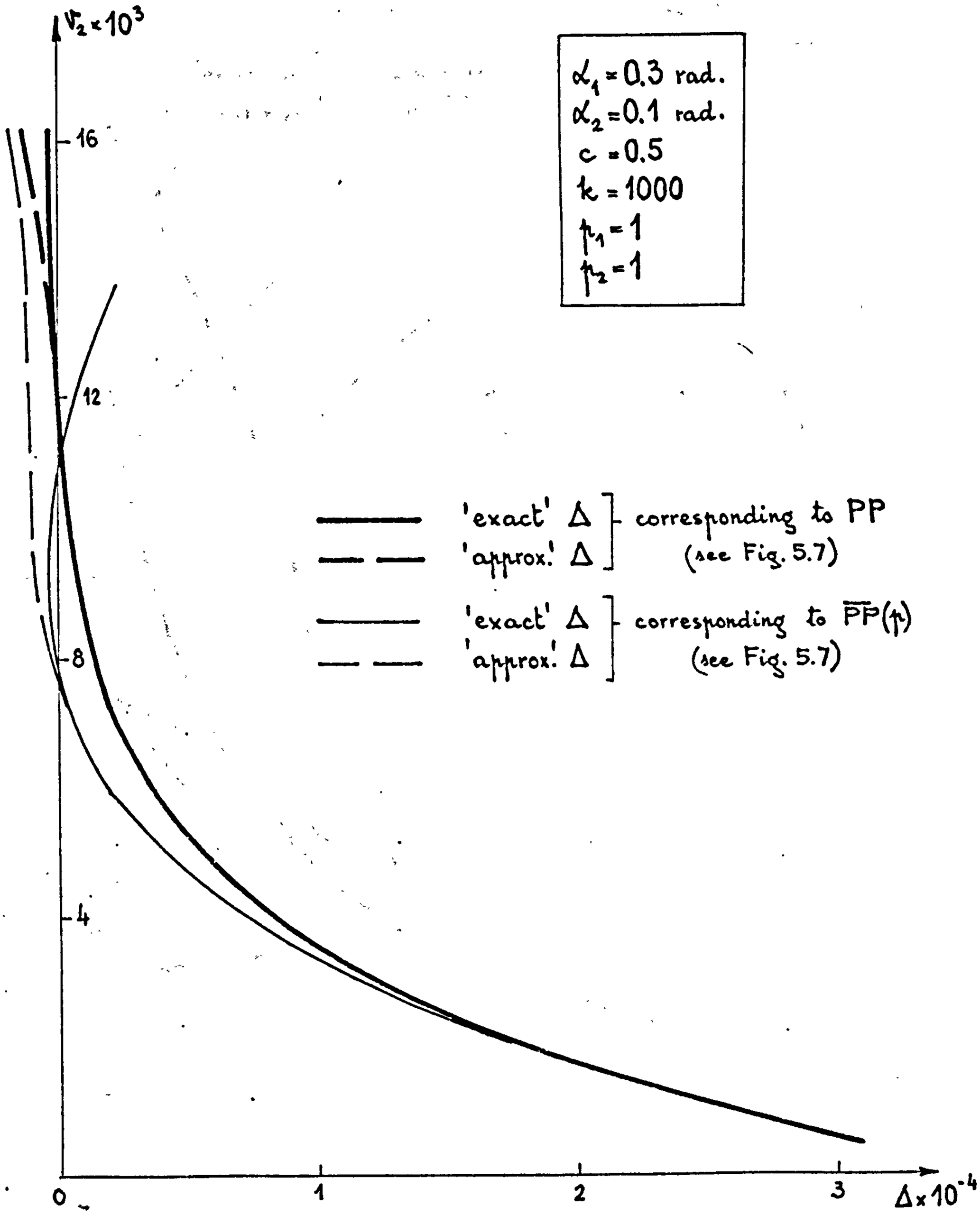
$V_2 \times 10^3$
16
12
8
4
0
1
2
3
$\Delta \times 10^{-4}$
$\alpha_1 = 0.3$ rad.
$\alpha_2 = 0.1$ rad.
$c = 0.5$
$k = 1000$
$\mu_1 = 1$
$\mu_2 = 1$
'exact' Δ] corresponding to PP
'approx.' Δ] (see Fig. 5.7)
'exact' Δ] corresponding to $\overline{PP}(\mu)$
'approx.' Δ] (see Fig. 5.7)

Fig. 5.15

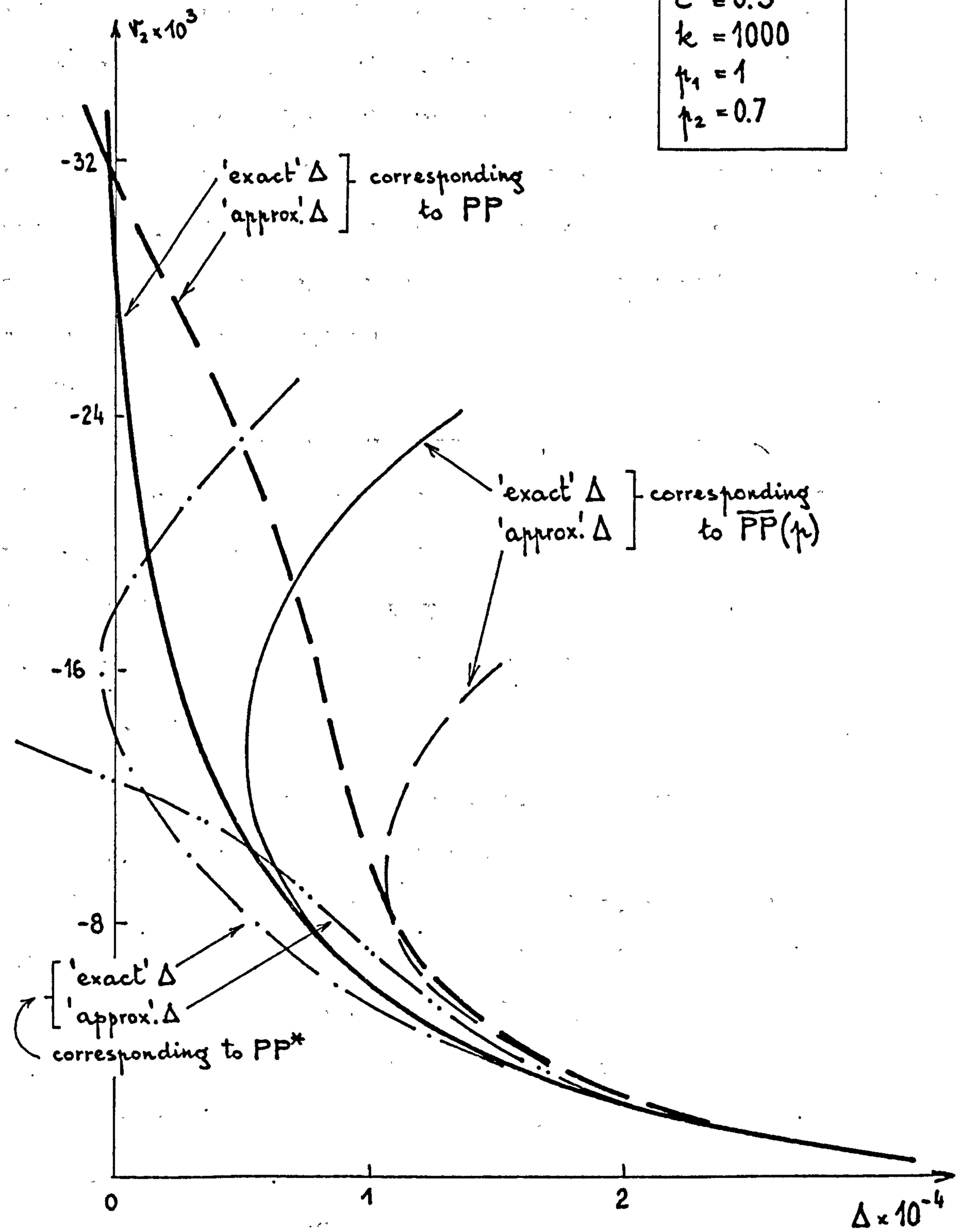
$\alpha_1 = 0.3$ rad.
$\alpha_2 = 0.1$ rad.
$c = 0.5$
$k = 1000$
$\mu_1 = 1$
$\mu_2 = 0.7$
$r_2 \times 10^3$
-32
-24
-16
-8
'exact' Δ
'approx.' Δ
corresponding to PP
'exact' Δ
'approx.' Δ
corresponding to $\overline{PP}(\mu)$
'exact' Δ
'approx.' Δ
corresponding to PP*
0
1
2
$\Delta \times 10^{-4}$

Fig. 5.16

ii) Significantly different results can arise from using the 'approximate' forms as Fig.5.16 depicts. Thus when $\overline{PP}(p)$ is used Δ is always positive and even PP^* yields coordinates of the critical point which are very different to those provided by the 'exact' PP. It must be outlined that the primary paths for the same model are less significantly different than the corresponding Δ-curves are. In other words, the effect of the approximations can yield greater inaccuracies with the stability criterion than with the primary path.

c. Conclusion

The following conclusions arise from above:

i) The stability criterion for the arch-model from Fig.5.2, that is the condition for the equilibrium states corresponding to the primary path to be stable, is given by eq.(5.23). The critical load corresponds to

$$\Delta = 0 \qquad (5.24)$$

ii) Simultaneously with eq.(5.24) other conditions from (5.16a) are also violated.

iii) In order to avoid inaccuracies, which can be very significant, the π_{ij}-coefficients in eq.(5.22) are computed according to eqs.(5.19), where the displacements v_i correspond to the 'exact' primary path PP (i.e. v_i are the accurate solutions of eqs.(5.8)). In view of eqs.(5.17) this is equivalent to saying that Δ represents the Jacobian of the equations (5.8).

The conclusions (i) and (ii) are also valid for the

one and two degree-of-freedom arch-models analysed by Croll and Walker (1972)*) and this suggests that they might be valid for mechanical arch-models with more degrees of freedom.

5.3.5 ELASTIC POSTBUCKLING BEHAVIOUR

So far the primary path depicting the stable prebuckling equilibrium states of the elastic arch-model and the stability criterion (5.23) supplying the coordinates of the critical point have been analysed.

The secondary path emerging from this critical point and depicting the stable equilibrium states of the elastic postcritical behaviour is investigated within this section. An 'exact' secondary path is found by using the 'exact' total potential, eq.(5.5), and the minimum of the total potential. Again the Powell's procedure is used to analyse the 'exact' secondary path and hence an 'approximate' secondary path is also necessary as an initial estimate of the 'exact' solution. An approach similar to that from the analysis of the primary path is employed to find this 'approximate' secondary path.

The analysis of the initial postbuckling behaviour will give information on which particular mode of buckling takes place at the critical point and whether a stiffening or unstiffening postcritical response occurs.

Footnote

*) see also Appendix V.3.

It is shown that the modes of buckling can be associated with the violation of criteria (5.16a).

a. 'Exact' Secondary path

For the sake of simplicity a transformed displacement space will be used to analyse the secondary path. Thus for a point $T\{\bar{v}_1, \bar{v}_2, \bar{v}_3, p\}$ one may write (Fig.5.17)

$$\bar{v}_i = v_i + w_i \qquad i = 1,2 \qquad (5.25)$$

where $S\{v_i, p\}$ is the point on the primary path corresponding to the same load p.

Virtually the static displacement w_i from eqs.(5.25) are analogous to the dynamic displacement w_i from Appendix V.3 so that eq.(5.3.2) can be used to express the total potential energy in terms of w_i.

It can be rewritten as

$$\Delta\Pi(w_i, p) = \Pi_0 + \frac{1}{1!}\sum_i \Pi_i w_i + \frac{1}{2!}\sum_i\sum_j \Pi_{ij} w_i w_j + \qquad (5.26)$$

$$\frac{1}{3!}\sum_i\sum_j\sum_k \Pi_{ijk} w_i w_j w_k + \frac{1}{4!}\sum_i\sum_j\sum_k\sum_l \Pi_{ijkl} w_i w_j w_k w_l + \cdots$$

where the notation (5.17) and

$$\Pi_0 = \Delta\Pi\Big|_S$$

$$\Pi_i = \frac{\partial \Delta\Pi}{\partial v_i}\Big|_S \qquad (5.27)$$

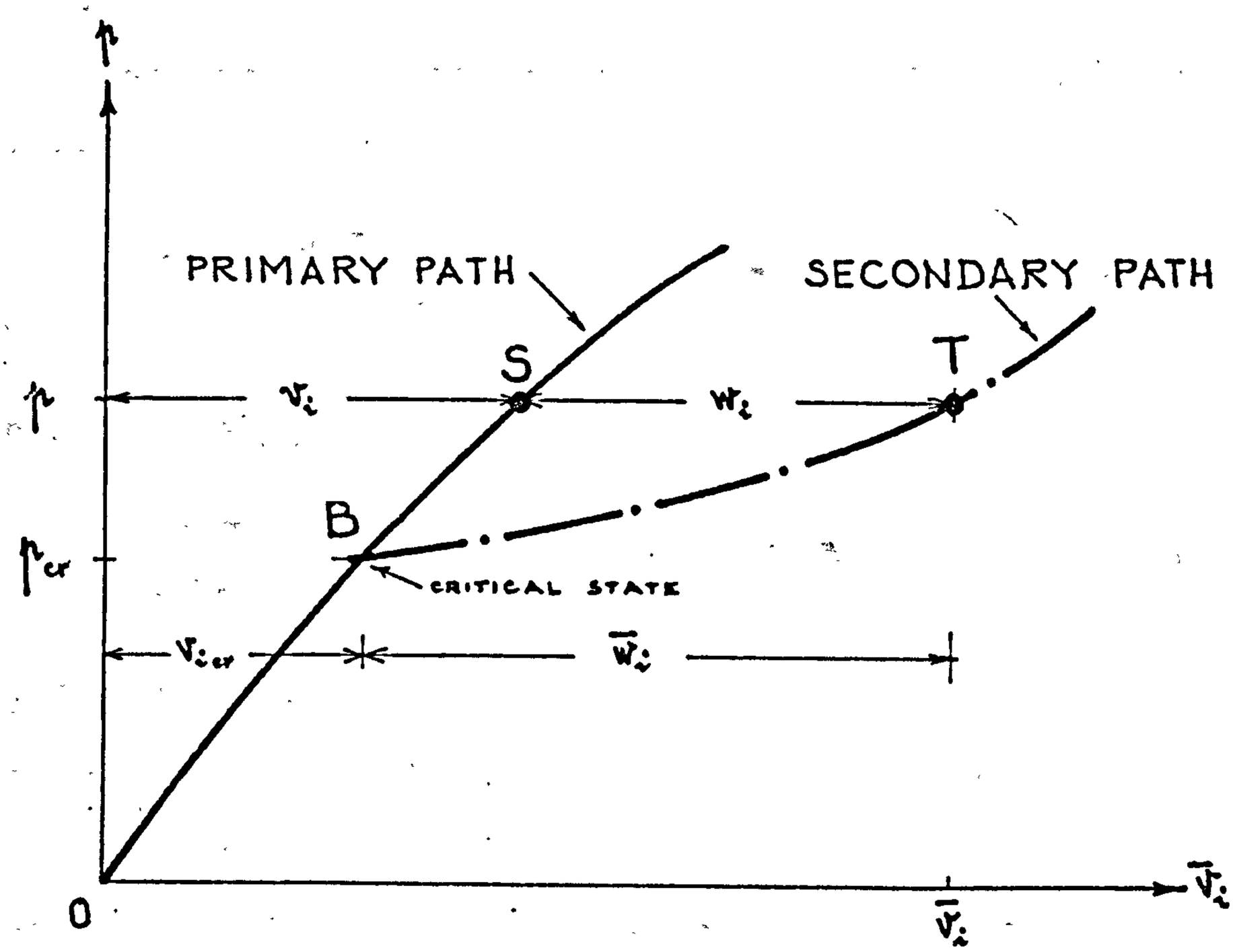

Fig. 5.17

$$\Pi\Pi_{ijk} = \left.\frac{\partial^3 \Delta\Pi}{\partial v_i \partial v_j \partial v_k}\right|_S$$

$$\Pi\Pi_{ijkl} = \left.\frac{\partial^4 \Delta\Pi}{\partial v_i \partial v_j \partial v_k \partial v_l}\right|_S \qquad (5.27)$$

are used.

The stationary conditions for the static equilibrium of the states S and T yield

$$\Pi_i = \left.\frac{\partial \Delta\Pi}{\partial v_i}\right|_S = 0 \qquad i = 1...3 \qquad (5.28)$$

and, respectively,

$$\frac{\partial \Delta\Pi}{\partial w_i} = 0 \qquad i = 1...3 \qquad (5.29)$$

Eqs(5.28) have been already used to find the state S on the primary path. Eqs.(5.29) can be used to find the corresponding state T on the secondary path.

Eqs.(5.29) with due alowance to eqs.(5.28) and to the fact that Π_0 does not depend on w_i yield

$$\sum_j \Pi\Pi_{ij} w_j + \frac{1}{2!} \sum_j \sum_k \Pi\Pi_{ijk} w_j w_k + \cdots = 0 \qquad i,j,k = 1...3 \qquad (5.30)$$

These homogeneous coupled equations have noncritical solution ($w_i \neq 0$) in restricted circumstances only and this means that no secondary path can be found unless

the state S complies with certain additional conditions.

If small displacements w_i are assumed, then eqs.(5.30) can be approximated by

$$\sum_j \Pi_{ij} w_j = 0 \qquad i,j = 1...3 \qquad (5.31)$$

which have non-critical solution if, and only if, eqs.(5.24) is true.

Therefore a secondary path given by eqs.(5.30) emerges from the primary path at the critical point B (Fig.5.17).

Using the 'exact' form of $\Delta\Pi$ given by eq.(5.5) and replacing v_i by $\bar{v}_i$ from eqs.(5.25), the eqs.(5.29) with eqs.(5.8) yield (see Appendix V.6)

$$\sum_i c_i \psi_i^* \frac{\partial \psi_i^*}{\partial w_j} + k u^* \frac{\partial u^*}{\partial w_j} = 0 \qquad i,j = 1...3 \qquad (5.32)$$

which are similar to eqs(5.8) but homogeneous. The angular and linear displacement in eqs.(5.32) (i.e. ψ_i^* and u^*, respectively) characterise the deformed state T in Fig.5.17. They have the same meaning as ψ_i and u but are measured about the equilibrium state S rather than about the undeformed state. Consequently relationships identical to eqs.(5.6) and (5.7) can be used with eqs. (5.32), provided that v_i are replaced by w_i and α_j $(j=1,2)$ are replaced by the angles $\theta_1 = \theta_5$ and $\theta_2 = \theta_4$, respectively, corresponding to the deformed state S (see eqs.(5.6.2) in Appendix V.6).

It should be noted that eqs.(5.32) are only apparently non-dependent on the load p. In fact the deformed state

S depends on p and consequently the angles θ_i in Appendix V.6 carry the indirect effect of the load on the equilibrium state T.

Due to its homogeneous form no solution of eqs.(5.32) can be found for certain values of p. In such cases the state S on the primary path is the solely possible equilibrium position.

The solution of eqs.(5.32), i.e. the 'exact' secondary path, can be found using a similar approach as for the 'exact' primary path, In fact by using the transformed space given by eqs.(5.25), the secondary path is found relative to the primary path in a manner similar to that in which the primary path is found relative to the undeformed state.

Here again an initial estimate of the solution is required and consequently an approximate solution using an approach similar to that from Section 5.3.3b is considered.

b. 'Approximate' Secondary path

An approximate form of eqs.(5.32) arises when eqs. (5.30) are truncated at

$$\sum_i \Pi_{ij} w_i + \frac{1}{2!}\sum_j\sum_k \Pi_{ijk} w_j w_k + \frac{1}{3!}\sum_j\sum_k\sum_\ell \Pi_{ijk\ell} w_j w_k w_\ell = 0 \qquad (5.33)$$

$$i,j,k,\ell = 1,2,3$$

where, analogous to previous developments, only the first three terms have been retained.

The Π-coefficients are given by eqs(5.17) and (5.27) and either the 'exact' form, eq.(5.5), or the approximate

form, eq.(5.9), of the total potential energy can be used. The latter yields

$$\Pi_{ij} = \pi_{ij} + \sum_k \pi_{ijk} \cdot v_{ks} + \frac{1}{2!} \sum_k \sum_\ell \pi_{ijk\ell} \cdot v_{ks} v_{\ell s}$$

$$\Pi_{ijk} = \pi_{ijk} + \sum_\ell \pi_{ijk\ell} \cdot v_{\ell s} \qquad i,j,k,\ell = 1 \ldots 3 \quad (5.34)$$

$$\Pi_{ijk\ell} = \pi_{ijk\ell}$$

where the π-coefficients are given in Table 5.1 and v_{is} are the displacements corresponding to the equilibrium state S on the primary path.

The perturbation technique is used again to linearise the coupled eqs.(5.33). Analogous to the developments from Appendix V.2 the sequence of linear perturbation equations becomes

$$\sum_j \Pi_{ij} \cdot \bar{w}_j' = 0 \qquad (5.35a)$$

$$\sum_j \Pi_{ij} \bar{w}_j'' = -2p' \sum_j \Pi_{ij}' \bar{w}_j' - \sum_j \sum_k \Pi_{ijk} \bar{w}_j' \bar{w}_k' \qquad (5.35b)$$

$$\sum_j \Pi_{ij} \bar{w}_j''' = -3p'^2 \sum_j \Pi_{ij}'' \bar{w}_j' - 3p'' \sum_j \Pi_{ij}' \bar{w}_j' - \qquad (5.35c)$$

$$3p' \sum_j \Pi_{ij}' \bar{w}_j'' - 3 \sum_j \sum_k \Pi_{ijk} \bar{w}_j'' \bar{w}_k' -$$

$$3p' \sum_j \sum_k \Pi_{ijk}' \bar{w}_j' \bar{w}_k' - \sum_j \sum_k \sum_\ell \Pi_{ijk\ell} \bar{w}_j' \bar{w}_k' \bar{w}_\ell'$$

$$i, j, k, \ell = 1,2,3$$

where Π are given by eqs.(5.34), Π' and Π'' are the first and second order derivatives of Π with respect to p and

$$\bar{w}_i = \bar{w}_i' \cdot \varepsilon + \frac{1}{2!} \bar{w}_i'' \cdot \varepsilon^2 + \frac{1}{3!} \bar{w}_i''' \cdot \varepsilon^3 \qquad , i = 1 \ldots 3 \tag{5.36}$$

$$p = p_{cr} + p' \cdot \varepsilon + \frac{1}{2!} p'' \cdot \varepsilon^2$$

In eqs.(5.35) and (5.36) the suffices of p and $\bar{w}_i$ denote their first, second,...derivatives with respect to the perturbation parameter ε, where ε is measured from the critical point B in Fig.5.17.

The first perturbation equations (5.35) are identical with eqs.(5.3) and, as already stated, a non-trival solution of $\bar{w}_i'$ (i=1..3) can be formed if, and only if, eq.(5.24) is fulfilled, that is if the Π-coefficients are computed for the critical state B.

Solving sequentially the sets of linear equations (5.35) and using eqs.(5.36), the approximate displacements of the state T on the secondary path arise as (see Fig.5.17)

$$\bar{v}_i = v_{icr} + \bar{w}_i \qquad i = 1,2,3 \tag{5.37}$$

where p is given by the second of eqs.(5.36).

Eqs.(5.37) provide the initial estimate of the solution of eqs.(5.32).

When using the perturbation technique with the

secondary path it is advisable to choose one of the displacements $\bar{w}_i$ as perturbation parameter since it is difficult to predict whether a stiffening ($p > p_{cr}$) or an unstiffening ($p < p_{cr}$) postcritical behaviour occurs (see Fig.5.20).

c.Discussion

Two approximate secondary paths can be obtained depending on how the sequence of eqs.(5.35) is solved. For either case $\bar{w}_1$ is supposed to be the perturbation parameter so that

$$\bar{w}_1' = 1 \qquad \bar{w}_1'' = \bar{w}_1''' = \dots = 0 \tag{5.38}$$

i) A secondary path can arise from the following sequence of solving the eqs.(5.35a...c):

- $\bar{w}_i'$ (i=2,3) come from eqs.(5.35a)

- if each equation $\underline{i}$ of the set (5.35b) is multiplied by $\bar{w}_i'$ and the results added, the left-hand side of the summation will be zero, on account of eqs.(5.35a), and therefore p' is given by

$$2p' \sum_i \sum_j \Pi_{ij}' \bar{w}_i' \bar{w}_j' = -\sum_i \sum_j \sum_k \Pi_{ijk} \bar{w}_i' \bar{w}_j' \bar{w}_k' \tag{5.39}$$

where $\bar{w}_i'$ are known from the previous step.

- $\bar{w}_i''$ (i=2,3) can be obtained from the first two of eqs.(5.35b) with due allowance to eqs.(5.37) and (5.38).

- similarly to p' in eq.(5.39), p'' follows from eqs.(5.35c) as

$$3\mu''\sum_i\sum_j \Pi'_{ij}\bar{w}_i'\bar{w}_j' = -3\mu'^2\sum_i\sum_j \Pi''_{ij}\bar{w}_i'\bar{w}_j' -$$

$$3\mu'\sum_i\sum_j \Pi'_{ij}\bar{w}_i'\bar{w}_j'' - 3\sum_i\sum_j\sum_k \Pi_{ijk}\bar{w}_i'\bar{w}_j'\bar{w}_k' - \qquad (5.40)$$

$$3\mu'\sum_i\sum_j\sum_k \Pi'_{ijk}\bar{w}_i'\bar{w}_j'\bar{w}_k' - \sum_i\sum_j\sum_k\sum_l \Pi_{ijkl}\bar{w}_i'\bar{w}_j'\bar{w}_k'\bar{w}_l'$$

$$i,j,k,l = 1\ldots3$$

$-\bar{w}_i'''$ (i=2,3) can be then obtained from the first two of eqs.(5.35c)

ii) Another secondary path can follow if one assumes that

$$\frac{\bar{w}_i'}{\bar{w}_1'} = \frac{\bar{w}_i''}{\bar{w}_1''} = \frac{\bar{w}_i'''}{\bar{w}_1'''} = \ldots \qquad j=1,2,3 \qquad (5.41)$$

in eqs.(5.35a...c). Eqs.(5.41) are always true (on account that the same coefficient matrix $\{\Pi_{ij}\}$ occurs in each set of perturbation equations) if the right-hand sides of eqs. (5.35band c) are zero, that is if

$$2\mu'\sum_j \Pi'_{ij}\bar{w}_j' = -\sum_j\sum_k \Pi_{ijk}\bar{w}_j'\bar{w}_k' \qquad (5.42a)$$

$$3\mu''\sum_j \Pi'_{ij}\bar{w}_j' = -3\mu'^2\sum_j \Pi''_{ij}\bar{w}_j' - \qquad (5.42b)$$

$$3\mu'\sum_j \Pi'_{ij}\bar{w}_j'' - 3\sum_j\sum_k \Pi_{ijk}\bar{w}_j''\bar{w}_k' -$$

$$3\mu'\sum_j\sum_k \Pi'_{ijk}\bar{w}_j'\bar{w}_k' - \sum_j\sum_k\sum_l \Pi_{ijkl}\bar{w}_j'\bar{w}_k'\bar{w}_l'$$

where $i,j,k,l = 1\ldots3$

Different values of p' and p" can arise from using different i in eqs.(5.42) due to the approximations introduced with eqs. (5.35). If so eqs.(5.39) and (5.40) can be used instead of eqs.(5.42a and b).

According to eqs.(5.36), eqs.(5.41) yield

$$\bar{w}_i = \bar{w}_i' \cdot \left(\varepsilon + \frac{\varepsilon^2}{2!} + \frac{\varepsilon^3}{3!} + \cdots\right) \quad , i = 1 \ldots 3 \qquad (5.43)$$

and this means that the secondary path (ii) is affine to the solution of the first perturbation eqs.(5.35a) throughout its length.

The secondary paths (i) and (ii) are coincident in the initial postbuckling range since, when ε is small, eqs.(5.36) yield

$$\bar{w}_i = \bar{w}_i' \cdot \varepsilon$$
$$p = p_{cr} + p' \cdot \varepsilon \qquad (5.36a)$$

amd since $\bar{w}_i'$ and p' are the same for both these secondary paths.

The above conclusions are true also for the 'exact' secondary paths. For instance, in Figs.5.18 and 5.19 the 'exact' secondary paths for two numerical applications are depicted. The same numerical data as in Figs.5.6 and 5.7 are analysed. In both cases the modes of buckling are antisymmetric, that is the initial post-buckling range

$$w_1 = -w_3 \quad \text{and} \quad w_2 = 0 \qquad (5.44)$$

For the sake of simplicity the secondary path is plotted

in the $p-\bar{v}_2-\theta_3$ system of coordinates where

$$\theta_3 = \frac{\bar{v}_1 - \bar{v}_3}{2} = \frac{w_1 - w_3}{2} \tag{5.45}$$

and $\bar{v}_i$ $(i=1..3)$ are given by eqs.(5.25) and represented in Fig.5.17. On account of the symmetry, the primary path will be represented in this system of coordinates by its projection on the $p-v_2$ plane from Figs.5.6 and 5.7.

Two 'exact' secondary paths have been computed for either case:

i) One is computed by finding the w_2, w_3 and p values corresponding to a certain w_1 from the full set of eqs. (5.32). This secondary path is plotted by broken lines in Figs.(5.18) and (5.19). It corresponds to the above 'approximate' path (i)

ii) Another secondary path is computed assuming that $w_1=w_3$ throughout the postbuckling behaviour. Due to this assumption the w_2 and p values corresponding to a certain w_1 (see Fig.5.17) have been found by solving exactly the first two equilibrium equations (5.32). This secondary path is plotted by unbroken lines in Figs. (5.18) and (5.19). This path corresponds to the above 'approximate' path (ii).

Both secondary paths are symmetric about the $p-O-\bar{v}_2$ plane and coincide for small displacements w_i.

It can be seen in Figs.5.18 and 5.19 that the secondary path can correspond to an increase of the load

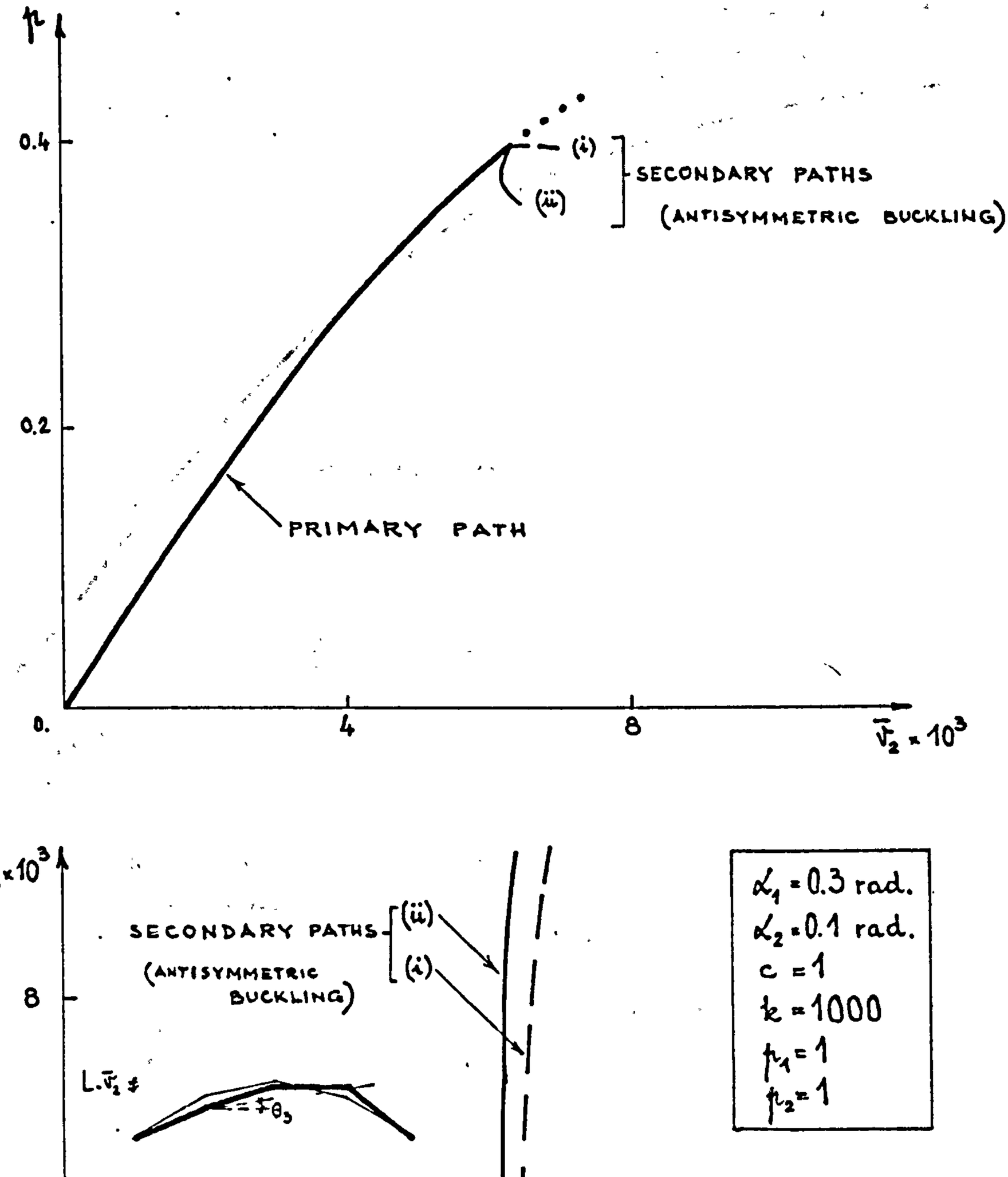
μ
0.4
0.2
0.
4
8
$\bar{V}_2 \times 10^3$
(i)
(ii)
SECONDARY PATHS
(ANTISYMMETRIC BUCKLING)
PRIMARY PATH
$\theta_3 \times 10^3$
SECONDARY PATHS
(ANTISYMMETRIC BUCKLING)
(ii)
(i)
$L.\bar{V}_2 \neq$
$= \mp\theta_3$
PRIMARY PATH
$\alpha_1 = 0.3$ rad.
$\alpha_2 = 0.1$ rad.
$c = 1$
$k = 1000$
$\mu_1 = 1$
$\mu_2 = 1$

Fig. 5.18

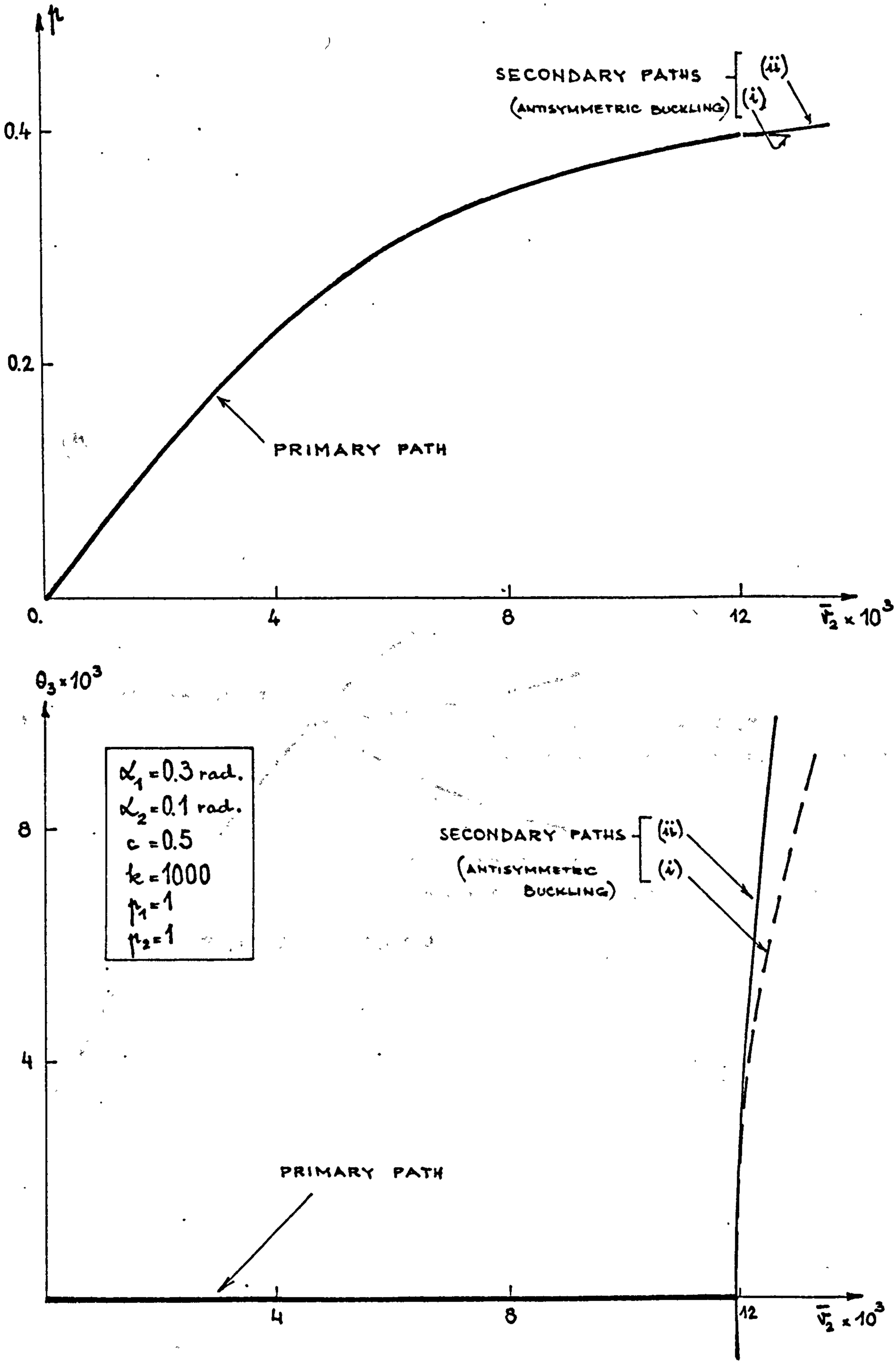
$\bar{r}_1$
0.4
0.2
SECONDARY PATHS
(ANTISYMMETRIC BUCKLING)
(iii)
(i)
PRIMARY PATH
0.
4
8
12
$\bar{r}_2 \times 10^3$
$\theta_3 \times 10^3$
$\alpha_1 = 0.3$ rad.
$\alpha_2 = 0.1$ rad.
$c = 0.5$
$k = 1000$
$\bar{r}_1 = 1$
$\bar{r}_2 = 1$
8
4
SECONDARY PATHS
(ANTISYMMETEC BUCKLING)
(ii)
(i)
PRIMARY PATH
4
8
12
$\bar{r}_2 \times 10^3$

Fig. 5.19

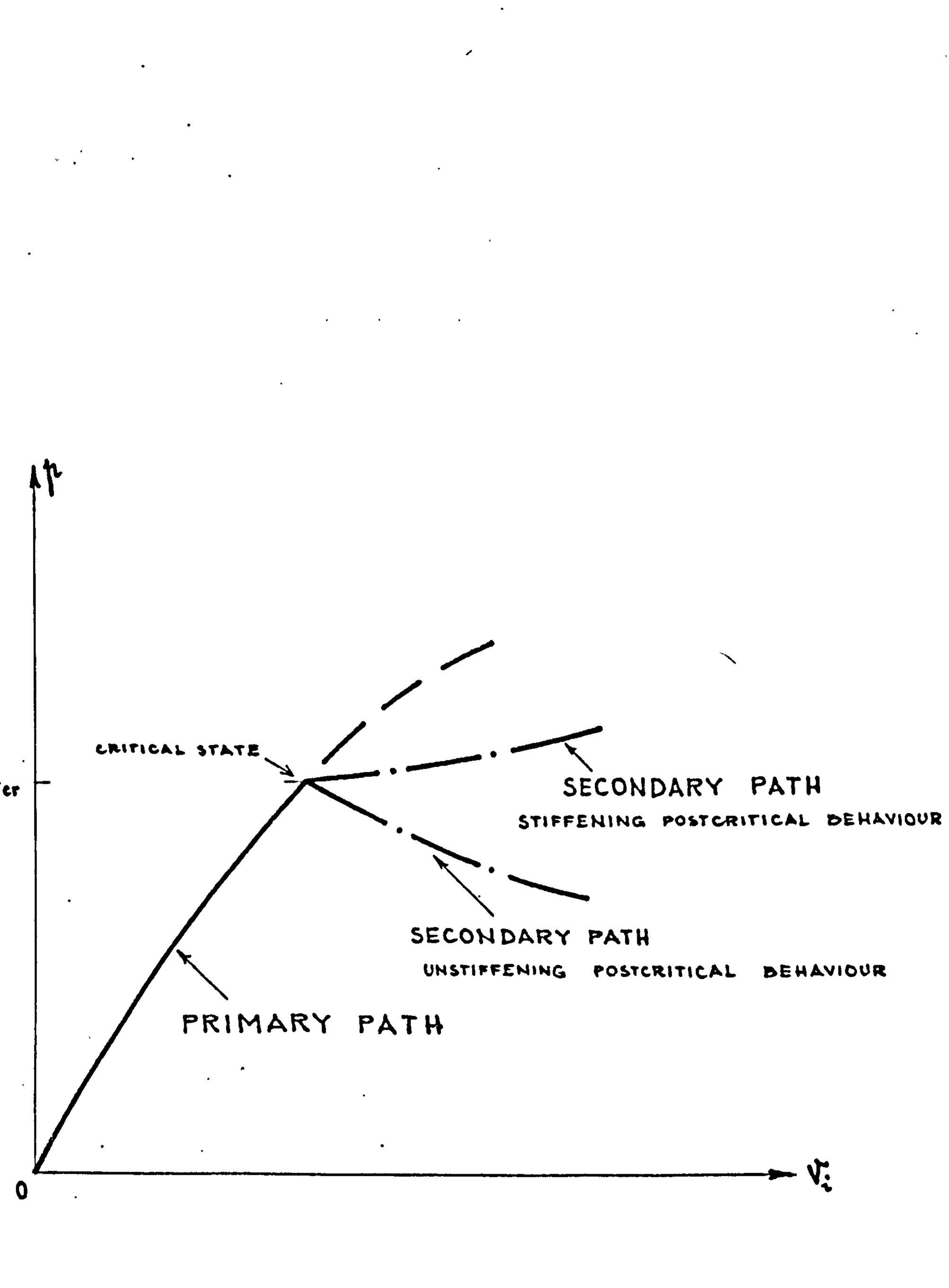
p
p_{cr}
CRITICAL STATE
SECONDARY PATH
STIFFENING POSTCRITICAL BEHAVIOUR
SECONDARY PATH
UNSTIFFENING POSTCRITICAL BEHAVIOUR
PRIMARY PATH
0
V_i

Fig. 5.20

p (see curve (ii) in Fig.5.19) or to a decrease of the p (see curve (ii) in Fig.5.18). The first situation corresponds to a stiffening postcritical behaviour (i.e. the load p must be increased in order to increase the postcritical deformation), whereas the latter corresponds to an unstiffening postcritical behaviour (i.e. the post-critical deformation increases as the load p decreases). These situations are depicted also in Fig.5.20.

Both models from Figs.5.18 and 5.19 display a bifurcation of equilibrium beyond the critical point and the corresponding deformed configuration (mode of buckling) is antisymmetric relative to the critical state (see eqs. (5.44)).

Different modes of buckling associated with either a stiffening effect or an unstiffening effect can be displayed by the arch-model from Fig.5.2 and this depends on the geometric, mechanical and loading characteristics of the structure.

In the next two sections these possible modes of buckling and some features of the initial postbuckling path are analysed in a general form.

d. Modes of buckling

The mode of buckling characterises geometrically the postcritical deformed state relative to the critical state. Different modes of buckling (i.e. snap-buckling, antisymmetric or symmetric bifurction) can be associated with the arch-model from Fig.5.2 and they are featured in Table 5.2.

It has been shown in Section 5.3.4a that, simultaneously with the stability criterion (5.23), one or a group of the first two criteria (5.16a) are also violated. In this section it is shown that a certain mode of buckling is associated to each such possible violation of the criteria (5.16a).

This association is proved below by analysing the first perturbation eqs.(5.35a), but the result is valid for small $\bar{w}_i$ too on account of eqs.(5.43) or (5.36a).

The use of the approximate eqs.(5.35) has been preferred here for the sake of simplicity. Nevertheless the same conclusions could be proved to be generally valid for small displacements $\bar{w}_i$ (initial postbuckling behaviour) by means of the dynamic criterion of stability.

When eq.(5.24) is fulfilled a secondary path emerges from the critical point and the approximate equations (5.35) can be used to find it.

Two distinct solutions can arise from the first perturbation equations (5.35a):

(i) $\underline{\bar{w}_1 = -\bar{w}_3 \neq 0 \quad \text{and} \quad \bar{w}_2 = 0}$ when

$$\Pi_{11} - \Pi_{13} = 0 \tag{5.46}$$

which yields, in terms of the criteria (5.16a),

$$\boxed{\begin{aligned} M_{22} &= 0 \\ M_{11} + M_{13} &= 0 \end{aligned}} \tag{5.47}$$

(ii) $\underline{\bar{w}_1 = \bar{w}_3 \neq 0 \quad \text{and} \quad \bar{w}_2 \neq 0}$ with the relationship

$$\bar{w}_2 = -\bar{w}_1 \cdot \frac{\varpi_{11} + \varpi_{13}}{\varpi_{12}} = -\bar{w}_1 \cdot \frac{2\varpi_{12}}{\varpi_{22}} \qquad (5.48)$$

when

$$\boxed{M_{11} - M_{13} = 0} \qquad (5.49)$$

Other solutions can arise either as particular cases of the previous distinct solution or as linear combination of them.

For instance:

iii) $\underline{\bar{w}_1 = \bar{w}_3 = 0}$ and $\underline{\bar{w}_2 \neq 0}$ arises from solution (ii) when simultaneously

$$\varpi_{12} = 0$$

$$\varpi_{22} = 0 \qquad (5.50)$$

which, in terms of the stability criteria (5.16a), yield

$$\boxed{\begin{array}{l} \varpi_{22} = 0 \\ M_{11} = 0 \end{array}} \qquad (5.51)$$

iv) $\underline{\bar{w}_1 = \bar{w}_3 \neq 0}$ and $\underline{\bar{w}_2 = 0}$ arises from solution (ii) when simultaneously

$$\varpi_{11} + \varpi_{13} = 0$$

$$\varpi_{12} = 0 \qquad (5.52)$$

which can be recast as

$$\boxed{\begin{array}{l} M_{11} - M_{13} = 0 \\ M_{22} = 0 \end{array}} \qquad (5.53)$$

v) $\underline{\bar{w}_1 = \bar{w}_3 \neq 0}$ and $\underline{\bar{w}_2 \neq 0}$ with both $\bar{w}_1$ and $\bar{w}_2$ indefinite arises either by combining solutions (iii) + (iv) or from solution (ii) when simultaneously

$$\pi_{11} + \pi_{13} = 0$$

$$\pi_{12} = 0 \qquad (5.54)$$

$$\pi_{22} = 0$$

The above solution (i) corresponds to an antisymmetric mode of buckling and coincides with eqs.(5.44). This mode of buckling takes place when eq.(5.46) is fulfilled simultaneously with eq.(5.24) which provides the critical point. Thus, on account of eq.(5.22), it follows that the condition (5.46) - or the equivalent eqs.(5.47) - is mathematically responsible for the violation of the stability criterion (5.23).

Similarly, solution (ii) corresponds to a symmetric mode of buckling, and the associated condition (5.49) is mathematically responsible for the violation of stability criterion (5.23) on account of eq.(5.22).

The criteria for snap-buckling to occur at joint B_2 and/or at joints B_1 and B_3 are derived in Appendix V.7. It is apparent that they are particular cases of solution (ii). Indeed the snap-buckling at joint B_2 is given by solution (iii), while the snap-buckling at joints B_1 and B_3 and the simultaneous snap-buckling at joints B_1, B_2, B_3 are given by solutions (iv) and (v), respectively, with $\pi_{11} = 0$.

It is noteworthy that the snap-buckling conditions yield $\Delta = 0$ too, which suggests that a secondary path emerges at the critical point. In fact this secondary path represents the dynamic snap which is always associated

with the snap-buckling (see Fig.5.10). This is proved in Appendix V.8.

From the above analysis the following conclusions concerning the modes of buckling can be drawn:

- The critical load of an arch-model as in Fig.5.2 is the lowest load for which the stability criterion (5.23) is isolated or, in other words, the lowest solution of eq.(5.24).

- Some other conditions from the criteria (5.16) are isolated simultaneously with $\Delta = 0$.

From the mathematical point of view these violated conditions are responsible for Δ being zero.

From the physical point of view each possible violation of stability criteria is associated with a certain mode of buckling. The modes of buckling that can occur with the arch-model from Fig.5.2 are presented in Table 5.2.

- Coupled modes of buckling occur (i.e. two or more critical points are coincident or nearly so) when at least two of the solutions (i)...(iv) are simultaneously possible.

For instance the snap-buckling at joints B_1 and B_3 (solution (iv) with $\pi_{11} = 0$), is always coupled with an antisymmetric mode of buckling, that is with the above solution (i).

- Information concerning the mode of buckling is provided by analysing solely the π_{ij}-coefficients associated with the primary path. However the need to

Table 5.2

solution	Buckling mode		Violated stability criteria, eqs.(5.16a)
(i)	$\bar{w}_1=-\bar{w}_3\neq 0$ and $\bar{w}_2=0$ 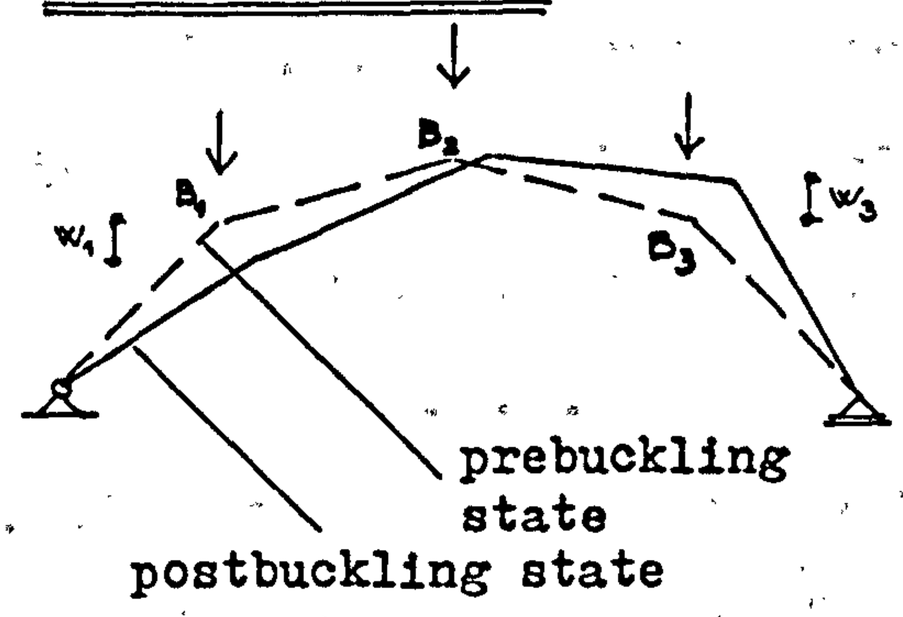	Antisymmetric buckling	$M_{22}=0$ $M_{11}+M_{13}=0$ $\Delta=0$
(ii)	$\bar{w}_1=\bar{w}_3\neq 0$ and $\bar{w}_2=-\bar{w}_1\frac{2\varpi_{12}}{\varpi_{22}}$ 	Symmetric buckling	$M_{11}-M_{13}=0$ $\Delta=0$
(iii)	$\bar{w}_1=\bar{w}_3=0$ and $\bar{w}_2\neq 0$ 	Snap-buckling at joint B_2	$\varpi_{22}=0$ $M_{11}=0$ $\Delta=0$
(iv)	$\bar{w}_1=\bar{w}_3\neq 0$ and $\bar{w}_2=0$ 	Symmetric buckling with $w_2=0$	$M_{22}=0$ $M_{11}-M_{13}=0$ $\Delta=0$
		Snap-buckling at joints B_1 and B_3	$\varpi_{11}=0$ $M_{11}=0$ $M_{22}=0$ $\Delta=0$

obtain further information about the postcritical behaviour leads to the complete analysis of the secondary path.

In the light of the above conclusions, the modes of buckling of the arch-models from Figs.5.6, 5.8 and 5.9 can be specified by analysing the variation of the criteria (5.16a) in the Figs.5.11...5.13, respectively.

Thus in Fig.5.11 it can be seen that the criterion $M_{22} > 0$ is violated simultaneously with eq.(5.23) and hence an antisymmetric mode of buckling occurs for the arch-model from Fig.5.6.

Fig.5.12 shows that a mode of buckling according to the above solution (iv) with $\Pi_{11}=0$ occurs for the arch-model from Fig.5.8. This mode of buckling is a coupling of an antisymmetric one and a snap-buckling at the joints B_1 and B_3.

According to Fig.5.13 another coupled mode of buckling, given by the above solution (v) and coupling a symmetric mode of buckling and a snap-buckling at joint B_2 arises for the arch-model from Fig.5.9.

e. Initial post-buckling behaviour

The mode of buckling provides some information about the geometry of the initial secondary path. Indeed the displacements $\bar{w}_i$ represent coordinates of the initial secondary path about the critical point.

Other two features of the initial secondary path, independent on the mode of buckling, are derived in this section. Alsc aspects associated with the stiffness

characteristics of the secondary path are discussed. Both the characteristics of the secondary path presented in this section and the modes of buckling from the previous section provide a better understanding of the elastic postbuckling response of the arch-model from Fig.5.2.

1. Two remarkable features of any secondary path associated with the present arch-model arise as a consequence of the eqs.(5.36a):

i) In the vecinity of the critical point the secondary path can be approximated by a straight line.

ii) This straight line is included in a plane which has the normal parallel to p - axis.

The first feature is an immediate consequence of eqs. (5.36a) which are actually the parametric equations of the secondary path when small displacements $\bar{w}_i$ are considered. Further details about these parametric equations are provided by the above analysis of the modes of buckling since the solutions found in Section 5.3.4d represent in fact the direction cosines of the straight line (i.e. the initial secondary path) at the critical point.

The second feature is again a consequence of the affinity of $\bar{w}_i$ given by eqs.(5.36a) and valid for small $\bar{w}_i$. Indeed for small ε it follows from eq.(5.36a) that

$$\bar{w}_i' = \frac{\bar{w}_i}{\varepsilon} \qquad , i = 1...3 \tag{5.55}$$

and hence eq.(5.39) yields

$$2p'\varepsilon = \frac{\sum_i \sum_j \sum_k \Pi_{ijk} \bar{w}_i \bar{w}_j \bar{w}_k}{\sum_i \sum_j \Pi'_{ij} \bar{w}_i \bar{w}_j} \simeq 0 \tag{5.56}$$

because π_{ijk} and π'_{ij} are always finite on account of their physical meaning.

Similarly from eqs.(5.40) and with due allowance to eq.(5.56) it follows that*)

$$3p'' \varepsilon^2 \simeq 0 \qquad (5.57)$$

so that the second of eqs.(5.36) yields

$$p \simeq p_{cr} \qquad (5.58)$$

Eq.(5.58) has already been mentioned in conjunction with the snap-buckling (see Appendix V.7).

2. As mentioned in Section 5.3.5c, it is of greatest interest to find out whether the structure displays a stiffening postbuckling behaviour or an unstiffening one. In terms of the secondary path that means whether the load p is to be increased or decreased, respectively, in order to advance along the secondary path (see Fig.5.20).

The above feature (ii) of the initial secondary path shows that the immediate postbuckling behaviour (i.e. the first small displacements about the critical state) does not require a variation of load p.

The dependence on p of the initial postbuckling behaviour can be visualised by studying the variation of the elastic forces from the devices B_i $(i = 1..3)$ and A in

---

Footnote

*) A development of eq.(5.57) for an antisymmetric mode of buckling is shown in Appendix V.9.

Fig.5.2 as the secondary path is travelled along. Thus when these forces are increased by the initial post-buckling behaviour that means that a stiffening effect occurs or, in other words, an increase of the load beyond p_{cr} is necessary. Contrarily an unstiffening postcritical behaviour occurs when the elastic forces decrease while the secondary path is travelled along. The variations of the elastic forces about their values corresponding to the critical state are proportional to the postbuckling variations of the corresponding displacements which can be computed as in Appendix V.6.

For an antisymmetric mode of buckling, for instance, with

$$\bar{w}_1 = -\bar{w}_3 \qquad \text{and} \quad \bar{w}_2 = 0 \tag{5.59}$$

eqs.(5.6.2) with eqs.(5.6.1) yield

$$\psi_1^* = -\frac{\bar{w}_1}{4}\cdot(4+\sin^2\theta_1+\sin^2\theta_2)+\frac{\bar{w}_1^2}{2}(\sin\theta_1-\sin\theta_2)$$

$$\psi_2^* = \bar{w}_1^2\sin\theta_2 \tag{5.60}$$

$$\psi_3^* = \frac{\bar{w}_1}{4}\cdot(4+\sin^2\theta_1+\sin^2\theta_2)+\frac{\bar{w}_1^2}{2}\cdot(\sin\theta_1-\sin\theta_2)$$

and

$$u^* = -\frac{\bar{w}_1^2}{2}\cdot(4+3\sin^2\theta_1+3\sin^2\theta_2) \tag{5.61}$$

where eqs.(5.10) have been used and terms in $\bar{w}_1^m$ with

$m > 2$ has been neglected. ψ_i^* $(i = 1..3)$ in eqs.(5.60) and u^* in eq.(5.61) denote the displacements ψ_i and u about the critical state of the arch-model while θ_1 and θ_2 characterise the geometry of the symmetric critical state (see Fig.5.4).

For small displacements $\bar{w}_1$ the terms in $\bar{w}_1^2$ can also be neglected so that it follows from eqs.(5.60) and (5.61) that

$$\psi_1^* = -\psi_3^* = -\frac{\bar{w}_1}{4}\cdot(4 + \sin^2\theta_1 + \sin^2\theta_2)$$

$$\psi_2^* = 0. \qquad (5.62)$$

and $$u^* = 0. \qquad (5.63)$$

Thus, for any small $\bar{w}_1$, the variations of M_1 and M_3 are mutually compensated (on account of symmetry) while the variations of F and M_2 are zero ; therefore no variation of p is required by the initial postbuckling response.

When $\bar{w}_i$ are no longer small a variation of the load p will be required to advance along the secondary path but whether an increase or a decrease of load will be necessary depends on the values ψ_i^* and u^* given by eqs.(5.60) and (5.61) and on the relative stiffnesses c_i and k from eqs.(5.4).

The above conclusion is also outlined by the numerical applications from Figs.5.18 and 5.19 for which an antisymmetric mode of buckling is recorded.

While the secondary paths (i) in both Fig.5.18 and

Fig.5.19 do not require any change in load p (i.e. they lie initially in a plane normal to p-axis), the secondary path (ii) models either an unstiffening postcritical behaviour, see Fig.5.18, or a stiffening one see Fig.5.19.

On account of the large value of k, u^* is the relavant displacement in either of the cases from Fig.5.18 and 5.19 so that the stiffening or unstiffening of the postcritical behaviour will depend crucially on the variation of elastic force F in device A from Fig.5.2. This variation ΔF along either of secondary paths (i) and (ii) and for either of models from Figs.5.18 and 5.19 is plotted in Fig.5.22 where u^* and ΔF have the meanings from Fig.5.21. The curves plotted in Fig.5.22 have the same graphic representation as the secondary paths from Figs.5.18 and 5.19, i.e. the broken and unbroken lines are associated with the secondary paths (i) and (ii), respectively.

From Fig.5.22 it follows that:

- ΔF associated with the secondary paths (i) in both Figs.5.18 and 5.19 are almost zero so that no variation of p is required when the initial postbuckling deformation is increased.

- ΔF associated with the secondary path (ii) in Fig.5.18 is increasingly negative which means that an amount of energy is released by the device A as the postbuckling deformation increases. A decrease of the external load p corresponds to this release of energy and therefore an unstiffening secondary path (ii) is displayed by the model from Fig.5.18.

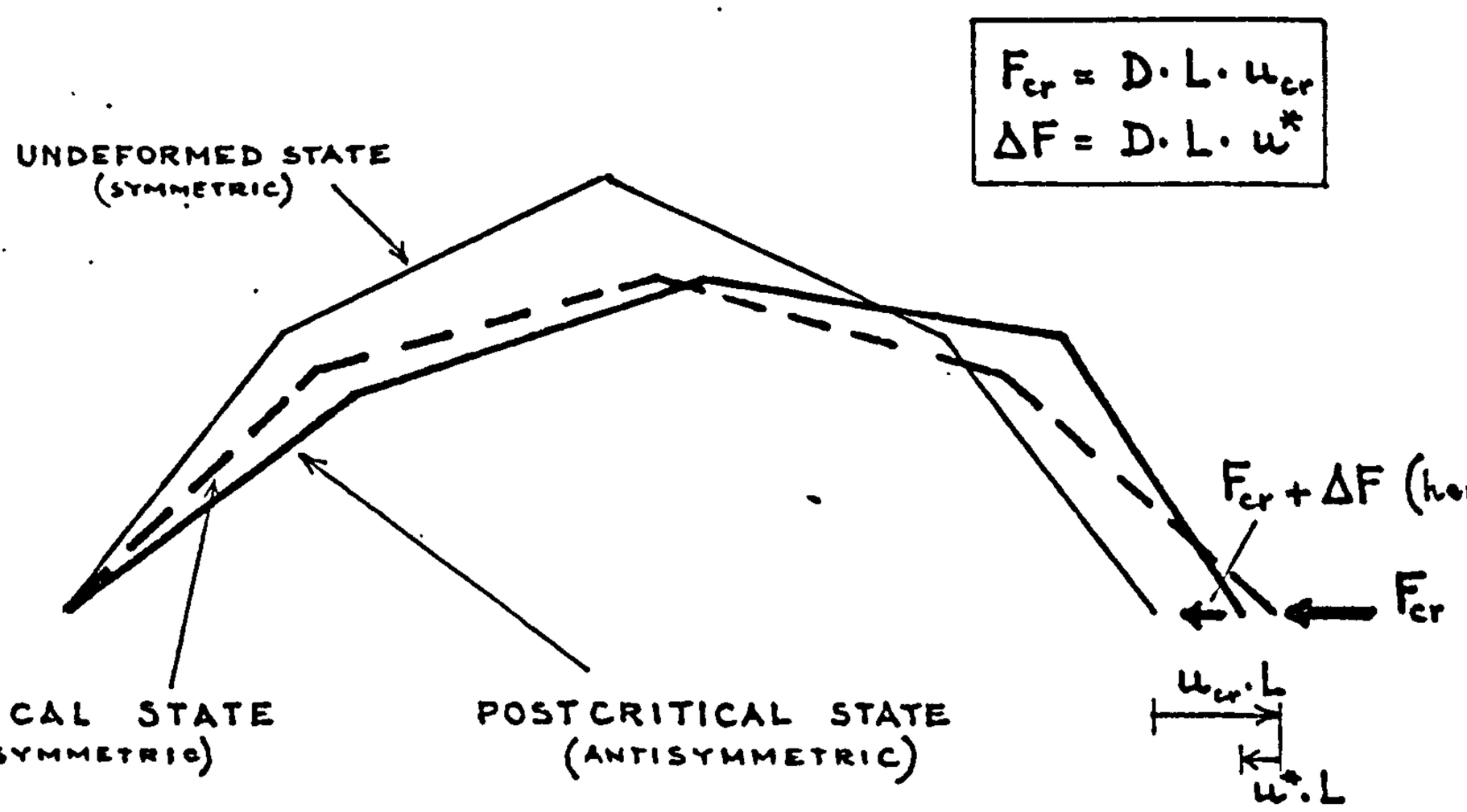

Fig. 5.21

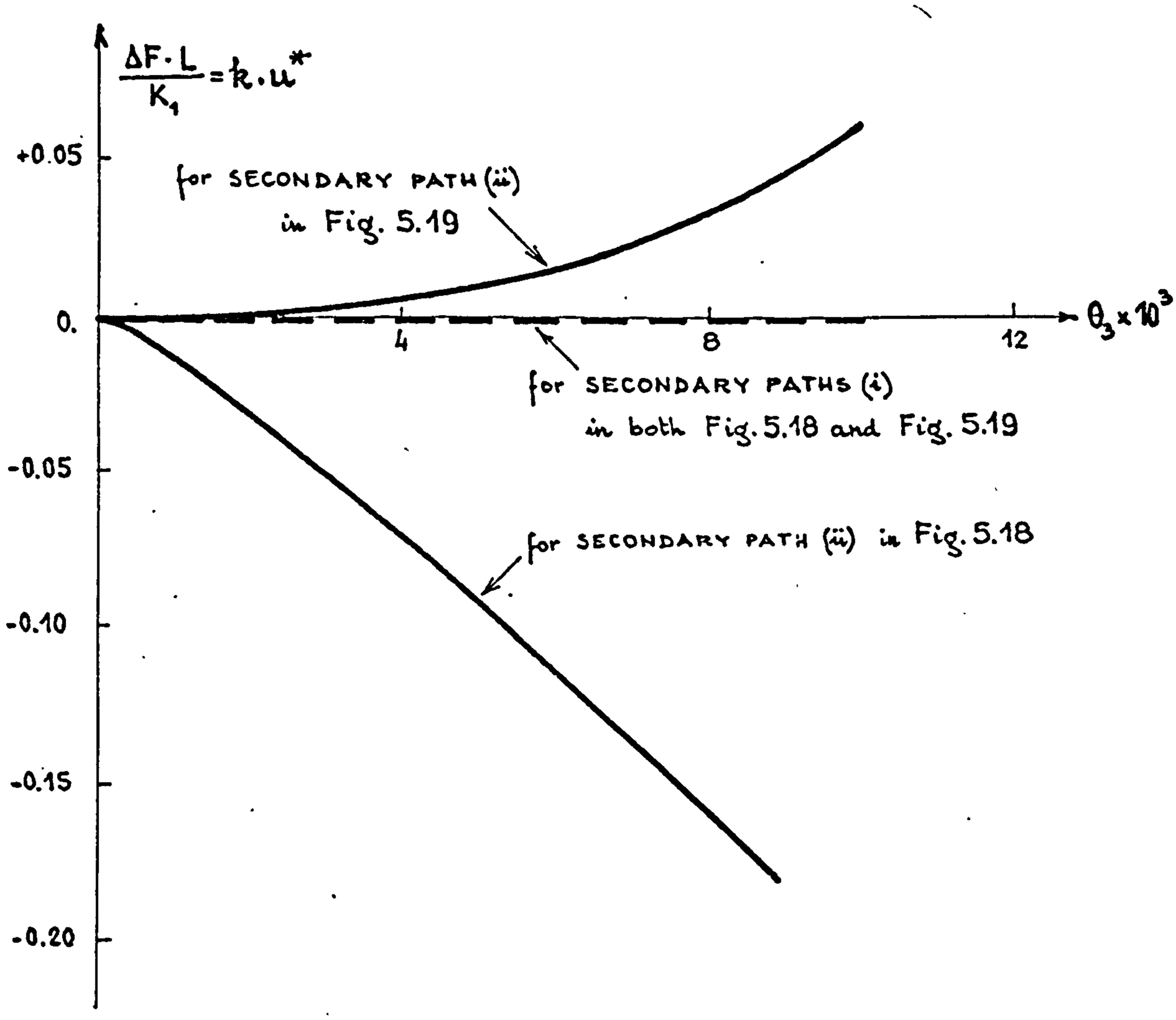

Fig. 5.22

- similarly, the stiffening secondary path (ii) of the model from Fig.5.19 is in accordance with the increasingly positive variation of ΔF associated with that secondary path.

f. Conclusion

The elastic postbuckling behaviour of the arch-model from Fig.5.2 has been analysed. Approaches to find the 'exact' and 'approximate' secondary paths are presented in Section 5.3.5a and b, respectively. The 'exact' secondary path is recommended to use for analysing the elastic postbuckling behaviour and the 'approximate' path is employed only as the initial estimate of the 'exact' solution.

Different elastic postbuckling responses can arise and they depend on the geometrical, mechanical and loading characteristics of the arch-model.

General features of the initial range of the secondary path are presented and discussed. It is shown that:

i) The modes of buckling displayed by a particular three degree-of-freedom arch-model is associated with the stability criterion (5.23) - see Section 5.3.5d. By mode of buckling is meant the configuration of the postbuckling deformed state relative to the critical deformed state. The modes of buckling which can be displayed by the three degree-of-freedom arch-model are summarised in Table 5.2.

ii) The stiffening or unstiffening of the postbuckling response is associated with the storage or release of

deformation energy in the mechanical devices A and B_i as the postbuckling deformation increases - see Section 5.3.5e Subsection 2.

5.3.6 CREEP EFFECTS ON PREBUCKLING BEHAVIOUR

So far the behaviour of the arch-model has been analysed assuming that the material is perfectly elastic. Yet the stiffness of the concrete is significantly time-dependent. Due to the concrete creep the deformed state of the arch-model subjected to a certain load p smaller than the elastic critical load p_{cr} will change continuously in time and a corresponding variation of internal forces will take place simultaneously. As long as bounded creep φ_∞ is assumed and no material failure is considered two situations can eventually arise: either the model reaches a critical state or the concrete creep reaches its final value while the model is still in a stable equilibrium position. The former case will occur when the load p, although smaller than the elastic p_{cr}, is larger than the critical load $p_{cr\,\varphi}$ corresponding to the final creep φ_∞ , whereas the latter case will occur when $p < p_{cr\,\varphi}$.

Again no closed-form solution of the problem can be found when creep is also considered. Consequently an incremental approach has to be set up in order to deal with the effects of the corresponding creep increment on the equilibrium state. The development of such an approach is presented and discussed within this section.

a. Constitutive relationships

The 'rate of creep' method*) will be used to model the creep of concrete. Using the notation (5.3) and integrating eq.(2.39b) upon the cross-section at the joint B_i (Fig.5.2 and 5.4) it follows that

$$d\psi_i = \frac{dM_i}{K_i} + \frac{M_{i\varphi}}{K_i} \cdot d\varphi \qquad i = 1...3 \qquad (5.64)$$

where

$d\varphi$ = variation of the creep coefficient of concrete

$d\psi_i$ = variation of the angular displacement ψ_i corresponding to $d\varphi$

dM_i = variation of the bending moment $M_{i\varphi}$ corresponding to $d\varphi$

If a small but finite creep increment is assumed eqs.(5.64) yield

$$\Delta\psi_i = \frac{\Delta M_i}{K_i} + \frac{M_{i\varphi}}{K_i} \cdot \Delta\varphi \qquad i = 1...3 \qquad (5.65)$$

Analogous to eqs.(5.65) it follows for the horizontal force that

$$\Delta U = \frac{\Delta F}{D} + \frac{F_\varphi}{D} \cdot \Delta\varphi \qquad (5.66)$$

where the same notation (5.3) has been used.

Eqs.(5.65) and (5.66) are the governing relationships of joints B_i and of the device A, respectively, when a

---

Footnote

*) See Table 2.2.

concrete creep according to the 'rate of creep' method is considered. They replace eqs.(5.3) which accounted for an elastic behaviour of concrete.

In setting up eqs.(5.65) and (5.66) the same creep increments $\Delta\varphi$ has been assumed to occur in each bending joint B_i as well as in the axial device A (see Fig.5.2).

Two consequences arise from using the form (2.39b) of the 'rate of creep' method rather than the form (2.39a):

(i) The incremental approach is not sensitive to the shape of the creep curve, that is the same effects occur for a certain $\Delta\varphi$ no matter whether the time development of creep is given by the curve 1a or the curve 1b from Fig.5.23.

(ii) when the approach is used sequentially for a $\varphi_{\infty 2} = n_2 \cdot \Delta\varphi$, the result for a smaller creep $\varphi_{\infty 1} = n_1 \cdot \Delta\varphi$ (with $n_1 < n_2$ where n_1, n_2 are integers) arises as an intermediate step (see Fig.5.23).

Both the above points will prove advantageous later when the curves $\gamma_{cr\varphi}$ versus φ_∞ are computed.

b. 'Exact' equilibrium equations

Using eqs.(5.3) and denoting the values of M_i and F at time t=0 by M_{io} and F_o one can recast the equilibrium eqs.(5.8) as

$$\sum_i M_{io} \cdot \frac{\partial \psi_{io}}{\partial V_{jo}} + F_o \cdot \frac{\partial U_o}{\partial V_{jo}} - \gamma \cdot P_j = 0 \qquad i,j = 1...3 \qquad (5.67)$$

In this form the elastic equilibrium equations represent in fact the virtual work written for three

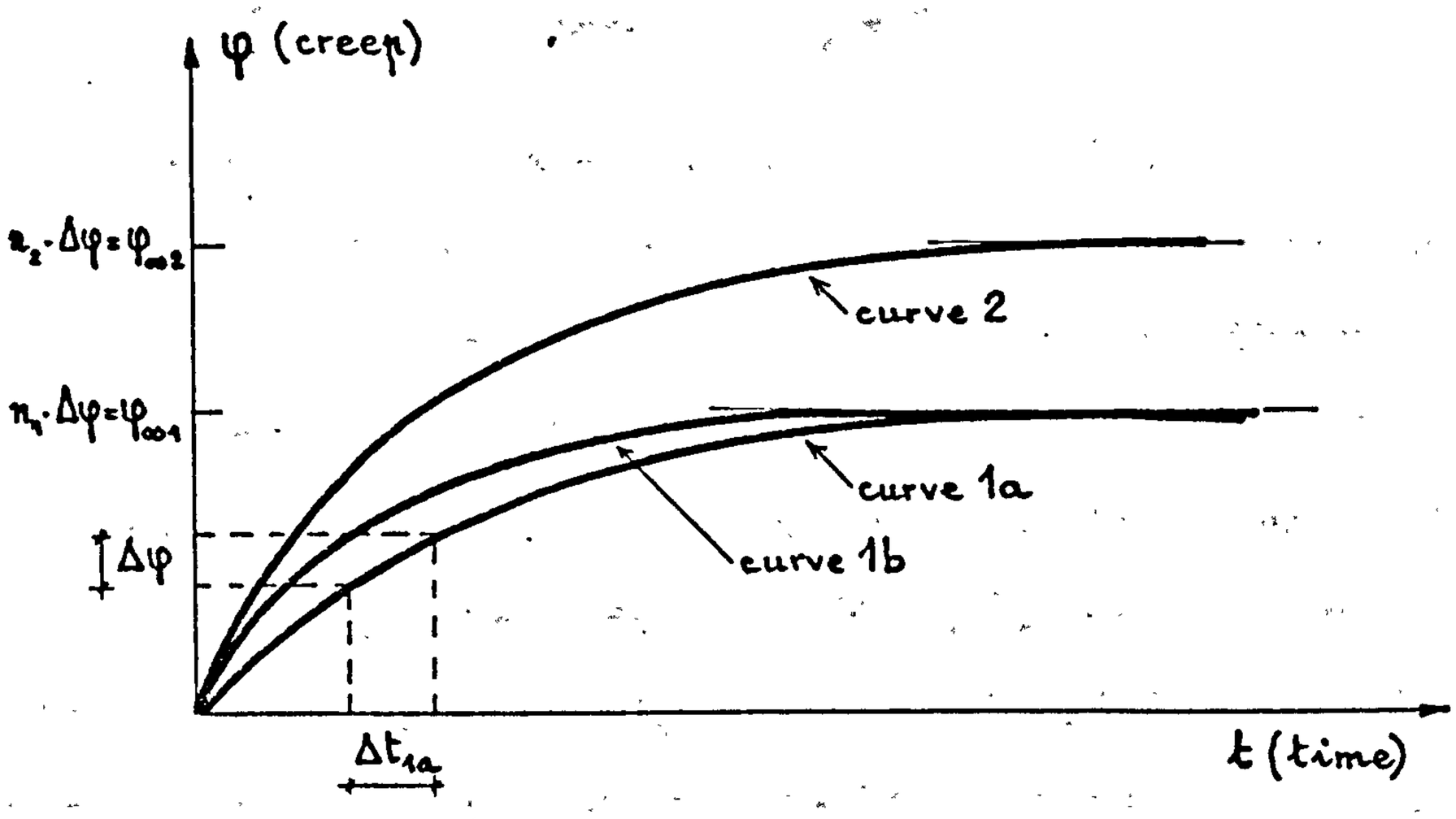

Fig. 5.23

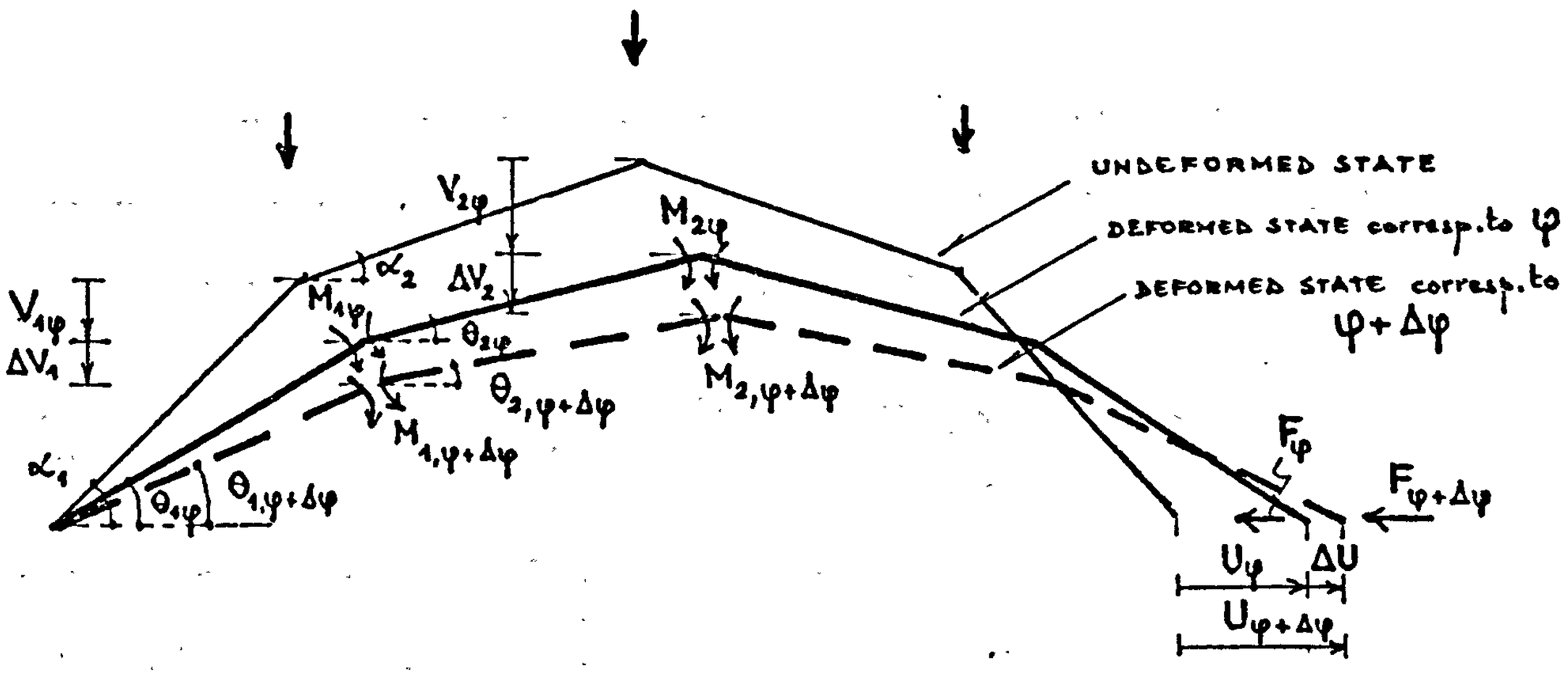

Fig. 5.24

independent virtual displacements

$$\delta V_j \neq 0 \qquad \text{and} \qquad \delta V_k = 0 \tag{5.68}$$

with $j \neq k$ and $j,k = 1,2,3$ (see Fig.5.4).

The principle of virtual work can be used to analyse the effects of a creep-increment on an equilibrium state.

Let us consider that the equilibrium state of the arch-model corresponding to a creep φ is characterised by the known internal forces $M_{i\varphi}$, F_φ and the known deformations $\theta_{j\varphi}$ and U_φ given by Fig.5.24. As the creep increases from φ to $\varphi+\Delta\varphi$ the new internal forces and deformations will be

$$\begin{aligned} M_{i,\varphi+\Delta\varphi} &= M_{i\varphi} + \Delta M_i \qquad i = 1\ldots3 \\ F_{\varphi+\Delta\varphi} &= F_\varphi + \Delta F \\ \theta_{j,\varphi+\Delta\varphi} &= \theta_{j\varphi} + \Delta\theta_j \qquad j = 1\ldots3 \\ U_{\varphi+\Delta\varphi} &= U_\varphi + \Delta U \end{aligned} \tag{5.69}$$

If no variation of the load is assumed over the $\Delta\varphi$-interval, the equilibrium of the deformed state corresponding to the $\varphi+\Delta\varphi$ can be written as

$$\sum_i M_{i,\varphi+\Delta\varphi} \cdot \frac{\partial\Delta\psi_i}{\partial\Delta V_j} + F_{\varphi+\Delta\varphi} \cdot \frac{\partial\Delta U}{\partial\Delta V_j} - \mu \cdot P_j = 0 \qquad i,j = 1\ldots3 \tag{5.70}$$

where the principle of virtual work has been used similarly to eqs.(5.67). Thus the internal forces correspond to the final deformed state while the variation of deformations corresponding to the virtual

displacements $\delta\Delta V_j$ are given by eqs. (5.1.2) *) with $\theta_i = \theta_{i\varphi}$ in eqs. (5.1.1).

Using eqs.(5.69) and eqs.(5.65) and (5.66), eqs.(5.70) yield

$$\sum_i K_i \cdot \Delta\psi_i \frac{\partial\Delta\psi_i}{\partial\Delta V_j} + D \cdot \Delta U \frac{\partial\Delta U}{\partial\Delta V_j} + \left[\sum_i M_{i\varphi} \frac{\partial\Delta\psi_i}{\partial\Delta V_j} + F_\varphi \frac{\partial\Delta U}{\partial\Delta V_j}\right] \cdot (1-\Delta\varphi) - p \cdot P_j = 0 \qquad i,j = 1\ldots3 \tag{5.71}$$

where, analogous to eqs.(5.6) and (5.7),

$$\sin\theta_{1,\varphi+\Delta\varphi} = \sin\theta_{1\varphi} - \frac{\Delta V_1}{L}$$

$$\sin\theta_{2,\varphi+\Delta\varphi} = \sin\theta_{2\varphi} - \frac{\Delta V_2 - \Delta V_1}{L} \tag{5.72}$$

and, respectively,

$$\Delta\psi_1 = \Delta\psi_3 = \theta_{1,\varphi+\Delta\varphi} - \theta_{2,\varphi+\Delta\varphi} - (\theta_{1\varphi} - \theta_{2\varphi})$$

$$\Delta\psi_2 = 2 \cdot \left[\theta_{2,\varphi+\Delta\varphi} - \theta_{2\varphi}\right] \tag{5.73}$$

$$\Delta U = 2L \sum_{j=1}^{2} \left[\cos\theta_{j,\varphi+\Delta\varphi} - \cos\theta_{j\varphi}\right]$$

Both equilibrium states corresponding to φ and to $\varphi + \Delta\varphi$ are symmetric.

By using the non-dimensional notation

Footnote

*) see Appendix V.1

$$\Delta v_i = \frac{\Delta V_i}{L} \qquad \Delta u = \frac{\Delta U}{L}$$

$$\bar{M}_{i\varphi} = \frac{M_{i\varphi}}{K_1} \qquad \Delta \bar{M}_i = \frac{\Delta M_i}{L} \tag{5.74}$$

$$\bar{F}_\varphi = \frac{F_\varphi \cdot L}{K_1} \qquad \Delta \bar{F} = \frac{\Delta F \cdot L}{K_1}$$

and the notation given by eqs.(5.4), eqs.(5.71) yield

$$\boxed{\sum_i c_i \, \Delta\psi_i \, \frac{\partial \Delta\psi_i}{\partial \Delta v_j} + k \, \Delta u \, \frac{\partial \Delta u}{\partial \Delta v_j} + \left[\sum_i \bar{M}_{i\varphi} \, \frac{\partial \Delta\psi_i}{\partial \Delta v_j} + \bar{F}_\varphi \, \frac{\partial \Delta u}{\partial \Delta v_j}\right] \cdot (1 - \Delta\varphi) - p \cdot p_j = 0} \qquad i,j = 1\ldots3 \tag{5.75}$$

while eqs.(5.65), (5.66) and (5.69) can be recast, respectively, as

$$\Delta \bar{M}_i = c_i \cdot \Delta\psi_i - \bar{M}_{i\varphi} \cdot \Delta\varphi \qquad i = 1\ldots3 \tag{5.65a}$$

$$\Delta \bar{F} = k \cdot \Delta u - \bar{F}_\varphi \cdot \Delta\varphi \tag{5.66a}$$

and

$$\bar{M}_{i,\varphi+\Delta\varphi} = \bar{M}_{i\varphi} + \Delta \bar{M}_i \qquad i = 1\ldots3$$

$$\bar{F}_{\varphi+\Delta\varphi} = \bar{F}_\varphi + \Delta \bar{F} \tag{5.67a}$$

$$u_{\varphi+\Delta\varphi} = u_\varphi + \Delta u$$

$$\theta_{i,\varphi+\Delta\varphi} = \theta_{i\varphi} + \Delta\theta_i \qquad i = 1,2$$

Eqs.(5.75) allow the Δv_j to be computed in a similar manner in which the v_j - displacements have been computed from eqs.(5.8). Since the same approach as in Section 5.3.3a is employed, an initial estimate of the solution

is required and the approximate form of eqs.(5.75) presented in the next section can be used to provide it.

After finding $\Delta' v_i$ the internal forces and deformations corresponding to $\varphi + \Delta\varphi$ and necessary to start the next step of analysis are found from eqs.(5.67a) with the help of eqs.(5.65a),(5.66a),(5.72) and (5.73).

The initial values for the first creep-increment are the forces and displacements corresponding to the instantaneous loading and they are determined according to Section 5.3.3.

Thus this step-by-step procedure provides the effects of concrete creep on the forces and displacements of the arch-model when the load is constant.

It is noteworthy that the form (5.70) of the equilibrium equation is virtually identical to the second variational principle derived by England (1968) for linear creep-elastic materials and continuous structures. According to this principle

$$\int \sigma_{ij} \cdot \delta\left(\frac{d\varepsilon_{ij}}{d\varphi}\right) dV - \sum_k P_k \cdot \delta\left(\frac{du_k}{d\varphi}\right) = 0 \qquad (5.76)$$

where σ_{ij} and ε_{ij} are the stresses and strains associated with the state of equilibrium at a certain instant t, P_k are the external forces on the structure and u_k are the displacements of the structure corresponding to P_k. "δ" in eq.(5.76) stands for small variations and is therefore analogous to "∂" in eqs.(5.70).

c. 'Approximate' equilibrium equations

In eqs.(5.70) the displacements $\Delta\psi_i$, ΔU and ΔV_j define the deformed state at the end of $\Delta\varphi$-increment about the deformed state existing at the beginning (i.e. at the instant when the creep is φ).

Eqs.(5.70) written in terms of the internal forces and the displacements of equilibrium state at the end of the previous creep increment (i.e. at the instant when the creep is φ) yield

$$\sum_i M_{i\varphi} \frac{\partial \Delta\psi_i^*}{\partial \Delta V_j^*} + F_\varphi \frac{\partial \Delta U^*}{\partial \Delta V_j^*} - \mu \cdot P_j = 0 \qquad i,j = 1\ldots3 \qquad (5.77)$$

where $\Delta\psi_i^*$, ΔU^* and ΔV_j^* are analogous to the above $\Delta\psi_i$, ΔU, ΔV_j but define the deformed state at instant φ about the state at instant $\varphi - \Delta\varphi$ (see Fig.5.25).

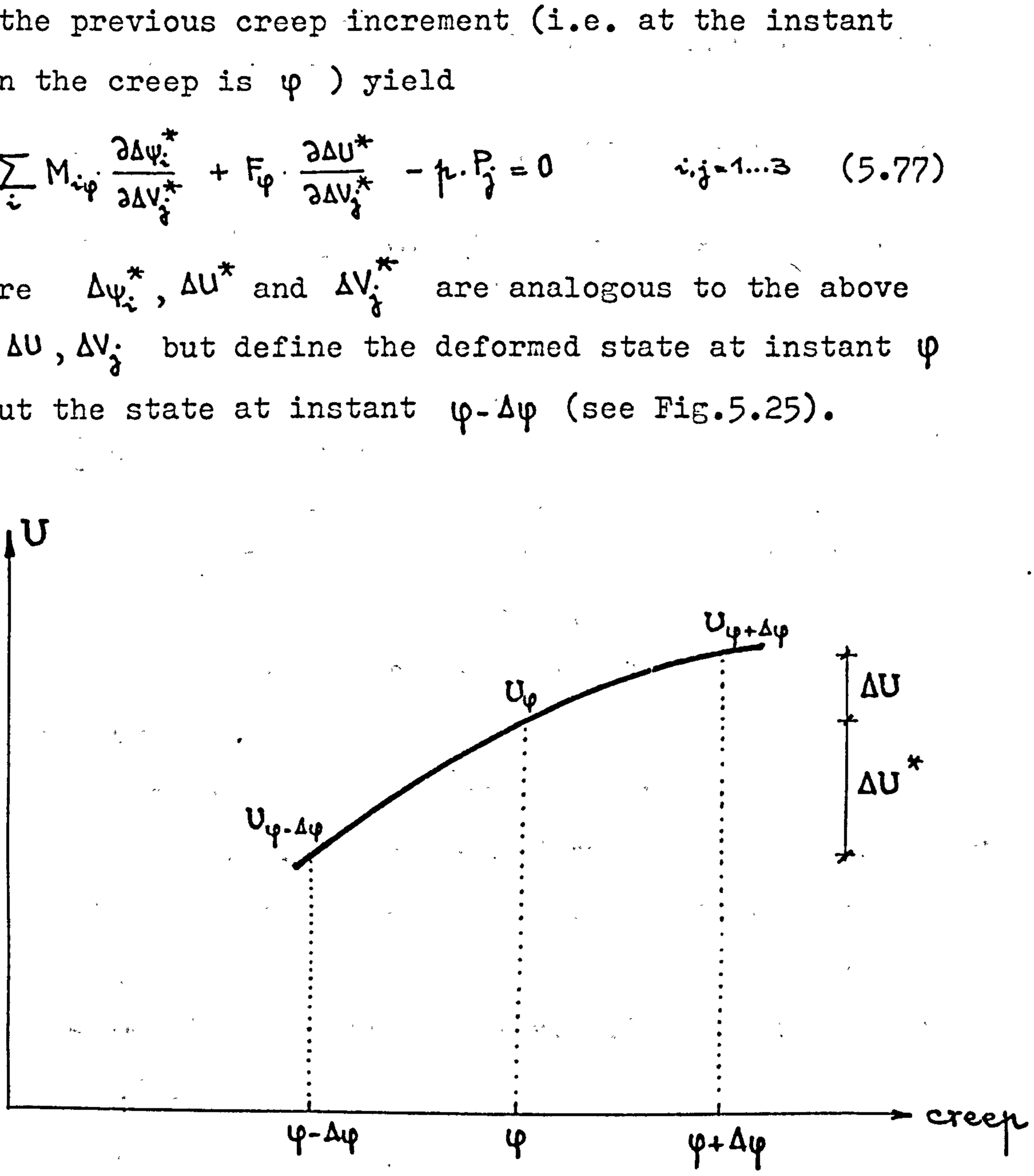

Fig. 5.25

Assuming that

$$\frac{\Delta\psi_i^*}{\Delta V_j^*} = \frac{\Delta\psi_i}{\Delta V_j} \qquad i,j = 1\ldots3 \qquad (5.78)$$

$$\frac{\Delta U^*}{\Delta V_j^*} = \frac{\Delta U}{\Delta V_j}$$

the following approximate form of eqs.(5.77) arises

$$\sum_i M_{i\varphi} \frac{\partial\Delta\psi_i}{\partial\Delta V_j} + F_\varphi \frac{\partial\Delta U}{\partial\Delta V_j} - p\cdot P_j = 0 \qquad i,j = 1\ldots3 \qquad (5.79)$$

Using now eqs.(5.79) in eqs.(5.71) it follows that

$$\sum_i K_i\,\Delta\psi_i \frac{\partial\Delta\psi_i}{\partial\Delta V_j} + D\cdot\Delta U \frac{\partial\Delta U}{\partial\Delta V_j} - p\cdot P_j\,\Delta\varphi = 0 \qquad i,j = 1\ldots3$$

or, with the notation (5.4) and (5.74),

$$\boxed{\sum_i c_i\,\Delta\psi_i \frac{\partial\Delta\psi_i}{\partial\Delta v_j} + k\,\Delta u \frac{\partial\Delta u}{\partial\Delta v_j} - p\,\Delta\varphi\cdot p_j = 0} \qquad (5.80)$$

Eqs.(5.80) are remarkably analogous in mathematical form with the 'exact' equations (5.8) analysing the instantaneous elastic deformed state due to the same load p, but

i) the geometry about which the displacements are measured in eqs.(5.80) is the deformed state at instant φ rather than the undeformed and unloaded state as it is in eqs.(5.8),

ii) $p\cdot\Delta\varphi$ is to be used in eqs.(5.80) rather than p in eqs.(5.8).

With just these differences the same technique can be used to solve both eqs.(5.80) and eqs.(5.8).

Since eqs.(5.80) are an approximate form of eqs.(5.75) due to assumptions (5.78), they are further used solely to provide the initial estimate of the solution Δv_j , $j=1...3$. For this aim the approximate solution of eqs.(5.80), that is the solution found analogous to Section 5.3.3, proved to be sufficient.

However, in order to emphasise the implications of assumptions (5.78), a comparison between the accurate solutions of eqs.(5.75) and (5.80) is presented and discussed in the next section.

d. Discussion and conclusion

When a 1st order theory is performed, that is the displacements of the arch-model are assumed so small that the equilibrium and compatibility equations can be written about the undeformed state, eqs.(5.78) become true and hence eqs.(5.80) are no longer approximate. In this case both eqs.(5.80) and eqs.(5.8) become algebraically linear and, according to the correspondence principle - see Flügge (1975)- it follows that *)

$$v_{i\varphi} = v_{i0} \cdot (1+\varphi) \qquad i=1...3$$

$$\psi_{i\varphi} = \psi_{i0} \cdot (1+\varphi) \qquad (5.81)$$

$$u_\varphi = u_0 \cdot (1+\varphi)$$

Footnote

*) A development of eqs.(5.81) and (5.82) based on the linear form of eqs.(5.8) and (5.80) is given in Appendix V.10.

and

$$\bar{M}_{i\varphi} = \bar{M}_{i0}$$
$$\bar{F}_{\varphi} = \bar{F}_{0} \qquad (5.82)$$

where the notation (5.74) have been used and the subscript '0' denotes the corresponding instantaneous values, i.e. at $\varphi = 0$.

The larger is the creep, the larger are the displacements and therefore the more significant the effects of assumptions (5.78). In fact eqs.(5.78) are inconsistent with the large displacements since it is not possible for both eqs.(5.70) and eqs.(5.79) to be simultaneously satisfied.

An idea of the effects of assumptions (5.78) is given by comparing the results of using eqs.(5.75) and (5.80) for a typical set of numerical data.

Step-by-step analyses based on eqs.(5.75) and (5.80) have been carried out and the accurate solutions of either set of equations have been found for the numerical data of the arch-model from Fig.5.7 and p=0·19. The results are plotted in Figs.5.26 and 5.27.

Fig.5.26 depicts the variation of displacements $v_{i\varphi}$ versus the creep characteristic φ and Fig.5.27 depicts the variation of internal forces $\bar{M}_{i\varphi}$ and $\bar{F}_{\varphi}$ versus the same φ.

The results of the 1st order analysis, that is according to eqs.(5.81) and (5.82), are also plotted considering the correct initial values, i.e. the large

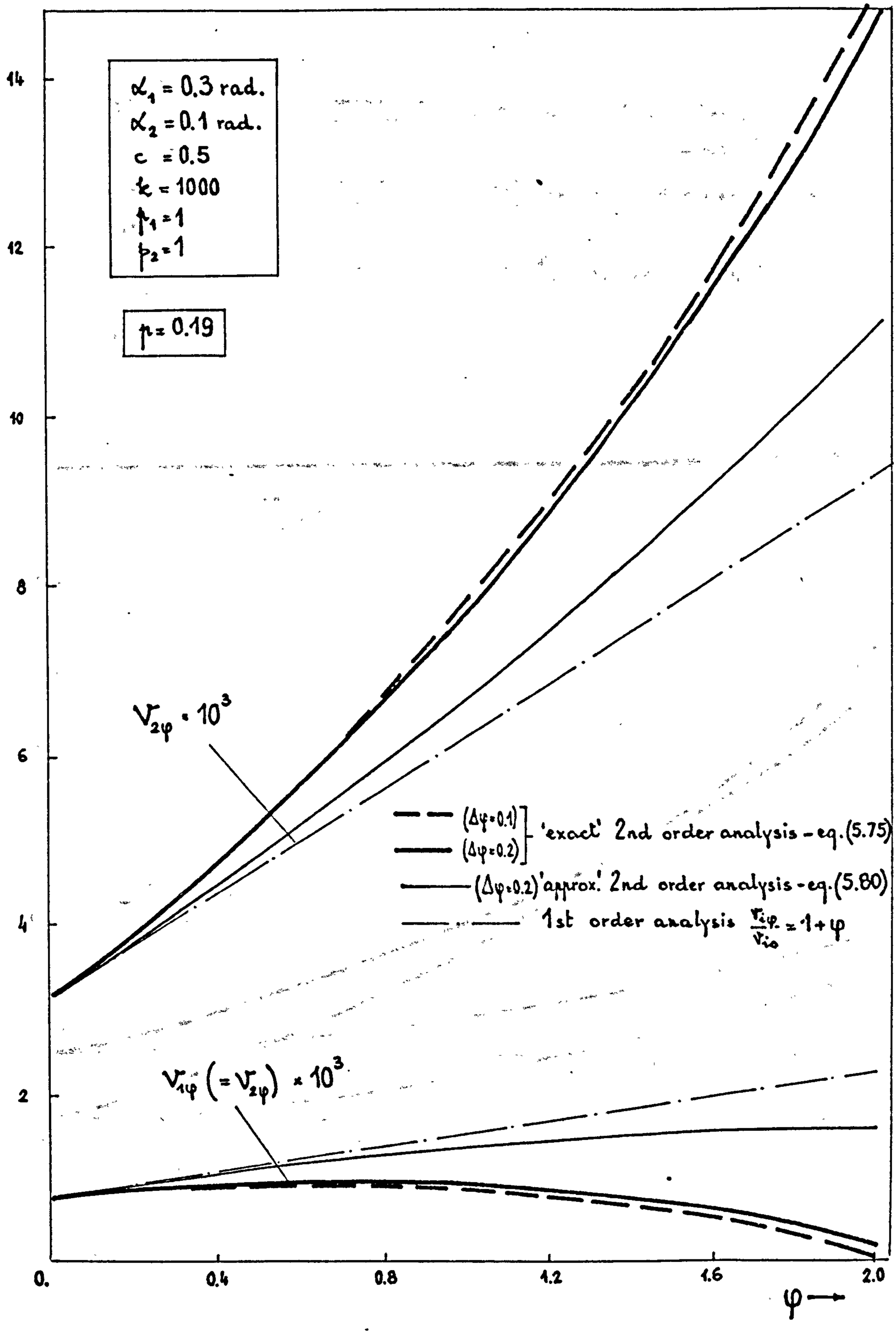
$\alpha_1 = 0.3$ rad.
$\alpha_2 = 0.1$ rad.
$c = 0.5$
$k = 1000$
$\mu_1 = 1$
$\mu_2 = 1$
$\mu = 0.19$
$V_{2\varphi} \cdot 10^3$
$V_{1\varphi} (= V_{2\varphi}) \cdot 10^3$
(Δφ=0.1)
(Δφ=0.2)
'exact' 2nd order analysis - eq.(5.75)
(Δφ=0.2) 'approx.' 2nd order analysis - eq.(5.80)
1st order analysis $\frac{V_{i\varphi}}{V_{i0}} = 1 + \varphi$
14
12
10
8
6
4
2
0.
0.4
0.8
1.2
1.6
2.0
φ →

Fig. 5.26

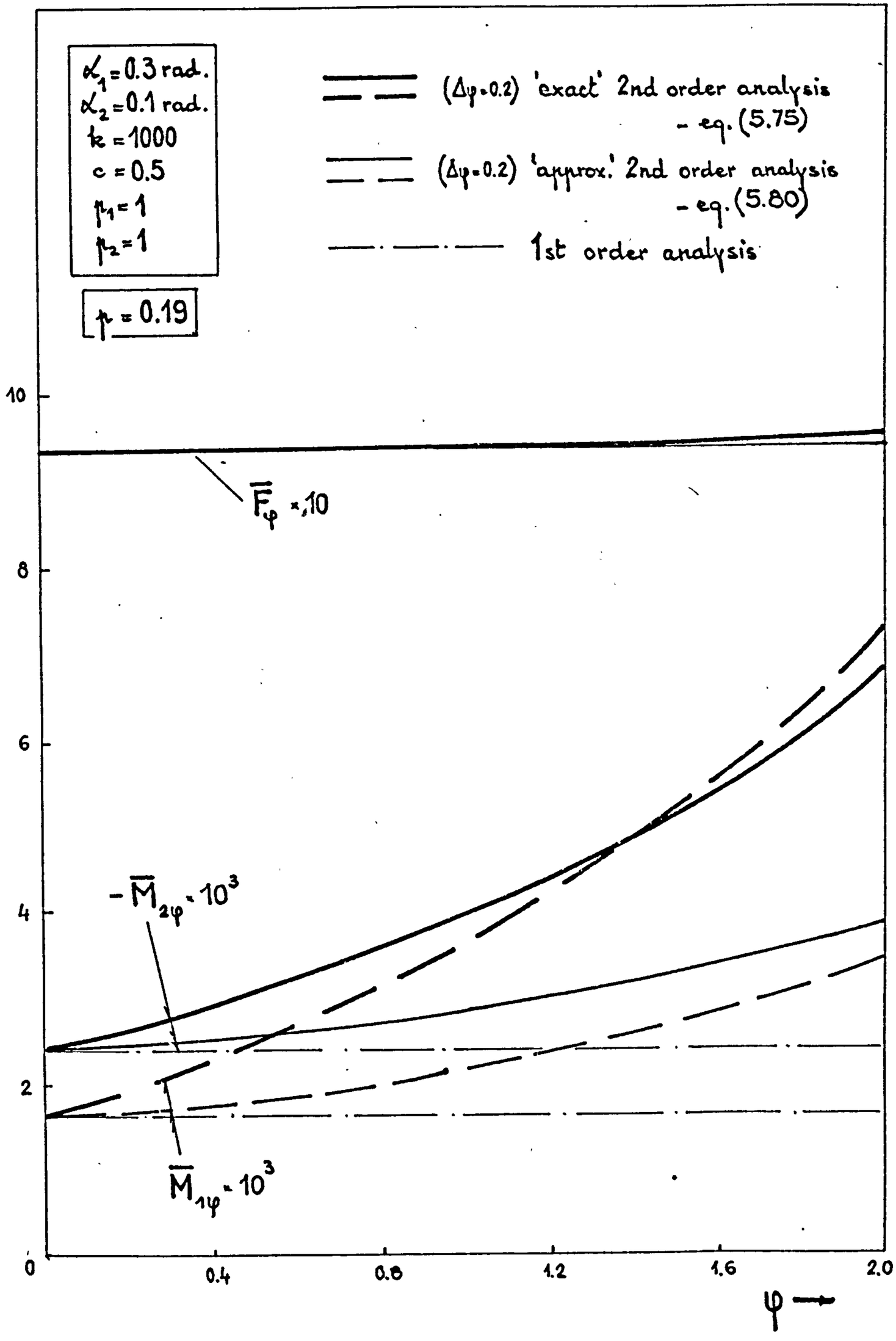
$\alpha_1 = 0.3$ rad.
$\alpha_2 = 0.1$ rad.
$k = 1000$
$c = 0.5$
$\mu_1 = 1$
$\mu_2 = 1$
$\mu = 0.19$
($\Delta\varphi = 0.2$) 'exact' 2nd order analysis - eq. (5.75)
($\Delta\varphi = 0.2$) 'approx.' 2nd order analysis - eq. (5.80)
1st order analysis
$\overline{F}_\varphi \cdot 10$
$-\overline{M}_{2\varphi} \cdot 10^3$
$\overline{M}_{1\varphi} \cdot 10^3$
10
8
6
4
2
0
0.4
0.8
1.2
1.6
2.0
$\varphi \longrightarrow$

displacements provided by eqs.(5.8) at $\varphi = 0$.

From Figs.5.26 and 5.27 it can be concluded that:

i) the increase of creep has a similar effect as the increase of load, that is the displacement v_2 increases while the displacement v_1 decreases (see also Fig.5.7), when the exact eqs.(5.75) are used.

ii) the results of eqs.(5.80) lie between the results provided by eqs.(5.75) and those provided by the 1st order analysis. In other words this means that eqs.(5.80) is less approximative than the 1st order analysis when larger displacements are involved. Nevertheless significant differences can arise from using the approximate eqs. (5.80) instead of the exact eqs.(5.75).

iii) The sharp increase of v_{20} while $\bar{F}_\varphi$ is almost constant suggests that the load p=0·19 is very close to the critical load producing snap-buckling at point B_2 and this will be confirmed later when the creep stability in analysed (see Fig.5.35).

iv) A creep increment $\Delta\varphi = 0{\cdot}2$ has been used for each step of analysis. In order to find out the sensitivity of the results at the magnitude of the creep increment the curves corresponding to $\Delta\varphi = 0{\cdot}1$ and to the solution of eqs.(5.75) have also been plotted. It is found that no significant differences occur when a smaller creep increment than $\Delta\varphi = 0{\cdot}2$ is considered.

5.3.7 CREEP EFFECTS ON STABILITY

As the concrete creep increases and the loading is held constant the forces and displacements in the arch-

model increase too (see Figs.5.26 and 5.27) and the structure advances towards buckling.

When the creep and the load are small, the final deformed state (i.e. the state corresponding to φ_∞) will be stable and the sole effect of concrete creep is to modify the values of forces and deformations of the structure. When large displacements are displayed these modifications are significantly larger.

When either the creep or the load is large, a critical state can be attained before the concrete creep reaches its final value and thus a creep buckling takes place. The more flexible is the structure (i.e. the larger are the displacements) the less are the value of φ or p when the creep buckling occurs.

The effects of concrete creep on the critical load $p_{cr\varphi}$ are analysed within this section and the dependence between the load $p_{cr\varphi}$ and the creep φ_∞ is sought. This dependence will provide the boundary of the range of parameters p and φ under which no creep instability can occur. It can be regarded as supplying either the maximum load $p_{cr\varphi}$ under which the arch-model displaying a certain creep φ_∞ is still stable or the maximum creep φ_{crp} which can be allowed for the arch-model to be stable under a certain load p (Fig.5.28).

This critical boundary depends not only on the geometry, mechanics and loading of the arch-model*), but also on the

---

Footnote

*) by loading here it is meant the values of p_1 and p_2 in eqs.(5.4).

path $p(\varphi)$, i.e. on the history of relative variation of ρ and φ, in view of the viscous behaviour of concrete.

Two types of paths will be analysed below:

i) a certain load ρ_o is assumed to be applied instantaneously and held constant until a creep φ occurs. Then the extra load $\Delta\rho$ which brings the model to a critical state is found (path (i) in Fig.5.29). The critical state is defined using the same dynamic criterion of stability as in Section 5.3.4, that is the deformed state at which small dynamic displacements applied instantaneously are no longer damped. This type of instability associated with the path (i) is further called 'elastic instability of the creeping structure.'

Path (i) models in fact the practical situation in which a structure sustains the dead load and a fraction of the live load for a certain period of time and then an instantaneous increase of the live load occurs.

ii) the total load p is applied instantaneously and held constant and the lowest value of φ_{cr} is found for which

$$\frac{d\varphi}{dv_{i\varphi}} = 0 \qquad (5.83)$$

that is the increase of one of the displacements $v_{i\varphi}$ is practically indefinite relative to the corresponding increase in creep (path (ii) in Fig.5.29). This path models the practical situation when a structure sustains a constant load. The type of instability associated with this loading is further called 'creep instability.'

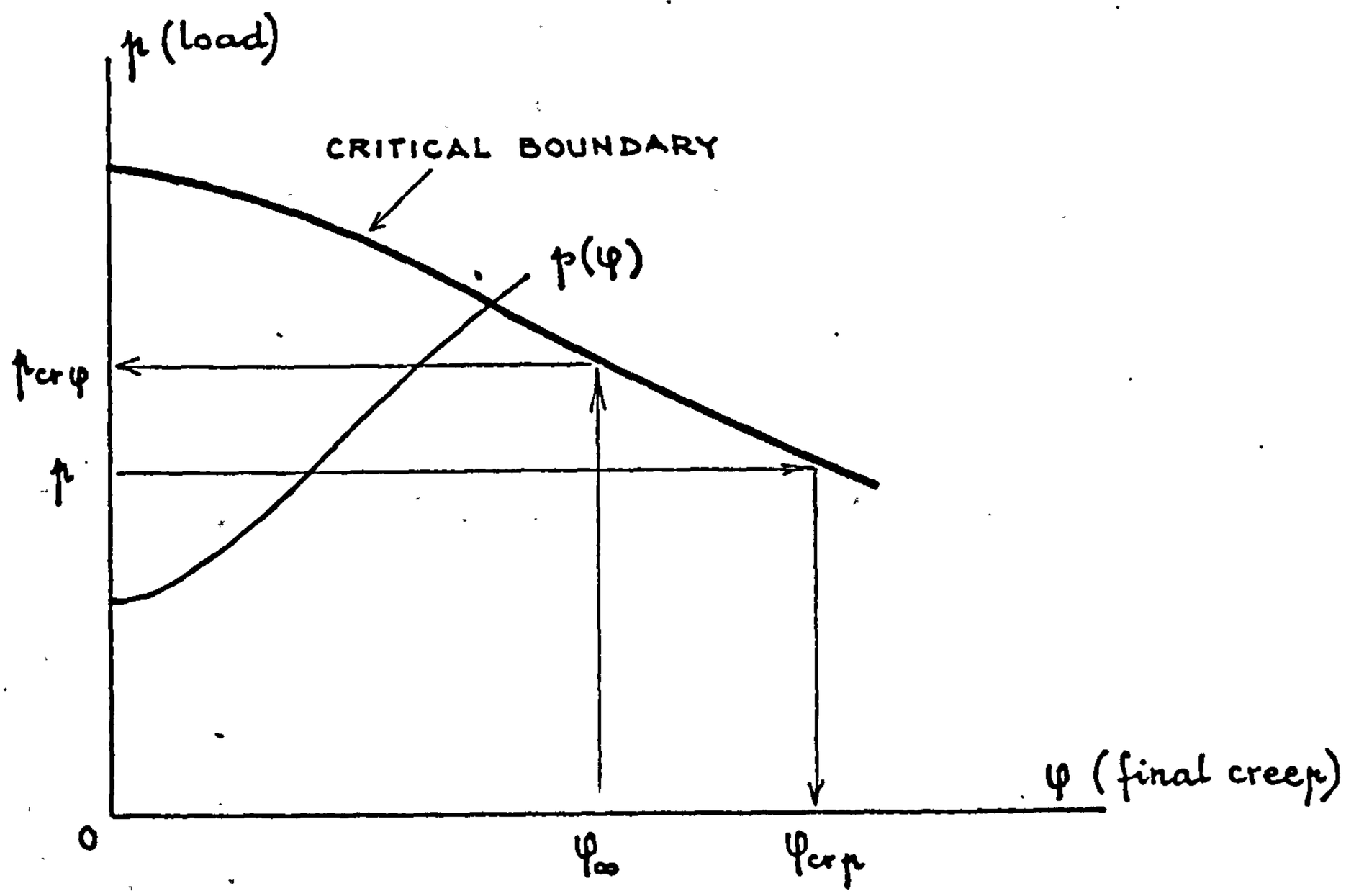

Fig. 5.28

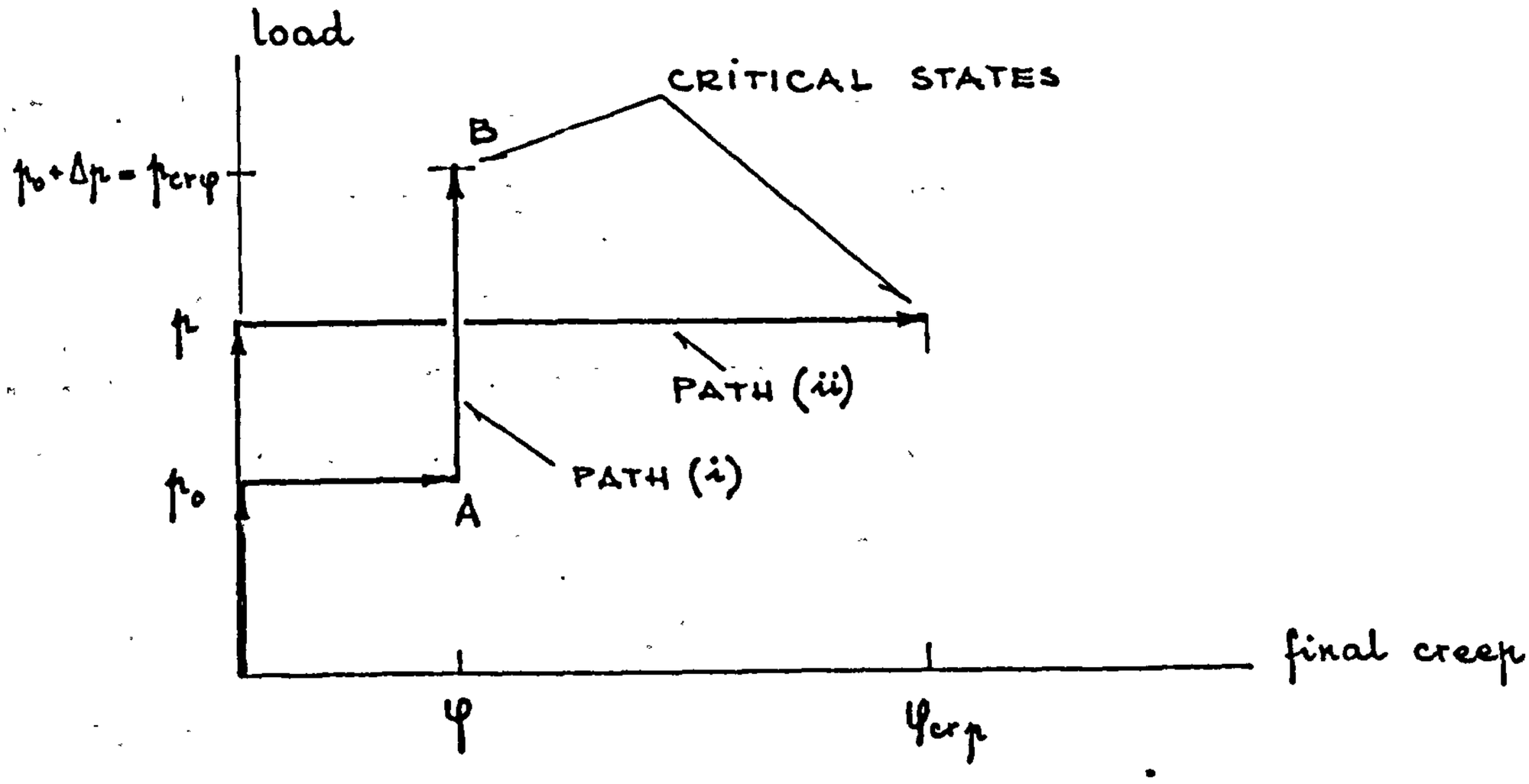

Fig. 5.29

Whereas for the 'elastic instability of creeping structure' the elastic stability criterion (5.23) is employed, for the 'creep instability' the stability criterion is given by eq.(5.83).

a. Elastic Instability of the Creeping Structure.

When the load is applied according to path (i) from Fig.5.28 the equilibrium equations (5.8) become

$$\frac{\partial \Delta\Pi}{\partial v_j} = \sum_i \left(\bar{M}_{i\varphi} + c_i \cdot \Delta\psi_i\right) \cdot \frac{\partial \Delta\psi_i}{\partial \Delta v_j} + \left(\bar{F}_\varphi + k \cdot \Delta u\right) \cdot \frac{\partial \Delta u}{\partial \Delta v_j} - \left(p_0 + \Delta p\right) \cdot p_j = 0 \qquad (5.84)$$

$$i, j = 1 \ldots 3$$

and eqs.(5.31) become

$$\Pi_{jl} = \left.\frac{\partial^2 \Delta\Pi}{\partial v_j \partial v_l}\right|_B = \sum_i \left(\bar{M}_{i\varphi} + c_i \cdot \Delta\psi_i\right) \left.\frac{\partial^2 \Delta\psi_i}{\partial \Delta v_j \partial \Delta v_l}\right|_B +$$

$$\left(\bar{F}_\varphi + k \cdot \Delta u\right) \left.\frac{\partial^2 \Delta u}{\partial \Delta v_j \partial \Delta v_l}\right|_B + \sum_i c_i \left.\frac{\partial \Delta\psi_i}{\partial \Delta v_j}\right|_B \cdot \left.\frac{\partial \Delta\psi_i}{\partial \Delta v_l}\right|_B + \qquad (5.85)$$

$$k \cdot \left.\frac{\partial \Delta u}{\partial \Delta v_j}\right|_B \cdot \left.\frac{\partial \Delta u}{\partial \Delta v_l}\right|_B \qquad i, j, l = 1 \ldots 3$$

where :

$\Delta\Pi$ - is the variation of the total potential energy when the model deforms from the state A to the state B (Fig.5.29)

$\bar{M}_{i\varphi}, \bar{F}_\varphi$ - are the forces corresponding to the state A

$\Delta\psi_i, \Delta u, \Delta v_j$ - are the displacements corresponding to the state B and measured about the deformed state A.

In writting the eqs.(5.84) and (5.85) the same approach as for the elastic primary path has been used with the difference that the deformed state A has been considered as the initial state rather than the undeformed and

unloaded state.

The deformed state A corresponding to p_o and φ is found by using the step-by-step procedure from the previous section.

The critical value of Δp is the lowest value of Δp for which the stability criterion (5.23) is no longer satisfied, where Δ is given by eq.(5.22) and π_{ij} are given by eqs.(5.85). The $\Delta\psi_i$, Δu and Δv_j displacements from eqs.(5.85) are given by the solution of eqs.(5.84) and equations (5.6) and (5.7) with the alterations that $\Delta\psi_i$, Δu and Δv_j replace ψ_i, u and v_j, respectively, and that the angles θ_{jA} should be considered rather than α_j. With these differences a similar approach to that presented in Section 5.3.3 and Section 5.3.4 is employed.

By varying φ, curve I from Fig.5.30 can be plotted. This curve depicts the dependence on creep of the critical load yielding elastic instability of creeping structure.

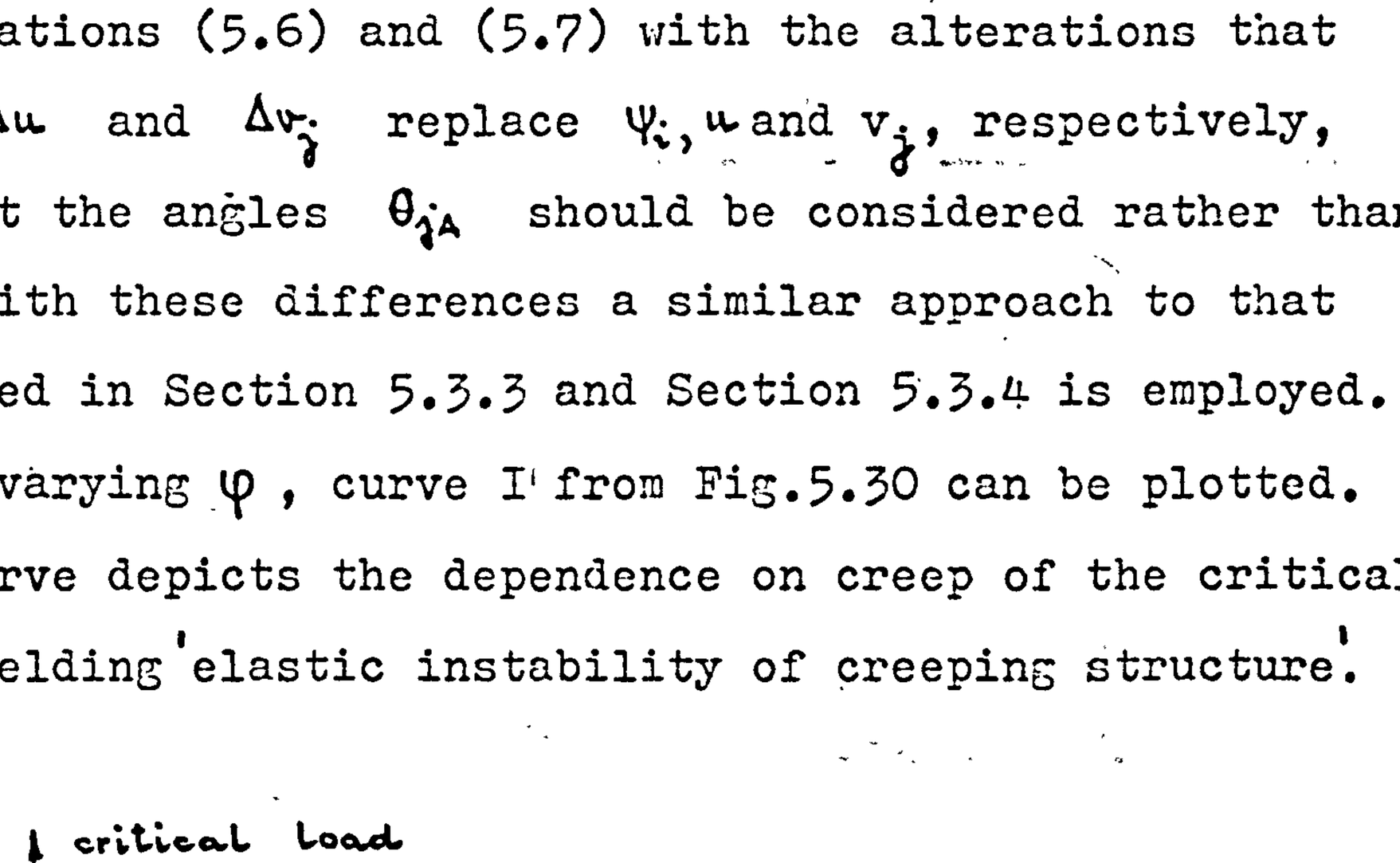

Fig. 5.30

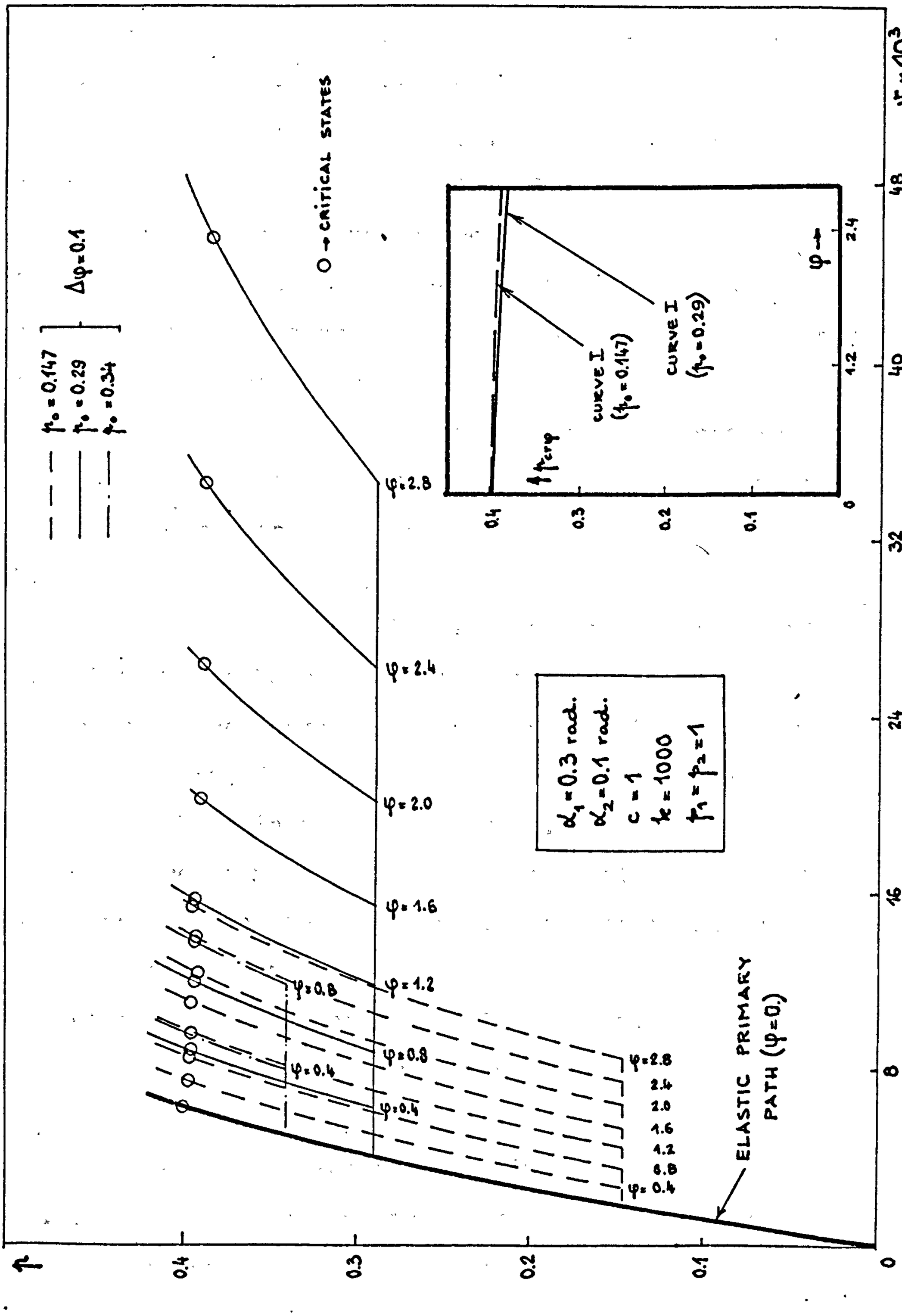
$V_2 \times 10^3$
48
40
32
24
16
8
0
0.1
0.2
0.3
0.4
$\psi \rightarrow$
0
1.2
2.4
ψ_{crip}
CURVE I (ψ_0=0.147)
CURVE I (ψ_0=0.29)
O → CRITICAL STATES
ψ=2.8
ψ=2.4
ψ=2.0
ψ=1.6
ψ=1.2
ψ=0.8
ψ=0.4
ψ_0=0.147
ψ_0=0.29
ψ_0=0.34
$\Delta\psi$=0.1
α_1=0.3 rad.
α_2=0.1 rad.
c = 1
k = 1000
$\tau_1 = \tau_2$=1
ELASTIC PRIMARY PATH (ψ=0.)
ψ=2.8
2.4
2.0
1.6
1.2
0.8
ψ=0.4

Fig. 5.31

At $\varphi = 0$ the critical load is given by the elastic value γ_{cr}. Different curves I emerging from the same point B_o should arise for different values of p_o.

Curve I is depicted in Fig.5.31 for the same numerical data as those from Fig.5.6. For the sake of simplicity only the curves corresponding to the increments $\Delta\varphi = 0{\cdot}4$ are plotted. The actual increase of $\Delta\varphi$ in carrying out the analysis has been $\Delta\varphi = 0{\cdot}1$. Three levels of p_o have been considered. The results depicted by Fig.5.31 are typical for the behaviour of the arch-model.

The following conclusions can be drawn on curve I:

i) it emerges from the point corresponding to the elastic critical load γ_{cr}

ii) it is insignificantly dependent on the level of p_o. Differences between curves I corresponding to different p_o are larger for large creep values, but in that range curve I is no longer of practical interest as will be shown in the next section.

iii) there is no significant drop in elastic critical load when the arch-model has previously crept under a lower sustained load.

Yet in the next section it will be shown that the concrete creep significantly affects the 'creep instability'.

b. Creep Instability

When the load is applied according to path (ii) from Fig.5.29 the step-by-step procedure presented in Section 5.3.6 can be employed. By increasing progressively the

coefficient φ , the corresponding displacements $v_{i\varphi}$ (i=1..3) arise from solving eqs.(5.75) and from

$$v_{i\varphi} = v_{i0} + \sum_{\varphi} \Delta v_i$$

To each value of p a certain value $\varphi_{cr\,p}$ can be found which brings the arch-model to a critical state, i.e. at a deformed state for which an infinitely small increase in creep yields a very large increase of one of the displacements v_i such that condition (5.83) is satisfied. A long-term snap-buckling occurs consequently.

It is worth emphasising that due to the time-dependent behaviour of the material a non-conservative stability problem arises and, therefore, the stability criteria from Section 5.3.4 based on the energy principles are no longer valid. Condition (5.83) is subsequently employed as criterion for creep instability.

The effects of the progressive increase of concrete creep on the forces and displacements of an arch-model are depicted in Figs.5.32 and 5.33. The same numerical data as in Fig.5.31 has been chosen.

The variation of bending moments $\bar{M}_{i\varphi}$ versus the creep φ is depicted in Fig.5.32 for different intensities of load p. It can be seen that the larger is p the more dramatic is the increase in $\bar{M}_2$. As a matter of fact in view of the relationship existing between moments and vertical displacements the condition (5.83) can well be replaced by

$$\frac{d\varphi}{d\bar{M}_{i\varphi}} = 0 \qquad (5.83a)$$

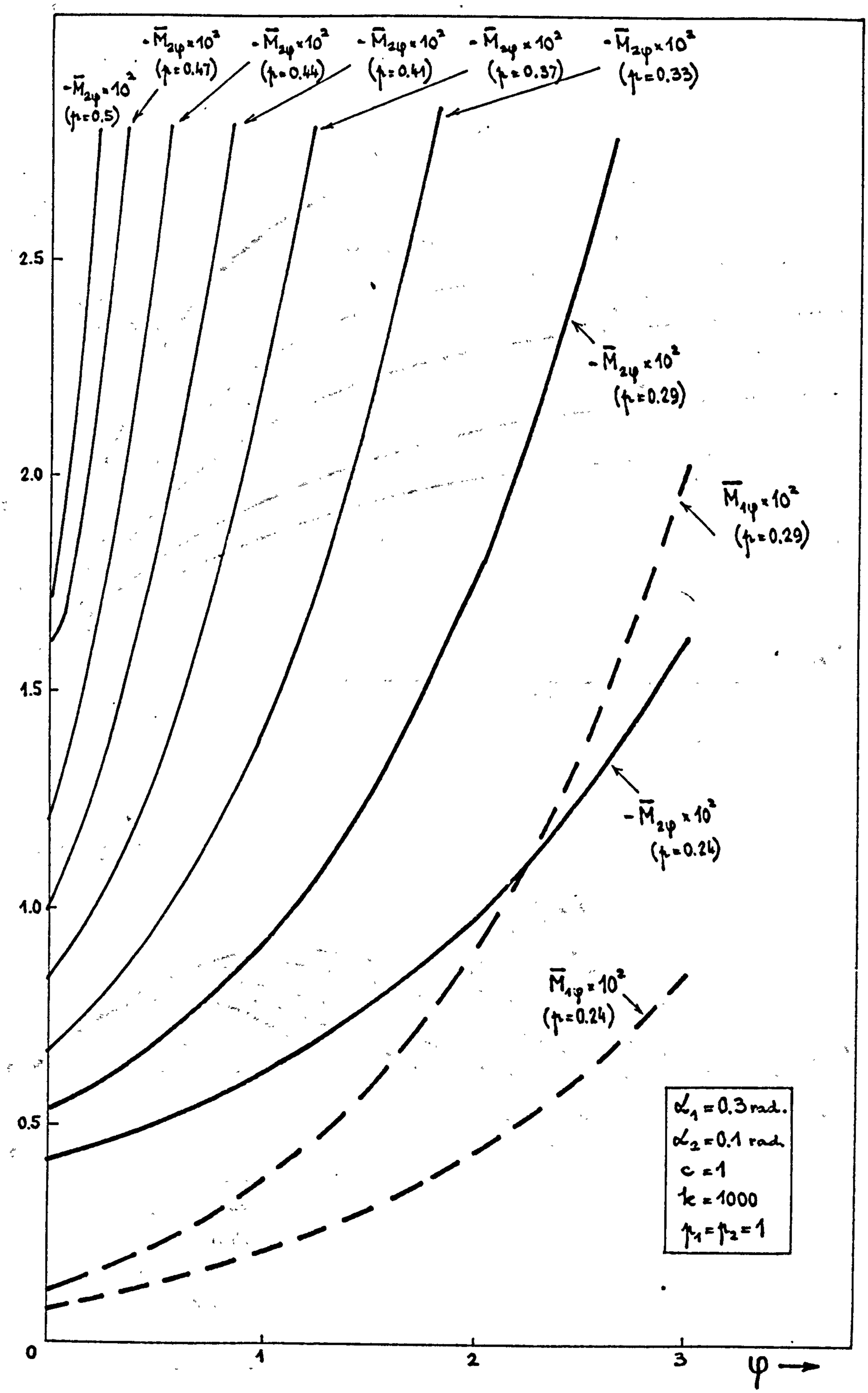
$-\bar{M}_{2\varphi}\times10^2$ (μ=0.5)
$-\bar{M}_{2\varphi}\times10^2$ (μ=0.47)
$-\bar{M}_{2\varphi}\times10^2$ (μ=0.44)
$-\bar{M}_{2\varphi}\times10^2$ (μ=0.41)
$-\bar{M}_{2\varphi}\times10^2$ (μ=0.37)
$-\bar{M}_{2\varphi}\times10^2$ (μ=0.33)
$-\bar{M}_{2\varphi}\times10^2$ (μ=0.29)
$\bar{M}_{1\varphi}\times10^2$ (μ=0.29)
$-\bar{M}_{2\varphi}\times10^2$ (μ=0.24)
$\bar{M}_{1\varphi}\times10^2$ (μ=0.24)
α_1 = 0.3 rad.
α_2 = 0.1 rad.
c = 1
k = 1000
$\mu_1=\mu_2=1$
2.5
2.0
1.5
1.0
0.5
0
1
2
3
φ →

Fig. 5.32

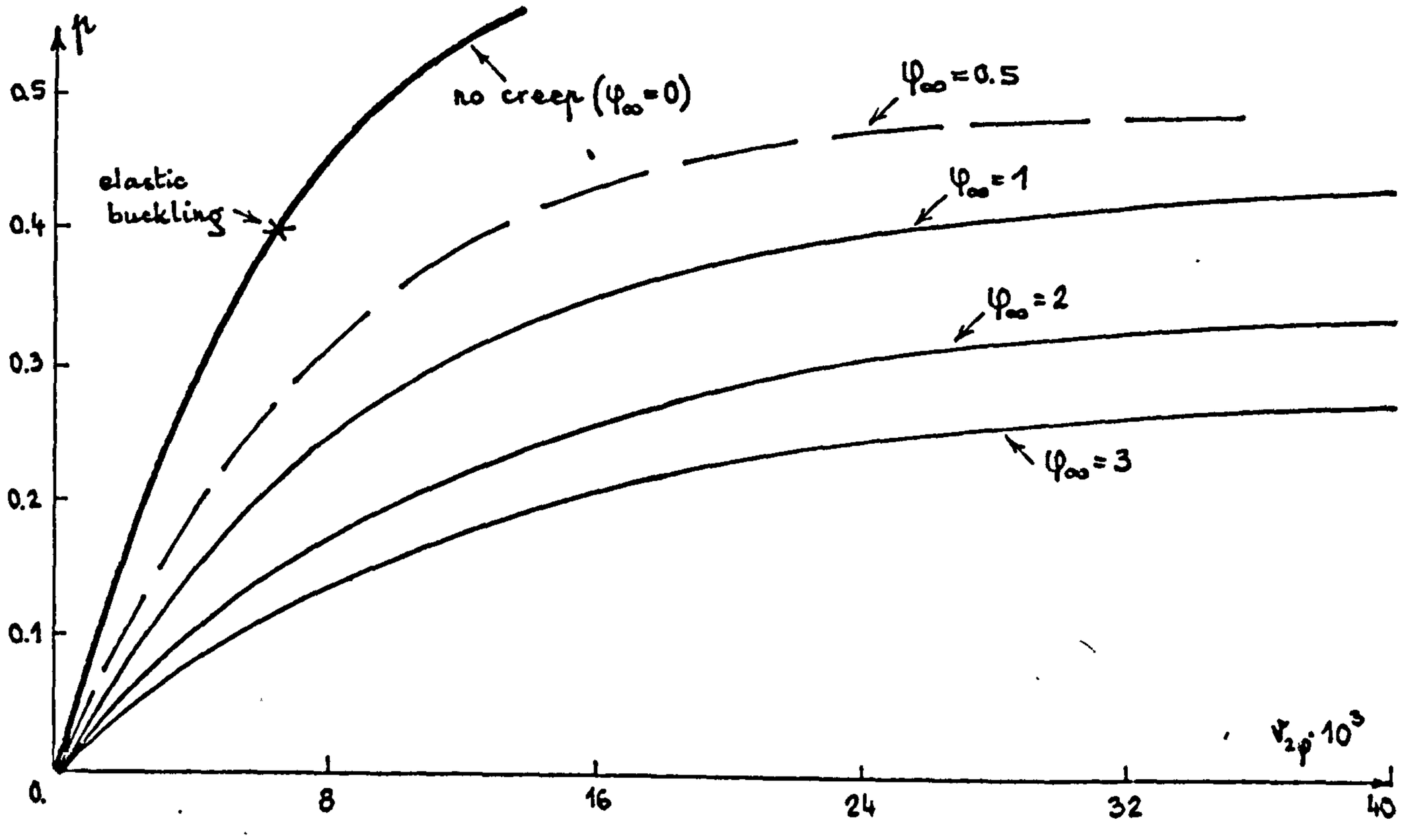

$\alpha_1 = 0.3$ rad.
$\alpha_2 = 0.1$ rad.
$c = 1$
$k = 1000$
$\mu_1 = \mu_2 = 1$

Fig. 5.33

The curves p versus $\nu_{2\varphi}$ and $\nu_{1\varphi}$ ($= \nu_{3\varphi}$) versus $\nu_{2\varphi}$ are plotted in Fig.5.33. Each curve correspond to a certain value of the final creep φ_∞. It can be seen that only when the final creep exceeds a certain limit the condition (5.83) yields a lower critical load than the elastic one. The curve depicting the values $\varphi_{cr\,p}$ corresponding to different p for the arch-model from Fig.5.33 is plotted in Fig.5.34. For convenience it is called curve II. Curve I associated with the 'elastic stability of creeping structure' is also depicted for comparison.

The point of intersection between the curve II and the axis $\varphi = 0$ corresponds to the elastic snap-buckling of the arch-model.

The curves from Fig.5.33 are descendent beyond the snap-point but that portion cannot be outlined by the approach described here.

c. Discussion and conclusion

The curves I and II from Fig.5.34 depicting the variation of the critical load with respect to the concrete creep are associated with the loading - paths (i) and (ii), respectively, from Fig.5.29.

In Figs.5.35 and 5.36 the same curves are plotted for the numerical data of the arch-models from Figs.5.7 and 5.9, respectively.

Curve I emerges from the point on the axis $\varphi = 0$ which corresponds to the elastic bifurcation of equilibrium, whereas curve II emerges from the point on the same axis which corresponds to the snap-buckling.

$\alpha_1 = 0.3$ rad.
$\alpha_2 = 0.1$ rad.
$c = 1$
$k = 1000$
$\mu_1 = \mu_2 = 1$

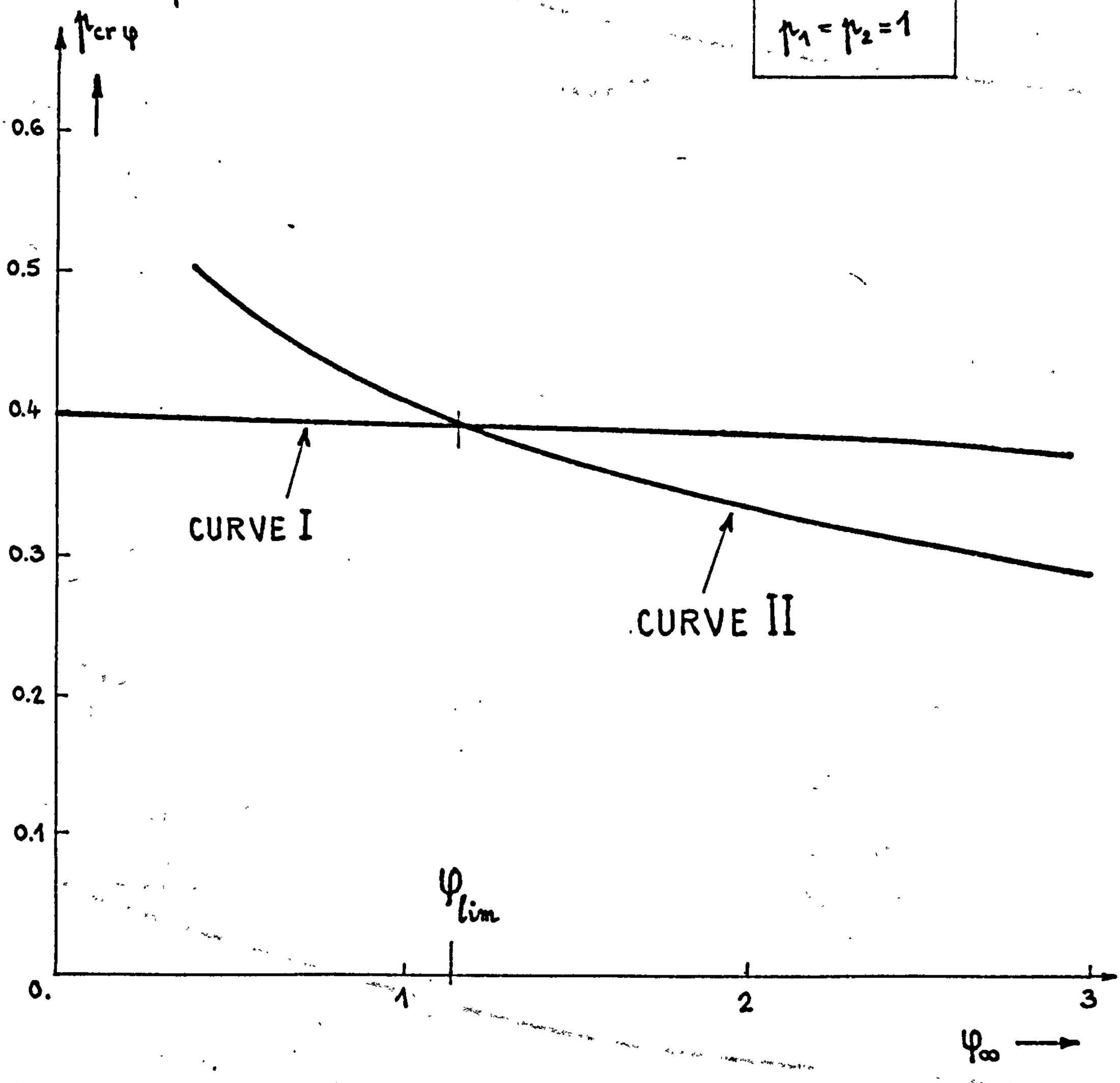

Fig. 5.34

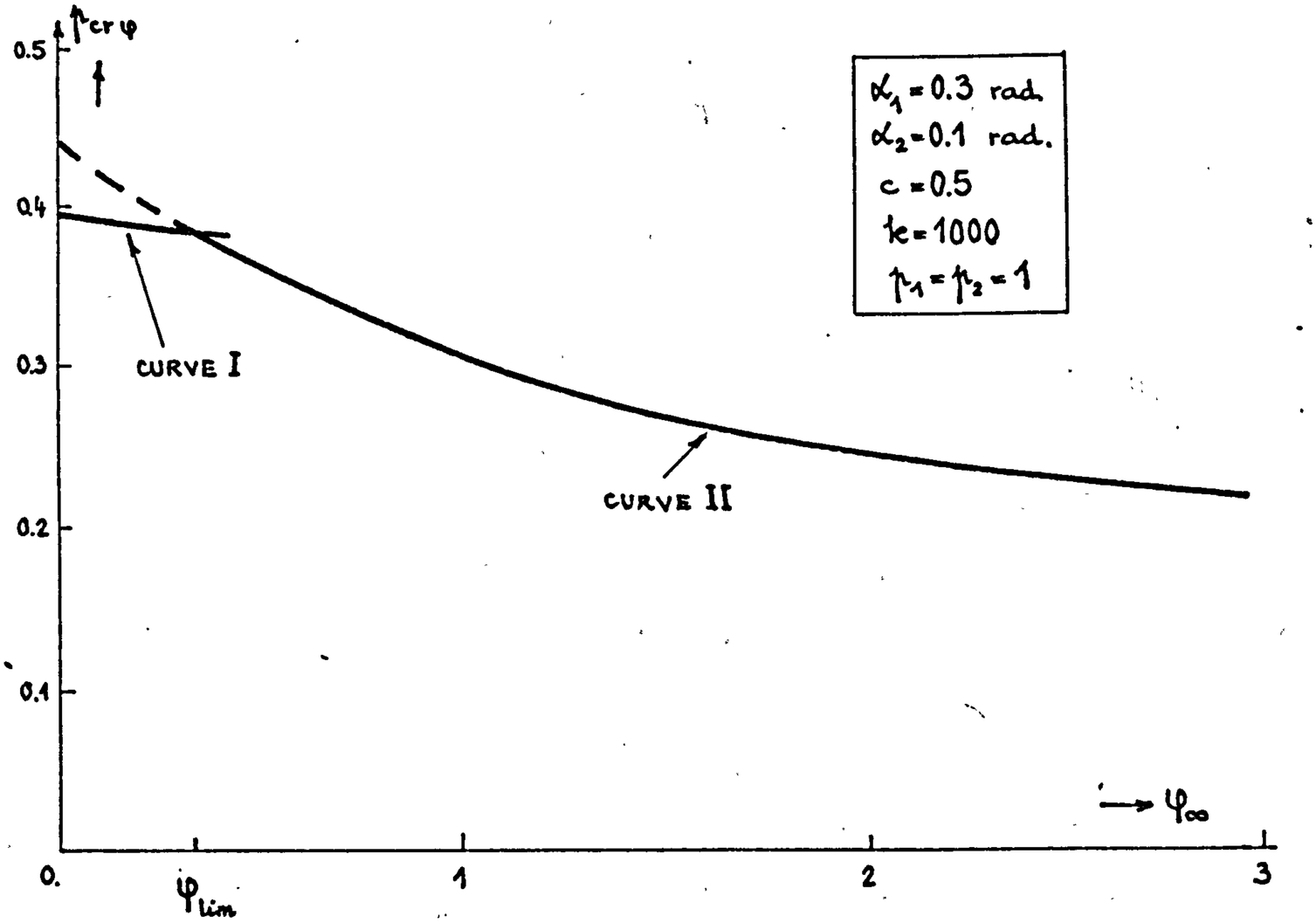

Fig. 5.35

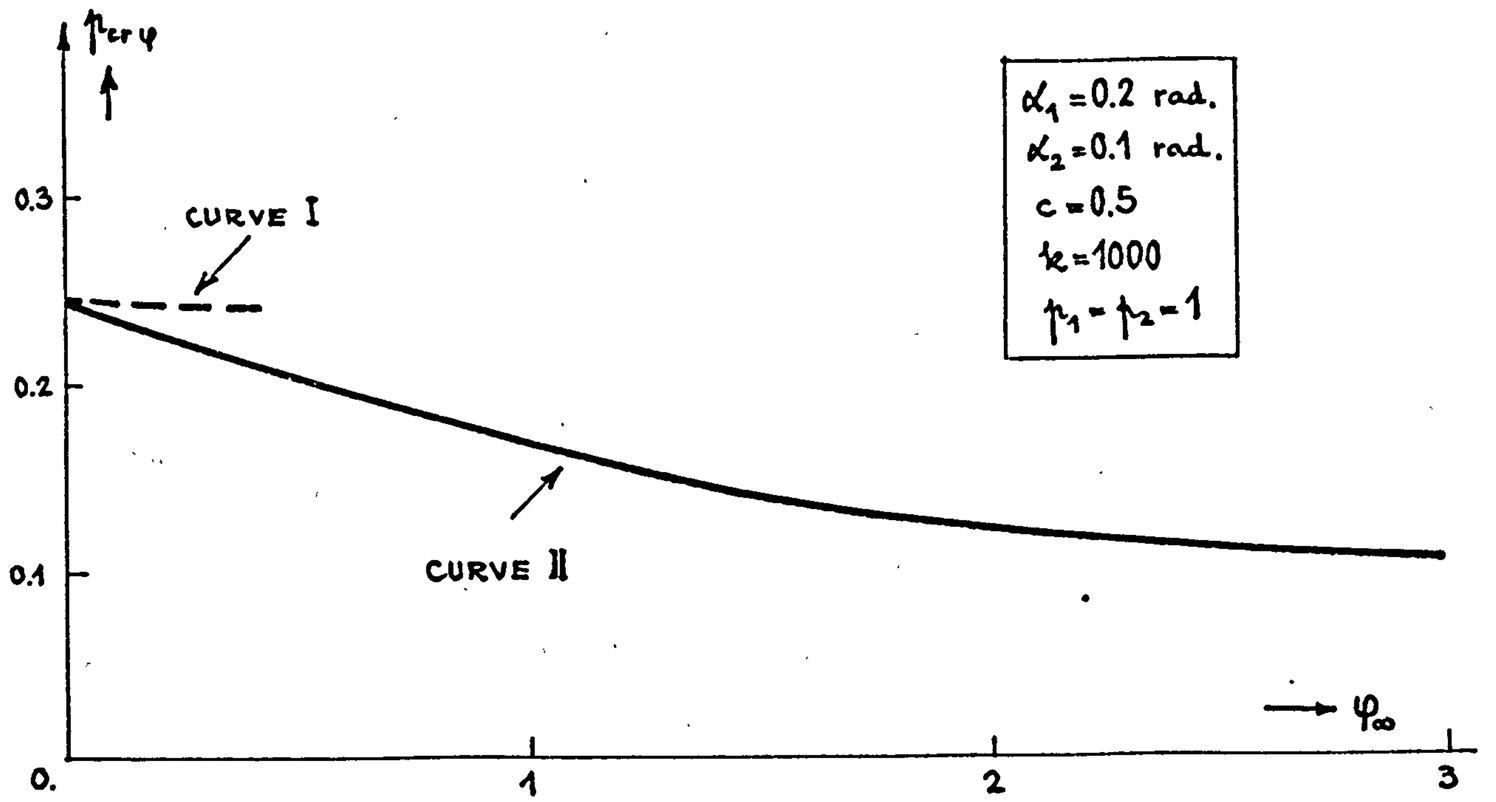

Fig. 5.36

Since the lowest critical load matters from a practical point of view, it follows that the critical load is provided by curve I for $\varphi < \varphi_{lim}$ and by curve II for $\varphi > \varphi_{lim}$.

The closer is the critical load corresponding to the elastic bifurcation to the critical load corresponding to the elastic snap-buckling, the smaller is the value of φ_{lim} in view of the sharper decay of curve II. As the instability of the arch-model analysed in Fig.5.36 is due to a snap-buckling (see Figs.5.9 and 5.13) solely curve II is depicted, that is $\varphi_{lim} = 0$.

Generally the more non-linear is the behaviour of an arch-model, the more significant is the decay of curve I and the more sensitive this curve is to the intensity of the sustained load p_o. On the other hand, in view of the same non-linearity, the critical load corresponding to the snap-buckling is closer to p_{cr} and consequently curve II emerges from a lower point (i.e. φ_{lim} is smaller).

The latter effect of the non-linear behaviour largely compensates for its former effect. In fact, since the initial portion curve I is insignificantly affected by non-linearity, it follows that curve I can well be approximated by a horizontal straight line emerging from p_{cr}.

Throughout this section the creep φ is used as independent variable describing the viscous behaviour of concrete. Nevertheless a critical time can be always associated with each φ_{cr} so long as the creep curve is known.

5.4 CORRESPONDENCE WITH ACTUAL ARCH-STRUCTURES

The mechanical arch-models are, in fact, approximations of actual arch-structures. The approximation is mainly because in an actual arch the bending and axial deformations are continuously distributed throughout its length, whereas in a mechanical model they are concentrated in discrete cross-sections linked by non-deformable members. In the arch-model from Fig.5.2 for instance, the bending rotations are concentrated in the joints B_i and the axial deformations are concentrated in the device A (i.e. the deformation U of the device A is associated with the axial deformation of an actual arch) so that the actual deformed state in Fig.5.37b is approximated by the deformed state plotted by the broken line.

One consequence of using the arch-model is that the load is also considered concentrated rather than distributed along the arch as is usually the case. Another consequence of using the arch-model is that the curved axis of the actual arch is replaced by a folded line although this should have little effect when a model with as many as three degrees-of-freedom is employed.

Within this section the relationships between the characteristic values of the arch-model from Fig.5.2 and their correspondents in an actual arch are derived. Then a comparison is carried out between the elastic critical loads resulting from existing closed-form solutions for some particular arch-structures and from the elastic analysis of the corresponding arch-model.

a. ACTUAL ARCH

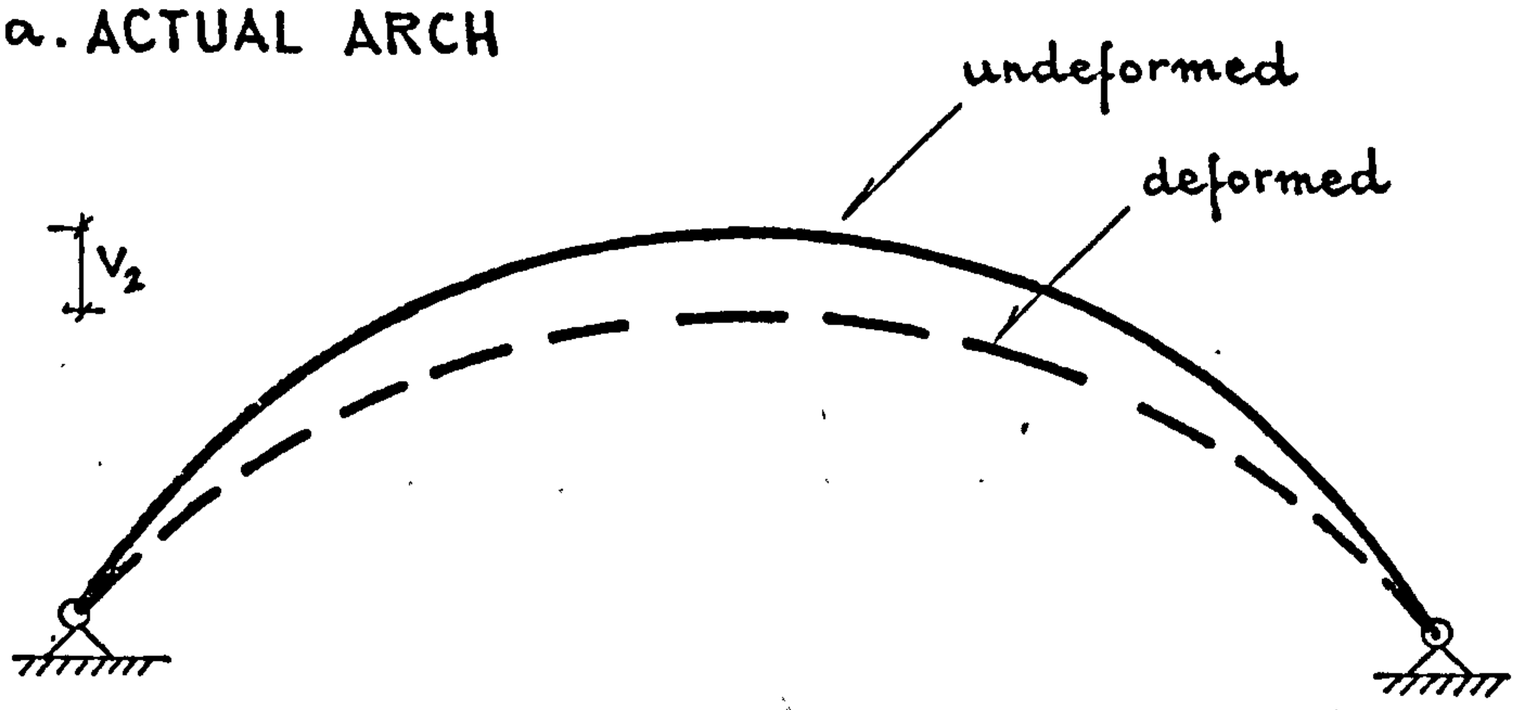

b. ARCH-MODEL

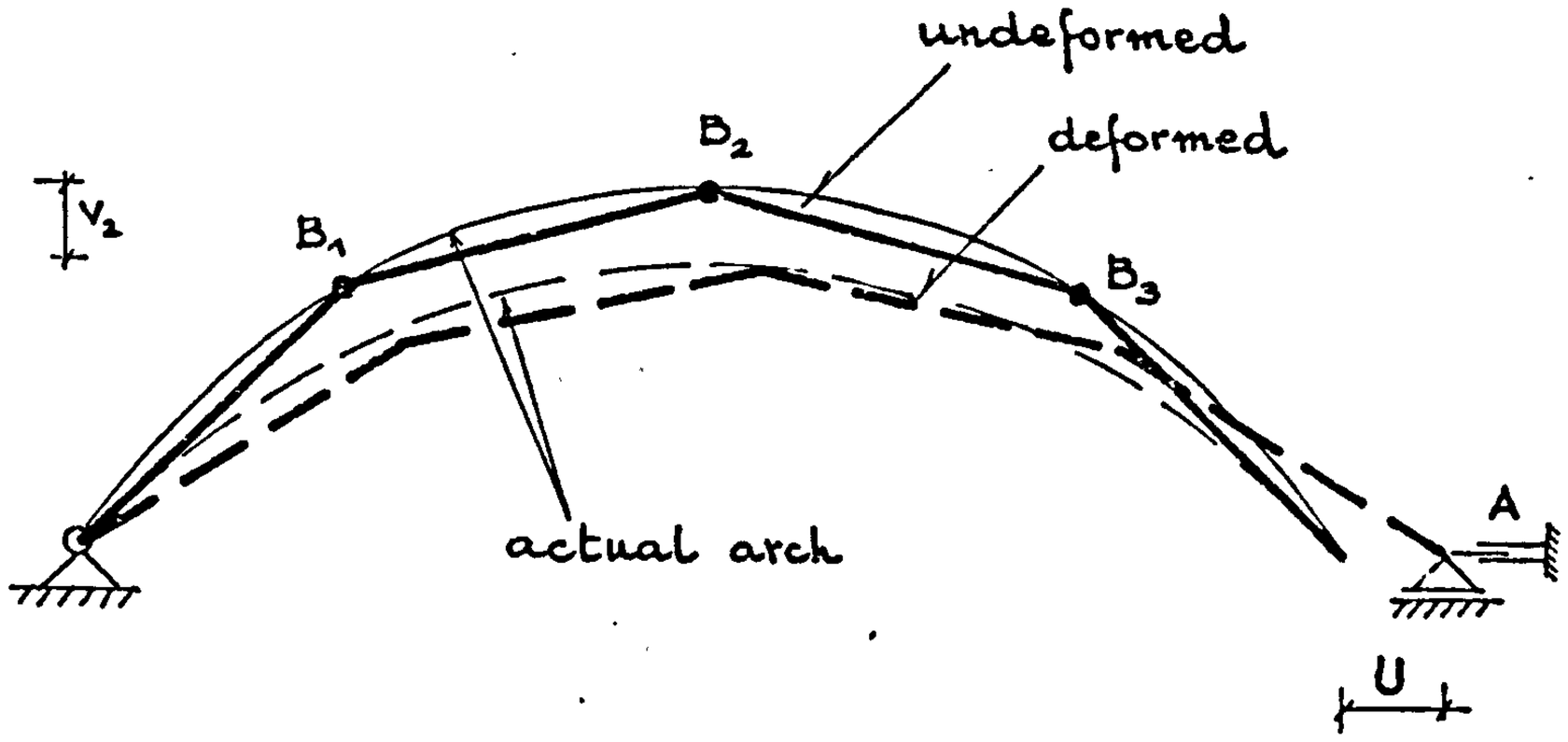

Fig. 5.37

Finally possibilities of improving the arch-model in order to approximate better the actual structures are presented and discussed.

5.4.1 MECHANICAL AND LOADING PARAMETERS.

The correspondence between the arch-model from Fig.5.2 and the double-hinged supported arch from Fig.5.38a is presented below.

The change in the total potential energy when the elastic arch is loaded is

$$\Delta\Pi^* = \frac{1}{2}\int_{H_1}^{H_2} M^*\psi^* ds + \frac{1}{2}\int_{H_1}^{H_2} N^*\cos\theta^* U^* dx - p\int_{H_1}^{H_2} Q^*V^* dx \quad (5.86)$$

where M^*, N^* are the forces in arch

V^* is the vertical displacement of the arch

ψ^*, U^* are the angular and axial deformations of the cross-section (see Fig.5.38b)

Q^* defines the load variation ($Q^*=1$ when the load is uniformly distributed)

p is the factor of proportionality of loading.

On account of elastic behaviour

$$M^* = EI^*\psi^*$$
$$N^*\cos\theta^* = EA^*U^* \quad (5.87)$$

where I^* and A^* are the second order moment and the area of the cross-section.

The superscript '*' indicates a value associated with the actual arch. All these values vary from one cross-section to another.

In order to be able to replace the continuous arch

a.

$$q = p \cdot Q^*$$

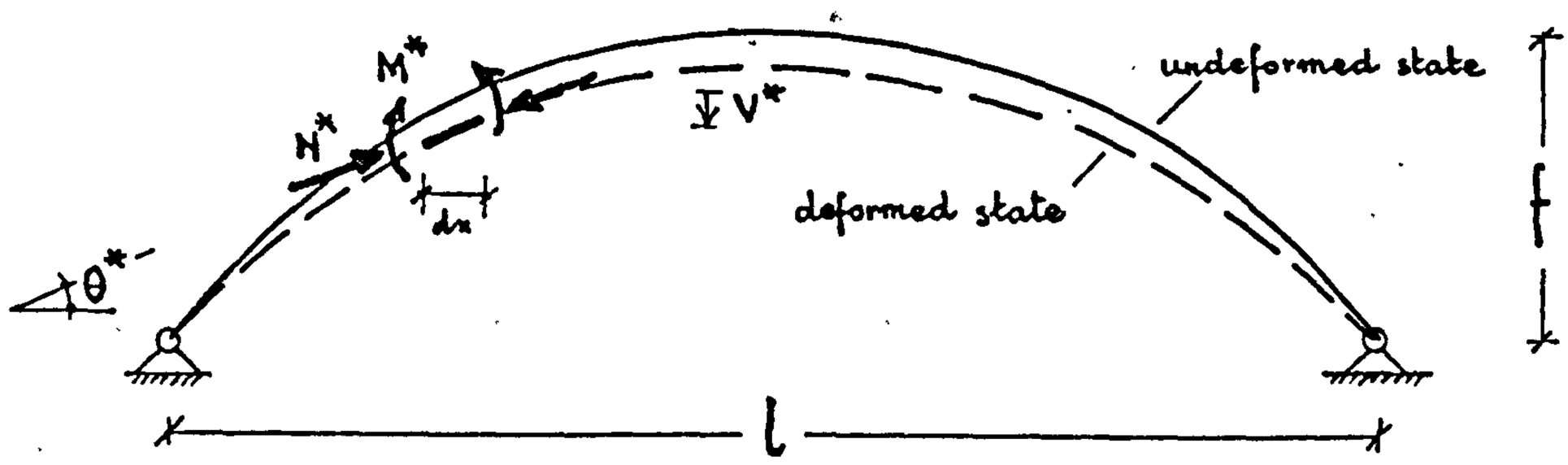

b.

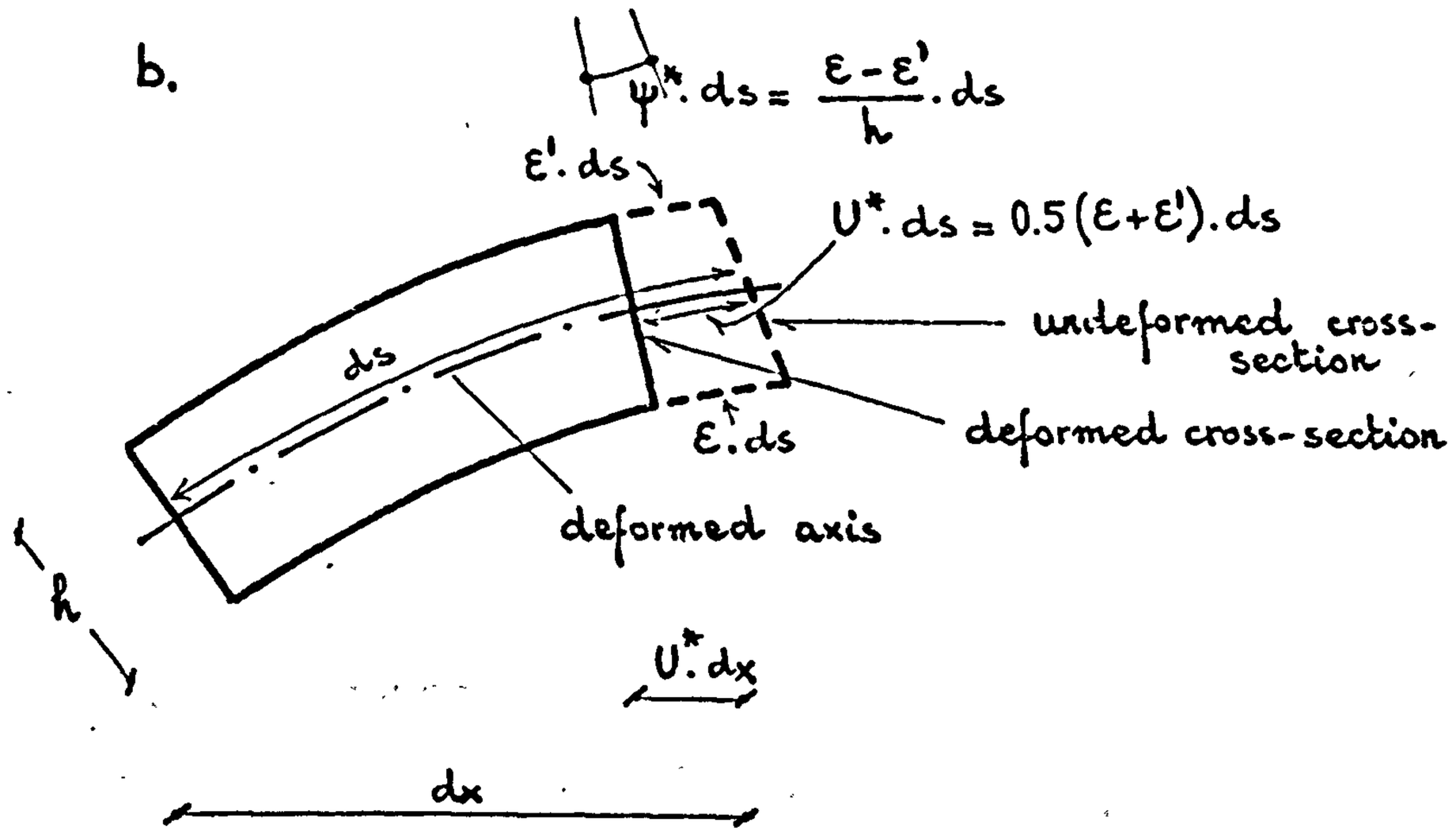

Fig. 5.38

with a discrete arch-model one assumes that the forces and the stiffness characteristics are replaced by their mean values along a segment $a_i b_i$ (see Fig.5.39a). Thus if

i) M_i is the mean value of the bending moments M^* between a_i and b_i

ii) F is the mean value of $N^* \cos\theta^*$ between H_1 and H_2

iii) I_i is the mean value of I^* between a_i and b_i

iv) A is the mean value of A^* between H_i and H_2

v) V_i is the mean value of V^* between a_i and b_i,

eq.(5.86) can be recast as [1]

$$\Delta\Pi^* = \frac{1}{2}\sum_{i=1}^{3} M_i \cdot \int_{a_i}^{b_i} \psi^* ds + \frac{1}{2} F \int_{H_1}^{H_2} U^* dx - p \sum_{i=1}^{3} V_i \cdot \int_{a_i}^{b_i} Q^* dx \qquad (5.88)$$

and eq.(5.87) can be written as

$$M_i = \frac{EI_i}{L} \int_{a_i}^{b_i} \psi^* ds \qquad i = 1...3$$

$$F = \frac{EA}{\ell} \int_{H_1}^{H_2} U^* ds \qquad (5.89)$$

Introducing the notation

Footnote

1) Eq.(5.88) assumes that the bending potential energy of segments $H_1 a_i$ and $b_3 H_2$ in Fig.5.39a can be neglected.

$$\psi_i = \int_{a_i}^{b_i} \psi^* \, ds \qquad i = 1...3$$

$$U = \int_{H_1}^{H_2} U^* \, dx \qquad (5.90)$$

$$\bar{P}_i = \int_{a_i}^{b_i} Q^* \, dx \qquad i = 1...3$$

eq.(5.88) yields

$$\Delta\Pi^* = \frac{1}{2} \sum_{i=1}^{3} M_i \psi_i + \frac{1}{2} F.U - \gamma \sum_{i=1}^{3} \bar{P}_i . V_i \qquad (5.91)$$

whereas eqs.(5.89) yield

$$M_i = \frac{EI_i}{L} . \psi_i \qquad i = 1...3$$

$$F = \frac{EA}{\ell} . U \qquad (5.92)$$

It can be seen that eqs.(5.91) and (5.92) are identical with eqs.(5.2) and (5.3), respectively, where

$$K_i = \frac{EI_i}{L} \qquad (5.93)$$

$$D = \frac{EA}{\ell}$$

In other words, eqs.(5.91) and (5.92) show that an actual arch such as that in Fig.5.39a can be replaced approximately by an arch-model like that in Fig.5.2 by using the above assumptions (i)...(v) and the stiffnesses (5.93).

The forces M_i and F of the arch-model will represent

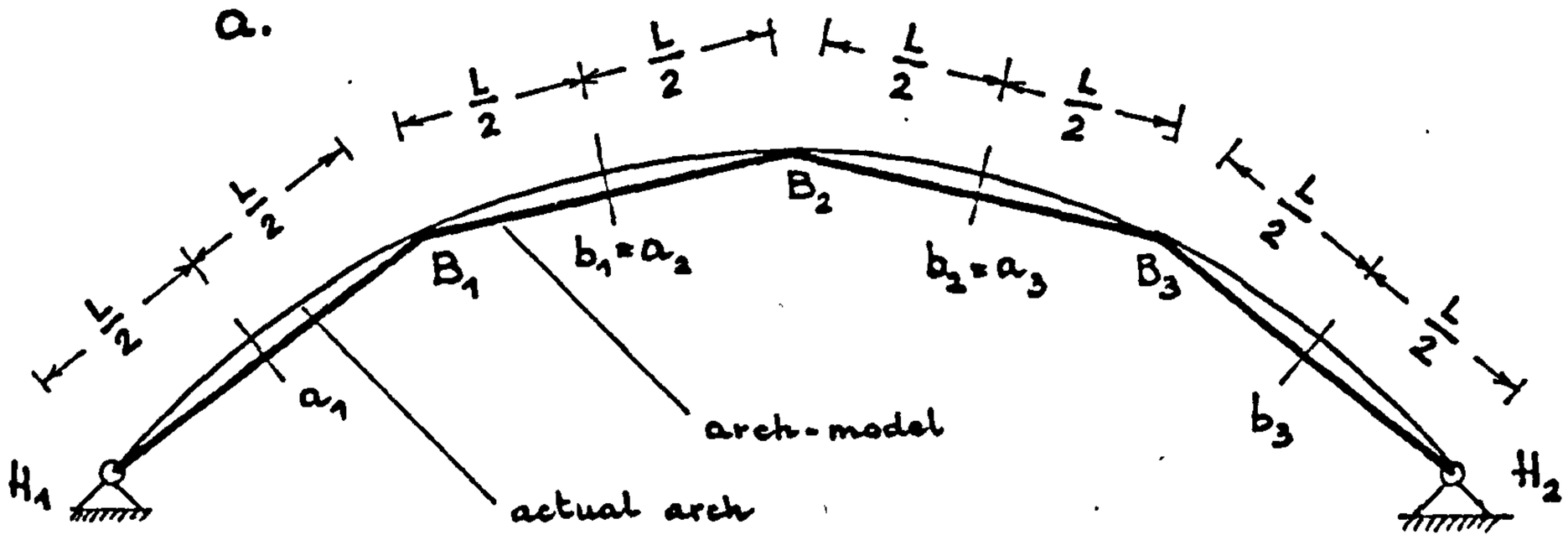
a.
L/2
L/2
L/2
L/2
L/2
L/2
L/2
L/2
B1
B2
B3
b1=a2
b2=a3
a1
b3
H1
H2
arch-model
actual arch

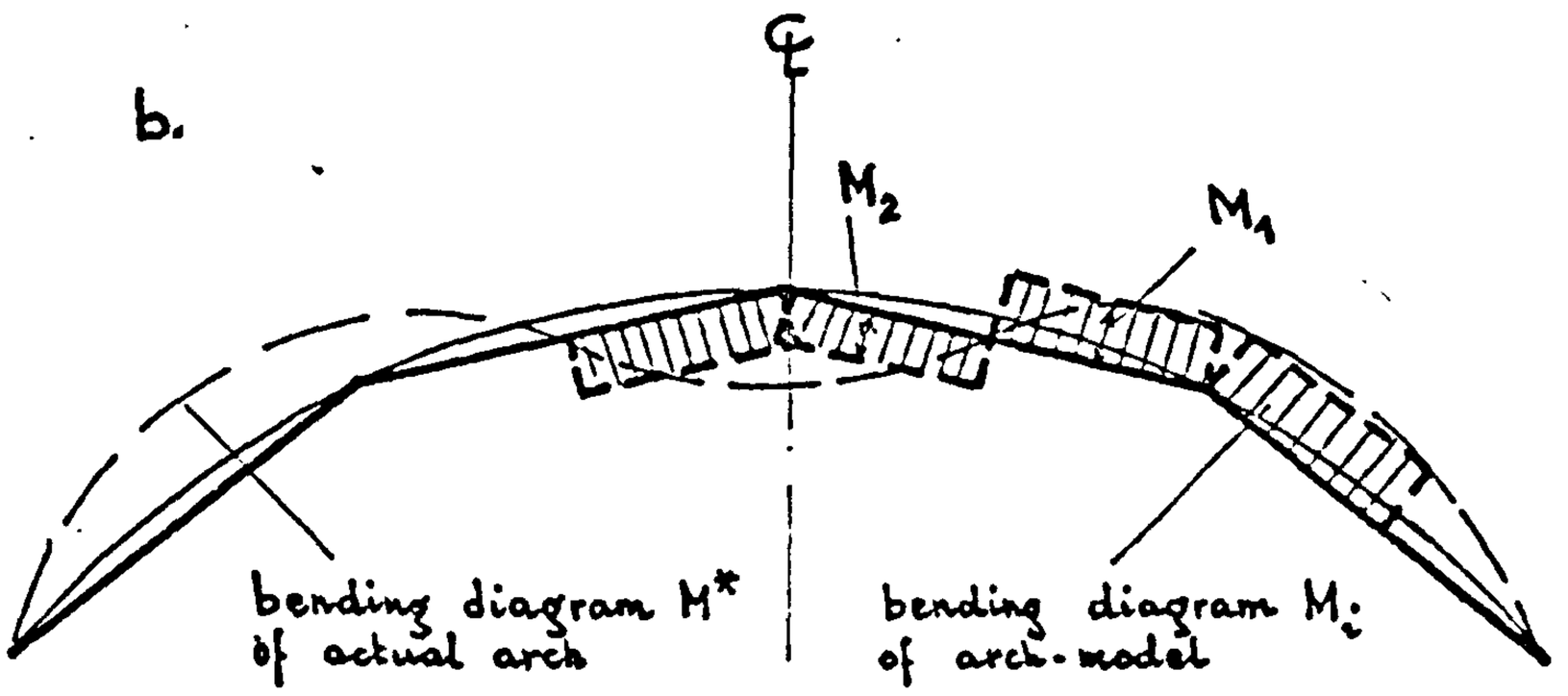
b.
M2
M1
bending diagram M*
of actual arch
bending diagram Mi
of arch-model

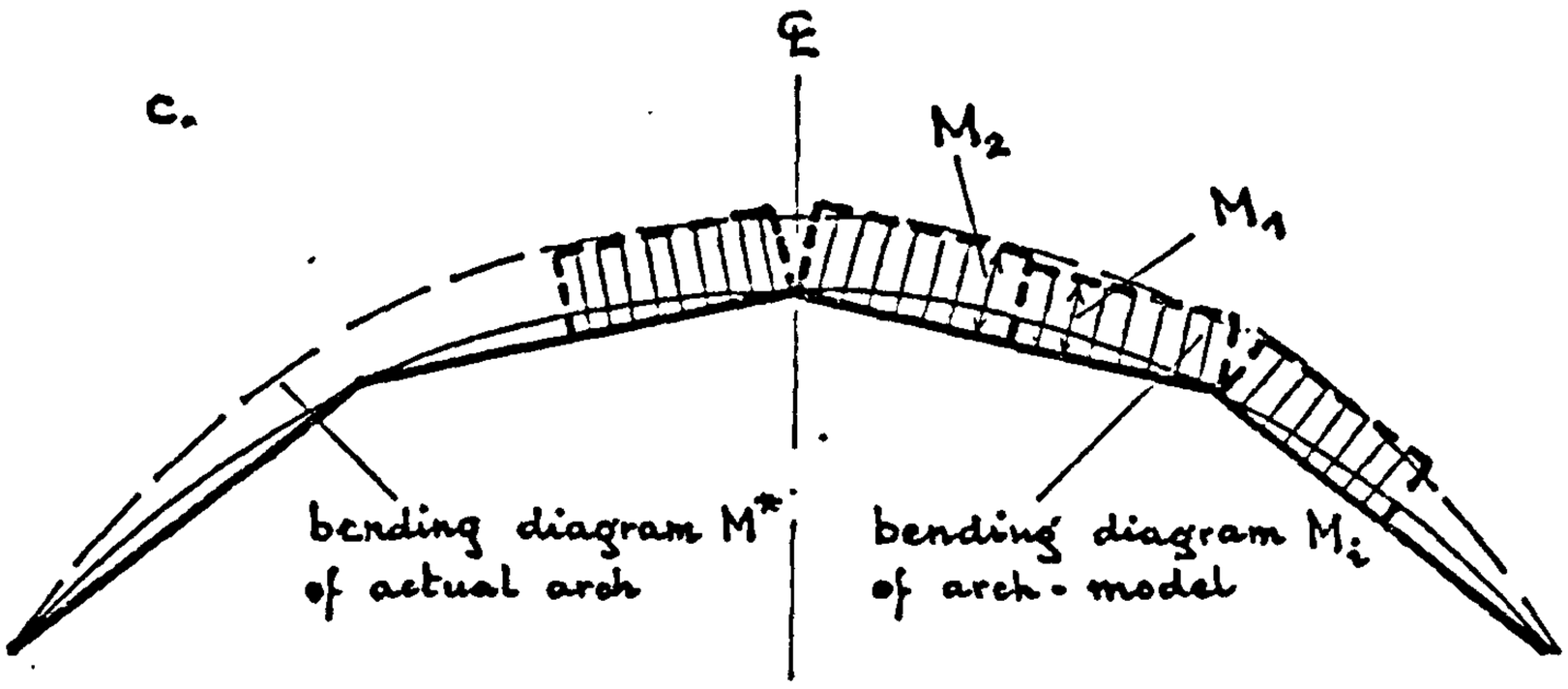
c.
M2
M1
bending diagram M*
of actual arch
bending diagram Mi
of arch-model

Fig. 5.39

the mean-values of the actual bending moments and axial forces of the continuous arch while the displacements ψ_i and U of the arch-model will represent the sums of the actual angular and axial deformations over lengths equal to $a_i b_i$ and $H_1 H_2$ respectively.

The closer are the constant values M_i and I_i to the actual variations of M^* and I^* along the segment $a_i b_i$ and the closer are the constant values F and A to the actual variations of $N^* \cos\Theta$ and A^* along the arch length $H_1 H_2$, the less approximate are the results provided by the arch-model.

For instance, two M^* - diagrams which are fairly well approximated by constant values of M_i are plotted in Figs. 5.39b and c.

The mechanical parameters c_i and k and the loading parameters p and p_i from eqs(5.4) can be associated with their corresponding parameters of the actual arch by using eqs.(5.90) and (5.93). The parameter p has the same meaning as in Fig.5.38, whereas

$$c_i = \frac{K_i}{K_1} = \frac{I_i}{I_1}$$

$$k = \frac{DL^2}{K_1} = \frac{A\ell^2}{I_1} \cdot \left(\frac{L}{\ell}\right)^3 = \lambda_1 \beta^3 \qquad (5.95)$$

$$p_i = \frac{\bar{P}_i L}{K_1} = \frac{L^2}{EI_1} \cdot \int_{a_i}^{b_i} Q^* dx$$

In eqs.(5.95) λ_1 is the slenderness of the arch relative to the rigidity of the cross-section B_1, that is

$$\lambda_1 = \frac{\ell}{\sqrt{\frac{I_1}{A}}} \qquad (5.96)$$

while, for the arch-model from Fig.5.2,

$$\beta = \frac{1}{2\cdot(\cos\alpha_1 + \cos\alpha_2)} \simeq 0.25 \qquad (5.97)$$

i) Constant load If the load is uniformly distributed $Q^* = 1$ and

$$f_i = \frac{l^3}{EI_i} \qquad (5.98)$$

ii) Arch with a constant, rectangular cross-section

If b and h are the width and the depth of the cross-section then

$$I_i = I^* = \frac{bh^3}{12}$$

$$A = A^* = bh$$

$$\lambda_1 = \frac{\ell}{h}\sqrt{12} = \lambda\sqrt{12} \qquad (5.99)$$

$$c_i = 1$$

$$k = 12\lambda^2\beta^3$$

where, similar to eq.(4.47),

$$\lambda = \frac{\ell}{h} \qquad (5.100)$$

Table 5.3 gives the k-values when $\lambda = 10....100$ and when β corresponds to f/l = 1/8...1/13 with $\alpha_1/\alpha_2 = 3$ (see Fig.5.4).

Table 5.3

Numerical values of k associated with the practical range of λ and β.

$\lambda = 1/h$	k when			
	$\beta = 0.26$ (f/l=1/8)	$\beta = 0.256$ (f/l=1/10)	$\beta = 0.254$ (f/l=1/13·3)	$\beta = 0.25$
10	21	20	20	19
20	84	81	79	75
30	185·5	178	174	166
40	336	322	315	300
50	525	504	492	469
60	756	726	708	675
73	1119	1074	1049	1000
100	2100	2016	1968	1877

The non-dimensional parameters n and m defined in eq.(4.31) can be computed for the arch-model so that

$$n_j = \frac{N_j}{bhf_c'} = \bar{N}_j \cdot \frac{E_c}{12f_c'} \cdot \frac{1}{(\beta\lambda)^2} \qquad j=1,2$$

$$m_i = \frac{M_i}{bh^2f_c'} = \bar{M}_i \cdot \frac{E_c}{12f_c'} \cdot \frac{1}{\beta\lambda} \qquad i=1,2,3 \qquad (5.101a)$$

or, using k rather than λ,

$$n_j = \bar{N}_j \cdot \frac{E_c}{f_c'} \cdot \frac{\beta}{k} \qquad j=1,2$$

$$m_i = \bar{M}_i \cdot \frac{E_c}{f_c'\sqrt{12}} \cdot \sqrt{\frac{\beta}{k}} \qquad i=1,2,3 \qquad (5.101b)$$

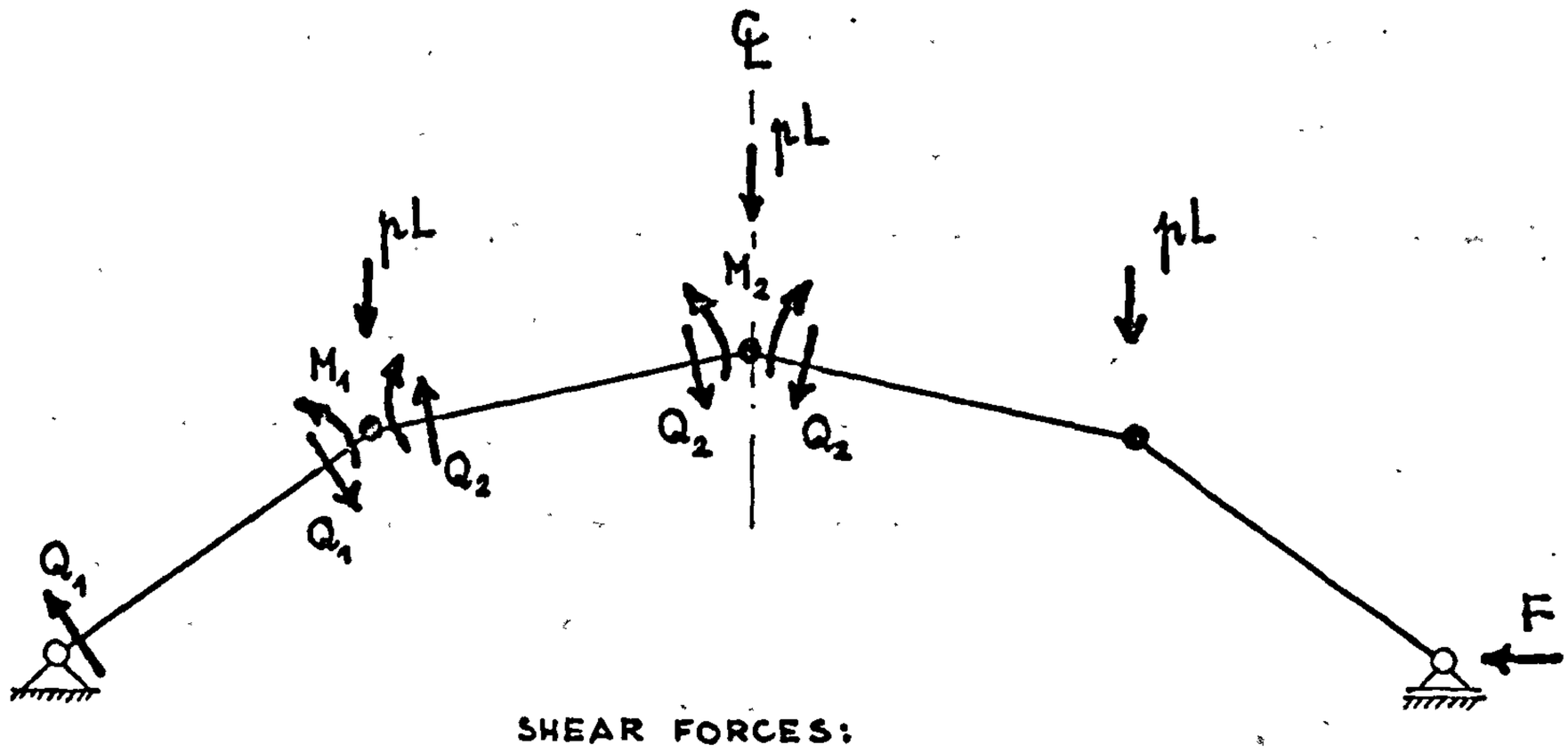

SHEAR FORCES:

$$Q_1 = \frac{M_1}{L}$$

$$Q_2 = \frac{M_2 - M_1}{L}$$

JOINT B_2

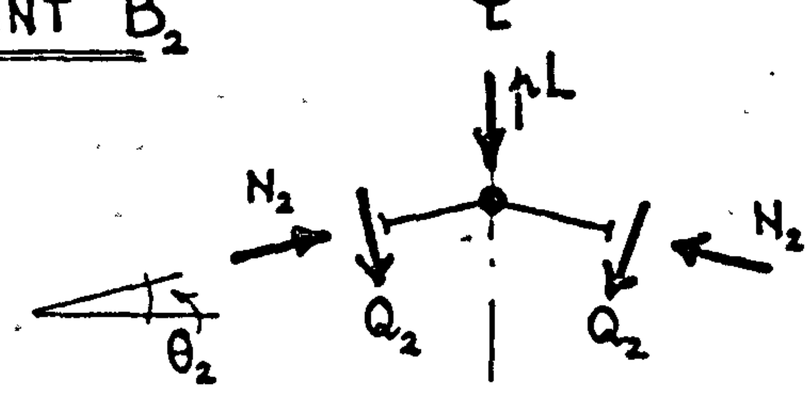

$$N_2 \cdot \sin\theta_2 = 0.5\,\mu L + Q_2 \cdot \cos\theta_2$$

JOINT B_1

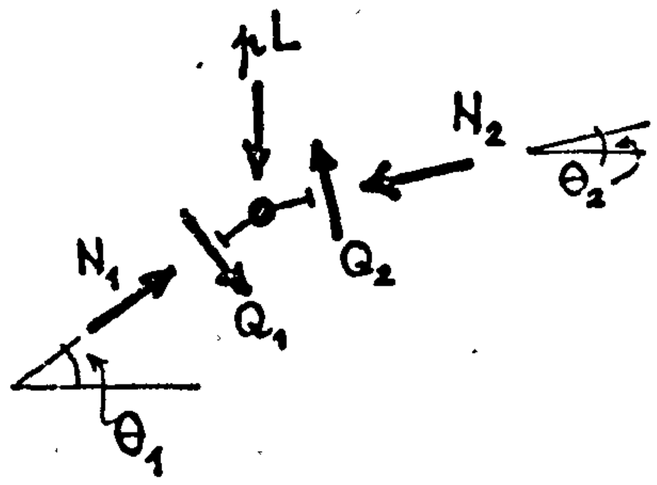

$$N_1 = \mu L \cdot \sin\theta_1 + N_2 \cdot \cos(\theta_1 - \theta_2) - Q_2 \cdot \sin(\theta_1 - \theta_2)$$

Fig. 5.40

In eqs.(5.101)

f'_c is the concrete strength in compression

E_c is the modulus of elasticity of concrete

$\bar{M}_i = c_i \cdot \psi_i$, according to eqs.(5.74) and (5.3)

$\bar{N}_j$ is the non-dimensional axial force in member j of the arch-model

M_i is the bending moment in joint B_i

N_j is the axial force in member j,

where N_j can be computed using the equilibrium of internal forces at the joint B_i (see Fig.5.40), and

$$N_j = \frac{EI}{L^2} \bar{N}_j \qquad j = 1,2$$

$$M_i = \frac{EI}{L} \bar{M}_i \qquad i = 1...3 \qquad (5.102)$$

5.4.2 COMPARISON WITH CLOSED-FORM SOLUTIONS

A comparison of the elastic critical loads and of modes of buckling obtained from known closed-form solutions and from the present arch-model is presented.

Two buckling problems are considered for which closed-form solutions are provided by Timoshenko and Gere (1961):

i) the buckling of double and triple hinged arches having a negligible axial deformability.

ii) the buckling of a double hinged arch when the initial shape is very flat (f/l very small)

In both cases a constant transverse load, a circular arch and a uniform cross-section are assumed.

It is worth emphasising that the mechanical arch-models have been devised chiefly in order to analyse the post-buckling behaviour. Nevertheless the present comparison

will prove that the three degree-of-freedom model from Fig.5.2 yields elastic critical loads which are in fairly good agreement with those provided by closed-form solutions and indicates the same mode of buckling as the analytic procedures.

Since the mechanical models with less degrees of freedom than three are not able to outline all the possible modes of buckling associated with an actual arch, it follows that the three degree-of-freedom arch-model provides the simplest approach to the analysis of actual arches having the flexibility continuously distributed along their length.

These facts suggest that the arch-model could be used to analyse approximately the buckling of actual arch-structures for which closed-form solutions cannot be found in view of the mathematical difficulties.

a. Buckling of circular arches with inextensible axis

Due to the assumption of inextensibility, the work done by the axialforces is neglected when the closed-form solution is computed*) and this weakness of the theoretical approach is required in order to simplify the mathematical solution.

When the arch-model from Fig.5.2 is employed, it is not possible to consider an infinite axial stiffness since

---

Footnote

*) see Timoshenko and Gere (1961) pp.297-302

that means $k=\infty$ from the second of equations (5.95). Nevertheless choosing a large value for k (i.e. a large slenderness λ), the effects of the axial shortening are much smaller than those of the bending rotations and hence a situation close to that assumed by the theoretical solution should arise.

The results of the numerical analysis are compared in Table 5.4. The instability of the arch-model is due to the same mode of buckling as that provided by the closed-form solution.

The value k=1000 corresponds to a slenderness $\lambda \simeq 70$ for the range of f/l=1/10...1/15 (see Table 5.3).

The agreement of the elastic critical loads from Table 5.4 is fairly good except for the triple-hinged arch. The large difference recorded with this arch is due to the fact that the bending diagram of the triple-hinged arch cannot be properly approximated by the discrete moments M_i in the arch-model (see discussion from Section 5.4.1 associated with Fig.5.39). In all cases the critical loads provided by the arch-model are smaller than those supplied by the closed-form solutions and this is partially due to the effect of axial deformability in the arch-model analysis.

b. Buckling of a very flat curved bar

The results provided by the arch-model and by a closed-form solution*) are compared for a double hinged

---

Footnote

*) see Timoshenko and Gere (1961), pp.305-310

Table 5.4

Type of arch and buckling mode	$\frac{f}{l}$	Numerical data				Critical load $(\frac{q_{cr} l^3}{EI})$	
		α_1 (rad)	α_2 (rad)	c	k	acc. to Timoshenko and Gere	acc. to arch-model
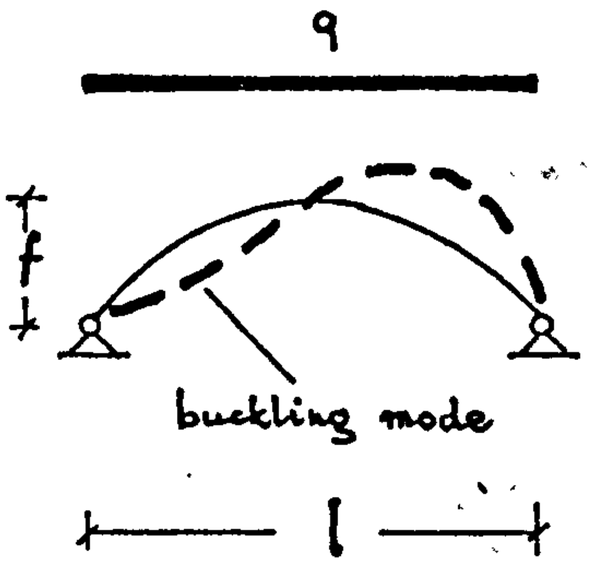	1/15	0.2	0.067			18.8	16.2
	1/13.3	0.225	0.075	1	1000	22.6	18.2
	1/10	0.3	0.1			28.6	23.6
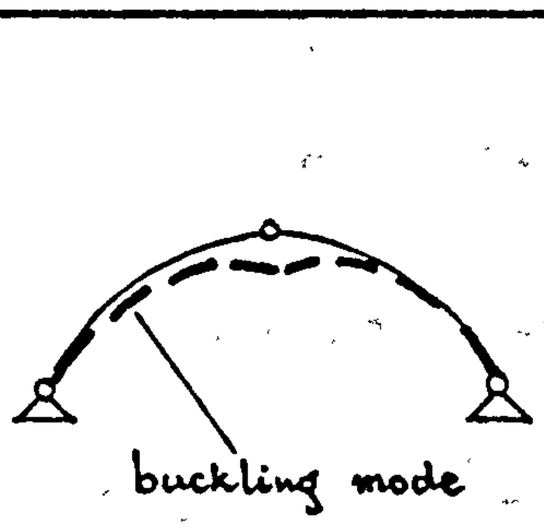	1/10	0.3	0.1	0	1000	23.4	15.8

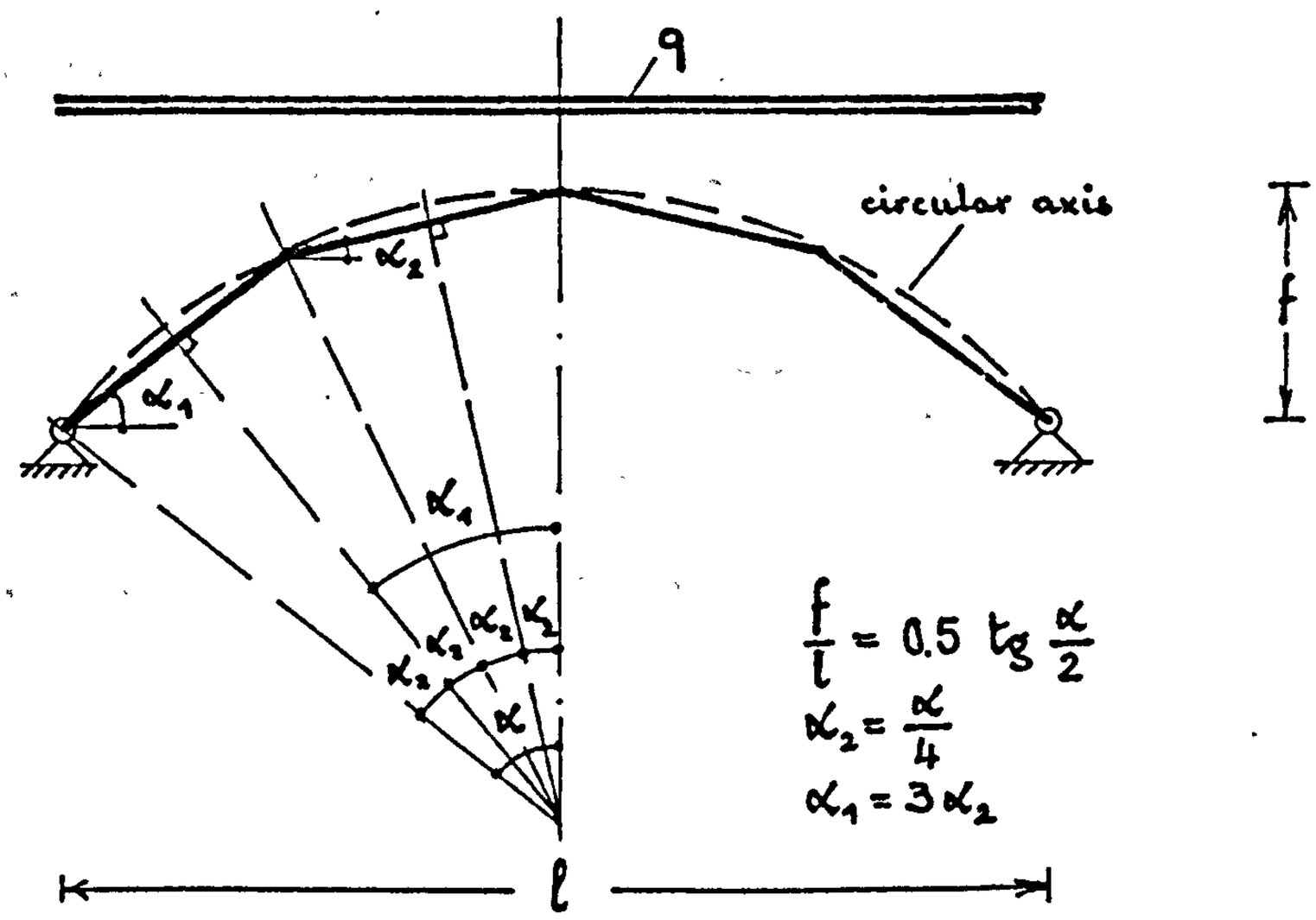

Fig. 5.41

circular bar having a uniform cross-section and

$$\frac{f}{\ell} = \frac{1}{30} \qquad (\alpha = 0.1334 \text{ rad in Fig.5.41})$$

$$\lambda = 40$$

From Fig.5.41 it arises that

$$\kappa_1 = \frac{3\alpha}{4} = 0.1 \text{ rad.}$$

$$\kappa_2 = \frac{\alpha}{4} = 0.033 \text{ rad.}$$

With these numerical values and

$$k = 12 \quad \lambda^2\beta^3 = 300$$

$$c = 1.0$$

$$p_1 = p_2 = 1.0$$

the arch-model analysis yields

$$q_{cr} = 6.30 \frac{EI}{\ell^3}$$

whereas the closed-form solution yields

$$q_{cr} = 7.78 \frac{EI}{\ell^3}$$

In both analyses the mode of buckling is a general snap, that is a simultaneous snap-buckling of joints B_i, $i = 1..3$.

5.4.3 LIMITATIONS AND POSSIBILITIES OF IMPROVEMENT.

When compared with a continuous, reinforcement concrete arch, two classes of approximations are associated with the solution presented in Section 5.3 for the arch model from Fig.5.2:

i) approximations arising from the fact that the continuously deformable arch-structure is replaced by a discretely deformable arch-model, and

ii) approximations related to the idealisation of the material behaviour.

The first class of approximations has been presented and discussed within Section 5.4.1. It has shown that when a discrete arch-model as that in Fig.5.1 is employed to approximate a continuously deformable arch, the following approximations are introduced (see Figs.5.4, 5.38 and 5.39a):

- the bending rotation ψ_i of the joint B_i represents the sum of the angular deformations ψ^* of all cross-sections of the actual arch between a_i and b_i

- the bending moment M_i in the joint B_i represents the mean value of the bending moments M^* in the actual arch between a_i and b_i

- the bending stiffness of the joint B_i represents the mean value of the bending stiffnesses of all cross-sections of the actual arch between a_i and b_i

- the axial displacement U of the device A represents the sum of the horizontal deformations U^* of all the cross-sections of the actual arch, i.e. between H_1 and H_2

- the axial force F in the device A represents the mean value of the horizontal projection $N^* \cos \theta^*$ of all the axial forces N^* in the actual arch, i.e. between H_1 and H_2

- the axial stiffness of the device A represents the mean value of the axial stiffness of all cross-sections

of actual arch, i.e. between H_1 and H_2

- the curved axis of the actual arch is replaced by a folded axis and the angles α_1 and α_2 are computed to ensure a good agreement of the two axes

- the commonly uniform load q between a_i and b_i is replaced by its resultant and the force is applied at joint B_i; only vertical loads are considered.

- the loading and deformability of the actual arch between H_1 and a_1 and between b_3 and H_2 are neglected.

The increase of the number of joints B_i will improve the approximations associated with the bending stiffness but will have no impact on the approximations related to the axial stiffness.

A consequence of this rougher approximation of axial deformability of the actual arch will be that modes of buckling and secondary paths associated with local instability, like that plotted in Fig.5.42, will not be properly emphasised by the arch-model. Nevertheless local buckling is more common with shells than it is with arches.

A possibility of improving this deficiency of the arch-model is to attach an axial device to each non-deformable member so that each joint AB_i in Fig.5.43 will be similar to the device B_i in Fig.5.3 but at the same time will partially restrain the axial displacement.

It is noteworthy that the increase of the number of degrees-of-freedom should not affect significantly the 'exact' analysis of the arch-model, as it is presented

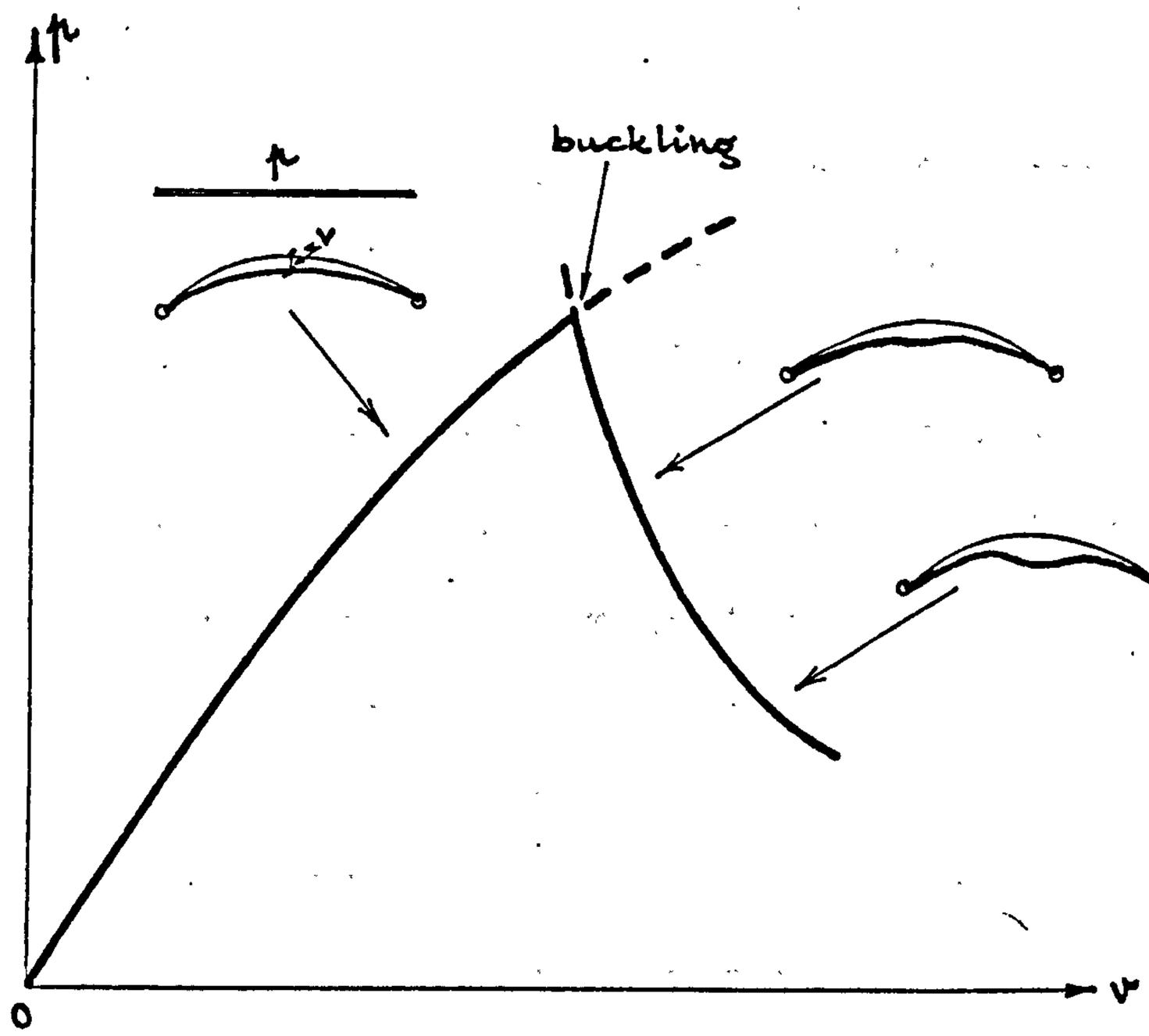

Fig. 5.42

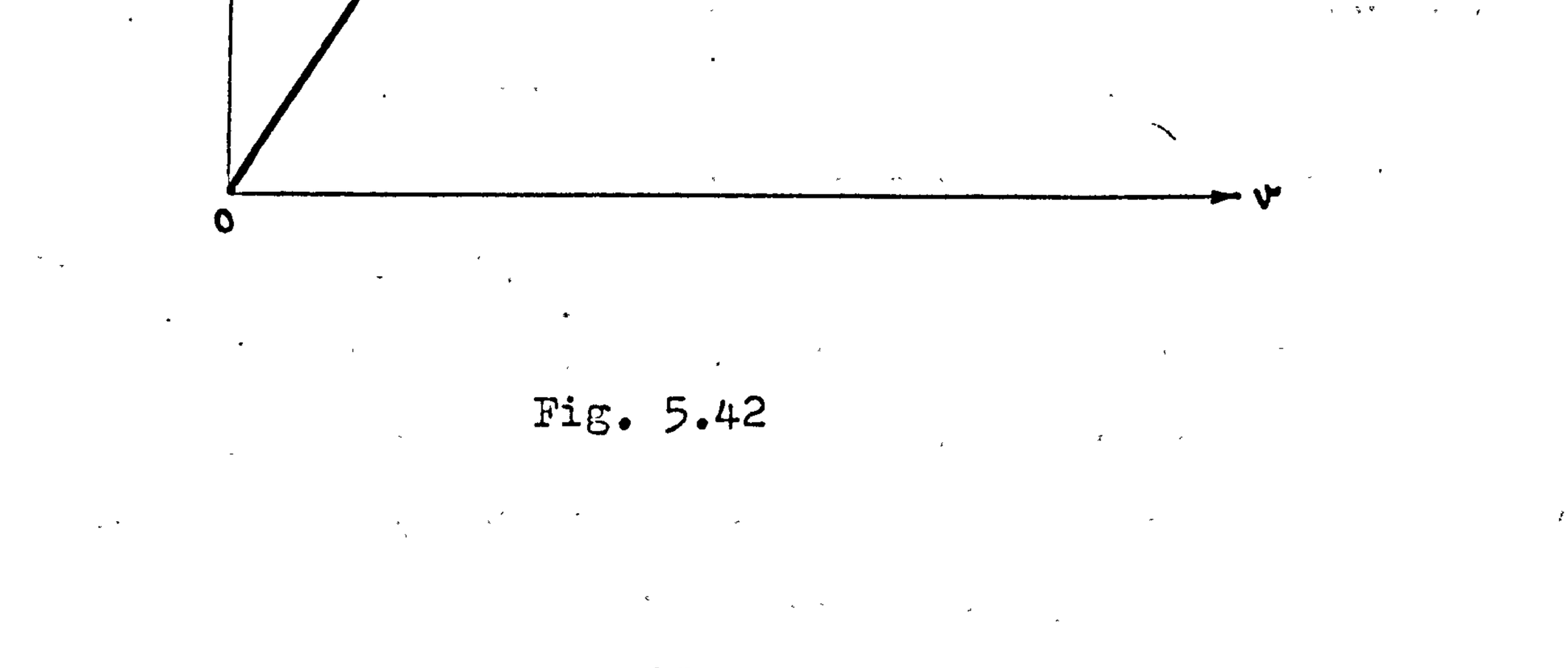

Fig. 5.43

in Section 5.3, but can increase significantly the mathematical difficulties associated with the 'approximate' solution.

The above class (ii) of approximations is connected with the assumptions relative to the material behaviour and presented in Section 5.3.2. An ideal viscoelastic behaviour has been considered in Section 5.3 when the arch-model is analysed theoretically and this idealisation is necessary if only to keep simple the mathematical approach associated with the arch stability and large displacements. In view of the complex structural behaviour it is no longer possible to consider the actual behaviour of the reinforced concrete, as it was when the column was analysed in chapter 4.

Among the assumptions relative to the material some are less significant. For instance, regarding reinforced concrete it is commonly assumed that the elastic modulus and creep characteristic of concrete are constant and equal in compression and tension (assumptions (iii) and (iv) from Section 5.3.2). Also due to the lack of consistent information about the non-linearity of the creep for a highly stressed concrete it is still acceptable to assume that the creep deformations are proportional to the instantaneous deformations up to failure*) (assumption (ii) from Section 5.3.2).

Nevertheless other assumptions may significantly

Footnote

*) This aspect is discussed earlier in Section 4.3.2d.

affect the solution. In this respect the most important assumptions are (i), (v) and (vii) from Section 5.3.2. Thus the plasticity and the cracking of a reinforced concrete cross-section significantly affect its stiffness, whereas a material failure can well precede the buckling.

The effects of the plasticity and cracking on the stiffness can be grossly taken into account by using simplified bending-moment/curvature curves based on those presented in chapter 4.

The smaller are the bending moments relative to the axial force, the less significant are the effects of plasticity and cracking (see Figs.4.32..4.34). Yet the attainment of the plastic range in any of the joints B_i can crucially affect the non-linear behaviour of the model and therefore the final solution.

As to whether the material failure precedes or not the structural buckling a further discussion is presented later in Section 6.2.

5.5 NUMERICAL APPLICATIONS. CONCLUSIONS

The elastic pre-buckling and post-buckling behaviour as well as the visco-elastic pre-buckling and buckling behaviour of the arch-model from Fig.5.2 have been analysed for the sets of numerical data given in Table 5.5.

The geometry of the arch-model (i.e. the angle α_1 and α_2) has been chosen to correspond to a funicular polygon for a uniform loading (i.e. $p_1 = p_2 = 1$). It arises from this condition that

$$\alpha_1 \simeq 3\alpha_2$$

The following structural parameters have been varied:

- $\frac{f}{\ell} = \frac{\sin\alpha_1 + \sin\alpha_2}{\cos\alpha_1 + \cos\alpha_2}$ · The smaller f/l, the more shallow the arch is.

- k The smaller k is, the more slender the arch.

- c When c=1 the arch has a uniform cross-section, whereas when c=0·5 the arch has a smaller bending stiffness at the apex.

- p_1 and p_2. When $p_1=p_2$ the loading is uniform, when $p_2 > p_1$ the load is larger at the apex, and when $p_2 < p_1$ the load is smaller at the apex.

Table 5.5

f/l	α_1 (rad)	α_2 (rad)	k	c	$p_1:p_2$
1/8	0·365	0·123	1000	1·0	1:1
			400		
			1000	0·5	
1/10	0·3	0·1	1000	1·0	1:1
			400		
			1000	0·5	1:1
					1:07
					0·7:1
1/13·3	0·225	0·075	1000	1·0	1:1
			400		
			1000	0·5	
	0·2	0·1	1000	1·0	1:1
			400		
			1000	0·5	

No more graphs depicting the results of these numerical applications aregiven here since they are similar to those already plotted in Figs.5.6...5.9, 5.11...513, 5.18,5.19 and 5.32...5.36.

The following conclusions can be drawn from these numerical analyses:

i) the non-linear behaviour, which is associated with the occurence of large displacements, is affected by all structural parameters: the smaller is the rise f or the more slender is the arch or the less stiff is the cross-section at the apex or the farther is the funicular polygon from the arch geometry, the more significantly non-linear is the overall behaviour of the arch-model both under instantaneous and under sustained loading.

ii) the more non-linear is the arch behaviour, the more significant are the differences between the results arising from the 'exact' and the 'approximate' formulations of the arch-model.

iii) when the elastic buckling is due to a bifurcation of equilibrium which precedes a snap-buckling, then the more significant the non-linearity, the closer the load p_{snap} is to p_{cr}, where p_{snap} corresponds to the snap-buckling and p_{cr} corresponds to the bifurcation.

iv) the closer p_{snap} is to p_{cr}, the smaller is φ_{lim} or, in other words, the more significant is the decay of the critical load due to the concrete creep

v) a smaller effect of the creep on the critical load is recorded than that given by the formula *)

Footnote

*) This approximate formula is used in design to account for the reduction of critical load due to creep. It provides a creep-dependent critical load which is similar to the elastic critical load, but the modulus of elasticity is reduced to account for the long-term deflections (see Section 4.6 and Gioncu (1974))

$$p_{cr\varphi} = \frac{p_{cr,el}}{1+\varphi}$$

and $p_{cr,el}$ should be taken to be equal with p_{snap} rather than with p_{cr}. Nevertheless no certain conclusion can be drawn in this latter respect as long as the actual behaviour of the reinforced concrete and the possibility of a material failure, which may precede the buckling, are not considered properly. More experimental work must be carried out and models able to account accurately for the actual structural and material behaviour must be devised before a positive conclusion could be achieved.

5.6 SUMMARY AND CONCLUSIONS

A three degree-of-freedom arch-model is presented in the present chapter and its elastic behaviour under instantaneous loading as well as the effects of concrete creep when the load is sustained are analysed.

1. Theoretical approaches to analyse the arch-model behaviour under load when large displacements are involved are presented in Section 5.3. The pre-buckling behaviour and the stability are analysed for both instantaneous and sustained loading, whereas the postcritical behaviour is investigated solely for instantaneous loading.

In each situation a so-called 'exact' solution as well as 'approximate' solutions are presented.

The 'exact' solution arises from an analysis in which only the assumptions from Section 5.3.2 are employed. Due to the large displacements the final coupled equations are non-linear. A standard subroutine

based on the Powell's procedure is used to provide the 'exact' solution of the non-linear coupled equations. In order to use this subroutine an initial estimate of the solution is required and an 'approximate' solution is always computed with this aim. Approximations can be used to reduce these non-linear equations to a sequence of linear coupled equations by using truncated Taylor's expansions of the 'exact' equations and the perturbation technique. These latter solutions are called 'approximate'. Different 'approximate' solutions arise for different perturbation parameters and their accuracy is dependent on the significance of the truncations of various expansions and on the choice of the perturbation parameter.

A comparison between the 'exact' and 'approximate' solutions of the primary path and stability criteria is presented and it is concluded that the larger are the displacements, the more significantly different are these solutions so that the approaches yielding the 'exact' solution are employed eventually.

The main conclusions of Section 5.3 are:

i) Among the five necessary and sufficient conditions (5.16a), which ensure that the elastic equilibrium of the symmetric arch-model is stable the last condition (i.e. $\Delta > 0$) is solely sufficient to ensure elastic stability. In other words none of the other conditions (5.16a) can be violated at a load lower than the critical load supplied by $\Delta = 0$.

Simultaneously with $\Delta = 0$ one or a group of the

left-hand sides of conditions (5.16a) reach also their zeros and, in fact, the violations of these latter conditions are mathematically responsible for $\Delta=0$. Moreover, it is shown that a certain mode of buckling (i.e. snap-buckling, antisymmetric or symmetric bucklings) is associated with each specific violation of conditions (5.16a).

These results achieved for the three degree-of-freedom arch-model, are proved to be true also for the one and two degree-of-freedom arch-models and thus suggest that they might be valid for models having more degrees of freedom.

ii) Both stiffening and unstiffening of the post-critical elastic behaviour have been recorded with the three degree-of-freedom arch-model depending on the specific mode of buckling and on the configuration of the critical deformed state. This latter factor is shown in Section 5.5 to depend on structural parameters such as the shallowness and the slenderness of the arch-model, and the position of the funicular polygon of loads relative to the initial geometry of the arch-model. Some general features of the initial geometry of the elastic post-buckling path are emphasised.

iii) A step-by-step procedure based on the principle of virtual work is developed to account for the effects of concrete creep. The 'rate of creep' method is employed to model the creep-dependent behaviour of concrete but no difficulty would arise if any other method were used

in view of the numerical approach.

iv) the creep effects on the stability of the arch-model are studied by considering both (1) the elastic stability of the model which has previously crept under a sustained, intermediate load (see Section 5.3.7a) and (2) creep stability, that is the indefinite increase of a creep-dependent displacement relative to the increase of creep when the model sustains a constant load (see Section 5.3.7b). Consequently, two curves depicting the relationship between the critical load and the concrete creep arise and they are called curve I and curve II, respectively in Figs 5.34...5.36.

At $\varphi = 0$ (i.e. when only the elastic stability under an instantaneous loading is considered) curve I corresponds to the elastic critical load, whereas curve II corresponds to the load associated with snap-buckling. Thus:

- when the elastic instability of the slender arch is due to a snap-buckling, the starting points of curve I and II are coincident (see Fig.5.36)

- when the elastic instability of the slender arch is due to a bifurcation of equilibrium, the starting point of curve I is below that of curve II (see Figs.5.34 and 5.35).

Since curve I decays almost negligibly as φ increases, this curve is of practical interest only in the latter case. Even then, however, curve I provides the critical load only for $\varphi_\infty < \varphi_{lim}$. When $\varphi_\infty > \varphi_{lim}$, the creep-dependent critical load of the slender arch is associated

with curve II (see Figs.5.34 and 5.35).

The closer the starting point of curve II is to that of curve I or, in other words, the more non-linear the elastic primary path is, the smaller is φ_{lim}.

It is therefore apparent that the more non-linear the pre-buckling behaviour is (i.e. the larger the transverse displacements are), the more the creep diminishes the critical load of the slender arch.

In fact the above effects of creep on the stability of a slender arch can be summarised as follows:

a. So long as the slender arch does not display large displacements, the creep affects its critical load very little. This situation occurs when the elastic primary path is fairly linear up to the buckling point and when the creep coefficient is relatively small (i.e. $\varphi_\infty < \varphi_{lim}$)

b. If the creep of concrete is important or if the structure exhibits large transverse displacements under instantaneous loading, the critical load of the slender arch is significantly diminished by the concrete creep. The larger the transverse displacements are *) the more damaging the creep effects.

Footnote

*) In Section 5.5 it has been shown that the arch exhibits larger transverse displacements when: the slenderness λ is larger, the shallowness f/l is smaller, the arch is more flexible at apex , the arch axis differs more from the funicular polygon.

2. The correspondence existing between the arch-model and an actual arch is analysed within Section 5.4. It is shown that the arch-model approximates the actual arch by

i) considering as forces (M_i or F in the devices B_i or A, respectively) and as stiffnesses (bending or axial, respectively) the mean values of the corresponding forces and stiffenesses in the actual arch.

ii) considering as displacements (angular or linear in the devices B_i or A, respectively) the sum of the corresponding deformations (bending or axial, respectively) of the actual arch.

iii) both the mean values and the summations are considered over an arch-length equal with the distance $a_i b_i$ for a device B_i and equal with the whole length $H_1 H_2$ for the device A (see Fig.5.39a).

Using this correspondence a comparison between closed-form solutions available for two particular types of arches and results of the arch-model analysis is performed in Section 5.4.2. It is shown that the arch-model provides critical loads on the conservative side and with a fairly good approximation. The same mode of buckling is displayed by both analyses. This suggests that the arch-model can be used to analyse approximately arches for which no closed-form solution is available.

The limitations arising from using the arch-model from Fig.5.2 in analysing actual structures are discussed in Section 5.4.3. Possibilities of improving both the arch-model and the assumptions are presented.

Chapter 6

CONCLUDING REMARKS CONCERNING THE ANALYSES OF SLENDER BEAM-COLUMNS AND ARCHES

A theoretical investigation has been carried out into the creep effects on two slender reinforced concrete structures.

i) One is a slender beam-column subject to combined axial load and bending moment, where the latter can be due to either an accidental out-of-straightness of the geometric axis or to a transverse loading.

ii) The other is a slender arch subject to gravitational, transverse loads.

Both the effects of structural slenderness, when the loading is instantaneous, and the combined effects of structural slenderness and concrete creep, when the loading is constant and sustained, are taken into consideration.

The analysis of the slender arch is mathematically more complex than that of a slender beam-column chiefly because the former has a more complex structural behaviour and can exhibit larger displacements at the critical state. Consequently different simplifications (that is different degrees of accuracy) have been used in performing the two analyses. Thus

- regarding the slender beam-column (chapter 4), the behaviour of both materials (concrete and reinforcement) is modelled as accurately as possible and no significant simplifications are associated with the structural analysis. The ultimate capacity is investigated in conjunction with both the material failure and the structural instability.

- regarding the slender arch (chapter 5), important

simplifications are employed with respect to both the material and the structural behaviour; thus a perfectly visco-elastic response is assumed to govern the material behaviour, while the structural analysis is carried out with the help of a three degree-of-freedom model. Only the ultimate capacity associated with the structural instability is investigated.

In view of these differences in performing the analyses of the beam-column and of the arch, two matters are further discussed below in Sections 6.1 and 6.2, respectively:

1. What are the similarities and the differences between the effects of concrete creep on the behaviour of slender beam-columns and that of slender arches?

2. Is it correct to assume that the ultimate capacity of slender arches can be associated with creep buckling or, in view of the large displacements exhibited by the structure and of the limited capability of deformation of concrete, is the ultimate capacity of the slender arch always exceeded through material failure before the buckling could be attained?

Then the underlying conclusions of the analyses of slender reinforced concrete beam-columns and arches are presented in Section 6.3 and suggestions for further research are given in Section 6.4.

6.1 EFFECTS OF CONCRETE CREEP

Due to the concrete creep two effects take place in a reinforced concrete cross-section:

i) stresses are redistributed from concrete to the restraining reinforcement

ii) the axial and rotational deformations of the cross-section are increased

The effect (i) means in most cases an unloading of the concrete with a corresponding loading of the reinforcement. Consequently:

- firstly, the effect(ii) is smaller than if the concrete creep were unrestrained. When a consistent analysis as that from chapter 4 is difficult to perform, this aspect is considered globally by using a reduced creep function φ of concrete

- secondly, it may be possible in certain circumstances (i.e. when the instantaneous failure of the cross-section is due to either the tension reinforcement attaining its limit strain or the compression concrete attaining its limit strain while the compression reinforcement yields and the tension reinforcement is still below the yielding stress) that a creep-dependent reduction of the load-bearing capacity of the cross-section occurs. Nevertheless this reduction is small so that the same interaction-diagram can be practically assumed for a cross-section no matter whether the loading is instantaneous or sustained.

The effect (ii) becomes significant when the structure is slender. Then, the creep-dependent increase in the structural deformability induces a corresponding increase in the internal forces which additionally increase the

deformations and so on. Consequently the ultimate capacity of the structure (either material failure or instability) is substantially reduced.

The combined effect of structural slenderness and concrete creep on the ultimate capacity of a reinforced concrete slender structure can be analysed as depicted in Fig.6.1. The principle of the analysis is the same no matter whether a slender beam-column or a slender arch or any other slender structure is considered. Thus:

1. the interaction- diagram is associated with the ultimate capacity (material failure) of the critical cross-section *). As already mentioned this interaction-diagram can be considered creep-independent.

2. the curves OA, OA' or OA" are associated with the response of the structure to loading, i.e. they depict the relationship between the actual axial force and the bending moment of the critical cross-section for various intensities of the load. This response is given by:

- the straight line OA when the structure is not slender ($\lambda = 0$) and the loading is either instantaneous ($\varphi = 0$) or sustained ($\varphi > 0$).

- the curve OA' when the structure is slender ($\lambda > 0$) and the loading is instantaneous ($\varphi = 0$)

- the curve OA" when the structure is slender ($\lambda > 0$) and

---

Footnote

*) i.e. that cross-section of the structure where the largest forces occur

the loading is constant and sustained ($\varphi > 0$).

The larger is λ , the farther is the curve OA' from the straight line OA. The larger is λ or φ , the farther is the curve OA" from the curve OA'. However the derivation of curves OA' and OA" depends on whether a slender beam-column or a slender arch is considered. Thus:

2a. when the slender beam-column is considered, only the bending moment is increased by slenderness and creep. For a certain load the axial force is the same while additional moments Δm_λ or $\Delta m_{\lambda\varphi}$ will occur as the loading is instantaneous or sustained, respectively (see Fig.6.2a).

2b. when the slender arch is considered, both the axial force and the bending moments can increase so that additional Δn_λ and Δm_λ or $\Delta n_{\lambda\varphi}$ and $\Delta m_{\lambda\varphi}$ will occur as the loading is instantaneous or sustained (Fig.6.2b).

With only these differences, the ultimate capacity of either the slender beam-columns or the slender arches can be performed by using the graphs plotted in Fig.6.1.

The critical load *) will correspond to a point B' on the curve OA' or B" on the curve OA" as the elastic buckling or the creep-dependent buckling, respectively, are considered (see Fig.6.3).

Footnote

*) i.e. the lowest intensity of load associated with the instability of the slender structure.

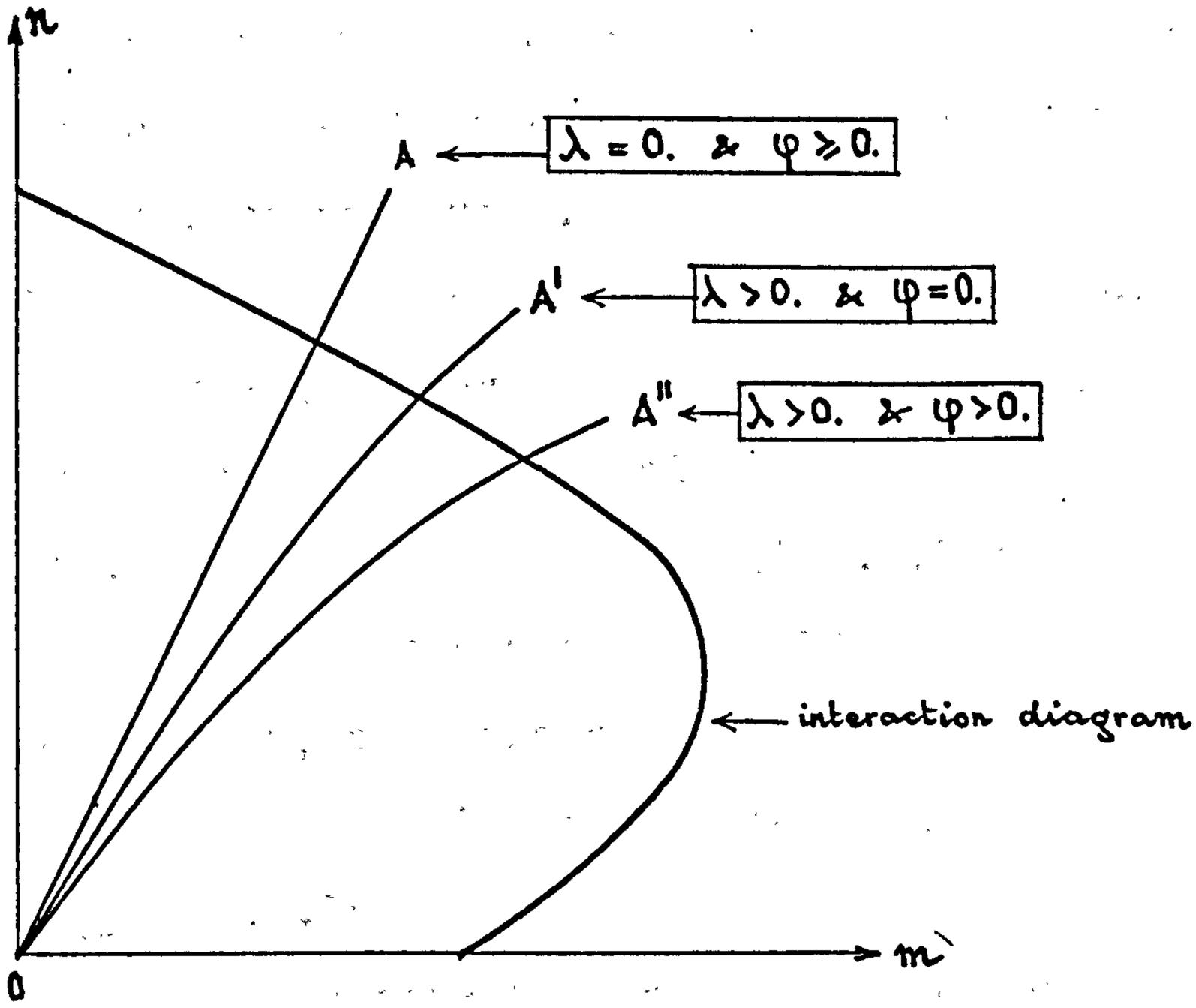

Fig. 6.1

a. SLENDER BEAM-COLUMN

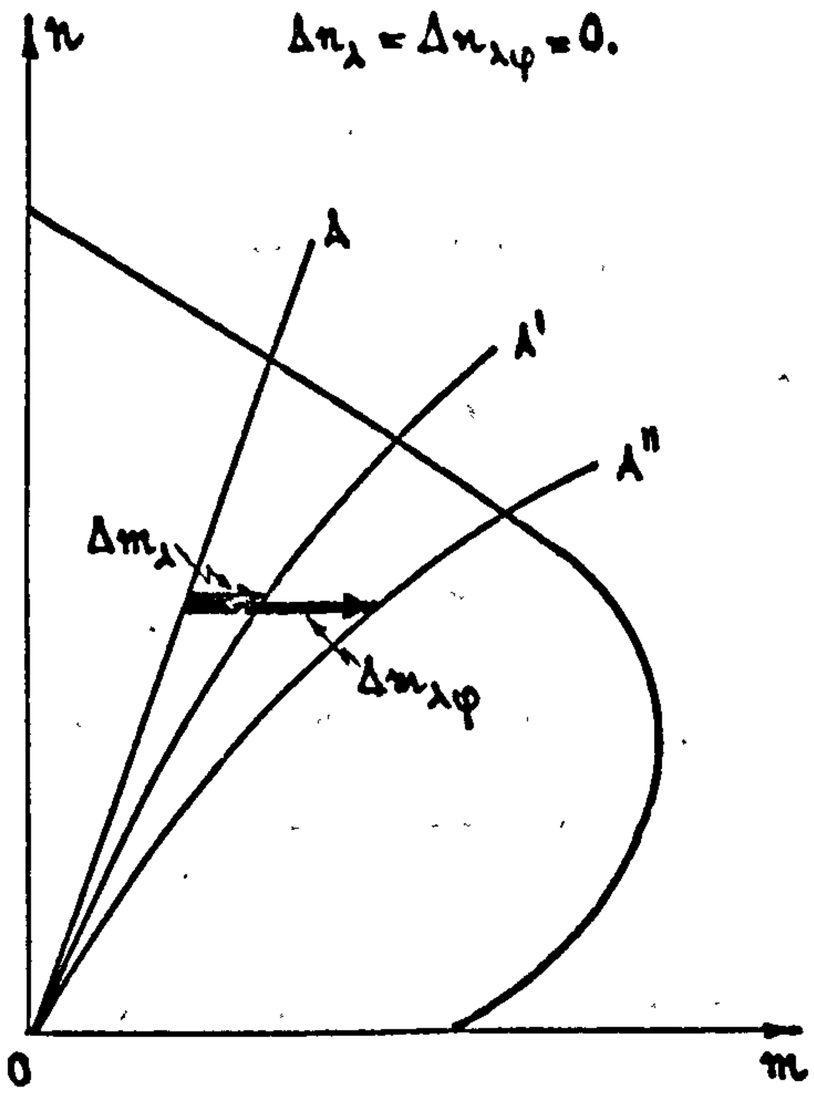

b. SLENDER ARCH

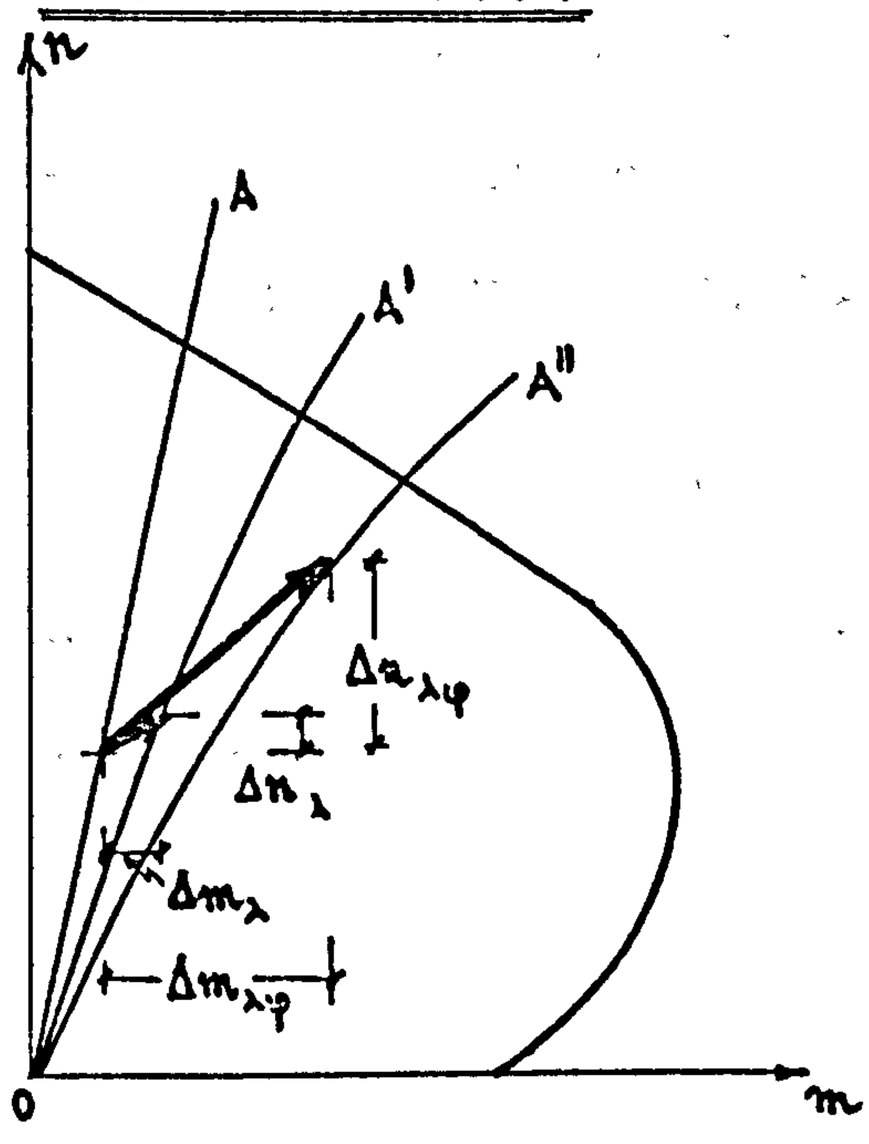

Fig. 6.2

As the points B' or B" are inside or outside the interaction-diagram, the ultimate capacity of the slender structure is associated with either structural stability or material failure, respectively. Thus:

- when the loading is instantaneous and B' is outside the interaction-diagram, the maximum instantaneous load which the structure can bear is associated with the material failure, i.e. with the load p_u (Fig.6.3a)**)

- when the loading is instantaneous and B' is inside the interaction-diagram, the maximum instantaneous load which the structure can bear is associated with the elastic critical load p_{cr} (Fig.6.3b)

- when the loading is constant and sustained and B" is outside the interaction-diagram, the ultimate capacity of the structure is associated with a creep-dependent material failure, i.e. with the sustained load $p_{u\varphi}$ (Fig.6.3a).

- when the loading is constant and sustained and B" is inside the interaction-diagram, the ultimate capacity of the structure is associated with the creep-buckling, i.e. with the load $p_{cr\varphi}$ (Fig.6.3b).

Considering the above mentioned aspects, the effects of concrete creep on the ultimate capacity of a slender

---

Footnote

**) Here the load p denotes (see also Fig.6.2):

η - according to eq.(4.31), p.96, when the slender beam-column is analysed

γ - according to eq.(5.1), p.226, when the slender arch is analysed.

a.

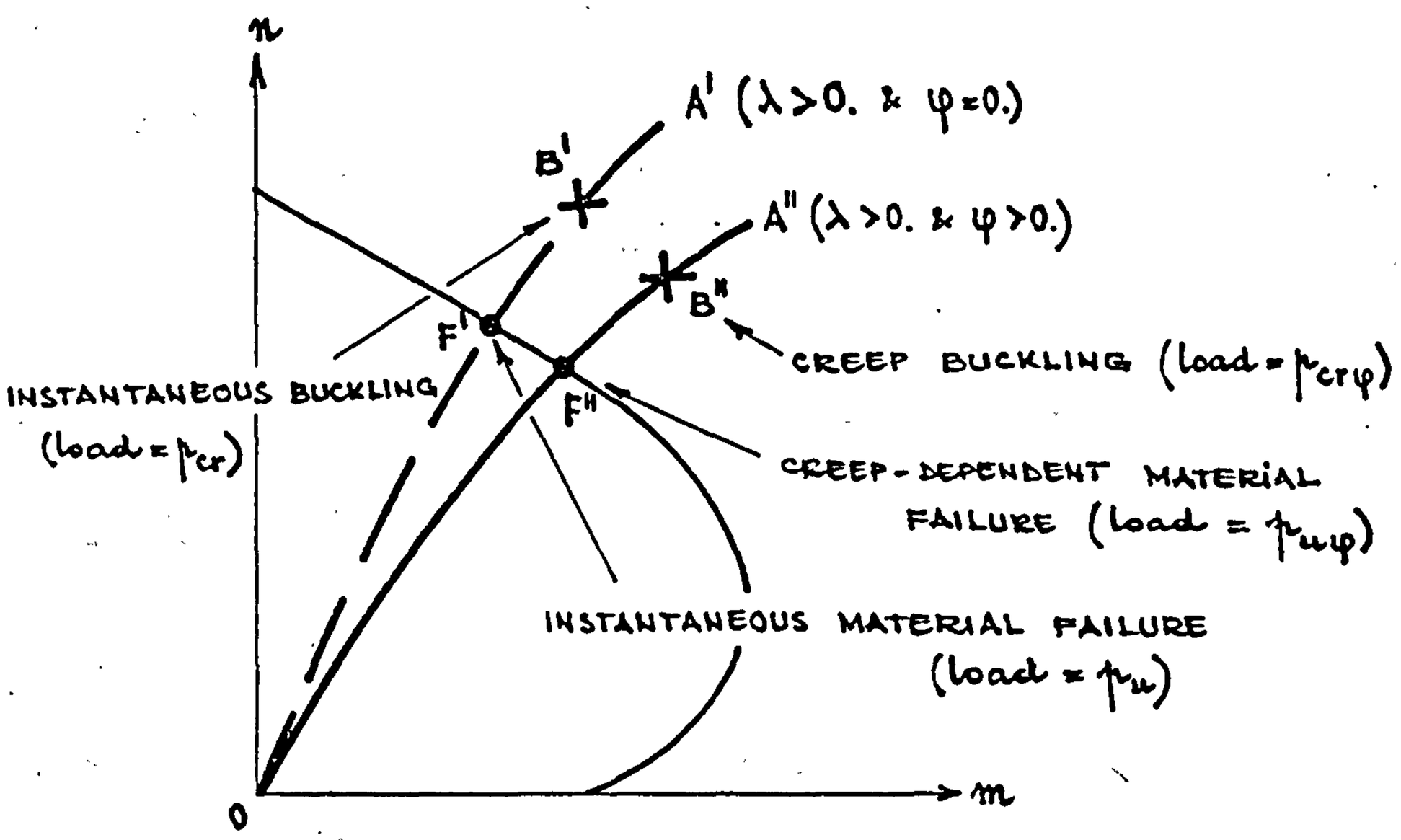

X STRUCTURAL INSTABILITY (BUCKLING)

● MATERIAL FAILURE

b.

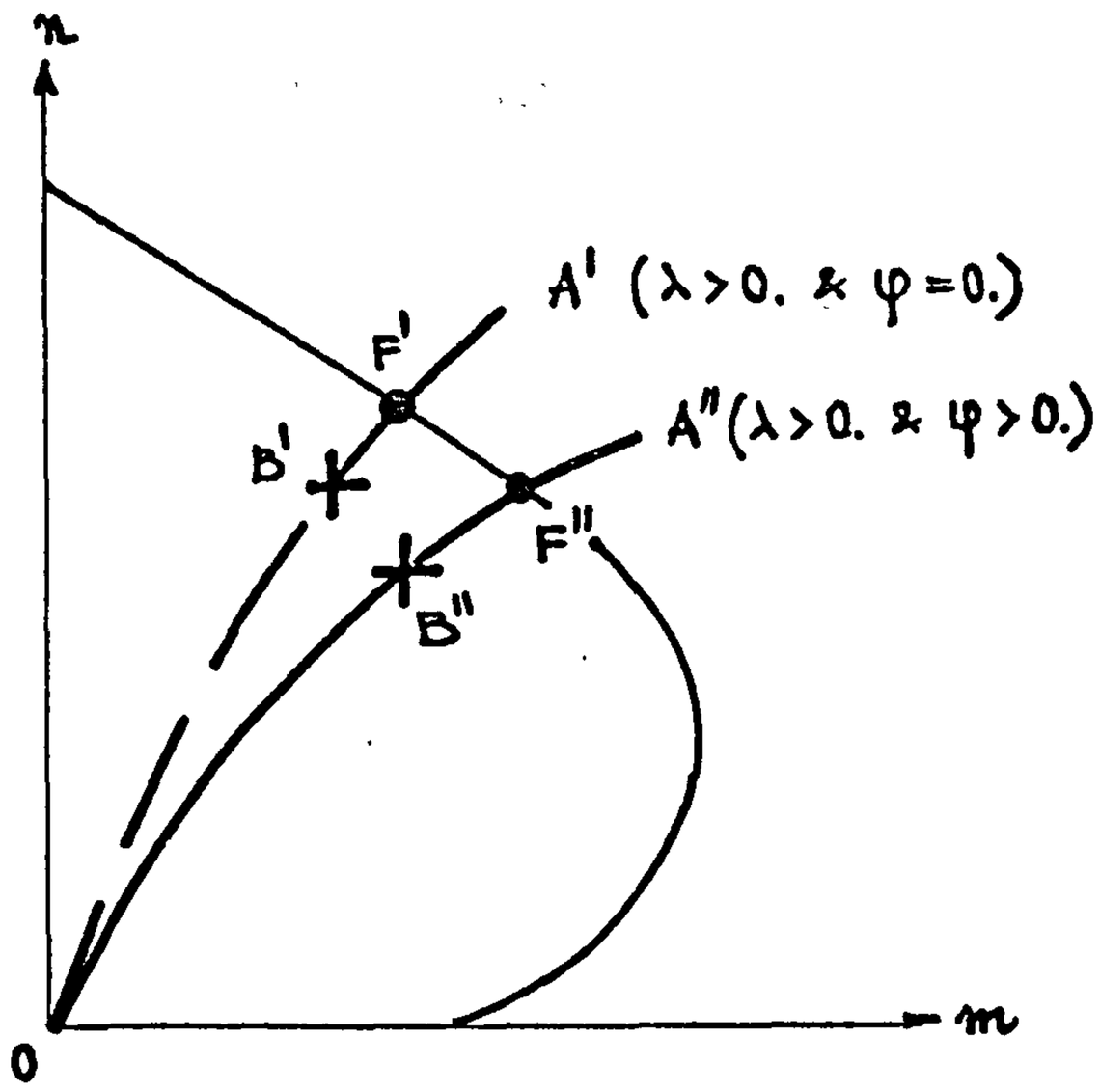

Fig. 6.3

beam-column or a slender arch can be summarised as:

When the ultimate capacity is due to a material failure (Fig.6.3a) the concrete creep always diminishes the load (i.e. $p_{u\varphi} < p_u$). Indeed it is apparent from Fig.6.2 that no matter whether a slender beam-column or a slender arch is considered, the curve OA" always attains the interaction-diagram at a lower load than the curve OA' does. The larger is φ, the smaller is $p_{u\varphi}$ compared to p_u (Fig.6.3a).

When the ultimate capacity is due to structural instability (Fig.6.3b) the effects of creep are more complex. Thus:

I. Regarding the slender beam-column, it has been shown in chapter 4 that the larger is φ, the smaller is $p_{cr\varphi}$ when compared with p_{cr}.

II. Regarding the slender arch it has been shown in chapter 5 that (see Section 5.3.7):

IIa. when the elastic instability of the slender arch is due to a snap-buckling, the larger is φ, the smaller is $p_{cr\varphi}$ when compared with p_{cr}.

The similarity between the situations I and IIa is not incidental. Indeed, in both situations the structural instability is associated with a vanishing stiffness, in other words, a displacement can be increased at the critical state without increasing the load or the concrete creep. In such structures the concrete creep has an effect similar to that of the load and, therefore, the creep buckling will occur at a lower load than the elastic buckling.

IIb. when the elastic instability of the slender arch

is due to a bifurcation of equilibrium, the creep-dependent critical load $p_{cr\varphi}$ is diminished by an increase in φ (similarly to the above cases IIa and I) provided that is larger than a certain limit φ_{lim}. If not (i.e. if $\varphi < \varphi_{lim}$), $p_{cr\varphi}$ is insignificantly affected by the concrete creep and one can consider $p_{cr\varphi} \simeq p_{cr}$.

The result is only apparently contradictory with those following from situations I and IIa. Indeed, the buckling by bifurcation of equilibrium is associated with relatively small displacements of the slender arch and thus additional creep-dependent displacements can not change the situation significantly so long as the creep is small ($\varphi < \varphi_{lim}$). It is, in fact, as if the arch were initially slightly shallower; then no significant reduction of the elastic critical load takes place, for instance, according to the theory of elastic stability. However, when the concrete creep becomes significant ($\varphi > \varphi_{lim}$), its effects on buckling are no longer negligible. The limit φ_{lim} was shown in chapter 5 to depend on the significance of the displacements of the arch. The larger these displacements are, the smaller φ_{lim} is and also the sharper the decay of $p_{cr\varphi}$ with the increase in φ. In other words the larger the displacements exhibited by the slender arch are, the closer the situation IIb is to the above situations IIa and I. The larger displacements are associated with arches having larger slenderness and/or higher shallowness and/or larger differences between the geometric axis and the funicular polygon.

6.2 CREEP BUCKLING AND MATERIAL FAILURE

The ultimate capacity of both slender beam-columns and slender arches was associated in the previous section with either material failure (Fig.6.3a) or structural instability (Fig.6.3b).

However the question arises whether both the situations depicted in Fig.6.3 are possible; in other words, whether the buckling, particularly the creep buckling, is not preceded always by a material failure.

Concerning the slender beam-column, an accurate answer to this question was given in chapter 4. The analysis performed there was consistent with the actual behaviour of both structure and materials and hence the ultimate capacity was associated with either material failure (Fig.6.3a) or structural instability (Fig.6.3b) whichever was the case. It was shown that the structural instability precedes the material failure when the axial force is about $0{\cdot}1 < n < 0{\cdot}5$ (see Fig.4.53, p.171). Indeed, no structural instability is possible when n is very small. On the other hand when n is very large, the moment-bearing capacity of the critical cross-section is small and hence a material failure occurs before the transverse displacements could increase too much. The more slender the beam-column is or the larger the concrete creep, the more extended this range of n is (i.e. the more likely is that the ultimate capacity of the slender beam-column is according to Fig.6.3b rather than to Fig.6.3a).

Concerning the slender arch, attention was given in chapter 5 only to the case where the ultimate capacity of

the slender arch is associated with structural instability (Fig.6.3b). In order to find an answer to the above question the results of numerical applications carried out for four slender arches are plotted in Figs.6.4..6.6. These graphs are identical to those in Fig.6.3 with:

i) the interaction diagram corresponding to *)

- a concrete strength f'_c = 25 MPa
- a reinforcement strength f_s = 300 MPa
- a reinforcement ratio ρ = 1%
- a relative cover of reinforcement a/h = 0·1

ii) the curves OA' and OA" (plotted by broken and continuous lines, respectively) corresponding to **)

- (in Fig.6.4) Two arches having a constant cross-section and the geometric axis coincident with the

---

Footnote

*) using the mechanical ratio of reinforcement ω given by eq.(4.49), see p.127, the interaction diagram in Figs.6.4..6.6 corresponds to ω=0·12 and a/h = 0·1

**) the curves OA' and OA", which depict the response of the slender arches to the instantaneous and the sustained loadings, respectively, follow from the analysis of the three degree-of-freedom arch-model (see Section 5.3) and from the correspondence between the discrete arch-model and the actual arch (see Sect.5.4.1). It is worth emphasising that Figs.6.4..6.6 depict results for arches of which both the elastic and the creep-dependent primary paths and critical states have been already analysed in chapter 5.

funicular polygon. These two arches have different values of the slenderness λ; one arch has a small slenderness (λ=40) while the other is rather slender (λ=70)

- (in Fig.6.5) an arch identical to that with λ=70 in Fig.6.4 but being more flexible at the apex (i.e. the ratio c between the flexural stiffnesses of the cross-sections at the apex of the arch and at the quarter of the arch is 0·5 rather than 1)

- (in Fig.6.6) an arch with λ=70 and c=0·5 but being shallower (i.e. the ratio between the rise f of the arch and its span l -see Fig.5.4, p.227- is $f/l \simeq 1/13{\cdot}3$ rather than f/l=1/10 as it is in Figs.6.4 and 6.5) and having the geometric axis non-coincident with the funicular polygon.

iii) all the curves OA" corresponding to a final creep φ_∞=2.

It is also noteworthy that the curves OA' and OA" in Figs.6.4..6.6 are plotted for the critical cross-section of each arch. Thus the curves m_2-n_2 depicted in Figs.6.4 and 6.5 are associated with the cross-section at the apex of the arches, while the curves m_1-n_1 depicted in Fig.6.6 are associated with the cross-section at the quarter of the arch.

The following conclusions can be drawn from Figs.6.4.. 6.6:

1./ For the arch with λ=40 in Fig.6.4 both p_{cr} (the elastic critical load) and $p_{cr\varphi}$ (the creep-buckling load)

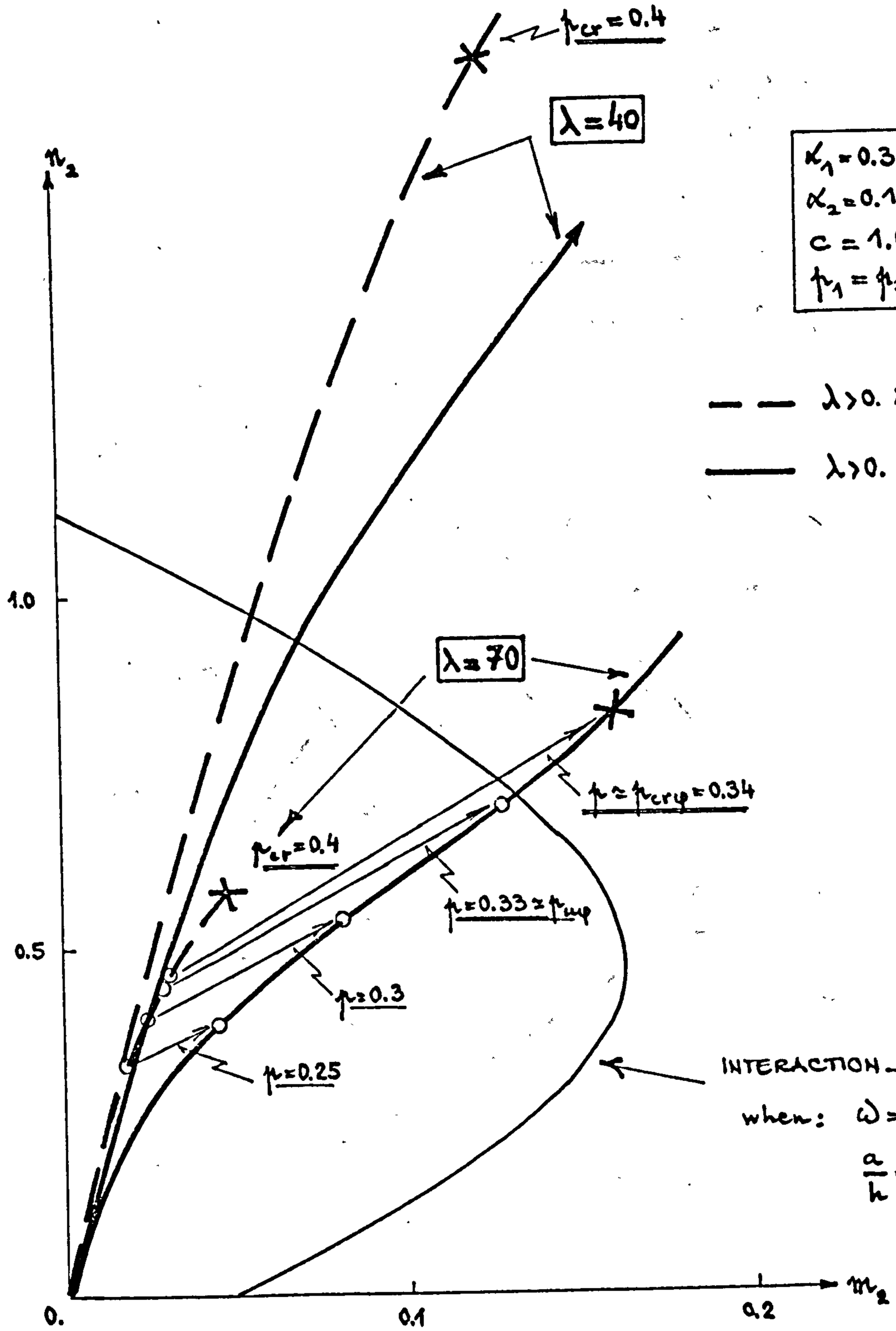
$\mu_{cr}=0.4$
$\lambda=40$
μ_2
$\kappa_1=0.3$ rad.
$\kappa_2=0.1$ rad.
$c=1.0$
$\mu_1=\mu_2=1.$
— — $\lambda>0.$ & $\varphi_\infty=0.$
—— $\lambda>0.$ & $\varphi_\infty=2.$
1.0
$\lambda=70$
$\mu\simeq\mu_{crip}=0.34$
$\mu_{cr}=0.4$
$\mu=0.33\simeq\mu_{crip}$
0.5
$\mu=0.3$
$\mu=0.25$
INTERACTION-DIAGRAM
when: $\omega=0.12$
$\frac{a}{h}=0.1$
0.
0.1
0.2
μ_2

Fig. 6.4

$\alpha_1 = 0.3$ rad.

$\alpha_2 = 0.1$ rad.

$c = 0.5$

$k = 1000$ $(\lambda = 70)$

$\mu_1 = \mu_2 = 1$

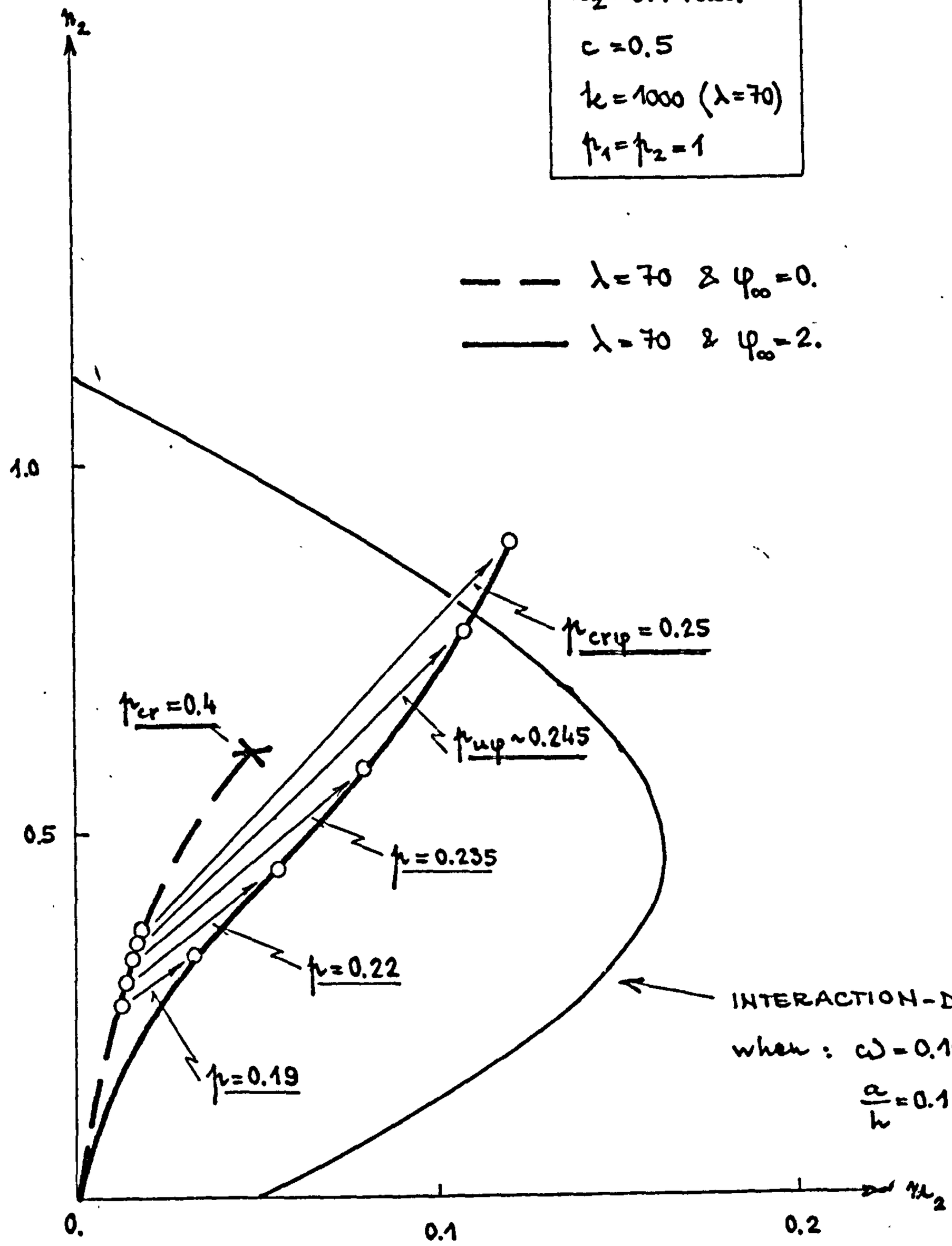

Fig. 6.5

$\alpha_1 = 0.2$ rad.
$\alpha_2 = 0.1$ rad.
$c = 0.5$
$k = 1000$ $(\lambda = 70)$
$\psi_1 = \psi_2 = 1.$

— — $\lambda = 70$ & $\varphi_\infty = 0.$
——— $\lambda = 70$ & $\varphi_\infty = 2.$

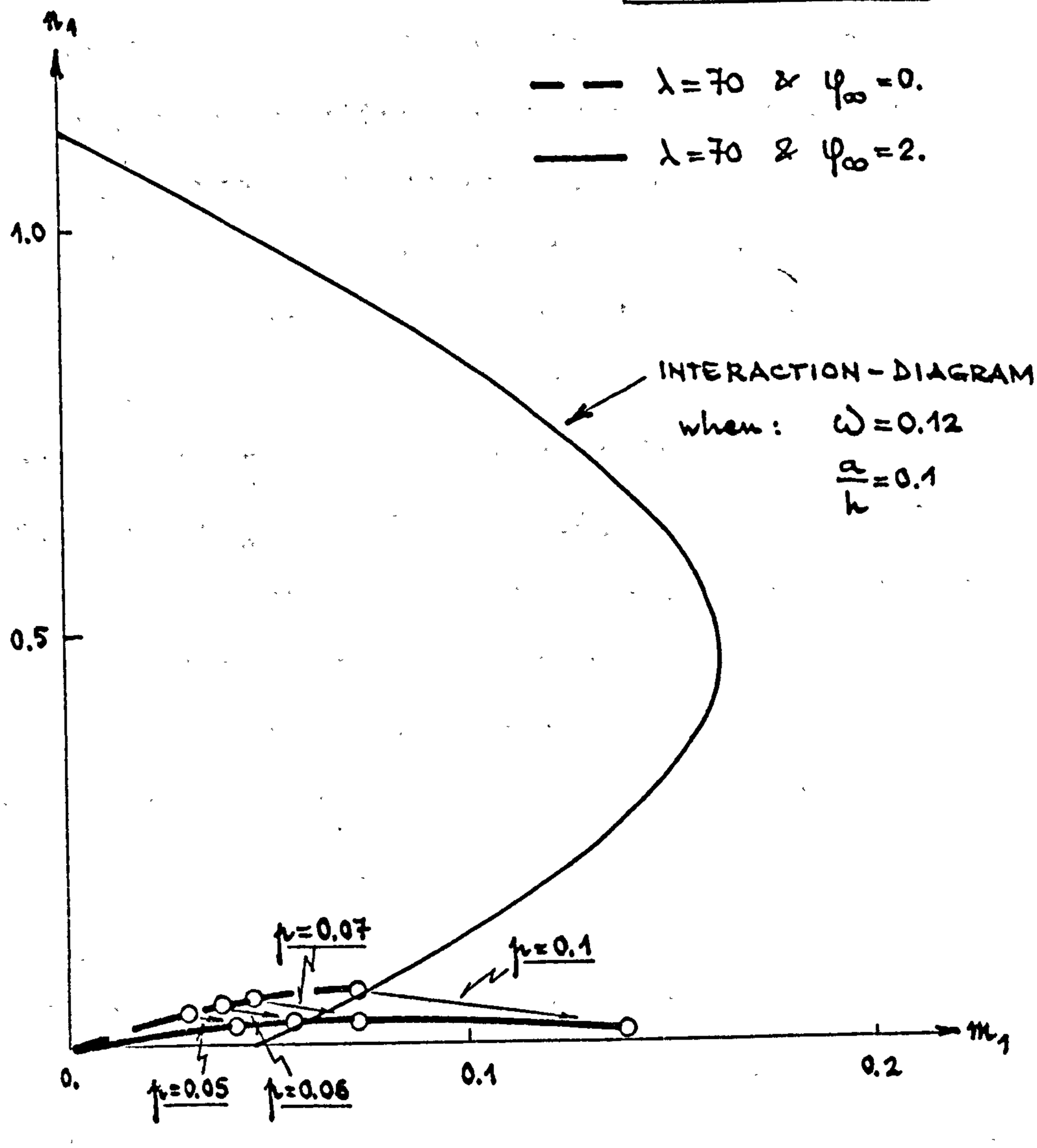

Fig. 6.6

are very high and the pre-buckling behaviour is geometrically almost linear (the curves CA' and OA" are almost straight lines). The ultimate capacity of such an arch is always associated with a material failure (see Fig.6.3a). This situation is typical for the range in which the reinforced concrete arches are generally designed.

2. When the slenderness is increased while the elastic buckling is still due to a bifurcation of equilibrium (i.e. the elastic prebuckling behaviour is associated with moderately large displacements), the structural instability precedes the material failure when the loading is instantaneous (see curve OA' for λ=70 in Fig.6.4). When the loading is sustained, the concrete creepdecreases both the load corresponding to the material failure ($p_{u\varphi} \simeq 0{\cdot}33$ in Fig.6.4) and the load corresponding to the creep-buckling ($p_{cr\varphi} \simeq 0{\cdot}34$ in Fig.6.4). Consequently the long-term ultimate capacity of such a slender arch is associated with a material failure which takes place as the critical state is approached but it is apparent in Fig.6.4 that $p_{u\varphi}$ is virually equal with $p_{cr\varphi}$.

Similar results are depicted by the arch in Fig.6.5 although the creep-dependent displacements of that arch are almost twice as much as those of the arch with λ=70 in Fig.6.4.

3. When the arch has a prebuckling behaviour which is geometrically very non-linear and thus the elastic

instability is associated with very large displacements, the ultimate capacity of the slender arch is due to a material failure for both instantaneous and sustained loadings. In Fig.6.6, for instance, p_{cr}=0·24 and $p_{cr\varphi}$ =0·12 *) while material failure occurs in the slender arch when p_u=0·1 and $p_{u\varphi}$ =0·06, respectively.

From the above conclusions it follows that the analysis carried out in chapter 5 and based on the assumption that the ultimate capacity of a slender arch is associated with the structural instability (Fig.6.3b) rather than with a material failure (Fig.6.3a) is valid provided that:

- the bending moments are not too large relative to the axial force. This restriction means that the arch should have the geometric axis coincident with or very close to the funicular polygon and should not be too shallow.

- the arch is slender. A value λ=70 arose from the numerical applications depicted in Fig.6.4..6.6 as being close to the lower limit of slenderness in which the analysis is valid.

6.3 CONCLUSIONS

The conclusions of the analyses of the slender beam-column (chapter 4) and of the slender arch (chapter5) have been presented in Sections 4.7 and 5.6, respectively.

Footnote

*) see Fig.5.36, p.319

Only a brief reminder of the main results is given below.

a. Concerning the slender beam-column

i) The response to loading and the ultimate capacity of the slender reinforced concrete beam-columns are analysed by means of a computer-model. With respect to both the assumptions and the method of solution used, the computer-model belongs to the 'general method' according to the classification given by the CEB-Buckling Manual (1973).

ii) The computer-model is able to analyse the reinforced concrete beam-column no matter whether this is short or slender or whether the loading is instantaneous or sustained.

iii) However, in its present form, the computer-model can analyse only the beam-columns bent in single curvature and having a rectangular, symmetrically reinforced cross-section.

Suggestions are made to extend the use of the computer-model to beam-columns having other shapes of the cross-section and/or being bent in double curvature.

iv) A thorough computer-analysis was performed of the effects which the main parameters can have on the ultimate capacity of reinforced concrete beam-columns. The following parameters were varied to cover most of the practical range:

- materials strength (concrete and reinforcement)
- reinforcement ratio
- reinforcement cover

- concrete creep
- member slenderness
- distribution of the initial bending moments along the member axis.

A comprehensive insight into the combined effects of the concrete creep, member slenderness and the other parameters is presented with the help of numerous graphs. It is shown that the larger the member slenderness and the concrete creep are, the more imperative it is to design the slender beam-column consistently with the actual behaviour of both concrete and reinforcement. The present computer-model provides such a design means.

v) The results of experimental tests carried out on slender columns subject to sustained, constant load are compared with the computer-analysis and a remarkably good agreement is found.

vi) The design formulae recommended by CEB-FIP and some national codes of practice were analysed and compared with the computer-analysis. It was shown that the design formulae are conservative so long as slenderness and the concrete creep are not too large. However some design formulae (e.g. ACI 318-71) can lead to a too conservative design. It was also shown that the design formulae proposed by CEB-FIP are in very good agreement with the computer-analysis for the range of parameters most often used in practice and this result is noteworthy since the CEB-FIP proposals followed from experimental evidence.

b. Concerning the slender arch.

i) The instability of a symmetric, double hinged arch is analysed with the help of a three degree-of-freedom arch-model and assuming that the material is perfectly visco-elastic.

ii) The discrete arch-model, which is made up from non-deformable members joined by deformable devices (see Fig.5.2, p.221), approximates the real arch by:

- concentrating the axial and rotational deformations in the discrete devices

- replacing the forces and the flexibilities (which are actually variable along the arch axis) with their mean values over the distance between two successive devices

iii) Although this simplified arch-model yields approximate solutions with regard to the actual arch, its use has been considered advantageous on account that:

- it simplifies considerably the analysis of both the elastic and the creep buckling in the range of large displacements.

- it is able to model all the possible modes of buckling associated with the real arch.

- it provides a solution whatever the particularities of the arch geometry or of the load distribution.*)

- it is suitable for computer programming so that a

Footnote

*) Due to the mathematical difficulties which are associated with the instability of arches, there are few particular arches for which closed-form solutions are known even when the material is perfectly elastic (see Timoshenko and Gere (1961)).

wide range of numerical data can be investigated.

- the degree of accuracy of the results for elastic buckling has proved reasonable when compared with known closed-form solutions.

iv) Theoretical approaches were presented to analyse both the elastic pre-and post-buckling behaviour of the arch-model and the effects of concrete creep on its prebuckling and buckling behaviour. Non-linear coupled equations are associated with these analyses and their accurate solution was found by using a standard sub-program available with NAG library.

v) These accurate solutions were compared with approximate solutions arising from using the perturbation technique. It was shown that the differences can be significant when the displacements are large.

vi) Five necessary and sufficient conditions are associated with the elastic buckling of a symmetric three degree-of-freedom arch-model and it was shown that one sufficiently provide the critical load. The other conditions provide information on the mode of buckling. Theoretical proofs were given and it was shown that a similar conclusion can be drawn for discrete model with one and two degree-of-freedom.

vii) With regard to the creep buckling it was shown that:

- when the elastic instability is due to a snap-buckling, the concrete creep reduces always the critical load. The larger is the creep, the lower is the corresponding critical load.

- when the elastic instability is due to a bifurcation of equilibrium no noticeable effect of creep takes place so long as the concrete creep is small. However, when the concrete creep φ exceeds a certain limit φ_{lim}, the creep-dependent critical load decays as the difference $\varphi - \varphi_{lim}$ increases.

viii) From the numerical applications carried out in chapter 5, it followed that the more slender or the shallower the arch is or the more different its geometric axis is from the funicular polygon, the larger the displacements are and consequently the more significant the creep effects.

ix) The analysis of the slender arch was carried out assuming that no material failure can precede the structural instability. This assumption was discussed earlier in this chapter (see Section 6.2) and the range of arches where it proves to be correct was outlined.

6.4 SUGGESTIONS FOR FURTHER RESEARCH

The research carried out and the results presented in this thesis suggest the following directions worthy of further investigation.

With regard to the slender beam-column (chapter 4)

1. The computer-model is built for a rectangular, symmetrically reinforced cross-section. It should be generalised for other types of cross-section. The only difficulty to solve would be to find the lower and upper limits in between the actual strain-distribution on the cross-section lies (see Fig.4.18, p.93 and Fig.4.25, p.105)

2. The computer-model is built for a beam-column bent

in single curvature. Columns bent in double curvature could be analysed in a similar manner provided that the behaviour of the cross-section under decreasing bending moments were modelled. There should be no difficulty in extending the method of solution presented in Section 4.3.3 to those columns.

Such solutions will create conditions for a structural analysis of reinforced concrete frames which can be performed automatically and consistently with the limit state design (see Section 4.3.7c).

With regard to the slender arches (chapter 5)

The analysis of the creep effects in slender reinforced concrete arches has been performed less accurately than that for slender beam-columns. Further research should be carried out in order to improve the results from both the material and the structural behaviour standpoints.

a. Regarding the material behaviour. The assumption of perfectly visco-elastic behaviour should be replaced by a governing relationship which is able to consider the actual response to loading of a reinforced concrete cross-section. Thus simplified n-m-h/r surfaces like those depicted in Fig.4.36a, see p.137, and Fig.4.42, see p.151, may be used. Such a governing relationship will provide better results when the plasticity and cracking of the concrete become relevant, that is when large bending moments occur on the cross-section. As shown in Section 6.2 these are precisely the situations where the present analysis is less correct since the

creep buckling is most likely preceded by a creep-dependent material failure.

b. Regarding the structural behaviour. The arch-model used in chapter 5 proved a convenient means of analysis. However further research should be done to ensure that the discrete model closely approximates the actual slender arch with the flexibility continuously distributed along its axis. Thus:

i) more degrees of freedom should be also investigated inorder to find the optimum number which provide the best compromise between the necessity of modelling the actual deformability of the structure and the simplicity of the analysis.

ii) the horizontal components of the displacements (in other words the axial flexibility of the slender arch) can significantly affect the structural behaviour and the mechanical devices in Fig.5.3, see p.221, can be improved to consider more appropriately these effects. Devices as shown in Fig.5.43, see p.339, could be used.

iii) the analysis of the elastic stability of the three degree-of-freedom arch-model are in agreement with those for models with one and two degree-of-freedom. They suggest that a general theory can be developed on the elastic stability and postbuckling behaviour of discrete arch-models. Such attempts have already been made (see Thompson (1969)).

iv) the additional effects of geometric imperfections combined with structural slenderness and concrete creep can be very damaging and a thorough investigation into

these aspects should be carried out.

The knowledge gained from the research presented in this thesis and the improvements mentioned above are of significant help when the creep effects in reinforced concrete thin shells are analysed. It is there that the combined creep and slenderness have the most significant effects in view of their reduced capacity for bearing bending moments.

APPENDICES

APPENDIX II.1

Age-Adjusted Effective Modulus Method.

A development of the basic formula used by Bazant's 'Age-Adjusted Effective Modulus'method is given below.

It has been shown in Section 2.1 that the stress induced by an imposed constant strain ε_0 is given by eq.(2.8) where R_φ represents the relaxation function (see Fig.2.2 and eq.(2.7)).

If the imposed strain ε has a time-development affine to the creep function,i.e.

$$\varepsilon(t,t_0) = \varepsilon_1 \cdot \varphi(t,t_0) \tag{2.1.1}$$

it follows from the analogy existing between eqs.(2.3a) and (2.11) that the induced stress is

$$\sigma(t,t_0) = E \cdot \varepsilon_1 \cdot R_\varphi(t,t_0) \tag{2.1.2}$$

Therefore,for an imposed strain of the form

$$\varepsilon(t,t_0) = \varepsilon_0 + \varepsilon_1 \cdot \varphi(t,t_0) \tag{2.1.3}$$

the induced stress follows from the superposition of eqs.(2.8) and (2.1.2) as

$$\sigma(t,t_0) = E \cdot \varepsilon_0 + E \cdot (\varepsilon_1 - \varepsilon_0) \cdot R_\varphi(t,t_0) \tag{2.1.4}$$

In eq.(2.1.3) ε_0 and ε_1 are constant and represent

$$\varepsilon_0 = \varepsilon(0,t_0)$$
$$\varepsilon_1 = \frac{\varepsilon(t,t_0) - \varepsilon(0,t_0)}{\varphi(t,t_0)} \tag{2.1.5}$$

On account of eqs.(2.1.5) and of the initial condition

$$\sigma(0,t_0) = E \cdot \varepsilon(0,t_0) \tag{2.1.6}$$

eq.(2.1.4) can be recast as

$$\boxed{\sigma(t,t_0) - \sigma(0,t_0) = E'' \cdot \left[\varepsilon(t,t_0) - \varepsilon(0,t_0) - \sigma(0,t_0) \cdot \frac{\varphi(t,t_0)}{E}\right]} \tag{2.1.7}$$

where

$$E'' = E \cdot \frac{R_\varphi(t,t_0)}{\varphi(t,t_0)} \tag{2.1.8}$$

and is called by Bazant the 'age-adjusted effective modulus'(1972).

E" provides directly the stress induced by a strain imposed according with eq.(2.1.3). Bazant proposes the use of eq.(2.1.7) for other

time-variations of $\mathcal{E}$ too.However,the more different the actual variation of $\mathcal{E}$ is from that given by eq.(2.1.3),the more approximate is the stress in eq.(2.1.7).

APPENDIX II.2 *)

The object of this appendix is to show the development of eqs. (2.40) and (2.42) when φ_r and φ_i corresponding to CEB creep function and rate of flow, respectively (see Table 2.2) are used. All the other governing relationships mentioned in Table 2.2 can be deduced in a similar manner.

Governing relationship (2.40).

From eqs.(2.24) and (2.29)

$$\frac{\partial \varphi_i(t-\tau, t_0+\tau)}{\partial \tau} = -\beta_1 \bar{\varphi}_{i\infty} e^{-\beta_1 \cdot (t_0+\tau)}$$

and from eqs.(2.22),(2.23),(2.27)

$$\frac{\partial \varphi_r(t-\tau, t_0+\tau)}{\partial \tau} = -\beta_2 \varphi_{r\infty} e^{-\beta_2 \cdot (t-\tau)}$$

Thus the derivative of eq.(2.30) is

$$\frac{\partial \varphi(t-\tau, t_0+\tau)}{\partial \tau} = -\beta_1 \bar{\varphi}_{i\infty} e^{-\beta_1 \cdot (t_0+\tau)} - \beta_2 \varphi_{r\infty} e^{-\beta_2 \cdot (t-\tau)}$$

and eq.(2.3a) becomes

$$\varepsilon(t,t_0) = \frac{\sigma(t,t_0)}{E} + \frac{\beta_1 \bar{\varphi}_{i\infty}}{E} \int_0^t \sigma(\tau,t_0) \cdot e^{-\beta_1 \cdot (t_0+\tau)} d\tau + \frac{\beta_2 \varphi_{r\infty}}{E} \int_0^t \sigma(\tau,t_0)\, e^{-\beta_2 \cdot (t-\tau)} d\tau \qquad (2.2.1)$$

The derivative of the previous equation with respect to t is

$$\frac{d\varepsilon}{dt} = \frac{1}{E} \cdot \frac{d\sigma}{dt} + \frac{\beta_1 \cdot \bar{\varphi}_{i\infty} \cdot e^{-\beta_1 \cdot (t_0+t)}}{E} \cdot \sigma + \frac{\beta_2 \varphi_{r\infty}}{E} \cdot \sigma - \frac{\beta_2^2 \varphi_{r\infty}}{E} \int_0^t \sigma(\tau,t_0)\, e^{-\beta_2 \cdot (t-\tau)} d\tau$$

Adding this equation to eq.(2.2.1) multiplied by β_2 it becomes

$$\frac{d\varepsilon}{dt} + \beta_2 \varepsilon = \frac{1}{E} \cdot \frac{d\sigma}{dt} + \frac{\beta_1 \bar{\varphi}_{i\infty} e^{-\beta_1 \cdot (t_0+t)} + \lambda_2}{E} \cdot \sigma + \frac{\beta_1 \beta_2 \bar{\varphi}_{i\infty}}{E} \int_0^t \sigma(\tau,t_0)\, e^{-\beta_1 \cdot (t_0+\tau)} d\tau$$

where the notation (2.41) has been used.

Eq.(2.40) is found as the derivative of the previous one, i.e.

$$\boxed{\frac{d^2\varepsilon}{dt^2} + \beta_2 \frac{d\varepsilon}{dt} = \frac{1}{E} \cdot \frac{d^2\sigma}{dt^2} + \frac{\frac{d\varphi_i}{dt} + \lambda_2}{E} \cdot \sigma + \frac{\beta_2 - \beta_1}{E} \cdot \frac{d\varphi_i}{dt} \cdot \sigma} \qquad (2.40)$$

where, according to eqs.(2.24) and (2.29),

$$\frac{d\varphi_i(t,t_0)}{dt} = \beta_1 \bar{\varphi}_{i\infty} e^{-\beta_1 \cdot (t+t_0)} = \beta_1 \cdot \varphi_i(\infty, t_0+t)$$

Governing relationship (2.42).

From eqs.(2.24) and (2.29)

$$\varphi_i(t-\tau, t_0+\tau) = \varphi_i(t,t_0) - \varphi_i(\tau,t_0) \qquad (2.2.2)$$

and from eq.(2.31)

*) see Constantinescu and Illston (1974)

$$\varphi_i(t-\tau, t_0+\tau) = \varphi_{i\infty}\left[1 - e^{-\beta_2 \cdot \varphi_i(t-\tau, t_0+\tau)}\right] = \varphi_{i\infty}\left\{1 - e^{-\beta_2 \cdot \left[\varphi_i(t,t_0) - \varphi_i(\tau,t_0)\right]}\right\} \qquad (2.2.3)$$

Therefore the derivative of eq.(2.32) with respect to $\varphi_i(\tau, t_0)$ becomes

$$\frac{\partial \varphi(t-\tau, t_0+\tau)}{\partial \varphi_i(\tau, t_0)} = -1 - \beta_2 \varphi_{i\infty} e^{-\beta_2 \cdot \left[\varphi_i(t,t_0) - \varphi_i(\tau,t_0)\right]} \qquad (2.2.4)$$

If $\varphi_i(t, t_0)$ replaces t as variable in eq.(2.3a), this becomes

$$\varepsilon\left[\varphi_i(t,t_0)\right] = \frac{\sigma\left[\varphi_i(t,t_0)\right]}{E} - \int_0^{\varphi_i(t,t_0)} \frac{\sigma\left[\varphi_i(\tau,t_0)\right]}{E} \cdot \frac{\partial \varphi(t-\tau, t_0+\tau)}{\partial \varphi_i(\tau,t_0)} \cdot d\varphi_i(\tau,t_0) \qquad (2.2.5)$$

and further using eq.(2.2.5)

$$\varepsilon\left[\varphi_i(t,t_0)\right] = \frac{\sigma\left[\varphi_i(t,t_0)\right]}{E} + \frac{1}{E} \cdot \int_0^{\varphi_i(t,t_0)} \sigma\left[\varphi_i(\tau,t_0)\right] \cdot d\varphi_i(\tau,t_0) + \frac{\beta_2 \varphi_{i\infty}}{E} \cdot \qquad (2.2.6)$$

$$\int_0^{\varphi_i(t,t_0)} \sigma\left[\varphi_i(\tau,t_0)\right] \cdot e^{-\beta_2 \cdot \left[\varphi_i(t,t_0) - \varphi_i(\tau,t_0)\right]} \cdot d\varphi_i(\tau,t_0)$$

The derivative of the previous equation with respect with $\varphi_i(t, t_0)$ is

$$\frac{d\varepsilon}{d\varphi_i} = \frac{1}{E} \cdot \frac{d\sigma}{d\varphi_i} + \frac{1+\beta_2 \varphi_{i\infty}}{E} \cdot \sigma - \frac{\beta_2^2 \varphi_{i\infty}}{E} \int_0^{\varphi_i} \sigma \cdot e^{-\beta_2 \cdot \left[\varphi_i - \varphi_i(\tau,t_0)\right]} d\varphi_i(\tau,t_0)$$

Adding to eq.(2.2.6) multiplied by β_2,

$$\frac{d\varepsilon}{d\varphi_i} + \beta_2 \varepsilon = \frac{1}{E} \cdot \frac{d\sigma}{d\varphi_i} + \frac{1+\beta_2 \cdot (1+\varphi_{i\infty})}{E} \cdot \sigma + \frac{\beta_2}{E} \cdot \int_0^{\varphi_i} \sigma \cdot d\varphi_i$$

Finally the diferentiation of the previous equation gives

$$\boxed{\frac{d^2\varepsilon}{d\varphi_i^2} + \beta_2 \frac{d\varepsilon}{d\varphi_i} = \frac{1}{E} \cdot \frac{d^2\sigma}{d\varphi_i^2} + \frac{1+\lambda_2}{E} \cdot \frac{d\sigma}{d\varphi_i} + \frac{\beta_2}{E} \cdot \sigma} \qquad (2.42)$$

where the notation (2.41) has been used.

Eq.(2.2.2), which is the source of the governing relationship (2.42), is always true regardless of the expression for φ_i. Therefore eq.(2.42) is not dependent on the mathematical function chosen for $F_i(t+t_0)$. This conclusion is valid for all the governing relationships from Table 2.2 using φ_i as variable.

APPENDIX III.1

Direct solutions to problems of time-dependent induced stresses in restrained concrete

D.R. CONSTANTINESCU (1), J.M. ILLSTON (2)

The creep effects on the stresses induced in a concrete member by imposed deformations having a history similar to the shrinkage of concrete are analysed.

Direct solutions of the problem are deduced using two governing relationships of concrete judged in reference [1] *as the best compromise between reality and simplicity.*

The results are obtained in a general form and the influences of the most important parameters are plotted and compared.

NOTATION

E – modulus of elasticity. Throughout the present paper E is assumed age-independent.

t_0 – the age of concrete on initial loading. For each problem t_0 is a constant.

t – the time after loading; $t = 0$ when the age of concrete is t_0.

$t + t_0$ – the actual age of concrete at the moment t.

τ – an intermediate time ($0 < \tau \leqslant t$).

$\sigma(t, t_0)$ – the stress at the time t, measured from the age t_0. The positive values denote tension.

$\varepsilon(t, t_0)$ – the total strain at the same time as $\sigma(t, t_0)$. The positive values denote dilatation.

$\varepsilon_\varphi(t, t_0)$ – as ε but creep strain only. $\varepsilon_\varphi = \varepsilon_{\varphi t} + \varepsilon_{\varphi r}$.

$\varepsilon_{\varphi r}$ – the recoverable component of ε_φ.

$\varepsilon_{\varphi t}$ – the irrecoverable component of ε_φ.

$\varepsilon_e(t, t_0) = \dfrac{\sigma(t, t_0)}{E}$; the elastic strain.

$\varphi(t, t_0) = \dfrac{\varepsilon_\varphi(t, t_0)}{\varepsilon_e(t, t_0)}$. For $E = \text{const.}$ $\varphi = \dfrac{\varepsilon_\varphi}{\sigma} \times E$, where $\dfrac{\varepsilon_\varphi}{\sigma}$ is the specific creep strain (creep function). Also $\varphi = \varphi_t + \varphi_r$.

$\varphi_t(t, t_0) = \dfrac{\varepsilon_{\varphi t}}{\varepsilon_e}$

$\varphi_r(t, t_0) = \dfrac{\varepsilon_{\varphi r}}{\varepsilon_e}$ when $\varepsilon_{\varphi r}$ is age-dependent.

$\varphi_r(t)$ $= \dfrac{\varepsilon_{\varphi r}}{\varepsilon_e}$ when $\varepsilon_{\varphi r}$ is age-independent.

β_1 – constant affecting the rate of time-development of φ_t.

β_2 – constant similar to β_1 but for φ_r.

$\bar{\varphi}_{t\infty}$ – the final value of φ_t including the influences of all the factors affecting the concrete creep, except the age of concrete.

$\varphi_{t\infty}$ $= \varphi_t(\infty, t_0) = \bar{\varphi}_{t\infty} \times e^{-\beta_1 t_0}$; the final value of $\varphi_t(t, t_0)$.

$\varphi_{r\infty}$ – the final value of $\varphi_r(t, t_0)$.

λ_2 $= \beta_2 \times (1 + \varphi_{r\infty})$.

$R(t)$ – a change in the unit length of the concrete due to an external cause (e.g. a temperature variation) or to an internal one (e.g. shrinkage). The positive value denote dilatation.

$\bar{K}$ – the final value of R.

K $= \bar{K} \cdot E_c$; the elastic final value of σ_c when $\alpha = 1$.

m – a positive integer used to model a R-function faster than $\dfrac{\varphi_t(t, t_0)}{\varphi_{t\infty}} = 1 - e^{-\beta_1 t}$.

n – the same as m but used to model a R-function slower than $1 - e^{-\beta_1 t}$.

α – the degree of restraint of the development of R.

A – the sectional area.

S – the elastic stiffness.

r_1, r_2 – the roots of the characteristic equation associated with the differential equation (4); see eq. (10).

σ_c^* – the particular solution of eq. (4).

(1) C. Eng., Lecturer in Concrete Structures, Faculty of Civil Engineering, Bucharest, Romania; currently undertaking research at King's College, London, England.

(2) B. Sc. (Eng.), Ph. D., C. Eng., M.I.C.E., Reader in Civil Engineering, King's College, London, England.

B, C – constants of integration.
a $= \alpha + \beta_2 \cdot (1 + \alpha \varphi_{r\infty})$
A_j – constants.

Subscripts

c – subscript associated with all the quantities concerning the concrete or, generally, the part of the structure providing a time-dependent behaviour.
s – similar to c but concerning the reinforcement or the part of the structure exhibiting elastic behaviour.

INTRODUCTION

In a previous paper [1] an examination was conducted into the various governing relationships that enable direct solutions to be found to problems involving the linear creep of ageing concrete. It was concluded that two creep methods, *rate of flow* [2] and *improved Dischinger* [3] [4], represent the best compromise between the reality of concrete behaviour and mathematical simplicity.

The governing differential equations for the two methods were shown to be as follows :

Rate of flow,

$$\frac{d^2\varepsilon}{d\varphi_i^2} + \beta_2 \frac{d\varepsilon}{d\varphi_i} = \frac{1}{E}\frac{d^2\sigma}{d\varphi_i^2} + \frac{1+\lambda_2}{E}\frac{d\sigma}{d\varphi_i} + \beta_2 \frac{\sigma}{E} \quad (1)$$

Improved Dischinger,

$$\frac{d\varepsilon}{dt} = \frac{1+\varphi_{r\infty}}{E}\frac{d\sigma}{dt} + \frac{\sigma}{E}\frac{d\varphi_i}{dt} \quad (2)$$

Both methods consider linear creep as the sum of recoverable and irrecoverable components, given here as creep coefficients, φ_r and φ_i, and it is important to note that in *rate of flow* the variable is the irrecoverable creep, φ_i, while *improved Dischinger* can be equally well expressed in terms of the time after loading, t.

ε is the total strain under time-dependent stress, σ, E is the elastic modulus, taken as independent of time, and the suffix ∞ indicates the final limiting value. β_2 is a constant defining the rate of occurrence of φ_r, and $\lambda_2 = \beta_2 \cdot (1 + \varphi_{r\infty})$.

In the present paper the application of the two methods to the direct solution of a particular relaxation problem is demonstrated, and the opportunity is taken to make a comparison between the two.

In the problem the concrete is subjected to an imposed time-dependent strain, R, which is inhibited in accordance with a degree of restraint, characterised by a relative stiffness function α. The concrete is taken to be bonded in parallel with an elastic material; in practice the simplest model is a symmetrically reinforced concrete member in which the concrete suffers a uniform time-dependent shrinkage. The solution to the problem consists of the history of stress in the concrete, from which the steel stress history can be easily found. Throughout the following section tensile stress and dilation are taken as positive.

ANALYTICAL TREATMENT

The history of the imposed strain is considered to have the general form,

$$R(t) = \bar{K} \times (1 - e^{-m\beta_1 t}) \quad \text{with} \quad m \geqslant 1 \quad (3a)$$

or

$$R(t) = \bar{K} \times (1 - e^{-\beta_1 t})^n \quad \text{with} \quad n \geqslant 1 \quad (3b)$$

These expressions are shown plotted in figure 1, and four cases can be identified.

(1) Imposed strain constant in time, corresponding to $m = \infty$.
(2) Imposed strain affine to the irrecoverable creep curve (given by $\varphi_i = \varphi_{i\infty} \times (1 - e^{-\beta_2 t})$), corresponding to $m = 1$ or $n = 1$ in equations (3).
(3) Imposed strain faster than the irrecoverable creep, corresponding to $m > 1$ in equation (3a). This case covers the zone between the previous two, which form the upper and lower bounds.
(4) Imposed strain slower than the irrecoverable creep, corresponding to $n > 1$ in equation (3b). This case covers the zone between the curve for case (2) as an upper bound, and the time axis as a lower bound.

The mathematical procedure is such that solutions can be found only for integer values of m or n. However the actual phenomena are continuous, and interpolation between successive integer values is a perfectly valid procedure.

The governing relation for *rate of flow* is considered first, in some detail. Regardless of the expression for R, the general equation of the problem is,

$$\frac{d^2\sigma_c}{d\varphi_i^2} + a \cdot \frac{d\sigma_c}{d\varphi_i} + \alpha\beta_2\sigma_c = -E_c\alpha \times \left(\frac{d^2R}{d\varphi_i^2} + \beta_2\frac{dR}{d\varphi_i}\right) \quad (4)$$

with $R(0) = 0$, and for a and α according to the following development.

For the reinforced concrete section, there are two coupled equations : equilibrium of the reinforced concrete section,

$$\sigma_c A_c + \sigma_s A_s = 0$$

compatibility of strains,

$$\varepsilon_c + R = \varepsilon_s.$$

Also, from the constitutive relation for the steel,

$$\sigma_s = E_s \varepsilon_s.$$

The governing relation of concrete, equation (1), is given again here,

$$\frac{d^2\sigma_c}{d\varphi_i^2} + (1+\lambda_2) \times \frac{d\sigma_c}{d\varphi_i} + \beta_2\sigma_c = E_c \times \left(\frac{d^2\varepsilon_c}{d\varphi_i^2} + \beta_2\frac{d\varepsilon_c}{d\varphi_i}\right) \quad (5)$$

Rearrangement and substitution leads to the equation (4) for the reinforced concrete member.

In these equations modulus of elasticity is denoted by E and sectional area by A. The subscripts c and s are associated with concrete and steel respectively.

The symbol α is a relative stiffness function given by

$$\alpha = \frac{E_s A_s}{E_c A_c + E_s A_s} \tag{6a}$$

and

$$a = \alpha + \beta_2 \cdot (1 + \alpha \varphi_{r\infty}) \tag{7}$$

Here α has been defined in terms of the particular problem of the reinforced concrete member, but it is quite general to any structure having one indeterminacy providing interaction between an elastic part and a visco-elastic part. Thus, in general,

$$\alpha = \frac{S_s}{S_s + S_c} \tag{6b}$$

where S_c and S_s are, respectively, the elastic stiffness of the visco-elastic part and the stiffness of the elastic part. In this form the solution is applicable to a wider range of practical problems associated with the effects of shrinkage, settlement and temperature variation. α is a constant for the structure and characterises its degree of restraint. It can have any value between 0 and 1; $\alpha = 0$ signifies that the structure is statically determinate, so that the imposed strain, R, causes no induced stress. $\alpha = 1$ signifies that the elastic part of the structure is indefinitely stiffer than the visco-elastic part, so that the imposed strain is completely resisted, as in the case of a plain concrete column built in at both ends. When $\alpha = 1$ equations (4) and (5) become identical.

It follows that, in these general terms, the elastic response in the concrete is given by

$$\sigma_{c,el} = - E_c \cdot \alpha \cdot R(t) \tag{8}$$

Similarly, the solution for the concrete stress is found from equation (4) with R given by equations (3).

The general solution is

$$\sigma_c = B e^{-r_1 \varphi_t} + C e^{-r_2 \varphi_t} + \sigma_c^* \tag{9}$$

where r_1 and r_2 are the roots of the characteristic equation associated to eq. (4),

that is

$$r_{1,2} = 0.5 \cdot (a \pm \sqrt{a^2 - 4 \alpha \beta_2}) \tag{10}$$

The constants of integration B and C, and the particular solution σ_c^* depend on the mathematical form of R. Considering each of the four cases listed earlier :

For $m > 1$, with m an integer (see Appendix)

$$\sigma_c^* = \frac{K \alpha}{\varphi_{t\infty}} \sum_{j=1}^{m} \frac{m!}{(m-j)!\,(j-1)!} \cdot \left(\frac{\varphi_t}{\varphi_{t\infty}}\right)^{m-j} \cdot Aj \tag{11}$$

where

$$K = \bar{K} \times E_c \tag{12}$$

and the constants A_j are given by

$$A_1 = \frac{(-1)^m}{\alpha}$$

$$\alpha \beta_2 A_2 + \frac{a}{\varphi_{t\infty}} A_1 = (-1)^m \times \left(\frac{1}{\varphi_{t\infty}} - \beta_2\right) \tag{13}$$

$$\frac{\alpha \beta_2}{j-1} A_j + \frac{a}{\varphi_{t\infty}} A_{j-1} + \frac{j-2}{\varphi_{t\infty}^2} A_{j-2} = (-1)^{m-j} \times \left(\frac{1}{\varphi_{t\infty}} - \frac{\beta_2}{j-1}\right) \quad \text{for } j = 3 \ldots m$$

Also

$$B = \frac{K \alpha m}{\varphi_{t\infty} \cdot (r_1 - r_2)} \cdot \left(1 + r_2 A_m + \frac{m-1}{\varphi_{t\infty}} A_{m-1}\right)$$

$$C = - \frac{K \alpha m}{\varphi_{t\infty}} A_m - B. \tag{14a}$$

Here $\varphi_{t\infty}$ denotes the final value of φ_t when the age of first loading is t_0, so that, according to [1]

$$\varphi_{t\infty} = \bar{\varphi}_{t\infty} \cdot e^{-\beta_1 t_0} \tag{15}$$

For $n > 1$ with n an integer the solution is similar to that above (see Appendix).

σ_c^* has the same general form as equation (11) — with n for m. Constants A_j are given by similar equations to (13), with identical left hand sides, and with right hand sides $-\frac{1}{\alpha}$, $-\frac{1}{\varphi_{t\infty}}$ and 0 (for $j = 3 \ldots n$), respectively.

The constants of integration are in this case,

$$B = \frac{K \alpha n}{\varphi_{t\infty} \cdot (r_1 - r_2)} \cdot \left(r_2 A_n + \frac{n-1}{\varphi_{t\infty}} A_{n-1}\right)$$

$$C = - \frac{K \alpha n}{\varphi_{t\infty}} A_n - B \tag{14b}$$

similarly to eqs. (14*a*).

For $m = 1$ the general solution (9) becomes (see Appendix)

$$\sigma_c = - K \cdot [B_1 \cdot (1 - e^{-r_1 \varphi_t}) + C_1 \cdot (1 - e^{-r_2 \varphi_t})] \tag{16}$$

where

$$B_1 = \frac{\alpha - r_2}{r_1 - r_2}$$

$$C_1 = 1 - B_1. \tag{17}$$

If the recoverable creep component is neglected, this devolves into the well known *rate of creep* solution [4], [5]

$$\sigma_c = - K \cdot (1 - e^{-\alpha \varphi_t}) \tag{18}$$

For $m = \infty$ the general solution becomes (see Appendix)

$$\sigma_c = - K \cdot \alpha \cdot (B_2 e^{-r_1 \varphi_t} + C_2 e^{-r_2 \varphi_t}) \tag{19}$$

where

$$B_2 = \frac{r_1 - \beta_2}{r_1 - r_2}$$

$$C_2 = 1 - B_2. \tag{20}$$

Again, neglect of the recoverable component yields the known solution [4], [5]

$$\sigma_c = - K \alpha e^{-\alpha \varphi_t} \tag{21}$$

The governing relationship for the *improved Dischinger* method (see equation 2) yields the following general equation for the problem

$$(1 + \alpha \varphi_{r\infty}) \cdot \frac{d\sigma_c}{d\varphi_t} + \alpha \sigma_c = - \alpha \frac{dR}{d\varphi_t} \cdot E_c \tag{22}$$

A similar method of solution to that already demonstrated can be used (see Appendix). Mathematically, it is somewhat more simple because of

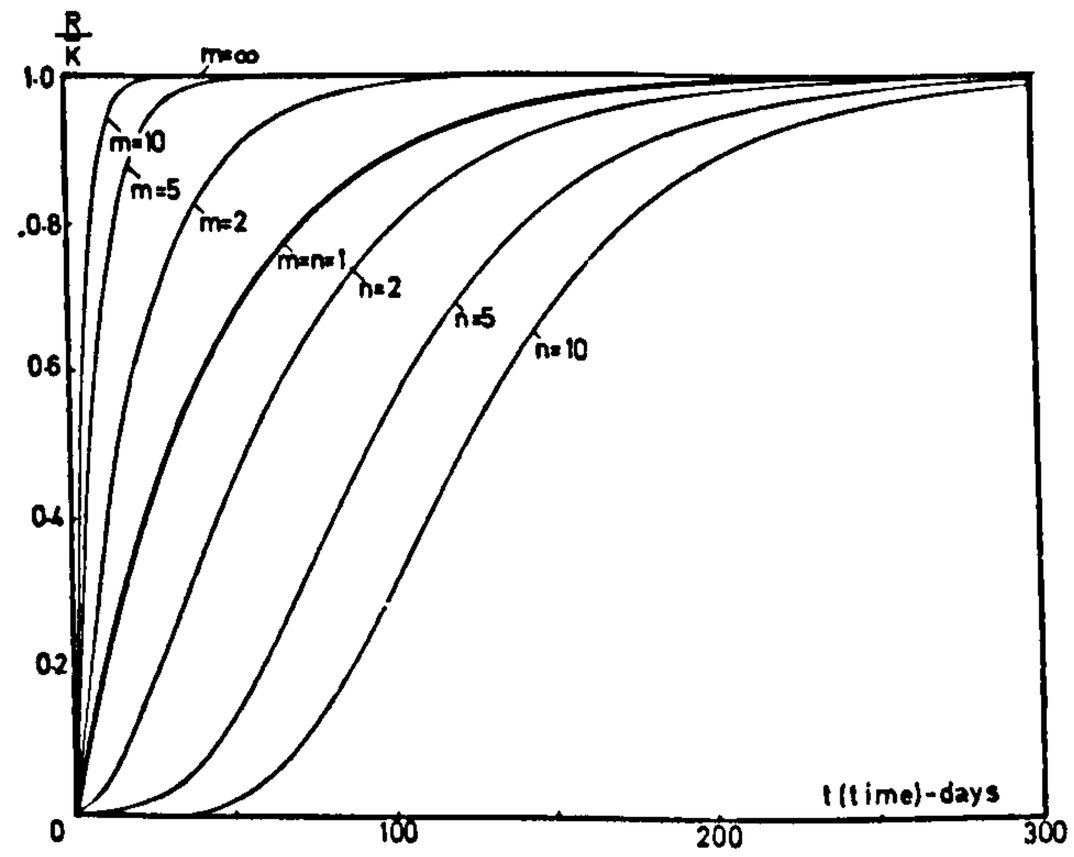

Fig. 1. — The time-development of the imposed strain R(t) according to eqs. (3).

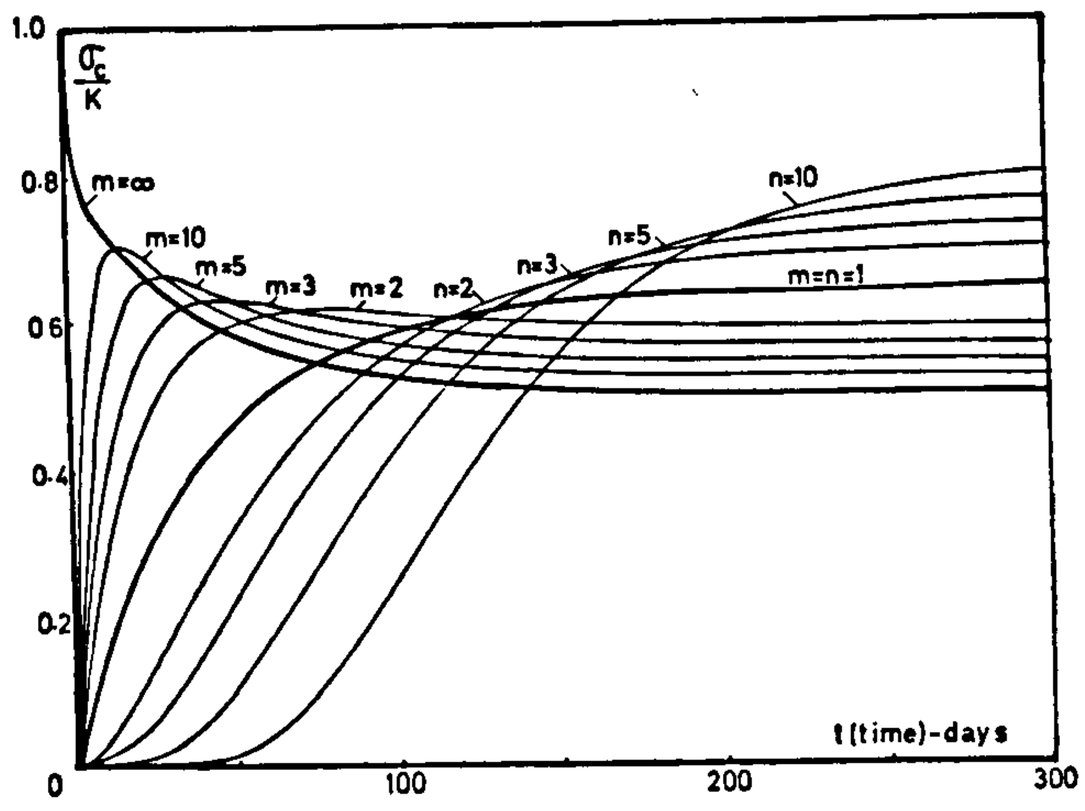

Fig. 2. — The stress-response $\sigma_c(t, t_0)$ according to the rate of flow solution [9] and induced by the imposed strains of figure 1; $t_0 = 28$ days and $\alpha = 1$.

the smaller order of differentiation in equation (22) compared to equation (4).

Thus for the limit cases, $m = 1$ and $m = \infty$, the solutions are

$$\sigma_c = -K \cdot (1 - e^{-\frac{\alpha\varphi_t}{1+\alpha\varphi_{r\infty}}}) \qquad (23)$$

and,

$$\sigma_c = -\frac{K\alpha}{1+\varphi_{r\infty}} \cdot e^{-\frac{\alpha\varphi_t}{1+\alpha\varphi_{r\infty}}} \qquad (24)$$

which are more straightforward than equations (16) and (19) from *rate of flow*.

Equations (16) and (19) give,
with $\beta_2 = \infty$, equations (23) and 24),
with $\beta_2 = 0$, equations (18) and (21).

COMPUTED RESULTS

The computed solutions to the relaxation problem, using the relations developed in the last section, are given in figures 2 ... 5. All the curves are based on the following numerical values [6].

$$\beta_1 = 0.022 \text{ days}^{-1} \qquad \bar{\varphi}_{t\infty} = 1.1$$
$$\beta_2 = 60 \qquad \varphi_{r\infty} = 0.24$$

The stress in the concrete is plotted non-dimensionally, as a ratio of σ_c to K, K being the final elastic value of $\sigma_{c,el}$ (from equations (8) and (12)) when the imposed strain is completely restrained ($\alpha = 1$). The rates of which the imposed strain is applied are defined by the values of m or n, as shown in figure 1.

A complete spectrum of results is given in figure 2 for the case when the relative stiffness function $\alpha = 1$, and the age of loading, $t_0 = 28$ days.

The maximum stress occurring is under the influence of two opposing effects. Firstly, when the strain is imposed rapidly (high values of m), there is insufficient time for immediate relief of stress by creep. This leads to high early stresses with a maximum when the whole strain is imposed instantaneously ($m = \infty$). Secondly, there is a decreasing creep capacity left in the concrete as it gets older. This leads to higher final stresses when the strain is imposed slowly,

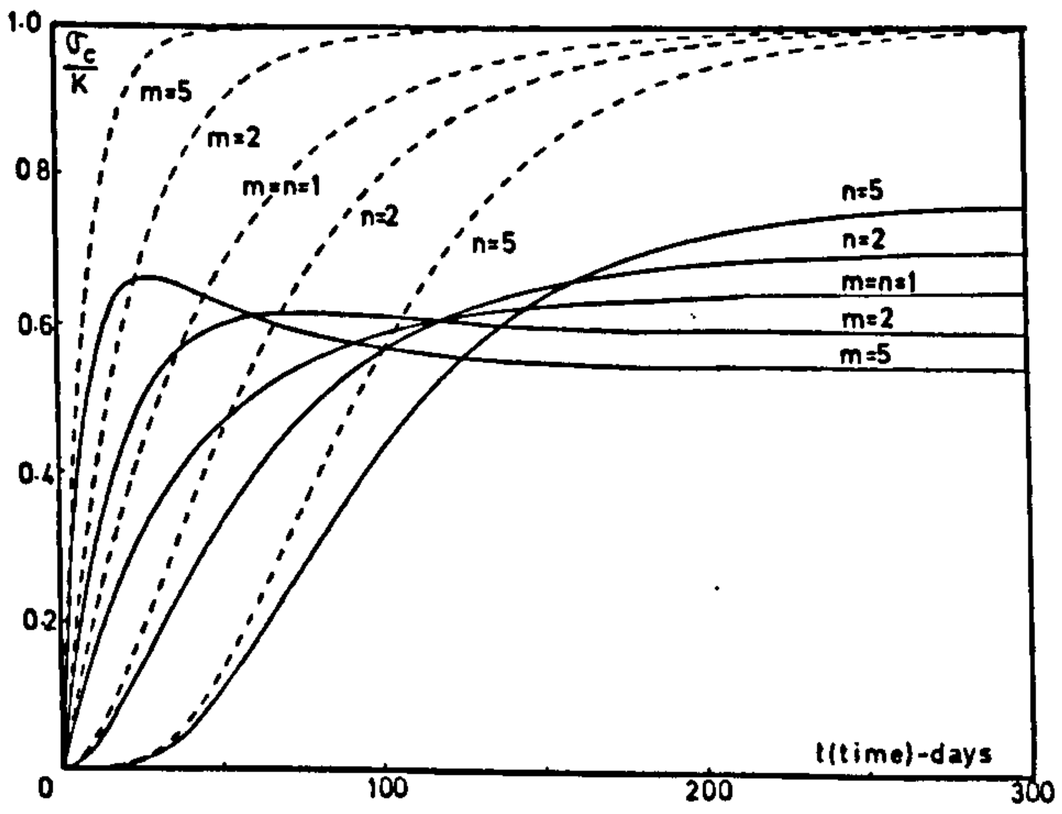

Fig. 3. — The effect of creep on the stress-response induced by the imposed strains of figure 1. The elastic solutions (8) are shown as dashed lines and the rate of flow solutions (9) are shown as full lines. $t_0 = 28$ days and $\alpha = 1$.

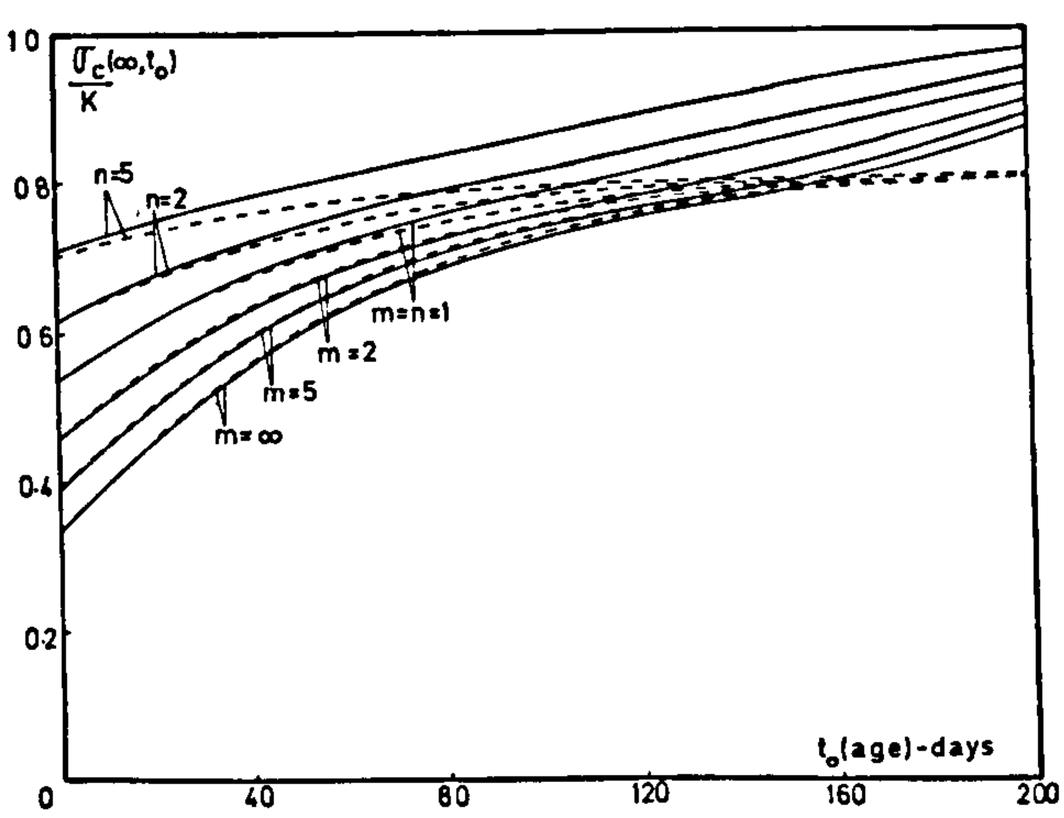

Fig. 4. — Comparison between the values of the final stress-response $\sigma_c(\infty, t_0)$ given by the rate of flow equation (4) — full line — and the Improved Dischinger equation (22) — dashed line; $\alpha = 1$.

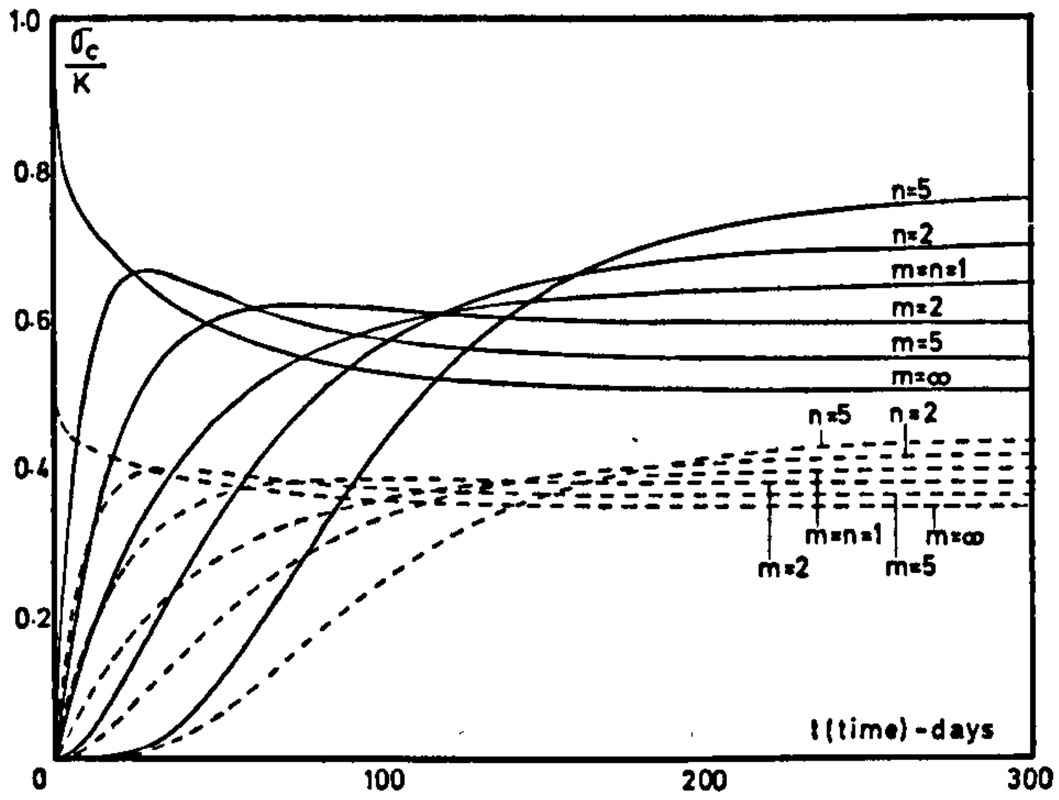

Fig. 5. — The influence of the degree of restraint α on the stress-response induced by a strain-history as in figure 1. The σ_c (t, t_0) values are computed according to the rate of flow equation (4) for $\alpha = 1$ (unbroken line) and $\alpha = 0.5$ (dashed line). The t-axis corresponds to the case $\alpha = 0$; $t_0 = 28$ days.

giving the highest for the greatest value of n. Clearly there must be an optimum rate of strain imposition which gives a lowest maximum stress. Here, this corresponds to $m = 2$.

The effectiveness of creep in relieving stress is demonstrated in figure 3. This shows the elastic solution to the problem as dashed lines, which are naturally of the same shape as the curves in figure 1, together with the corresponding curves for the creep solution. It can be seen that the faster the imposed strain is applied (high m, low n) the greater the stress relief, shown here by the lower final stresses.

In figures 2 and 3, only the *rate of flow* solution is given, but, in fact, for this comparatively early age of loading the *improved Dischinger* solution is virtually identical. The difference between the methods is shown in figure 4, in which the final concrete stress is plotted against the age of loading. The maximum value of age of loading is 200 days, at which the mathematical solution starts to become unstable. As can be seen, the assumption in the *improved Dischinger* method that the recoverable creep occurs instantaneously, leads, for high ages of loading (and low rates of irrecoverable creep), towards the final value of stress

$$\sigma(\infty, t_0) = \frac{K\alpha}{1 + \varphi_{r\infty}} = 0.805\, K\alpha$$

for any value m or n. In the *rate of flow* method the rate of recoverable creep decreases with age, and this suggests that the stress relief in a very old concrete would be very small. Figure 4 emphasises the difference between the two methods, but it does not make any judgement between them. Intuitively, *rate of flow* appears to be the better representation of reality, but there is insufficient evidence to make any sort of decisive quantitative comparison.

The curves of figures 2, 3 and 4 were all computed for the case of complete restraint, $\alpha = 1$ — the plain concrete column with built in ends. In figure 5, the effect of partial restraint is shown ($\alpha < 1$). If $\alpha = 0$, then there is no restraint at all, and consequently there is no induced stress. On figure 5 this is represented by $\sigma_c = 0$, that is, by the time axis, for all values of m and n. The intermediate value $\alpha = 0.5$, gives rise to the group of curves shown dashed, and it can be seen that the spread of results is reduced in comparison with those for $\alpha = 1$.

CONCLUSIONS

Previously it was concluded [1] that the governing relationships embodied in the *rate of flow* and *improved Dischinger* methods are the best compromise between reality and simplicity. Here both methods were demonstrated in the direct solution of a general structural relaxation problem. In one particular form this is the problem of the symmetrically reinforced concrete column in which the concrete suffers a time-dependent shrinkage. It was found :

(a) That for chosen functional form of the imposed strain-time relation, there is an optimum rate of time development that gives rise to the lowest maximum stress in the concrete. Practically for an imposed strain developing in time faster than the creep of the concrete ($m > 1$) a stress-value greater than the maximum stress corresponding to the optimum rate can appear only for a short time, in the first two months after loading.

(b) That, at low ages, there is virtually no difference between the solutions given by the two methods used. As the starting age of the strain imposition becomes greater, the solutions diverge : for a very old concrete, *rate of flow* predicts very little stress relief due to creep, while *improved Dischinger* predicts a final stress value of about 0.805 $K\alpha$.

APPENDIX

The object of this appendix is to show, firstly, the derivation of the solutions of eqs. (4) and (22) when R is given by eq. (3*a*) with $m > 1$ or by eq. (3*b*) with $n > 1$. Finally reference is made to the differences occurring when the limit cases $m = 1$ ($n = 1$) and $m = \infty$ are considered.

Solution of eq. (4)

Eq. (4) has the general solution (9) in which σ_c^* is a particular solution, B and C are constants of integration and r_1, r_2 are the roots of the algebraic equation associated with eq. (4) in its homogeneous form and are given by eq. (10).

The initial conditions of the problem (at $t = 0$, then $\varphi_t = 0$) for both eqs. (3) and m (or n) finite are

$$\sigma_c = 0$$

$$E_c \cdot \frac{\mathrm{d}\varepsilon_c}{\mathrm{d}\varphi_t} = \frac{\mathrm{d}\sigma_c}{\mathrm{d}\varphi_t} \qquad \text{(a)}$$

Using the solution (9) these initial conditions

$$B + C = -\sigma_c^*(\varphi_i = 0)$$

$$r_1 \cdot B + r_2 \cdot C = \frac{d\sigma_c^*}{d\varphi_i}(\varphi_i = 0) + \alpha \cdot E_c \cdot \frac{dR}{d\varphi_i}(\varphi_i = 0) \qquad (b)$$

leading to B and C as functions of R.

σ_c^* can be found according to eq. (11) regardless of whether R is given by eq. (3*a*) or by eq. (3*b*). But the particular expressions of constants A_j, and B and C depend on which equation is used.

1 - If it is eq. (3*a*) and if $m > 1$ and integer, the binomial theorem can be used and hence, using also, from [1], $\varphi_i(t, t_0) = \bar{\varphi}_{i\infty}\, e^{-\beta_1 t_0}(1 - e^{-\beta_1 t})$

$$R(t) = \bar{K} \cdot \left[1 - \left(1 - \frac{\varphi_i}{\varphi_{i\infty}}\right)^m\right] = -\bar{K} \cdot \sum_{j=1}^{m} \frac{(-1)^{m-j} \cdot m!}{j!\,(m-j)!} \cdot \left(\frac{\varphi_i}{\varphi_{i\infty}}\right)^{m-j} \qquad (c)$$

The constants A_j from σ_c^* can be established by introducing eqs. (11) and (c) in eq. (4) and by equating the coefficients of φ_i^j. So eqs. (13) are derived.

Further from eqs. (11) and (c)

$$\sigma_c^*(\varphi_i = 0) = \frac{K\,\alpha\, m}{\varphi_{i\infty}} \cdot A_m$$
$$\frac{d\sigma_c^*}{d\varphi_i}(\varphi_i = 0) = \frac{K\,\alpha\, m(m-1)}{\varphi_{i\infty}^2} \cdot A_{m-1} \qquad (d)$$

and, respectively,

$$\alpha \cdot E_c \cdot \frac{dR}{d\varphi_i}(\varphi_i = 0) = \frac{K\,\alpha\, m}{\varphi_{i\infty}} \qquad (e)$$

Using eqs. (d) and (e) in eq. (b) the solutions (14a) are obtained.

2 - If eq. (3b) is used and if $n > 1$ and integer, a similar method of solution can be applied. The only difference arises from the relation

$$R(t) = \bar{K} \cdot \left(\frac{\varphi_i}{\varphi_{i\infty}}\right)^n \qquad (f)$$

instead of eq. (c).

Thus using this $R(t)$, eq. (11) is still valid but

$$A_1 = -\frac{1}{\alpha}$$
$$\alpha\,\beta_2\, A_2 + \frac{a}{\varphi_{i\infty}} A_1 = -\frac{1}{\varphi_{i\infty}} \qquad (g)$$
$$\frac{\alpha\,\beta_2}{j-1} A_j + \frac{a}{\varphi_{i\infty}} A_{j-1} + \frac{j-2}{\varphi_{i\infty}^2} A_{j-2} = 0, \quad \text{for } j = 3 \ldots n$$

Eqs. (g) are identical to eqs. (13) but with a different right-hand side. Eq. (f) also gives

$$\alpha \cdot E_c \cdot \frac{dR}{d\varphi_i}(\varphi_i = 0) = 0 \qquad (h)$$

instead of eq. (e) so that the constants B and C for R given by eq. (3*b*) are found as in eqs. (14*b*).

With eqs. (g) and (14*b*) instead of eqs. (13) and (14*a*), respectively, the general solution (9) can be found similarly to the previous case, when R is given by eq. (3*a*).

Solution of eq. (22)

The general solution of eq. (22) can be found either directly following the same approach as used for eq. (4), or indirectly taking $\beta_2 = \infty$ into the previous equations.

For both eqs. (3) the general solution is

$$\sigma_c = A_0 \cdot e^{-\frac{\alpha\varphi_i}{1+\alpha\varphi_{r\infty}}} + \sigma_c^* \qquad (i)$$

where A_0 is obtained from the initial condition

$$\sigma_c = 0 \;\rightarrow\; A_0 = -\sigma_c^*(\varphi_i = 0)$$

and σ_c^* is still given by eq. (11). For R given by eq. (3*a*) and for $m > 1$ and integer, for instance, the constants A_j are given by

$$A_1 = \frac{(-1)^m}{\alpha}$$
$$\frac{\alpha}{j-1} A_j + \frac{1 + \alpha\,\varphi_{r\infty}}{\varphi_{i\infty}} A_{j-1} = \frac{(-1)^{m-j}}{\alpha \cdot (j-1)}, \qquad (j)$$
$$\text{for } j = 2 \ldots m$$

which are similar to eqs. (13) and the constant of integration A_0 is given by

$$A_0 = -\frac{K\,\alpha\, m}{\varphi_{i\infty}} A_m.$$

Solution for m = 1 (n = 1)

This case is simpler than the previous ones because $R = \bar{K} \cdot \varphi_i$ and so the particular solutions of both eqs. (4) and (22) become $\sigma_c^* = -K$. So

1 - When eq. (4) is used the constants B and C from (9) (here denoted by B_1 and C_1) can be found similarly to eqs. (b) from

$$B_1 + C_1 = K$$
$$r_1 B_1 + r_2 C_1 = K\,\alpha. \qquad (k)$$

Eqs. (16) and (17) are obtained.

2 - When eq. (22) is used the constant A_0 from (*i*) is given by $A_0 = -K$ and hence eq. (23) is obtained.

Solution for m = ∞

For $m = \infty$ both eqs. (4) and (22) become homogeneous because R is a constant. So $\sigma_c^* = 0$ in the solutions (9) and (*i*).

Using the initial conditions

$$\sigma_c(\varphi_i = 0) = -K \cdot \alpha \qquad (m)$$
$$E_c \cdot \frac{d\varepsilon_c}{d\varphi_i}(\varphi_i = 0) = \frac{d\sigma_c}{d\varphi_i}(\varphi_i = 0) + \sigma_c \cdot \frac{d\varphi}{d\varphi_i}(\varphi_i = 0)$$

for the solution (9), and the first of eqs. (*m*) for the solution (*i*), eqs. (19) and eq. (24) are obtained, respectively.

RÉSUMÉ

Solutions directes au problème des contraintes qui se développent en fonction du temps dans un béton bridé.
— *On évalue les effets du fluage sur les contraintes engendrées dans un élément de béton par des déformations imposées. Le cas répond à toute une gamme de problèmes pratiques.*

L'exemple le plus simple en est le problème d'un béton armé symétriquement et où se produit un retrait.

Les solutions directes au problème sont obtenues à l'aide des méthodes Dischinger améliorées et de vitesse d'écoulement, que, dans un article précédent, on a considérées comme le meilleur compromis entre la réalité physique et la simplicité mathématique.

On examine et compare sous une forme graphique les influences des paramètres les plus importants, tels que la vitesse de déformation imposée, le degré d'empêchement et l'âge du béton.

Les résultats des deux méthodes sont pratiquement égaux lorsque la déformation est imposée dans les deux premiers mois du béton, et diffèrent de plus en plus à mesure que l'âge où la déformation est imposée augmente.

REFERENCES

[1] CONSTANTINESCU D.R., ILLSTON J.M. — *Direct methods of analysing the structural effects of linear creep of ageing concrete.* Materials and Structures. November-December 1974.

[2] ENGLAND G.L., ILLSTON J.M. — *Methods of computing stress in concrete from a history of measured strain.* Civil Engineering and Public Works Review, April, May, June 1965.

[3] DISCHINGER F. — *Elastische und plastiche Verformungen der Eisenbetontragwerke und insbesondere der Bogenbruchen.* Bauingenieur, No. 5/6, 1939.

[4] RÜSCH H., JUNGWIRTH D., HILSDORF H. — *Kritische Sichtung der Verfahren zur Berucksichtigung der Einflusse von Kriechen und Schwinden des Betons auf das Verhalten der Tragwerke.* Beton und Stahlbetonbau, Nos. 3, 4 and 6, 1973.

[5] ILLSTON J.M., ENGLAND G.L. — *Creep and shrinkage of concrete and their influence on structural behaviour — a review of methods of analysis.* The Structural Engineer, July, 1970.

[6] ILLSTON J.M., JORDAAN I.J. — *Creep prediction for concrete under multiaxial stress.* J.A.C.I., March 1972.

[7] COURBON J. — *L'influence du fluage linéaire sur l'équilibre des systèmes hyperstatiques en béton précontraint*, Ann. ITBTP, Feb. 1968.

APPENDIX IV.1

The effects of the M_1-distribution.

The effects of the distribution of M_1 along the member length are analysed below for a perfectly elastic material. M_1 are the first order bending moments, i.e. the moments computed on the undeformed state of the member.

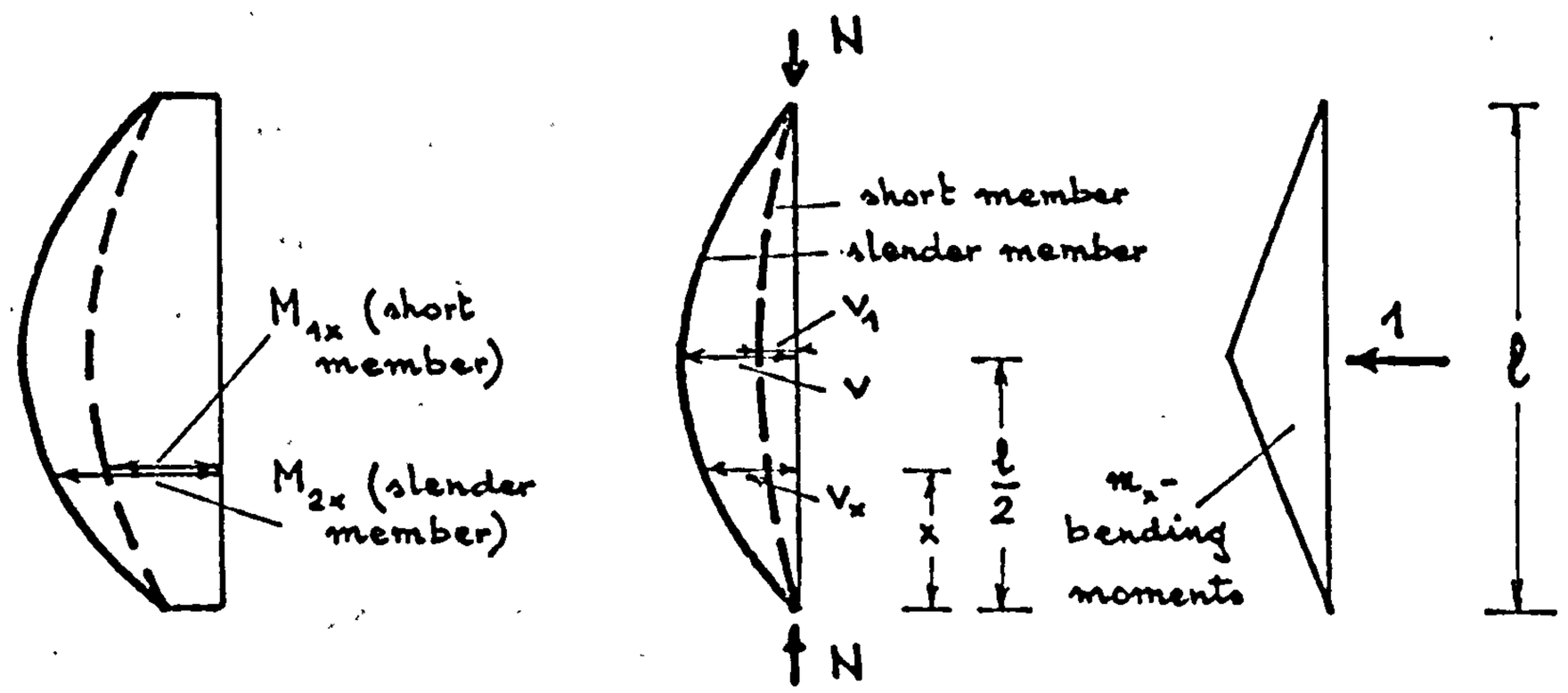

Fig.4.1.1

When the M_1-diagram has a general form as in Fig.4.1.1 the elastic deflection at the midlength follows from Castigliano's theorem as

$$v = \int_0^l \frac{M_{2x} \cdot m_x}{EI} dx = \frac{\pi^2}{N_{cr} \cdot l^2} \int_0^l M_{2x} \cdot m_x \, dx \qquad (4.1.1)$$

where N_{cr} is given by eq.(4.7) with K=E.I

Assuming that v has a sinusoidal distribution, i.e.

$$v_x = v \cdot \sin \frac{\pi x}{l} \qquad (4.1.2)$$

and on account that

$$M_{2x} = M_{1x} + N \cdot v_x \qquad (4.1.3)$$

it follows from eq.(4.1.1) that the midlength deflection of the slender member is

$$\boxed{v = \frac{N \cdot v}{N_{cr}} + v_1} \qquad (4.1.4)$$

where v_1 is the midlength deflection of the short member and is given by

$$v_1 = \int_0^l \frac{M_{1x} \cdot m_x}{EI} dx \qquad (4.1.5)$$

analogous to eq.(4.1.1).

On account that

$$M_2 = M_1 + N \cdot v \qquad (4.1.6)$$

where M_1 and M_2 are the midlength values of M_{1x} and M_{2x}, respectively, eq.(4.1.4) can be recast as

$$\frac{M_2 - M_1}{N} = \frac{M_2 - M_1}{N_{cr}} + \nu_1 \tag{4.1.7}$$

which is in accordance with Fig.4.8.

Eq.(4.1.7) yields

$$\boxed{M_2 = M_1 + \frac{N.\nu_1}{1 - \frac{N}{N_{cr}}}} \tag{4.1.8}$$

Two particular situations are considered below:

1. When M_{1x} <u>has a sinusoidal distribution</u>, i.e.

$$M_{1x} = M_1 . \sin \frac{\pi x}{\ell} \tag{4.1.9}$$

it follows from eq.(4.1.5), similar to eq.(4.1.4), that

$$\nu_1 = \frac{M_1}{N_{cr}} \tag{4.1.10}$$

so that eqs.(4.1.4) and (4.1.8) yield

$$\nu = \frac{M_2}{N_{cr}} \tag{4.1.11}$$

and, respectively,

$$M_2 = \frac{M_1}{1 - N/N_{cr}} \tag{4.1.12}$$

From eqs.(4.1.11) and (4.1.12) it follows that

$$\nu = \frac{\nu_1}{1 - N/N_{cr}} \tag{4.1.13}$$

2. When M_{1x} <u>has a constant distribution</u> it follows from eq.(4.1.5) that

$$\nu_1 = \frac{M_1}{N_{cr}} . \gamma \tag{4.1.14}$$

where

$$\gamma = \frac{\pi^2}{4} - 1 \tag{4.1.15}$$

With ν_1 given by eq.(4.1.14), eqs.(4.1.4) and (4.1.8) yield

$$\nu = \frac{M_2}{N_{cr}} + \frac{M_1 . (\gamma - 1)}{N_{cr}} \tag{4.1.16}$$

and, respectively,

$$M_2 = \frac{M_1}{1 - N/N_{cr}} \cdot \left[1 + \frac{N}{N_{cr}} \cdot (\gamma - 1)\right] \tag{4.1.17}$$

whereas eq.(4.1.13) is replaced by

$$\nu = \frac{\nu_1 / \gamma}{1 - N/N_{cr}} \cdot \left[1 + (\gamma - 1) \cdot \left(1 + \frac{N}{N_{cr}}\right)\right] \tag{4.1.18}$$

It is apparent that eqs.(4.1.11)...(4.1.13) follow from eqs. (4.1.16)...(4.1.18), respectively, with $\gamma = 1$. Since in the case 2 $\gamma > 1$ it results, as expected, that ν and M_2 are larger in the case 2 than in the case 1 for the same value of M_1.

Any possible distribution of M_1 for a single-curved beam-column lies always between the case 1 as lower limit and case 2 as upper limit where M_1 is equal with the midlength moment of the respective distribution.

In either of the above cases 1 and 2 the first order bending moment M_1 can be due either to a transverse load or to an accidental out-of-straightness e_x of the member axis. In the latter case

$$M_{1x} = N \cdot e_x \tag{4.1.19}$$

and the cases 1 and 2 correspond, respectively, to

$$e_x = e_o \cdot \sin \frac{\pi x}{\ell} \tag{4.1.20}$$

and to

$$e_x = e_o \tag{4.1.21}$$

where e_0 is the midlength out-of-straightness.

From eq.(4.1.19) it follows that

$$M_1 = N \cdot e_o \tag{4.1.22}$$

and thus eqs.(4.1.13) and (4.1.12) associated with the above case 1 yield

$$v = \frac{e_o}{1 - \frac{N}{N_{cr}}} \tag{4.1.23}$$

and, respectively,

$$M_2 = \frac{M_1}{1 - \frac{N}{N_{cr}}} \tag{4.1.24}$$

which are identical to eqs.(4.5) and (4.6), respectively.

The above developments are based on following assumptions:

(i) the distribution of v_x is sinusoidal - see eq.(4.1.2)

(ii) the material is perfectly elastic

(iii) the cross-section is constant along the member length

(iv) the deflections v_x are moderately large so that the compatibility equation is linear.

In fact the assumption (i) is accurate in the case 1. Its effect on the results corresponding to the case 2 should be small so long as the deflections v are not large.

Significant differences could occur when a reinforced concrete member is considered since then the stiffness will be variable along the member due to the variation of M_2. This aspect is analysed in Section 4.4.

APPENDIX IV.2

The development of eqs.(4.16) and (4.17)

1.When the 'rate of creep' method is assumed to govern the time-dependent behaviour of the device B in Fig.4.4 the constitutive relationship becomes (see Table 2.2)

$$d\theta_t = \frac{1}{K}\cdot dM_{2t} + \frac{M_{2t}}{K}\cdot d\varphi_t \qquad (4.2.1)$$

which yields (see Fig.4.9a)

$$d\nu_t = \frac{1}{N_{cr}}\cdot dM_{2t} + \frac{M_{2t}}{N_{cr}}\cdot d\varphi_t \qquad (4.2.1a)$$

From Fig.4.9a it follows that

$$M_{2t} = M_1 + N.\nu_t = N_{cr}.\nu_t \qquad (4.2.2)$$

and further (see the component ν_t in Fig.4.9a)

$$dM_{2t} = N.\, d\nu_t \qquad (4.2.3)$$

By using eqs.(4.2.2) and (4.2.3),eq.(4.2.1a) yields

$$d\nu_t = \frac{N}{N_{cr}}\cdot d\nu_t + \nu_t.\, d\varphi_t$$

or

$$\frac{d\nu_t}{\nu_t} = \frac{d\varphi_t}{1-N/N_{cr}} \qquad (4.2.4)$$

By integrating eq.(4.2.4) it follows that

$$\nu_t = C_1.\exp\left(\frac{\varphi_t}{1-N/N_{cr}}\right) \qquad (4.2.5)$$

The constant C_1 can be found from the initial condition (see Fig.4.9a),i.e.

$$\text{at time } t=0 \longrightarrow \nu_t=\nu_0=C_1 \qquad (4.2.6)$$

so that eq.(4.2.5) becomes*)

$$\boxed{\nu_t = \nu_o\cdot\exp\left(\frac{\varphi_t}{1-N/N_{cr}}\right)} \qquad (4.16)$$

2.When the 'improved rate of creep' method is used rather than the above 'rate of creep' method , eq.(4.2.1a) becomes (see Table 2.2)

$$d\nu_t = \frac{1+\varphi_{r\infty}}{N_{cr}}\, dM_{2t} + \frac{M_{2t}}{N_{cr}}\cdot d\varphi_{it} \qquad (4.2.7)$$

where $\varphi_{r\infty}$ and φ_{it} are the recoverable and the irrecoverable components of the creep so that (see eq.(2.21))

$$\varphi_i = \varphi_{r\infty} + \varphi_{it}$$

---

*) Eq.(4.16) was developed by Warner(1974)

Similarly to eq.(4.2.5) it follows from eq.(4.2.7) that

$$\nu_t = C_1 \cdot \exp\left(\frac{\varphi_{it}}{1-(1+\varphi_{r\infty})\cdot\frac{N}{N_{cr}}}\right) \tag{4.2.8}$$

The condition at time t=0 is

$$\nu_t = \nu_o \cdot (1+\varphi_{r\infty}) = C_1 \tag{4.2.9}$$

since the recoverable creep is assumed to occur instantaneously according to the 'improved rate of creep' method.

With eq.(4.2.9), eq.(4.2.8) yields

$$\boxed{\nu_t = \nu_o \cdot (1+\varphi_{r\infty}) \cdot \exp\left(\frac{\varphi_{it}}{1-(1+\varphi_{r\infty})\cdot\frac{N}{N_{cr}}}\right)} \tag{4.17}$$

APPENDIX IV.3

The development of ΔM_u and $\Delta M_{u\infty}$ in Fig.4.10a

In Section 4.2.2b it has been shown that

$$\Delta M_{u\infty} = N \cdot v_\infty = M_u \cdot \frac{v_\infty}{\frac{M_{1\infty}}{N} + v_\infty} \tag{4.3.1}$$

according to Fig.4.10a.

From Fig.4.10a it also follows that

$$M_{1\infty} + N \cdot v_o = N_{cr} \cdot v_o$$

and hence

$$v_o = \frac{\frac{M_{1\infty}}{N}}{\frac{N_{cr}}{N} - 1}$$

or

$$v_o = \frac{M_{1\infty}}{N} \cdot F_2 \tag{4.3.2}$$

where

$$F_2 = \frac{N/N_{cr}}{1 - N/N_{cr}} \tag{4.3.3}$$

According to the 'rate of creep' method the final deflection v_∞ in Fig.4.10a is given by eq.(4.16),i.e.

$$v_\infty = v_o \cdot \exp\left(\frac{\varphi_\infty}{1 - N/N_{cr}}\right)$$

which becomes after using eq.(4.3.2)

$$v_\infty = \frac{M_{1\infty}}{N} \cdot F_1 F_2 \tag{4.3.4}$$

where

$$F_1 = \exp\left(\frac{\varphi_\infty}{1 - N/N_{cr}}\right) \tag{4.3.5}$$

and F_2 is given by eq.(4.3.3)

By using eq.(4.3.4), eq.(4.3.1) yields

$$\boxed{\Delta M_{u\infty} = M_u \cdot \frac{F_1 F_2}{1 + F_1 F_2}} \tag{4.3.6}$$

Similarly it follows from Fig.4.10a or from eq.(4.13) that

$$\Delta M_u = \frac{N}{N_{cr}} \cdot M_u$$

which, taking into account that from eq.(4.3.3)

$$\frac{N}{N_{cr}} = \frac{F_2}{1 + F_2}$$

becomes

$$\boxed{\Delta M_u = M_u \cdot \frac{F_2}{1 + F_2}} \tag{4.3.7}$$

It can be shown that $\Delta M_{u\infty}$ is always larger than ΔM_u. Thus if the expansion of F_1 is used it follows that

$$F_1 = 1 + \frac{\varphi_\infty}{1-N/N_{cr}} + \mathcal{R} \simeq 1 + \frac{\varphi_\infty}{1-N/N_{cr}} \qquad (4.3.8)$$

where the rest $\mathcal{R}$ is definitely positive.

Eq.(4.3.8) can be recast as

$$F_1 \simeq \frac{1-N/N_{cr}+\varphi_\infty}{1-N/N_{cr}}$$

which introduced in eq.(4.36) yields

$$\Delta M_{u\infty} = M_u \cdot \frac{F_2}{1+F_2-\phi_1} \qquad (4.3.9)$$

where

$$\phi_1 = \frac{\varphi_\infty}{1-N/N_{cr}+\varphi_\infty} > 0 \qquad (4.3.10)$$

By using eq.(4.3.7), eq.(4.3.9) yields

$$\Delta M_{u\infty} \simeq \Delta M_u \cdot \frac{1+F_2}{1+F_2-\phi_1} \qquad (4.3.11)$$

Since ϕ_1 is always positive it follows from eq.(4.3.11) that

$$\boxed{\Delta M_{u\infty} > \Delta M_u} \qquad (4.3.12)$$

and that the larger the creep is (i.e. the larger φ_∞) or the larger $\frac{N}{N_{cr}}$ is (i.e. the smaller N_{cr} or the larger N), the larger $\Delta M_{u\infty}$ is when compared with ΔM_u.

APPENDIX IV.4

Set of programs and subprograms to analyse the beam-column from Fig.4.11

The theoretical background of this set of programs and subprograms is presented in Chapter 4 (see Section 4.3).Nevertheless, for the sake of keeping the exposition clear, the basic aspects are only presented there.Some more details are given below.

(i) Three subscripts are associated with the partition from Fig.4.17. Thus:

J1 - defines the cross-section

J2 - defines the stripe of a cross-section

J3 - defines the instant of time

(ii) Two integer constants,denoted by K2C and ISL, are used as indicators of the type of member failure and of the cross-section where the failure is recorded,respectively. Thus when a main program stops two integer values are printed out and,if ISL > 1,the value'ISL-1' denotes the J1-cross-section in Fig.4.17a where failure occurs while K2C can be:

=1 the starting value

=2 material failure (see assumption (x) in Section 4.3.2)

=3 material failure (see Fig.4.14c)

=4 material failure (see Fig.4.14b)

=6 the tensile reinforcement yields (see Section 4.3.3c)

=7 instability by divergence of equilibrium (see Fig.4.27)

=9 equilibrium impossible in SCTDEF-subprogram (similar to K2C=7

=10 normal exit,i.e.the final solution is found.

(iii) The subroutines RESSCT and CRRES which provide the resultan $\bar{N}$, $\bar{M}$ and $\Delta\bar{N}$, $\Delta\bar{M}$,respectively, when the strain distribution is known (see Figs.4.18 and 4.25) are not detailed here since they are similar to the subprogram MN from CEB-Buckling Manual (1973),Appendix A2.

(iv) The subroutine FRECR1 provides the increase in concrete strain due to creep-increment in a Δt-interval as if the concrete creep were fully unrestrained. This subroutine is built such that any creep law and any time-partition can be used. However,in accordance with the conclusion arising from Table 2.2, the 'improved Dischinger' method

is employed in the present form of FRECR1 and the time-partition in Fig. 4.17c is

$$t_j = t_{j-1} + \Delta t_j^2 \quad , \quad j=1,2,... \tag{4.4.1}$$

where

$$\Delta t_j = \Delta t_{j-1} + 1day \tag{4.4.2}$$
$$t_0 = 0.$$
$$\Delta t_0 = 0.$$

It is noteworthy that the same results occured when the 'rate of creep' method has been used rather than the 'improved rate of creep' method (see Table 2.2).Also,no relevant improve in the accuracy resulted when a time-partition closer than that given by eqs.(4.4.1) and(4.4.2) has been considered.

The following Tables are attached to the present Appendix:

Table 4.4.1 Main programs
Table 4.4.2 Subprograms
Table 4.4.3 Subprograms attached by the main programs and by other subprograms
Table 4.4.4 Flow chart of the program EXC07C
Table 4.4.5 Flow chart of the subprogram DEFSCT
Table 4.4.6 Flow chart of the subprogram SCTDEF
Table 4.4.7 Flow chart of the subprogram CRDEF
Table 4.4.8 Flow chart of the subprogram CREFF
Table 4.4.9 Flow chart of the subprogram DSLCOL

Table 4.4.1 Main programs

	Program	To compute	Output
SHORT COLUMN (CROSS-SECTION) WITHOUT CREEP	EXC01	the interaction-diagram $n_u - m_u$ and the curve $n_u - \frac{h}{r_u}$ for a cross-section under instantaneous load n_u=ultimate axial force m_u=ultimate bending moment $\frac{1}{r_u}$=ultimate curvature	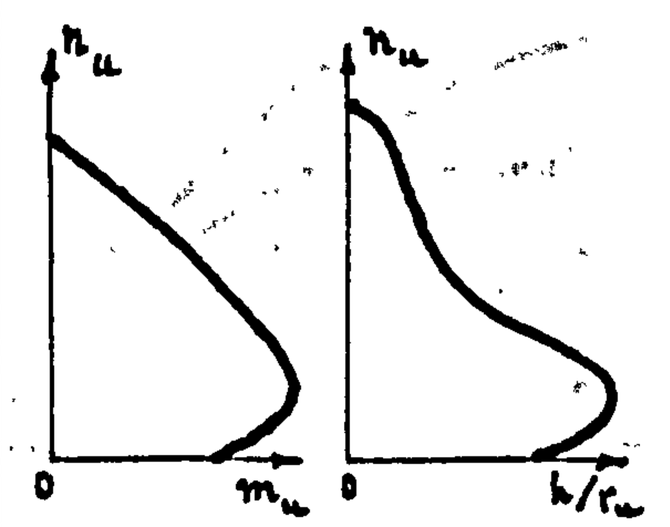
	EXC02	the m - $\frac{h}{r}$ curve up to the failure of the cross-section for a certain constant n and an instantaneous loading.	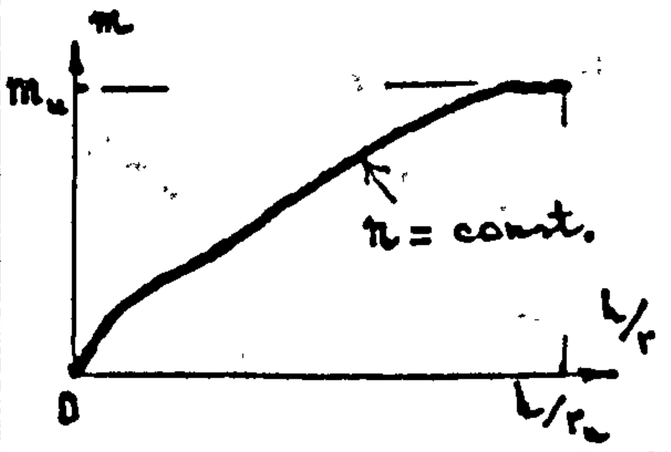
WITHOUT CREEP	EXC03A	the $m_1 - m_2$ curve for the midlength cross-section of a slender column when n is constant, the distribution of m_1 along the column is known and the loading is instantaneous. m_1=first order bending moment m_2=second order bending moment	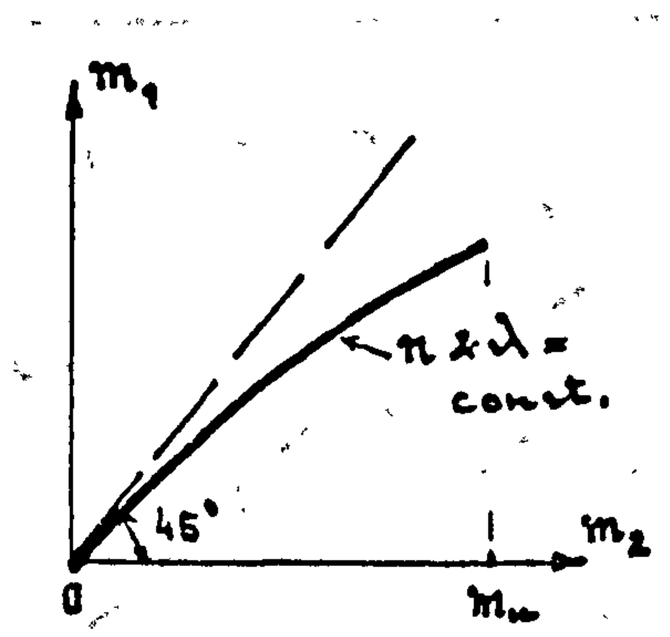
SLENDER COLUMN	EXC04A	the n - m_2 curve for the midlength cross-section of a slender column when the eccentricity m_1/n is constant, its distribution along the column is known and the loading is instantaneous. λ=slenderness of member	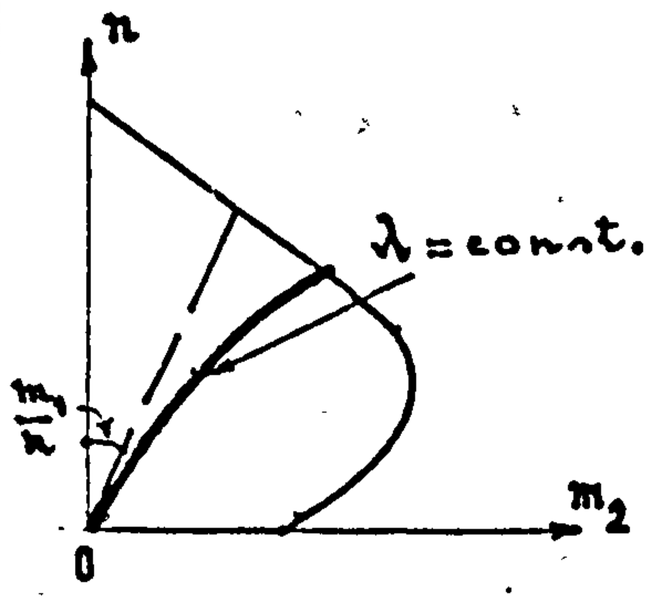
	EXC03B	the interaction-diagram for the midlength cross-section of a slender column when n is held constant and the loading is instantaneous.	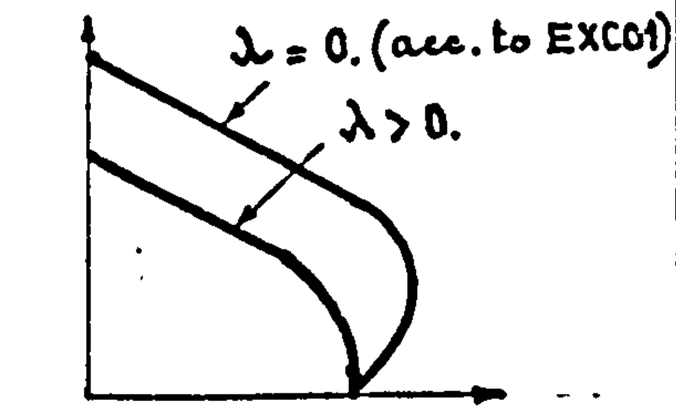

Table 4.4.1 (cont.)

CROSS-SECTION WITH CREEP	EXC06A	the redistribution of stresses and strains on a cross-section due to the concrete creep	see Figs.4.22 and 4.24
	EXC06E	(as EXC02, but including the effects of concrete creep)	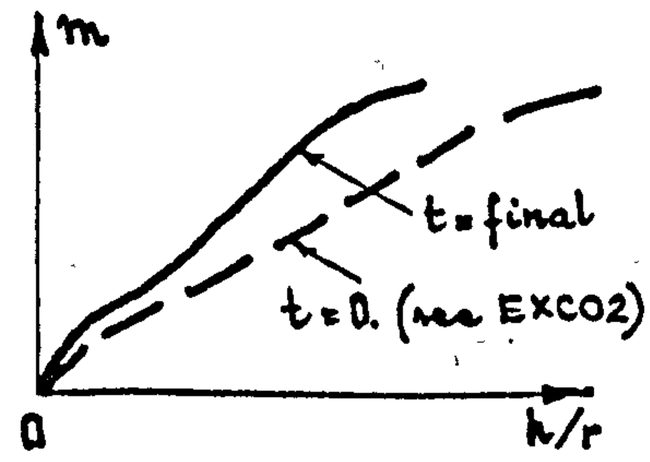
	EXC06H	(as EXC01, but including the effects of concrete creep)	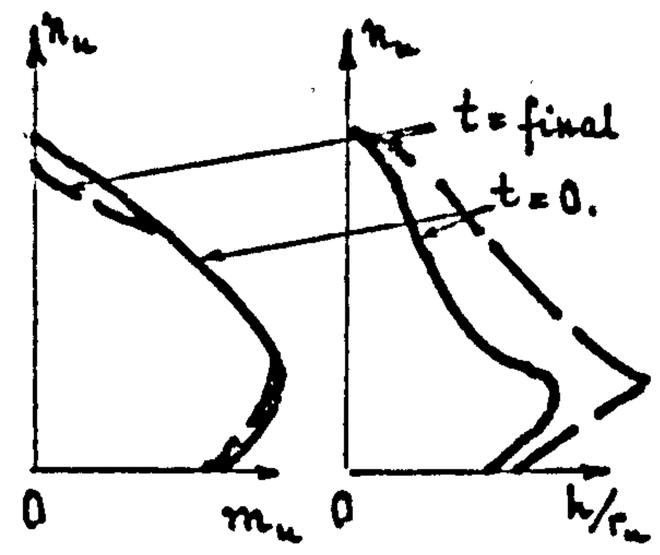
SLENDER COLUMN WITH CREEP	EXC07C	(as EXC03A, but including the effects of concrete creep) m_{10}= m_1 at time t=0. m_{20}= m_2 corresponding to m_{10} at time t=0. $m_{2\infty}$= m_2 corresponding to m_{10} at time t= final	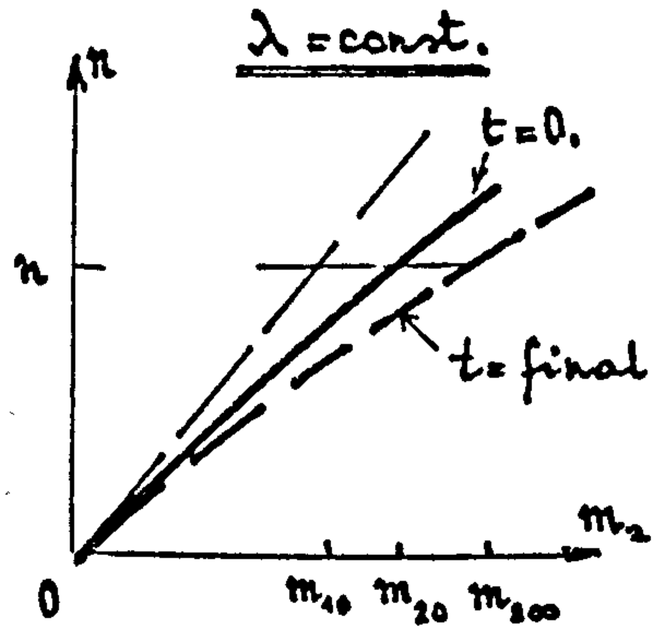
	EXC07B	(as EXC03B, but including the effects of concrete creep)	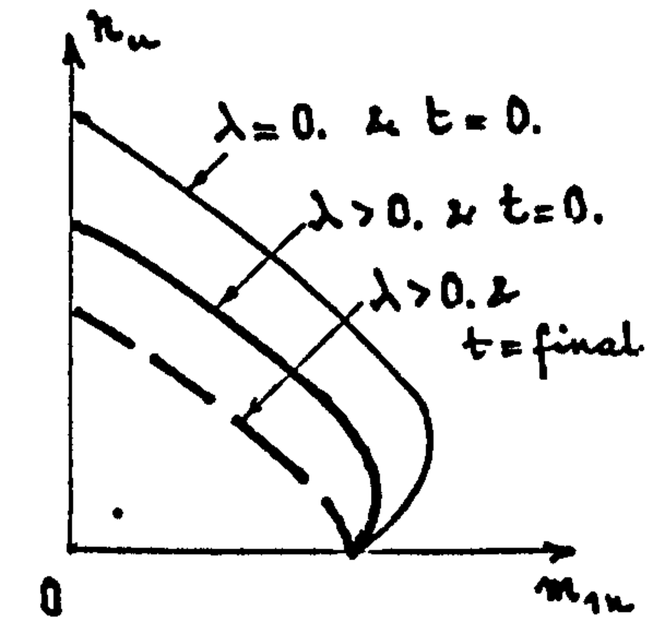

Table 4.4.2 Subprograms

To consider	Subprogram	To compute	
MATERIAL BEHAVIOUR	PHLST	the stress σ_s corresponding to a strain ε_s on the σ-ε curve of the reinforcement.	see Fig.4.12b
	PHLCOC	(as PHLST, but for concrete subject to instantaneous compr.)	see Fig.4.12a
	PHLTEC	(as PHLST, but for concrete subject to instantaneous tension)	see assumption (ii) in Section 4.3.2a
	FRECR1	the increase of a concrete strain in a time-interval due to an unrestrained creep.	see eq.(4.21)
	CONTR1	checking out whether a 'material failure' occured.	see assumptions (ix)...(xi) in Section 4.3.2a
CROSS-SECTION ANALYSIS	STEEL	the resultant forces in reinf. ($\bar{n}_s$ & $\bar{m}_s$) when the strain distrib. is known.	
	RESSCT	the resultant forces on the reinforced-concrete cross-section ($\bar{n}$ & $\bar{m}$) when the strain distrib. is known.	
	DEFSCT	the strain distribution on a cross-section when the forces n and m are known.	see Table 4.4.5 and Section 4.3.3b (instantaneous load)
	DGRINT	the interaction-diagram of a cross-section for instantaneous loading.	see Section 4.3.3b (instantaneous load)

Table 4.4.2 (cont.)

CROSS - SECTION ANALYSIS	ULT1CO	(as DGRINT, but m_u correspond to a given eccentricity,i.e. to a given ratio m_u/n_u)	
	COPHL	the variation of concrete stress corresponding to an instantaneous variation of strain when the existing stress-strain state is known.It can account for any kind of variation (i.e.loading,unloading, reloading) both in compr. & tension	see Fig.4.13a
	STPHL	(as COPHL,but for reinforcement)	see Fig.4.13b
	CRRES	the change in $\bar{n}$ and $\bar{m}$ when the variation of strain distribution is known.The strain variation may be either instantaneous or creep-dependent.	
	SCTDEF	the actual variation of the stress and strain distributions on the cross-section due to an inst. variation of the bending moment (Δm) when n is constant and the existing stress and strain distributions are known.	see Table 4.4.6
	CREFF	the summation of the effects of a time-increment on cross-section	see Table 4.4.3
	CRDEF	(as SCTDEF, but due to an unrestrained creep rather than to Δm). n and m are assumed constant.	see Table 4.4.7 and Section 4.3.3b (creep effects).
	CRINT	(as DGRINT but including the creep effects).	

Table 4.4.2 (cont.)

MEMBER ANALYSIS	ASLCOL	the m_2 -value at the column midlength when n and m_1 distributions along the slender column are known. No creep effects.	similar to DSLCOL but without creep and with m_1 applied on the undeformed state.
	DSLCOL	the slenderness effects on forces, curvatures, stresses and strains when n and m_1 are known. To be used with both instantaneous and sustained loading.	see Table 4.4.9 and Section 4.3.3c
	USLCOL	the ultimate bending m_{1u} corresponding to an axial force n and a certain distribution of m_1/n along the slender member. No creep effects.	
	SLINT	(as USLCOL but m_1 rather than m_1/n are known).	

Table 4.4.3 Subprograms attached by the main programs and by other subprograms.

	Called sub-program / Calling (User)	which account for: Material behaviour					'Cross-section' behaviour											'Member' behaviour			
		PHLST	PHLCOC	PHLTEC	FRECR1	CONTR1	STEEL	RESSCT	DEFSCT	DGRINT	ULT1CO	COPHL	STPHL	CRRES	SCTDEF	CRDEF	CREFF	CRINT	ASLCOL	DSLCOL	USLCOL	SLINT
SUBPROGRAMS	STEEL	x																				
	RESSCT	+	x	x			x															
	DEFSCT	+	+	+			+	x														
	DGRINT	+	+	+			+	x														
	ULT1CO	+	+	+			+	+		x												
	COPHL		x	x																		
	STPHL	x																				
	CRRES	+	+	+								x	x									
	SCTDEF	+	+	+		x						+	+	x								
	CRDEF	+	+	+	+	x						+	+	x								
	CREFF	+	+	+	x	+						+	+	+		x						
	CRINT	+	+	+	x	+	+	+	x	x		+	+	+		x						
	ASLCOL	+	+	+		+	+	+	x													
	DSLCOL	+	+	+	+	+						+	+	+	x							
	USLCOL	+	+	+		+	+	+	+	x									x			
	SLINT	+	+	+		+	+	+	+										x			
PROGRAMS	EXC01	+	+	+			+	x		●												
	EXC02	+	+	+			+	x	x													
	EXC03A	+	+	+		+	+	+	x	x									x			
	EXC03B	+	+	+		+	+	+	+	x	x								x			●
	EXC04A	+	+	+		+	+	+	+	x	x								x			
	EXC06A	+	+	+	x	+	+	+	x	x		+	+	+		x	●					
	EXC06E	+	+	+	x	+	+	+	x	x		+	+	+		x						
	EXC06H	+	+	+	x	+	+	+	x	x		+	+	+		x		●				
	EXC07B	+	+	+	+	x	+	+	x	x		+	+	+	x	+	x	x	+	x	x	x
	EXC07C	+	+	+	+	+	+	+	x	x		+	+	+	x	+	x		+	x		

N.B. 1.The subprograms called directly by the user are denoted by (x). Those subprograms which are used indirectly (i.e. they are used by a directly called subprogram) are denoted by (+). When a main program becomes a subroutine for other programsit is denoted by (●).

2.Concrete creep is considered every time FRECR1 is called.

Table 4.4.4 Flow chart of the program EXC07C (abridged)

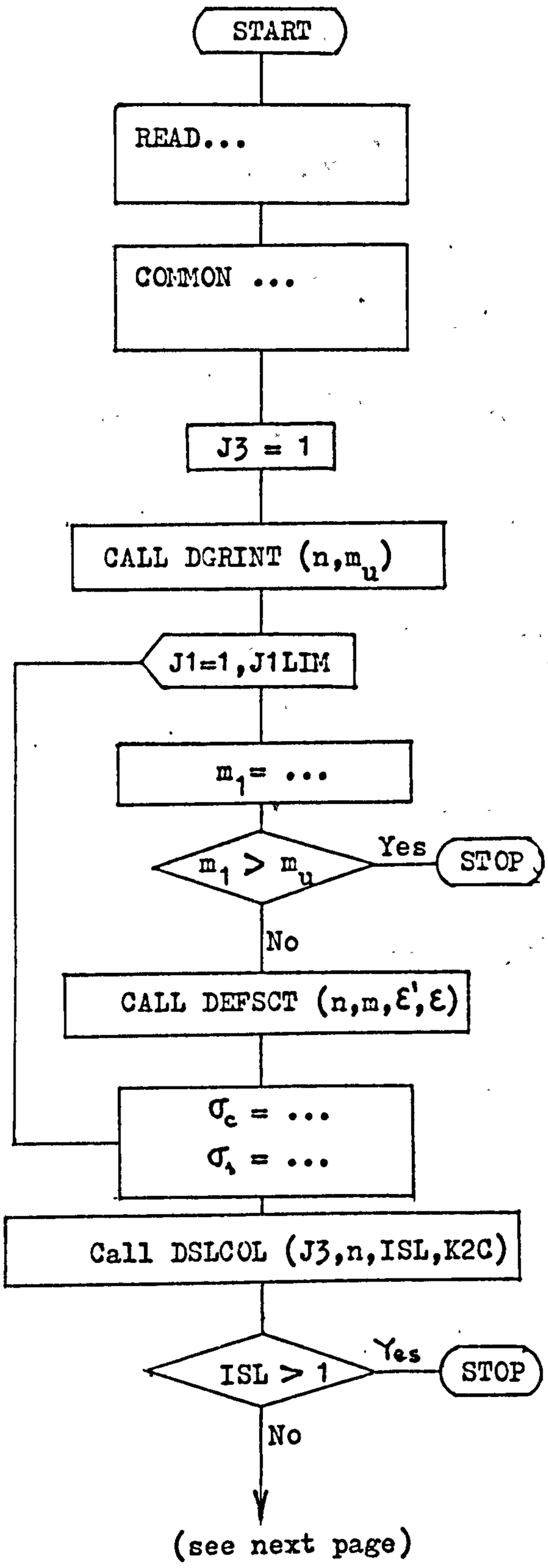

Comments:

- Read the parameters associated with the loading,materials, cross-section and member.

- To store the stress and strain distributions,the curvatures,the bending moments on each discrete cross-section at each discrete instant of time.

ANALYSIS OF INSTANTANEOUS BEHAVIOUR
(at time t=0.)

- Compute the instantaneous ultimate moment (m_u) of the cross-section.

'Cross-section analysis' of each discrete cross-section.

- Compute the 1st order bending moments.

- Checking the safety. 'STOP' if material failure occurs instantaneously.

-Find the strain distribution due to n and $m=m_1$.

- Compute the stress distributions in concrete and reinforcement.

'Member analysis' of instantaneous behaviour.

- Checking the safety. 'STOP' if instantaneous failure occurs due to slenderness.

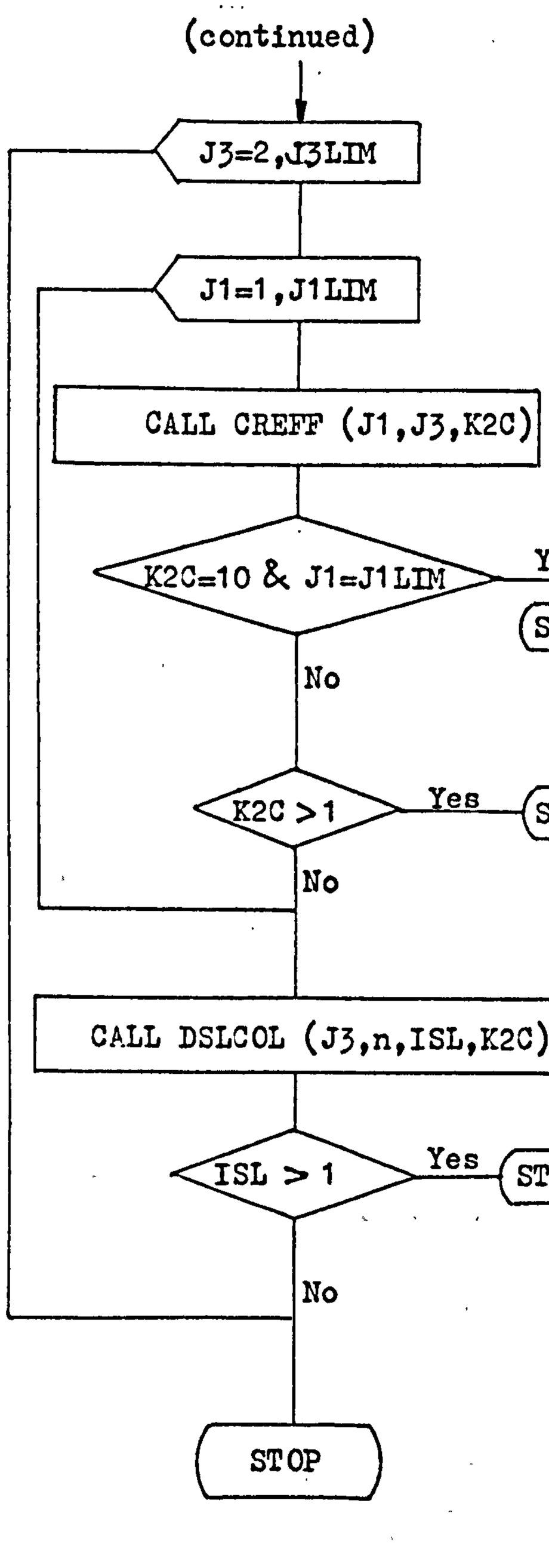

ANALYSIS OF THE EFFECTS OF SUCCESIVE TIME-INCREMENTS.

'Cross-section analysis' of creep effects.

- Compute the increase of stress and strain distributions.

- Checking the creep rate.'STOP' if the creep effect is no longer relevant.

- Checking the safety.'STOP' if material failure occurs due to combined effects of creep and slenderness.

'Member analysis'of long-term behaviour.

- Checking the safety.'STOP' if instability of member occurs.

Table 4.4.5 Flow chart of the subroutine DEFSCT (abridged)

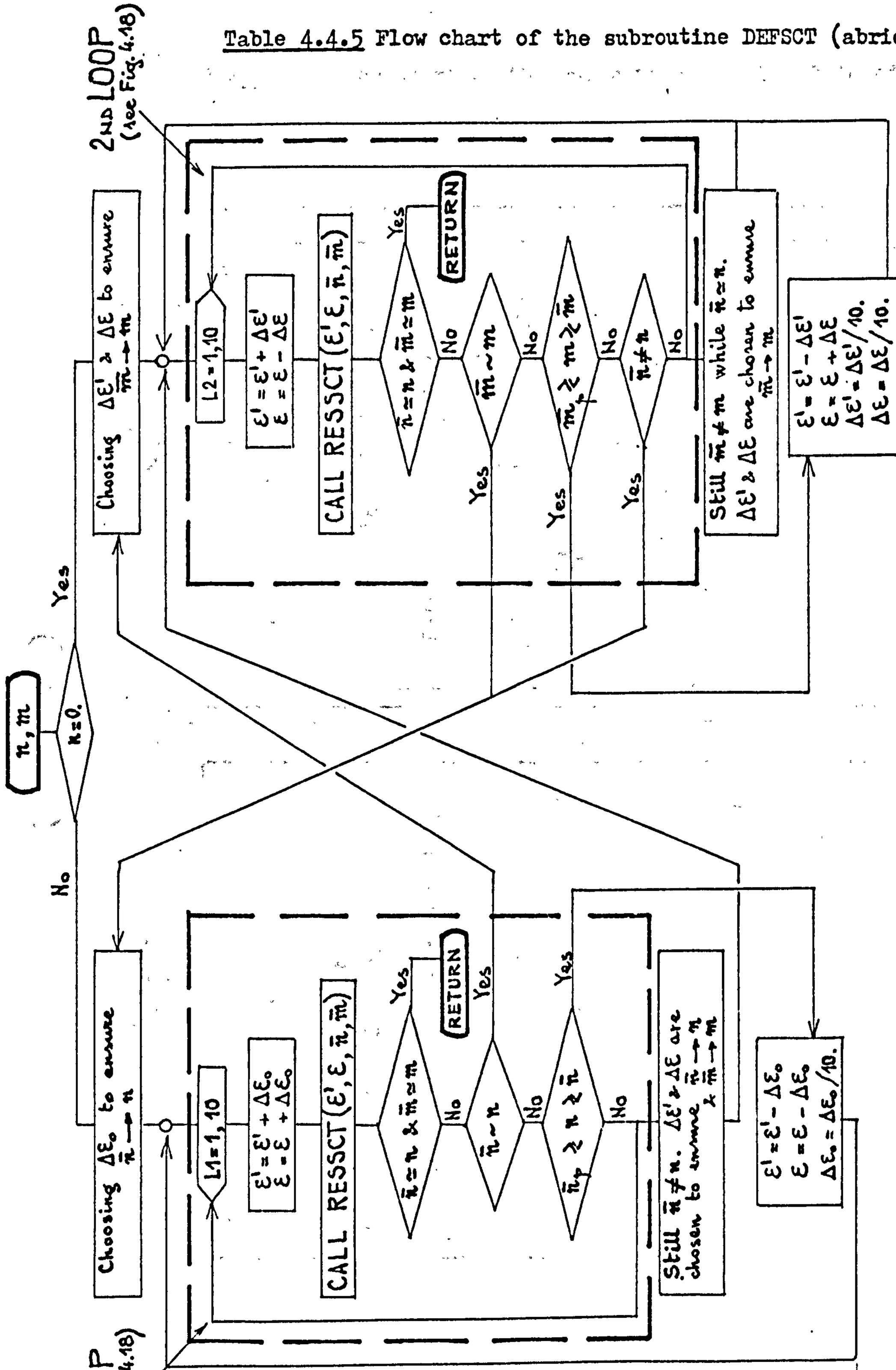

Table 4.4.6 Flow chart of the subroutine SCTDEF (abridged)

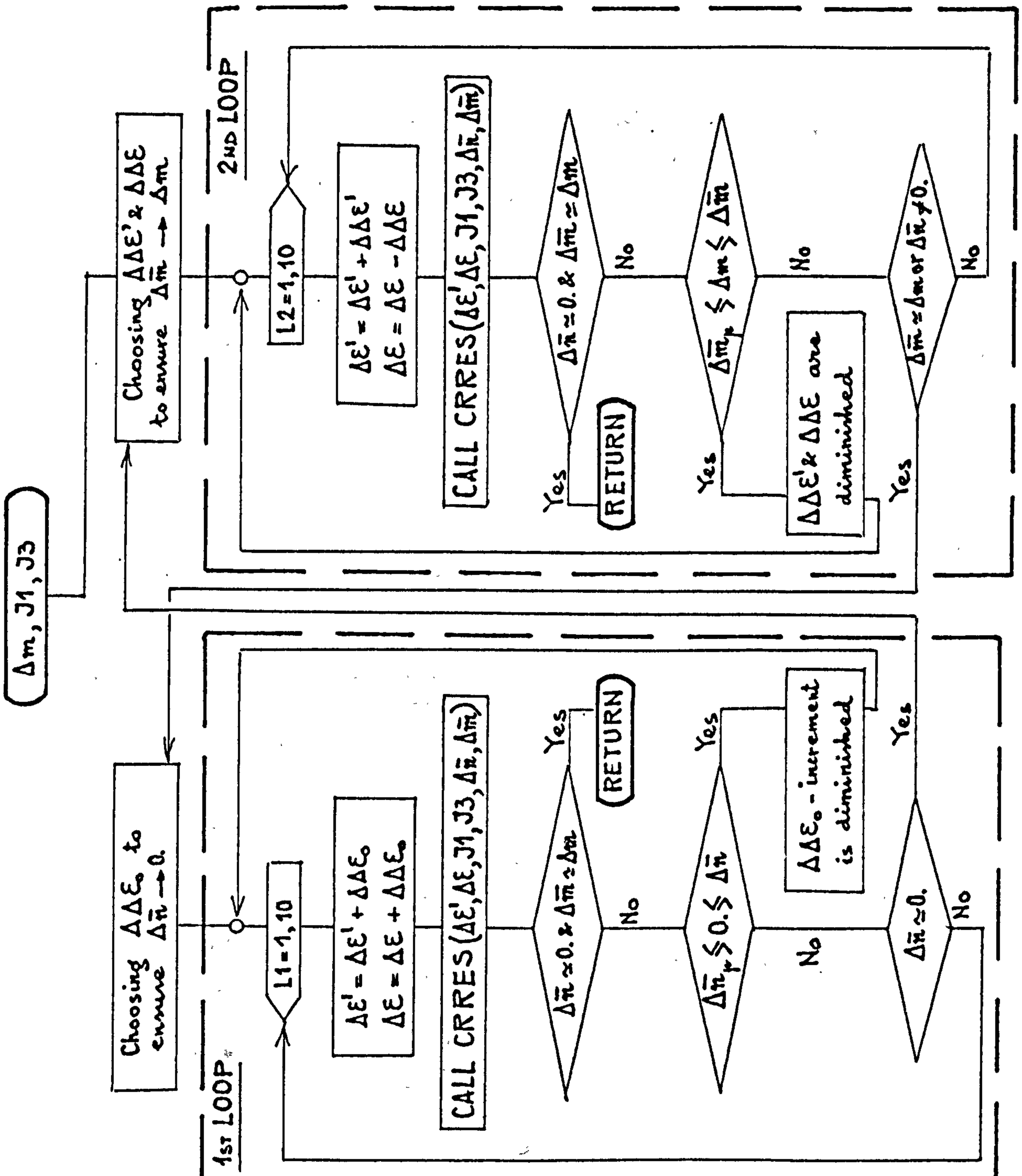

Table 4.4.7 Flow chart of the subroutine CRDEF (abridged)

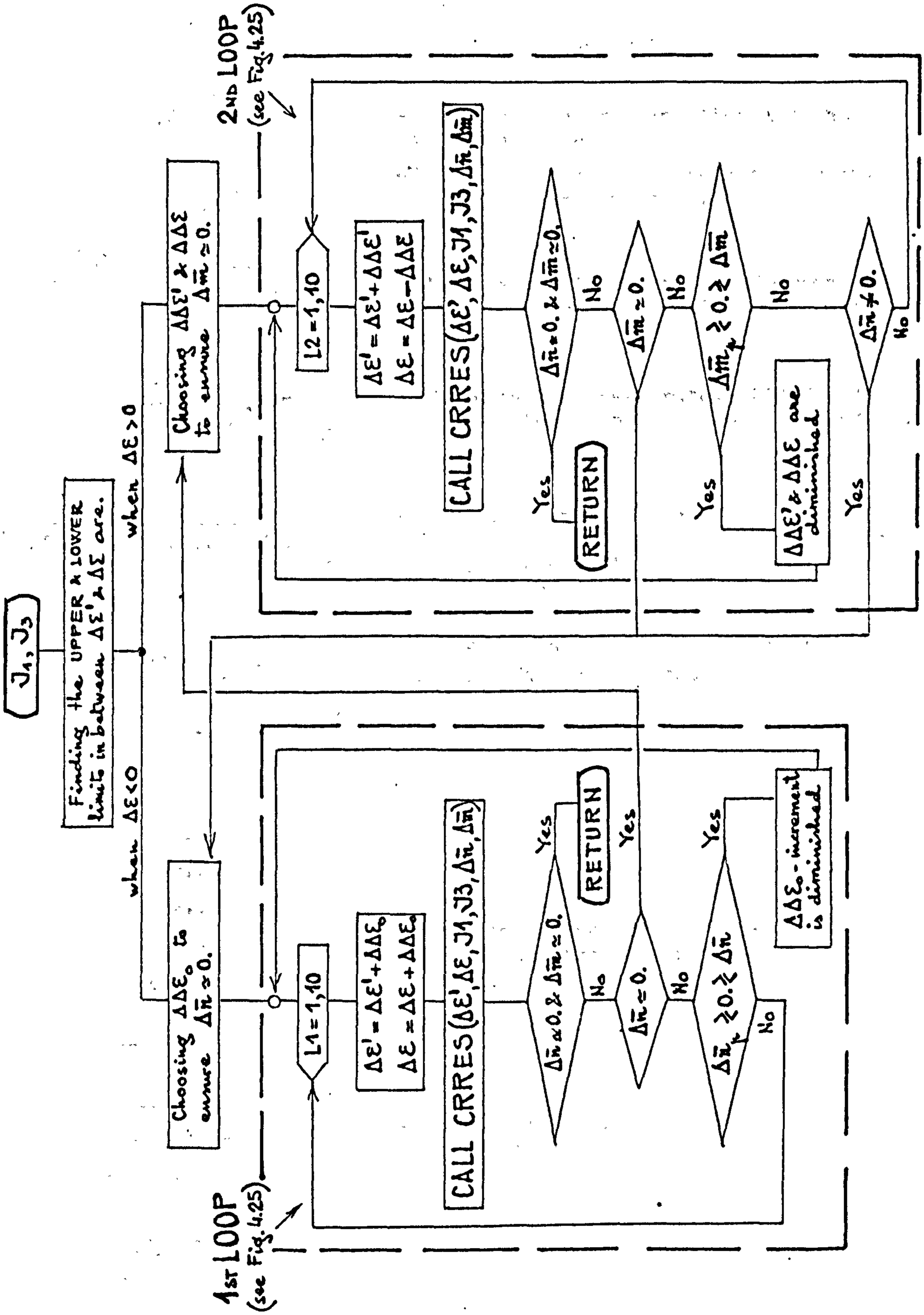

Table 4.4.8 Flow chart of subroutine CREFF (abridged)

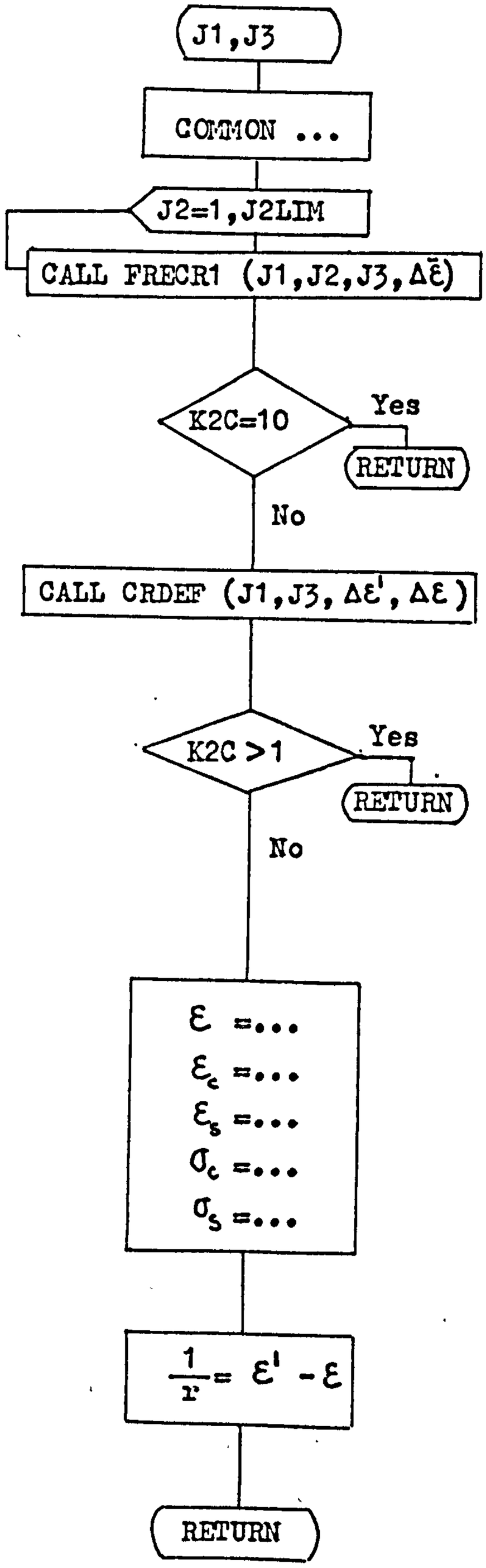

Comments

- Denoting the cross-section and the instant of time.

-The existing distributions of stresses and strains are attached.

- Compute the increase $\Delta\bar{\varepsilon}$ of creep strain as if unrestrained by reinforcement

- Checking the creep rate.'RETURN' if the concrete creep is no longer relevant.

- Find the actual variation of strain distribution by taking into account the restraining effect of reinforcement on the concrete creep.

- Checking the safety.'RETURN' if material failure occurs.

- Compute the new distributions of strains and stresses on the cross-section.

- Compute the curvature of the cross-section.

Table 4.4.9 Flow chart of the subroutine DSLCOL (abridged)

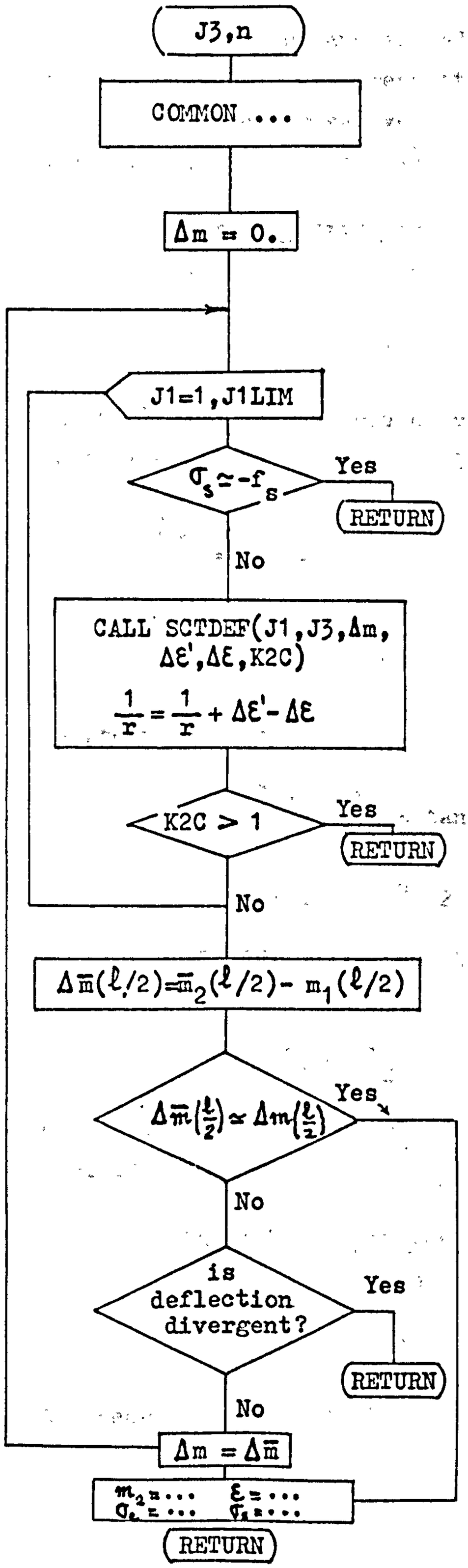

Comments

- Denoting the time instant.

- The existing distributions of stresses, strains,curvatures and bending moments are attached.

- Staring value of Δm at midlength.

STEP-BY-STEP ANALYSIS OF SLENDERNESS EFFECT

'Cross-section' effects of Δm- values.

'RETURN' if the tensile reinforcement yields (the member has no more bending capacity).

- Find the variation of strain distribution due to Δm and the corresponding increase in curvature.(see the second of eqs.(4.41))

- Checking the safety.'RETURN' if material failure occurs.

see the first of eqs.(4.41)

- Checking the convergence of the 'member analysis'. 'Yes' when the final solution is obtained.

- Checking the instability of column. 'RETURN' when the column is unstable (see Fig.4.27)

- Starting values of the new step.

- Compute the new moments,strains and stresses on each cross-section

APPENDIX V.1

The first and second order partial derivatives of Ψ_i and u from eqs.(5.7) with respect to v_i are detailed within this Appendix.

These derivatives are used by the 'exact' equations (5.8) and (5.19),i.e. by the 'exact' primary and secondary paths.

Partial derivatives of first order.

With the notation

$$D_i = \frac{(-1)^i}{\cos\theta_i} \qquad ,i=1,2 \qquad (5.1.1)$$

where θ_1 and θ_2 are given by eqs.(5.6), the first order partial derivatives of Ψ_i and u follow from eqs.(5.7) as

$$\begin{aligned}
&\frac{\partial\psi_1}{\partial v_1} = D_1 - D_2 && \frac{\partial\psi_2}{\partial v_1} = D_2 && \frac{\partial\psi_3}{\partial v_1} = 0\\
&\frac{\partial\psi_1}{\partial v_2} = D_2 && \frac{\partial\psi_2}{\partial v_2} = -2D_2 && \frac{\partial\psi_3}{\partial v_2} = D_2 \qquad (5.1.2)\\
&\frac{\partial\psi_1}{\partial v_3} = 0 && \frac{\partial\psi_2}{\partial v_3} = D_2 && \frac{\partial\psi_3}{\partial v_3} = D_1 - D_2
\end{aligned}$$

and,respectively,

$$\begin{aligned}
&\frac{\partial u}{\partial v_1} = \frac{\partial u}{\partial v_3} = \tan\theta_1 - \tan\theta_2 \qquad (5.1.3)\\
&\frac{\partial u}{\partial v_2} = 2\tan\theta_2
\end{aligned}$$

In eqs.(5.1.2) and (5.1.3)

$$\begin{aligned}
\theta_1 &= \theta_5\\
\theta_2 &= \theta_4
\end{aligned} \qquad (5.1.4)$$

on account of the symmetric loading and geometry of arch-model (see Fig.5.4).

Partial derivatives of second order.

With the notation (5.1.1) and

$$DD_i = (-1)^i D_i^3 \sin\theta_i \qquad ,i=1,2 \qquad (5.1.5)$$

the second order partial derivatives of Ψ_i and u follow as

$$\frac{\partial^2\psi_1}{\partial v_1^2}=DD_1-DD_2 \qquad \frac{\partial^2\psi_2}{\partial v_1^2}=DD_2 \qquad \frac{\partial^2\psi_3}{\partial v_1^2}=0$$

$$\frac{\partial^2\psi_1}{\partial v_2^2}=-DD_2 \qquad \frac{\partial^2\psi_2}{\partial v_2^2}=2DD_2 \qquad \frac{\partial^2\psi_3}{\partial v_2^2}=-DD_2$$

$$\frac{\partial^2\psi_1}{\partial v_3^2}=0 \qquad \frac{\partial^2\psi_2}{\partial v_3^2}=DD_2 \qquad \frac{\partial^2\psi_3}{\partial v_3^2}=DD_1-DD_2 \qquad (5.1.6)$$

$$\frac{\partial^2\psi_1}{\partial v_1\partial v_2}=DD_2 \qquad \frac{\partial^2\psi_2}{\partial v_1\partial v_2}=-DD_2 \qquad \frac{\partial^2\psi_3}{\partial v_1\partial v_2}=0$$

$$\frac{\partial^2\psi_1}{\partial v_1\partial v_3}=0 \qquad \frac{\partial^2\psi_2}{\partial v_1\partial v_3}=0 \qquad \frac{\partial^2\psi_3}{\partial v_1\partial v_3}=0$$

$$\frac{\partial^2\psi_1}{\partial v_2\partial v_3}=0 \qquad \frac{\partial^2\psi_2}{\partial v_2\partial v_3}=-DD_2 \qquad \frac{\partial^2\psi_3}{\partial v_2\partial v_3}=DD_2$$

and, respectively,

$$\frac{\partial^2 u}{\partial v_1^2}=\frac{\partial^2 u}{\partial v_3^2}=D_1^3-D_2^3$$

$$\frac{\partial^2 u}{\partial v_2^2}=-2D_2^3 \qquad (5.1.7)$$

$$\frac{\partial^2 u}{\partial v_1\partial v_2}=D_2^3$$

$$\frac{\partial^2 u}{\partial v_1\partial v_3}=0$$

The symmetry of arch-model has been again used in deriving eqs.(5.1.6) and (5.1.7).

APPENDIX V.2

The steps by which eqs.(5.14a...c) are developed from eqs. (5.13) are shown in this Appendix. For more details on the perturbation technique refer to Croll and Walker (1972).

(i) A parameter ε is chose to measure the progress along the primary path (see Fig.5.5).This parameter is denoted as the perturbation parameter.

(ii) The variables v_j and p are assumed single-valued continuous functions of ε , so that they may be written in form of MacLaurin's expansions

$$v_j(\varepsilon) = v_j(0) + \frac{\varepsilon}{1!}\frac{dv_j}{d\varepsilon}\Big|_0 + \frac{\varepsilon^2}{2!}\frac{d^2v_j}{d\varepsilon^2}\Big|_0 + \frac{\varepsilon^3}{3!}\frac{d^3v_j}{d\varepsilon^3}\Big|_0 + \dots \qquad j=1,2,3 \qquad (5.2.1)$$

$$p(\varepsilon) = p(0) + \frac{\varepsilon}{1!}\frac{dp}{d\varepsilon}\Big|_0 + \frac{\varepsilon^2}{2!}\frac{d^2p}{d\varepsilon^2}\Big|_0 + \frac{\varepsilon^3}{3!}\frac{d^3p}{d\varepsilon^3}\Big|_0 + \dots$$

where '0' stands for the origin of coordinates (v_j,p) and thus

$$v_j(0) = 0 \ , \ j=1\dots3 \qquad \text{and} \qquad p=0 \qquad (5.2.2)$$

When the displacement v_2 is chosen as perturbation parameter, for instance, eqs.(5.2.1) denote the two planar curves $p(v_2)$ and $v_1(v_2)$ in Fig.5.5. Theses curves fully define the actually spatial path. The values $\frac{d..}{dv_2}\Big|0$, $\frac{d^2..}{dv_2^2}\Big|0$, . . . represent the slope,curvature, . . . of each planar curve at the origin 0 of axes and,therefore, the less truncated the expansions (5.2.1) are,the more accurate the 'approximate' primary path is for large displacements v_2.

(iii) As a consequence of the condition of stationary total potential energy

$$E_i(v_j,p) = \frac{\partial \Delta\Pi}{\partial v_i} = 0 \qquad i,j=1\dots3 \qquad (5.2.3)$$

which is true for all ε-values on the primary path, the following conditions must be necessarily valid too

$$\frac{d^nE_i}{d\varepsilon^n} = 0 \qquad \begin{matrix} i=1,2,3 \\ n=1,\dots \end{matrix} \qquad (5.2.4)$$

The truncations of both the expansions (5.2.1) and the sequence of perturbation equations (5.2.4) are consistent with the approximations introduced with eqs.(5.13).

Using eqs.(5.2.1) in eqs.(5.13), the initial conditions (5.2.2) and the shorthand notation

$$v_j^{(m)} = \left.\frac{d^m v_j}{d\varepsilon^m}\right|_0 \qquad j=1,2,3$$

$$p^{(m)} = \left.\frac{d^m p}{d\varepsilon^m}\right|_0 , \tag{5.2.5}$$

eqs.(5.2.4) yield

$$\frac{dE_i}{d\varepsilon} \to \frac{\partial \Pi_i}{\partial \rho} \rho' + \sum_j \Pi_{ij} v_j' = 0 \tag{5.14a}$$

$$\frac{d^2E_i}{d\varepsilon^2} \to \frac{\partial \Pi_i}{\partial \rho} \rho'' + \sum_j \Pi_{ij} v_j'' = -\sum_j \sum_k \Pi_{ijk} v_j' v_k' \tag{5.14b}$$

$$\frac{d^3E_i}{d\varepsilon^3} \to \frac{\partial \Pi_i}{\partial \rho} \rho''' + \sum_j \Pi_{ij} v_j''' = -3\sum_j \sum_k \Pi_{ijk} v_j'' v_k' - \sum_j \sum_k \sum_l \Pi_{ijkl} v_j' v_k' v_l' \tag{5.14c}$$

where i,j,k,l=1,2,3.

APPENDIX V.3

The development of criteria (5.16).

The dynamic criterion is employed. Small external disturbances are assumed and the conditions for the dynamic response of a three degree-of-freedom structure to remain small are derived. An approach similar to that used by Croll and Walker (1972) is employed.

Small dynamic displacements w_i are assumed about the equilibrium state $S(v_i,p)$ and Lagrange's equations are used to analyse the dynamic equilibrium.

At any instant t the dynamic equilibrium of a system with a finite number of degrees of freedom yields

$$\frac{\partial \Delta\Pi}{\partial w_i} = -m_i \ddot{w}_i \qquad i=1,2,3 \qquad (5.3.1)$$

where $\Delta\Pi$ is the total potential energy , m_i are the generalized masses associated with w_i and $\ddot{w}_i$ is the second order derivative of w_i with respect to t.

The generalized Taylor expansion of $\Delta\Pi$ about the equilibrium state yields

$$\Delta\Pi(w_i,p) = \Delta\Pi\Big|_s + \frac{1}{1!}\sum_i \frac{\partial \Delta\Pi}{\partial v_i}\Big|_s . w_i + \frac{1}{2!}\sum_i\sum_j \frac{\partial^2 \Delta\Pi}{\partial v_i \partial v_j}\Big|_s . w_i w_j + \cdots \qquad (5.3.2)$$

where v_i are corresponding displacements of the equilibrium state S.

On account of static equilibrium

$$\frac{\partial \Delta\Pi}{\partial v_i}\Big|_s = 0 \quad ,$$

eqs.(5.3.1) with eqs.(5.3.2) yield

$$\sum_j \frac{\partial^2 \Delta\Pi}{\partial v_i \partial v_j}\Big|_s . w_j = -m_i \ddot{w}_i \qquad i=1,2,3 \qquad (5.3.3)$$

where the terms of higher order have been neglected as a consequence of 'small dynamic displacements' assumption.

Assuming that the dynamic displacements have the general form

$$w_i = \bar{w}_i \, e^{\bar{\omega} t \sqrt{-1}} \qquad i=1,2,3 \qquad (5.3.4)$$

where $\bar{w}_i$ are the initial disturbances,then eqs.(5.3.3) may be recast as

$$\frac{1}{m_i}\sum_j \left.\frac{\partial^2 \Delta\Pi}{\partial v_i\,\partial v_j}\right|_S \cdot w_j = \bar{\omega}^2 \cdot w_i \qquad i,j=1,2,3 \qquad (5.3.5)$$

Eqs.(5.3.5) provide the eigen values $\bar{\omega}^2$ as solutions of the determinantal equation

$$|A| = 0 \qquad (5.3.6)$$

where the element A_{ij} of the square matrix A is

$$A_{ij} = \frac{1}{m_i} \cdot \left.\frac{\partial^2 \Delta\Pi}{\partial v_i\,\partial v_j}\right|_S - \delta_{ij} \cdot \bar{\omega}^2 \qquad (5.3.7)$$

and δ_{ij} is the Kronecker Delta.

The equilibrium state S is stable in the sense described above when w_i in eqs.(5.3.4) are damping and this is sufficiently ensured when $\bar{\omega}$ (i.e. the natural vibration frequencies) are real and hence when all the solutions $\bar{\omega}^2$ of eq.(5.3.6) are positive.

When the three degree-of-freedom model is considered, eq.(5.3.6) yields

$$\begin{vmatrix} \frac{1}{m_1}\cdot\Pi_{11}-\bar{\omega}^2 & \frac{1}{m_1}\cdot\Pi_{12} & \frac{1}{m_1}\cdot\Pi_{13} \\ \frac{1}{m_2}\cdot\Pi_{12} & \frac{1}{m_2}\cdot\Pi_{22}-\bar{\omega}^2 & \frac{1}{m_2}\cdot\Pi_{23} \\ \frac{1}{m_3}\cdot\Pi_{31} & \frac{1}{m_3}\cdot\Pi_{32} & \frac{1}{m_3}\cdot\Pi_{33}-\bar{\omega}^2 \end{vmatrix} = 0$$

or, after expanding,

$$(\bar{\omega}^2)^3 - (\bar{\omega}^2)^2 \cdot \sum_{i=1}^{3} \frac{\Pi_{ii}}{m_i} + \bar{\omega}^2 \cdot \sum_{i=1}^{3} \frac{m_i M_{ii}}{m_1 m_2 m_3} - \frac{\Delta}{m_1 m_2 m_3} = 0 \qquad (5.3.8)$$

where

$$\Pi_{ij} = \left.\frac{\partial^2 \Delta\Pi}{\partial v_i\,\partial v_j}\right|_S \qquad (5.3.9)$$

$$\Delta = |\Pi_{ij}| = \begin{vmatrix} \Pi_{11} & \Pi_{12} & \Pi_{13} \\ \Pi_{21} & \Pi_{22} & \Pi_{23} \\ \Pi_{31} & \Pi_{32} & \Pi_{33} \end{vmatrix} \qquad (5.3.10)$$

and M_{ij} is the minor of Π_{ij} in the determinant Δ.

Eq.(5.3.8) is a cubic equation of form

$$x^3 + a_1 \cdot x^2 + a_2 \cdot x + a_3 = 0$$

of which roots x_i (i=1...3) are such that

$$\begin{cases} x_1 + x_2 + x_3 = -a_1 \\ x_1x_2+x_2x_3+x_1x_3 = a_2 \\ x_1x_2x_3 = -a_3 \end{cases}$$

In order to have $x_i > 0$ it is necessary to have

$a_1 < 0$, i.e. $\sum_i \frac{\varpi_{ii}}{m_i} > 0$ in eq.(5.3.8)

$a_2 > 0$, i.e. $\sum_i m_i M_{ii} > 0$ in eq.(5.3.8)

$a_3 < 0$, i.e. $\Delta > 0$ in eq.(5.3.8)

These conditions are sufficiently fulfilled when

$$\begin{cases} \varpi_{ii} > 0 \\ M_{ii} > 0 \\ \Delta > 0 \end{cases} \quad , \; i=1,2,3 \qquad (5.16)$$

APPENDIX V.4

Conditions associated with the violation of the stability criterion (5.23).

Two degree-of-freedom arch-model.

J.G.A.Croll and A.C.Walker (1972) have shown that the stability criteria for a symmetric two degree-of-freedom arch-model as in Fig.5.1 are given by*)

$$\Pi_{11} > 0$$
$$\Delta = \Pi_{11}^2 - \Pi_{13}^2 > 0 \qquad (5.4.1)$$

where the notation (5.17) has been used.

It can be shown that the first of the above stability criteria can not be violated so long as the second one is fulfilled.

Indeed when Π_{11} vanishes then

$$\Delta = -\Pi_{13}^2 < 0$$

and hence the second of the equations (5.4.1) arises as the only necessary and sufficient condition for the equilibrium state to be stable.

Three degree-of-freedom arch-model.

It can be shown that, similarly to the above conclusion, the last of the criteria (5.16a) set up for the symmetric arch-model in Fig.5.2 is solely sufficient to secure the stability of equilibrium. In other words, none of the other conditions (5.16a) can be violated so long as $\Delta > 0$.

The notation (5.17) and eq.(5.22) are used below and M_{ij} denotes the minor of Π_{ij} in Δ.

The criteria (5.16a) are always fulfilled for the undeformed and unloaded state (see Appendix.V.5). As the load p increases one of the criteria (5.16a) can be violated and the various situations which may occur are analysed below:

(i) It is not possible to have $\Pi_{11}=0$ before any other of

---

*) See Section 7.2.1

the conditions (5.16a) be violated since it yields

$$M_{22}=\Pi_{11}^2-\Pi_{13}^2=-\Pi_{13}^2<0 \qquad (5.4.2)$$

(ii) If it assumed that $M_{22}=0$ when the other conditions (5.16a) are fulfilled then

$$M_{22}=\Pi_{11}^2-\Pi_{13}^2=0$$

which yields either

$$\Pi_{11}=\Pi_{13} \qquad (5.4.3)$$

or

$$\Pi_{11}=-\Pi_{13} \qquad (5.4.4)$$

The former condition yields $\Delta=0$ while the latter yields -see eq.(5.22)-

$$\Delta=2\,\Pi_{11}(\Pi_{11}\Pi_{22}-2\Pi_{12}^2+\Pi_{13}\Pi_{22})=-4\Pi_{11}\Pi_{12}^2 \qquad (5.4.5)$$

It arises that the simultaneous violation of both above conditions (i.e. $\Pi_{11}=0$ and $M_{22}=0$) is not possible unless $\Delta=0$ too.

(iii) It is not possible to have $\Pi_{22}=0$ when all other conditions (5.16a) are fulfilled since it yields

$$M_{11}=\Pi_{11}\Pi_{22}-\Pi_{12}^2=-\Pi_{12}^2<0 \qquad (5.4.6)$$

(iv) If it is assumed that $M_{11}=0$ at a lower load than $\Pi_{22}=0$, in other words when $\Pi_{22}>0$, then

$$\Pi_{11}\Pi_{22}=\Pi_{12}^2 \qquad (5.4.7)$$

Thus

$$M_{13}=\Pi_{12}^2-\Pi_{13}\Pi_{22}=\Pi_{22}(\Pi_{11}-\Pi_{13}) \qquad (5.4.8)$$

and eq.(5.22) yields

$$\Delta=(\Pi_{11}-\Pi_{13})(M_{11}-M_{13})=-\Pi_{22}(\Pi_{11}-\Pi_{13}) \qquad (5.4.9)$$

which is impossible so long as $\Delta>0$.

From the above situations (i)...(iv) it can be concluded that the stability criterion $\Delta>0$ sufficiently secures that none of the other conditions (5.16a) is violated.

It is also evident that one or a group of the first two criteria (5.16a) are violated simultaneously with the stability criterion (5.23).

APPENDIX V.5

Stability of the unloaded arch - model.

It is shown that the criteria (5.16a) are always fulfilled by the unloaded and undeformed arch-model from Fig.5.2 as long as it has $\alpha_1 > \alpha_2 > 0$.

From eqs.(5.20) it follows that, at $p=0$ and $v_i=0$ $(i=1..3)$,

$$\Pi_{ij}\big|_0 = \pi_{ij} \tag{5.5.1}$$

where π_{ij} are given by Table 5.1.

Since

$$\begin{aligned}
\pi_{11} &= 2\left[(A_{11}+A_{12})^2+cA_{12}^2+k(B_{11}-B_{12})^2\right] > 0\\
\pi_{22} &= 4\left[A_{12}^2(1+2c)+2kB_{12}^2\right] > 0\\
\pi_{12} &= -2\left[A_{12}(A_{11}+A_{12})+2cA_{12}^2-2kB_{12}(B_{11}-B_{12})\right]\\
\pi_{13} &= 2\left[cA_{12}^2+k(B_{11}-B_{12})^2\right] > 0
\end{aligned} \tag{5.5.2}$$

where A_{ij}, B_{ij} and c, k are positive constants given by eqs.(5.11) and (5.4), respectively, it follows from eqs.(5.5.2) that

$$\begin{aligned}
\pi_{11}-\pi_{13} &= 2(A_{11}+A_{12})^2 > 0\\
M_{22} &= (\pi_{11}-\pi_{13})(\pi_{11}+\pi_{13}) > 0\\
M_{11} &= \pi_{11}\pi_{22}-\pi_{12}^2 = 4A_{12}^2(A_{11}+A_{12})^2+8cA_{12}^2\left[(A_{11}+A_{12})^2+A_{11}^2+A_{11}A_{12}+A_{12}^2\right]+16kB_{12}^2(A_{11}+A_{12})^2+\\
&\quad 8kA_{12}^2(B_{11}-B_{12})^2+8kA_{12}B_{12}(B_{11}-B_{12})+16kcA_{12}^2\left[(B_{11}-B_{12})^2+B_{11}B_{12}\right]\\
M_{11}-M_{13} &= 2M_{11}-\pi_{22}(\pi_{11}-\pi_{13}) = 2M_{11}-\\
&\quad 8A_{12}^2(A_{11}+A_{12})^2-16cA_{12}^2(A_{11}+A_{12})^2-16kB_{12}^2(A_{11}+A_{12})^2
\end{aligned} \tag{5.5.3}$$

So long as $\alpha_1 > \alpha_2$ eqs.(5.11) yield $B_{11} > B_{12}$ so that it follows from eqs.(5.5.3) that

$$\begin{aligned}
&M_{11} > 0\\
&M_{11}-M_{13} > 0\\
&\Delta = (\pi_{11}-\pi_{13})(M_{11}-M_{13}) > 0
\end{aligned} \tag{5.5.4}$$

It is noteworthy that the above proof is 'approximate' since the Π_{ij}-coefficients in Table 5.1 are approximate. However, the effect of the approximations in the vecinity of the unloaded and undeformed state is insignificant (see Figs.5.14...5.16).

An 'exact' proof can be carried out similarly. It would imply the use of eqs.(5.19) rather than of eqs.(5.20) with $\psi_i=0, i=1..3,$ and $u=0$ and with the partial derivatives of ψ_i and u given by Appendix V.1 where $\theta_i=\alpha_i$.

APPENDIX V.6

The development of eqs.(5.32)

Using eqs.(5.25) in eqs.(5.6) and (5.7) it follows that:

$$\begin{aligned}
&\sin\bar{\theta}_1=\sin\alpha_1-(v_1+w_1)=\sin\theta_1-w_1\\
&\sin\bar{\theta}_2=\sin\alpha_2-(v_2+w_2)+v_1+w_1=\sin\theta_2-w_2+w_1\\
&\sin\bar{\theta}_4=\sin\theta_4-w_2+w_3\\
&\sin\bar{\theta}_5=\sin\theta_5-w_3
\end{aligned} \qquad (5.6.1)$$

and, respectively,

$$\begin{aligned}
&\bar{\psi}_1=\bar{\theta}_1-\bar{\theta}_2-(\alpha_1-\alpha_2)=\bar{\theta}_1-\bar{\theta}_2-(\theta_1-\theta_2)+\psi_1=\psi_1^*+\psi_1\\
&\bar{\psi}_2=\bar{\theta}_2+\bar{\theta}_4-2\alpha_2=\bar{\theta}_2+\bar{\theta}_4-(\theta_2+\theta_4)+\psi_2=\psi_2^*+\psi_2\\
&\bar{\psi}_3=\bar{\theta}_5-\bar{\theta}_4-(\theta_5-\theta_4)+\psi_3=\psi_3^*+\psi_3\\
&\bar{u}=\sum_J\cos\theta_j-2(\cos\alpha_1+\cos\alpha_2)=\sum_J(\cos\bar{\theta}_j-\cos\theta_j)+u=u^*+u
\end{aligned} \qquad (5.6.2)$$

where:

- θ,ψ,u have the same meaning as in eqs.(5.6) and (5.7) -see also Fig.5.4- and denote the displacements of the deformed state S from Fig.5.17, measured about the unloaded and undeformed state 0.
- $\bar{\theta},\bar{\psi},\bar{u}$ are similar to θ,ψ,u but denote the displacements of the state T from Fig.5.17 about the state 0.
- θ^*,ψ^*,u^* are similar to θ,ψ,u but denote the displacements of the state T about the state S.

Eqs.(5.8) are valid for any state of equilibrium and hence are valid for the state T too, so that it can be rewritten as

$$\sum_{i=1}^{3} c_i\cdot\psi_i\cdot\frac{\partial\psi_i}{\partial\bar{v}_j}+k\cdot\bar{u}\cdot\frac{\partial\bar{u}}{\partial\bar{v}_j}-p\cdot p_j=0 \qquad ,j=1\ldots3 \qquad (5.6.3)$$

where the notation corresponding to T in Fig.5.17 are used.

On account of eqs.(5.25) and (5.6.2) it follows that

$$\frac{\partial\bar{\psi}_i}{\partial\bar{v}_j}=\frac{\partial\psi_i}{\partial v_j}=\frac{\partial\psi_i^*}{\partial w_j} \qquad \text{where } i,j=1\ldots3 \qquad (5.6.4)$$

$$\frac{\partial\bar{u}}{\partial\bar{v}_j}=\frac{\partial u}{\partial v_j}=\frac{\partial u^*}{\partial w_j}$$

so that

$$\bar{\psi}_i \cdot \frac{\partial \bar{\psi}_i}{\partial \bar{v}_j} = (\psi_i^* + \psi_i) \cdot \frac{\partial \bar{\psi}_i}{\partial \bar{v}_j} = \psi_i^* \cdot \frac{\partial \psi_i^*}{\partial w_j} + \psi_i \cdot \frac{\partial \psi_i}{\partial v_j} \qquad (5.6.5)$$

$$\bar{u} \cdot \frac{\partial \bar{u}}{\partial \bar{v}_j} = (u^* + u) \cdot \frac{\partial \bar{u}}{\partial \bar{v}_j} = u^* \cdot \frac{\partial u^*}{\partial w_j} + u \cdot \frac{\partial u}{\partial v_j}$$

With due allowance to eqs.(5.8) eqs.(5.6.2) and (5.6.5)

yield

$$\boxed{\sum_{i=1}^{3} c_i \cdot \psi_i^* \cdot \frac{\partial \psi_i^*}{\partial w_j} + k \cdot u^* \cdot \frac{\partial u^*}{\partial w_j} = 0} \qquad (5.32)$$

APPENDIX V.7

Stability criteria associated with elastic snap-buckling.

The development of the stability criteria associated with a snap-buckling of the model from Fig.5.2 is presented. The derivation is based on the analysis of the primary path.

The model attains a critical state of snap-buckling when a certain stiffness vanishes or,in other words,when an increase of a displacement v_i can take place without any variation of loading and of other displacements v_j $(j \neq i)$.

Snap-buckling at joint B_2.

The equilibrium equations (5.13) for the primary path can be regarded as a functional between the variables p and v_i so that their total differentials can be written as $(i = 1...3)$

$$d\left(\frac{\partial \Delta\Pi}{\partial v_i}\right) = \frac{\partial^2 \Delta\pi}{\partial v_i \partial p} dp + \frac{\partial^2 \Delta\pi}{\partial v_i \partial v_1} dv_1 + \frac{\partial^2 \Delta\pi}{\partial v_i \partial v_2} dv_2 + \frac{\partial^2 \Delta\pi}{\partial v_i \partial v_3} dv_3 = 0 \qquad (5.7.1)$$

With due allowance to symmetry and to eqs.(5.12) and (5.17), the above equations yield

$$p_i . dp = \Pi_{i2} . dv_2 + 2\, \Pi_{i1} . dv_1 \qquad i=1..3 \qquad (5.7.2)$$

As mentioned above,the stability criteria for a snap-buckling at joint B_2 are

$$\begin{aligned} dv_2 &\neq 0 \\ dv_1 &= 0 \\ dp &= 0 \end{aligned} \qquad (5.7.3)$$

and they are necessarily and sufficiently satisfied in eqs.(5.7.2) when

$$\Pi_{i2} = 0 \quad , \quad i=1...3 \qquad (5.7.4)$$

With eqs.(5.7.4),the determinant given by eq.(5.22) becomes

$$\Delta = \begin{vmatrix} \Pi_{11} & 0 & \Pi_{13} \\ 0 & 0 & 0 \\ \Pi_{13} & 0 & \Pi_{11} \end{vmatrix} = 0 \qquad (5.7.5)$$

and hence the stability criteria (5.7.4) can be recast in terms of eqs. (5.16a) as

$$\begin{vmatrix} \Pi_{22} = 0 \\ M_{11} = 0 \\ \Delta = 0 \end{vmatrix} \qquad (5.7.6)$$

Snap-buckling at joints B_1 and B_3.

Due to the symmetry of the arch-model, a simultaneous snap-buckling at joints B_1 and B_3 occurs.

By using the snap-buckling conditions

$$\begin{aligned} dv_1 &= dv_3 \neq 0 \\ dv_2 &= 0 \\ dp &= 0 \end{aligned} \qquad (5.7.7)$$

in eqs.(5.7.2), the stability criteria follow as

$$\varpi_{i1} = 0 \quad , \quad i=1..3 \qquad (5.7.8)$$

which yield, according to eq.(5.22),

$$\Delta = \begin{vmatrix} 0 & 0 & 0 \\ 0 & \varpi_{22} & 0 \\ 0 & 0 & 0 \end{vmatrix} = 0 \qquad (5.7.9)$$

The criteria (5.7.8) can be recast in terms of the eqs.(5.16a) as

$$\left\| \begin{aligned} W_{11} &= 0 \\ M_{11} &= 0 \\ M_{22} &= 0 \\ \Delta &= 0 \end{aligned} \right. \qquad (5.7.10)$$

Snap-buckling at joints $B_1 \ldots B_3$.

Local snap-buckling has been considered with the two previous cases. When both eqs.(5.7.4) and (5.7.8) are fulfilled, a simultaneous snap-buckling takes place at the joints B_1, B_2, B_3.

Thus, according to eq.(5.22), Δ becomes

$$\Delta = |0| = 0 \qquad (5.7.11)$$

and all criteria (5.16a) are violated simultaneously.

Since the untruncated form of eqs.(5.13) has been used, the above stability criteria are accurate provided that the 'exact' ϖ_{ij}-coefficients (i.e.given by eqs.(5.20)) are employed.

APPENDIX V.8

Approximate secondary path associated with an elastic snap-buckling.

The snap-buckling at joint B_2 will be considered below. According to the stability criteria (5.7.4) or (5.7.6) *) the solutions of the perturbation equations (5.35a..c) are **)

$$\bar{w}_1' = \bar{w}_1'' = \bar{w}_1''' = 0$$
$$\bar{w}_3' = \bar{w}_3'' = \bar{w}_3''' = 0 \qquad (5.8.1)$$

With eqs.(5.8.1), eqs.(5.42a) and (5.42b) yield

$$2p'\varpi_{i2}' = -\varpi_{i22}\bar{w}_2'$$
$$3p''\varpi_{i2}' = -3p'^2\varpi_{i2}'' - 3p'\varpi_{i2}'\frac{\bar{w}_2''}{\bar{w}_2'} - 3\varpi_{i22}\bar{w}_2'' - 3p'\varpi_{i22}'\bar{w}_2' - \varpi_{i222}\bar{w}_2'^2 \qquad (5.8.2)$$

where i=1...3.

Since

$$\varpi_{i2}' = \frac{d\varpi_{i2}}{dp} = \varpi_{i22}\cdot\frac{dv_2}{dp} + 2\varpi_{i12}\cdot\frac{dv_1}{dp} \qquad ,i=1..3 \qquad (5.8.3)$$

the first of eqs.(5.8.2) yield

$$2p'\left(\frac{dv_2}{dp}\varpi_{i22} + 2\frac{dv_1}{dp}\varpi_{i12}\right) = -\varpi_{i22}\bar{w}_2' \qquad ,i=1..3 \qquad (5.8.4)$$

Taking into account that the ϖ_{ij}-coefficients are always finite (due to their physical meaning) and that, according to eqs.(5.7.3), *)

$$\frac{dv_2}{dp} = \infty \qquad (5.8.5)$$

eqs.(5.8.4) yield

$$\boxed{p' = 0} \qquad (5.8.6)$$

Analogous to eqs.(5.8.3)

$$\varpi_{i2}'' = \frac{d^2\varpi_{i2}}{dp^2} = \varpi_{i222}\left(\frac{dv_2}{dp}\right)^2 + 4\varpi_{i122}\left(\frac{dv_1}{dp}\right)\left(\frac{dv_2}{dp}\right) + 2\varpi_{i112}\left(\frac{dv_1}{dp}\right)^2$$
$$\varpi_{i22}' = \frac{d\varpi_{i22}}{dp} = \varpi_{i222}\cdot\frac{dv_2}{dp} + 2\varpi_{i122}\cdot\frac{dv_1}{dp} \qquad ,i=1...3 \qquad (5.8.7)$$

---

*) see Appendix V.7

**) see solution (iii) from Section 5.3.5d.

With eq.(5.8.6), eqs.(5.8.4) yield

$$p' \frac{dv_2}{dp} = -0.5\bar{w}_2' \tag{5.8.8}$$

and hence

$$\begin{aligned} p'\,\Pi''_{i2} &= 0.25\Pi_{i222}\,\bar{w}_2'^2 + 0. \\ p'\,\Pi'_{i22} &= -0.5\Pi_{i222}\,\bar{w}_2' + 0. \end{aligned} \tag{5.8.9}$$

where eqs.(5.8.7) have been used.

By using eqs.(5.8.9) it follows from eqs.(5.8.2) that

$$3p''\Pi'_{i2} = -0.75\Pi_{i222}\bar{w}_2'^2 + 1.5\Pi_{i22}\bar{w}_2'' - 3\Pi_{i22}\bar{w}_2'' + 1.5\Pi_{i222}\bar{w}_2'^2 - \Pi_{i222}\bar{w}_2'^2$$

or

$$3p''\Pi'_{i2} = -0.25\Pi_{i222}\bar{w}_2'^2 - 1.5\Pi_{i22}\bar{w}_2'' \quad , \quad i=1\ldots3 \tag{5.8.10}$$

Eqs.(5.8.10) yield

$$\boxed{p'' = 0} \tag{5.8.11}$$

in a manner similar to that in which eq.(5.8.6) followed from eqs.(5.8.4)

Choosing w_2 as perturbation parameter and using eqs.(5.8.1), (5.8.4), (5.8.11) in eqs.(5.36), the approximate secondary path follows as

$$\left\| \begin{aligned} \bar{w}_1 &= \bar{w}_3 = 0 \\ \bar{w}_2 &= \text{indefinite} \\ p &= p_{cr} \end{aligned} \right. \tag{5.8.12}$$

In fact this 'approximate' secondary path is associated with the dynamic snap-buckling (see Fig.5.10).

APPENDIX V.9

Evaluation of p' and p'' for an antisymmetric buckling.

The antisymmetric buckling is given by (see Table 5.2)

$$\bar{w}_1' = -\bar{w}_3' \neq 0 \quad \text{and} \quad \bar{w}_2' = 0 \tag{5.9.1}$$

so that eq.(5.46) yields

$$2p' = -\bar{w}_1' \cdot \frac{\sum_i (\Pi_{i11} - 2\Pi_{i13} + \Pi_{i33})}{\sum_i (\Pi_{i11} - \Pi_{i13})} = -\bar{w}_1' \cdot \frac{0}{2(\Pi_{11} - \Pi_{13})} = 0 \tag{5.9.2}$$

while

$$3p'' = -\bar{w}_1'^2 \cdot \frac{\sum_i (\Pi_{i111} - 3\Pi_{i113} + 3\Pi_{i133} - \Pi_{i333})}{\sum_i (\Pi_{i11} - \Pi_{i13})} = \tag{5.9.3}$$

$$= -\bar{w}_1'^2 \cdot \frac{\Pi_{1111} - 4\Pi_{1113} + 3\Pi_{1133}}{\Pi_{11} - \Pi_{13}}$$

on account of eqs.(5.35a) and (5.9.2).

It is apparent from eq.(5.9.2) that eq.(5.56) is true for an antisymmetric 'approximate' secondary path no matter whether the displacements in eqs.(5.9.1) are large or small.

When small displacements $\bar{w}$ are assumed, eq.(5.9.3) yields

$$3p''\varepsilon^2 = -\bar{w}_1^2 \frac{\Pi_{1111} - 4\Pi_{1113} + 3\Pi_{1133}}{\Pi_{11}' - \Pi_{13}'} \approx 0 \tag{5.9.4}$$

where eqs.(5.55) have been used.

It is noteworthy that eqs.(5.9.2) and (5.9.4) are approximate since the perturbation equations (5.35a..c) and their summation versus i have been used.

APPENDIX V.10

Eqs.(5.81) and (5.82) are derived below from eqs.(5.80) and (5.8) when the 1st order theory is employed, that is when the displacements are small and hence both the equilibrium and compatibility equations are written on the undeformed state.

Consequently both eqs.(5.8) and (5.80) become linear and

$$\frac{\partial \Delta \psi_i}{\partial \Delta v_k} = \frac{\partial \psi_{i0}}{\partial v_{k0}}$$
$$\frac{\partial \Delta u}{\partial \Delta v_k} = \frac{\partial u_0}{\partial v_{k0}} \qquad (5.10.1)$$

where the subscript $\underline{0}$ denotes the instantaneous values, i.e. at $\varphi = 0$.

On account of the analogy of linear eqs.(5.8) and (5.80) and with due allowance to eqs.(5.10.1), it arises that the solutions of these two sets of equations are proportional, that is

$$\Delta v_k = v_{k0} \cdot \Delta\varphi \qquad ,k=1\ldots3 \qquad (5.10.2)$$

where v_{k0} are the solutions of eqs.(5.8).

Since the compatibility equations are linear, it follows that

$$\Delta \psi_i = \psi_{i0} \cdot \Delta\varphi$$
$$\Delta u = u_0 \cdot \Delta\varphi \qquad (5.10.3)$$

where, according to eqs.(5.3), (5.4) and (5.74),

$$\psi_{i0} = \frac{M_{i0}}{K_i} = \frac{\bar{M}_{i0}}{c_i} \qquad ,i=1\ldots3$$
$$u_0 = \frac{F_0}{DL} = \frac{\bar{F}_0}{k} \qquad (5.10.4)$$

Assuming that the first creep-increment $\Delta\varphi$ is considered and using eqs.(5.10.3) and (5.10.4), the governing equations (5.65a) and (5.66a) yield

$$\Delta \bar{M}_i = \bar{M}_{i0} \cdot \Delta\varphi - \bar{M}_{i0} \cdot \Delta\varphi = 0$$
$$\Delta \bar{F} = \bar{F}_0 \cdot \Delta\varphi - \bar{F}_0 \cdot \Delta\varphi = 0 \qquad (5.10.5)$$

When the creep attained the value φ it follows from eqs.(5.10.2), (5.10.3) and (5.10.5) that

$$
\begin{aligned}
v_{k\varphi} &= v_{k0} + \sum_{\varphi} \Delta v_k = v_{k0}\cdot(1+\varphi) \qquad ,k=1..3 \\
\psi_{i\varphi} &= \psi_{i0} + \sum_{\varphi} \Delta \psi_i = \psi_{i0}\cdot(1+\varphi) \qquad ,i=1..3 \\
u_{\varphi} &= u_0 + \sum_{\varphi} \Delta u = u_0 \cdot(1+\varphi)
\end{aligned}
\tag{5.10.6}
$$

and

$$
\begin{aligned}
\overline{M}_{i\varphi} &= \overline{M}_{i0} + \sum_{\varphi} \Delta \overline{M}_i = \overline{M}_{i0} \qquad , \; i=1...3 \\
\overline{F}_{\varphi} &= \overline{F}_0 + \sum_{\varphi} \Delta F = \overline{F}_0
\end{aligned}
\tag{5.10.7}
$$

Eqs.(5.10.6) and (5.10.7) are identical to eqs.(5.81) and (5.82).

APPENDIX V.11

Computer programs analysing the behaviour of the visco-elastic arch-model.

A set of programs and subprograms has been built in order to analyse the arch-model from Fig.5.2. The theoretical formulae on which these programs are based are presented in Section 5.3.

The computing is advantageously used with the theoretical analysis of the arch-model because the equations largely employ matrices and summations. In addition a standard subroutine available with the NAG-library (1972) allows for the solutions of the non-linear coupled equations to be found accurately. This subroutine,called C05NAF, is based on the Powell procedure (1970). The user must supply:

(i) an estimate of the solution.As shown in Section 5.3 an 'approximate' solution is used in this respect.

(ii) a subroutine which computes the values of the left-hand-side of the coupled equations. Here this subroutine is called FUNCT when the elastic behaviour is analysed and VFUNCT when the creep effect is studied (see Table 5.11.2).

(iii) a subroutine which monitors the intermediate and final solutions computed by C05NAF. Here this subroutine is called MONIT (see Table 5.11.2).

(iv) the required degree of accuracy. A value of 10^{-10} has been judged as providing sufficient accuracy of the 'exact' solution.

(v) the step-length necessary for the Jacobian to be computed by the subroutine. A value equal with 0.1 has been proved successful.

In solving the three coupled equations associated with the three degree-of-freedom model the unknowns can be chosen either equal with the displacements v_i (i=1...3) or equal with the load p and two of the displacements v_i. In the former case the 'exact' solution will correspond to the same load p as the 'approximate' solution, whereas in the latter the 'exact' and 'approximate' solutions will correspond to the same displacement v_j , where v_j is that displacement v_i not chosen as unknown (see Fig.5.11.1).

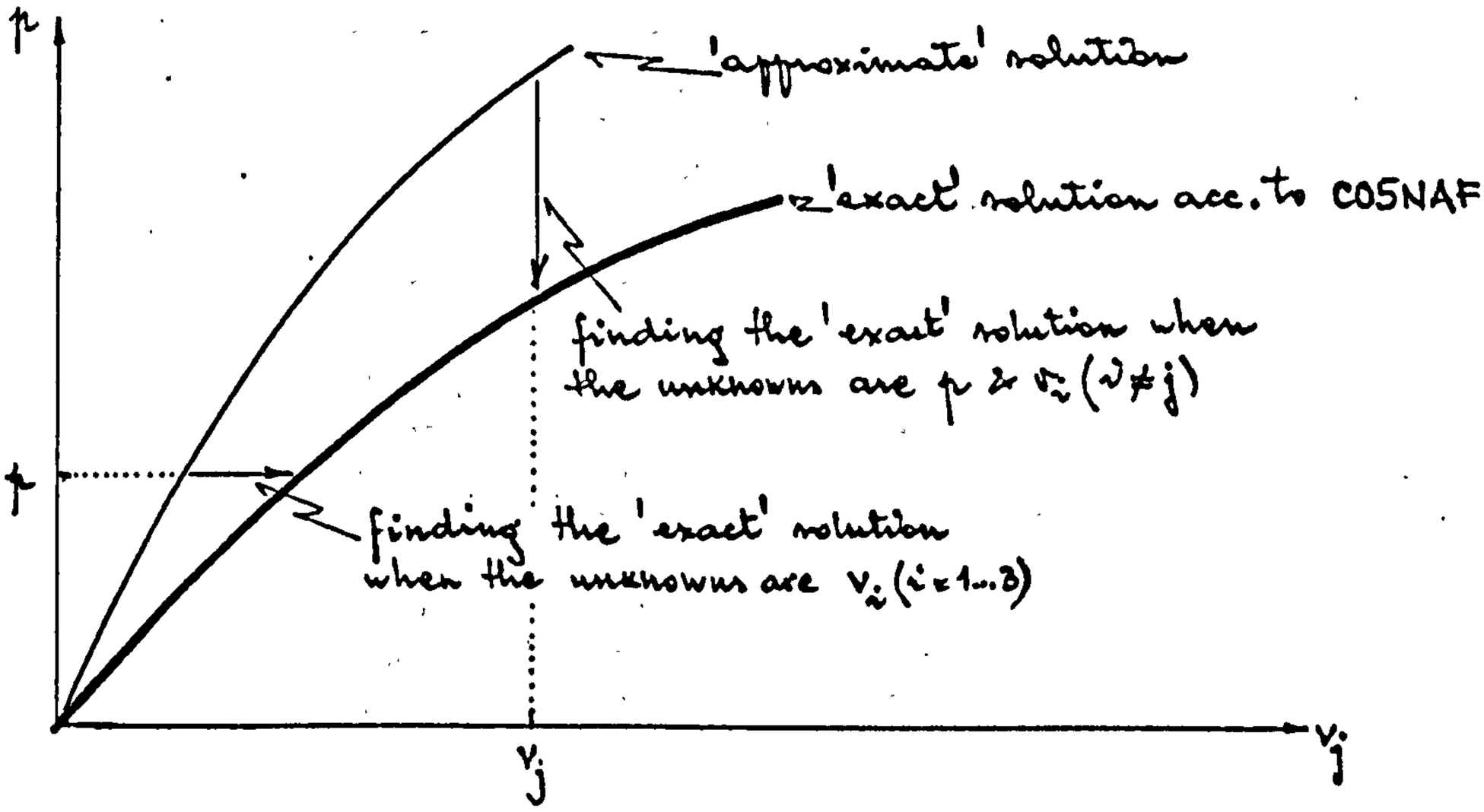

Fig.5.11.1

Two types of problems associated with the behaviour of the three degree-of-freedom model can be solved by using the present set of programs and subprograms:

1. a complete analysis of the elastic pre- and post-buckling response to loading.

2. an analysis of the creep effects on the pre-buckling response and instability.

A simplified flow-chart of the solution of these two problems is depicted in Fig.5.11.2.

Only the general features of the computer programs are presented in this Appendix. The main programs are listed in Table 5.11.1 while the subroutines computing the main aspects involved by the theoretical analysis are listed in Table 5.11.2. Details about both the scope and the basic equations of the main programs and subroutines are given in Table 5.11.1 and 5.11.2.

In Table 5.11.3 the subroutines attached to each main program are indicated.

Tables attached to Appendix V.11:

Table 5.11.1: Main programs.

Table 5.11.2: Subroutines.

Table 5.11.3: Subroutines attached by the main programs.

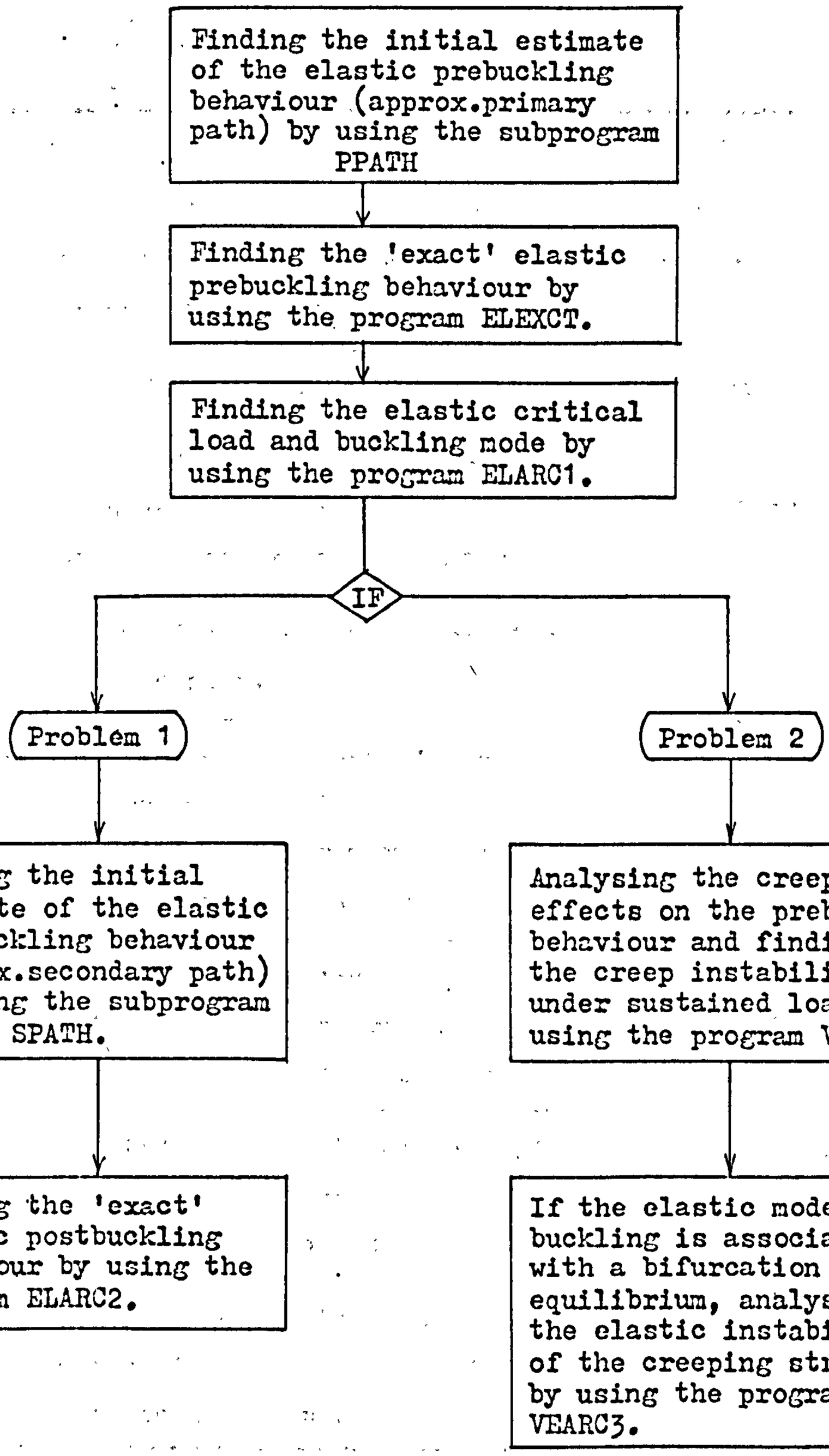
Finding the initial estimate of the elastic prebuckling behaviour (approx.primary path) by using the subprogram PPATH
Finding the 'exact' elastic prebuckling behaviour by using the program ELEXCT.
Finding the elastic critical load and buckling mode by using the program ELARC1.
IF
Problem 1
Problem 2
Finding the initial estimate of the elastic postbuckling behaviour (approx.secondary path) by using the subprogram SPATH.
Analysing the creep effects on the prebuckling behaviour and finding the creep instability under sustained loading by using the program VEARC1.
Finding the 'exact' elastic postbuckling behaviour by using the program ELARC2.
If the elastic mode of buckling is associated with a bifurcation of equilibrium, analysing the elastic instability of the creeping structure by using the program VEARC3.

Fig.5.11.2

Table 5.11.1. Main programs.

Program	Scope	Associated with
ELPERF	To build up the 'approximate' primary path when $\varepsilon = p$.	Section 5.3.3b
ELIMP	As ELPERF but $\varepsilon = v_1$ or v_2	Section 5.3.3b
ELEX	To build up the elastic primary path using the 'exact' solution of the 'approximate' equations.	eqs. (5.13)
ELEXCT	To build up the 'exact' elastic primary path.	Section 5.3.3a
ELARC1	To find out the 'exact' and 'approximate' critical points on the 'exact' primary path. (instantaneous loading)	Section 5.3.4
ELARC2	To find out the 'exact' primary and secondary paths under instantaneous loading.	Section 5.3.3a and 5.3.5a
VEARC1	To find the 'exact' effects of the concrete creep when the loading is sustained.	Section 5.3.6b
VEARC3	To find the critical load of a creeping structure for certain φ and p_0.	Section 5.3.7a

Table 5.11.2 Subroutines.

Subroutine	Scope	Using	Variantes
PICOEF	To compute the Π-coefficients of the 'approx.'form of the potential	Table 5.1	
PPATH	To analyse the 'approximate' elastic primary path when $\varepsilon = p$	eqs.(5.14a, b and c)	for $\varepsilon = v_1$ or $\varepsilon = v_2$
APROX	To compute the initial estimate for the 'exact' solution of the elastic primary path.	PPATH	
T3COEF	To compute the 'approximate' Π-coefficients for a point on the primary path.	eqs.(5.34)	
BIFUR	To find the bifurcation point on the 'approx.' primary path	T3COEF and eq.(5.24).	
FUNCT	To compute the left-hand side of eqs.(5.8).	eqs.(5.6)... (5.8) and Appendix V.1	p or v_1 or v_2 is held constant.
MONIT	To monitor the output of C05NAF		
AJACOB	To compute the 'exact' Π - coefficients.	eqs.(5.19)& Appendix V.1	
EXBIF	To find the 'exact' critical point on the 'exact' primary path.	AJACOB and eq.(5.24)	
TCODER	To compute the 'exact' $\frac{d\Pi}{dp}_{ij}$	eqs.(5.19)& finite diff.	
SPATH	To analyse the 'approx.' secondary path when $\varepsilon = v_2$	eqs.(5.35a.. ..c)	for $\varepsilon = v_1$
STRESS	To compute the forces $\bar{M}_i$ and $\bar{F}$ corresponding to a deformed state when the loading is either instantaneous or sustained.	eqs.(5.3), (5.65a), (5.66a) & (5.67a).	

Table 5.11.2 (cont.)

Subroutine	Scope	Using	Variantes
CRPATH	To compute the 'approximate' effect of a creep-increment on the arch displacements.	eqs.(5.80)	
VEDEF	To compute the 'exact' increase of displacements due to a creep-increment when p = const.	eqs.(5.75) and VFUNCT	
VFUNCT	To compute the left-hand side of eqs.(5.75).	eqs.(5.72), (5.73) and Appendix V.1	
ELSTAB	To find the critical load of the creeping structure.	eqs.(5.84) and (5.85).	

Table 5.11.3 Subroutines attached by the main programs.

Subroutines / Main programs	PICOEF	PPATH	APROX	T3COEF	BIFUR	COSNAF	FUNCT	MONIT	AJACOB	EXBIF	TCODER	SPATH	STRESS	CRPATH	VEDEF	VFUNCT	ELSTAB
ELPERF	x	x															
ELIMP	x	x															
ELEX	x	x	x			x		x									
ELEXCT	x	x	x			x	x	x									
ELARC1	x	x	x	x	x	x	x	x	x	x	x						
ELARC2	x	x	x	x	x	x	x	x	x	x	x	x	x				
VEARC1	x	x	x			x	x	x					x	x	x	x	
VEARC3	x	x	x			x	x	x	x				x	x	x	x	x

REFERENCES.

ACI (1966). Symposium on reinforced concrete columns. Publication SP-13 Detroit,377 pp.

ACI 318 (1971). Building code requirements for reinforced concrete. Detroit,76 pp.

Agent R.(1972). The inelastic analysis of reinforced concrete slender structures supporting travelling cranes. International Colloquium on Plastic Analysis,Iasi Sept. Vol.I pp.113-126

Ali I., Kessler C.E.(1965). Rheology of concrete.A review of research. Eng.Experiment Station,Univ.of Illinois Bulletin 476,101 pp.

Argyris J.H., Kelsey S.(1960). Energy theorems and structural analysis. Butterwords,48 pp.

Arutyunyan N.K.(1966). Some problems in the theory of creep. Pergamon Press,290 pp.

Bazant Z.P.(1968). Creep stability and buckling strength of concrete columns. Mag.of Concrete Research,Vol.20 June pp.85-94.

Bazant Z.P.(1972). Prediction of concrete creep effects using age-adjusted effective modulus method. Journal ACI,April pp.212-216.

Bazant Z.P.(1973). Comparison of approximate linear methods for concrete creep. ASCE,Journal of the Structural Division, ST9 pp.1851-1873.

BSI (1970). B.S.1881:Part 4:Methods of testing concrete for strength. 28 pp.

BSI (1972). CP 110:Part 1:Code of practice for structural use of concrete. November,154 pp.

Calin G., Constantinescu D.R.(1973). Creep effect on stresses induced by the seasonal variation of temperature (Efectul curgerii lente asupra eforturilor produse de variatia de temperatura sezoniera). Symposium ICB,Bucharest April

Carlson R.L., Breindel W.W.(1960). On the mechanism of column creep. in Creep of Structures (edited by N.J.Hoff),Colloquium IUTAM Stanford,Springer 1962 pp.272-290.

CEB-FIP (1970). International recommendations for the design and construction of concrete structures.Principles and Recommendatio FIP 6th Congress,Prague June,80 pp.

CEB (1972). Structural effects of time-dependent behaviour of concrete - Manual.2nd draft, Bulletin d'information CEB No.80 February,118 pp.

CEB (1973). Effects structuraux du fluage et des déformations différées du béton - Manual.Final draft, Bulletin d'information CEB No.94 August,62 pp.

CEB (1973). Buckling Manual. Final draft, Bulletin d'information CEB No.93 May.

Chapman J.C., Erickson B., Hoff N.J.(1960). A theoretical and experimental investigation of creep buckling. Int.Journal of Mechanical Science Vol.1 Nos.2/3 April pp.145-174.

Chilver A.H., Johns K.C.(1969). Coupled modes of buckling in some continuous systems. IUTAM Symposium on Instability of Continuous Systems (ed. by H.Leipholz).Hennenalb,Springer pp.334-337.

Chiorino M.A.(1967). Rheologic phenomena and thermal variations in road slabs of prestressed concrete (Fenomeni reologici e variazioni termiche nelle sovrastrutture stradali in calcestruzzo precompresso). Giornale del Genio Civile,105 February pp.137-157.

Chovichien V., Gutzwiller M.J., Lee R.H.(1973). Analysis of reinforced concrete columns under sustained load. Journal ACI,Oct. pp.692-699.

Constantinescu D.R.(1972). The creep of concrete (Curgerea lenta a betonului). Institutul de Constructii Bucuresti,90 pp.

Constantinescu D.R.(1974). On the governing relationship of concrete in the range of linear creep (Asupra legii fizice a betonului in domeniul curgerii lente lineare). Studii si Cercetari de Mecanica Aplicata, Vol.33 No.1 Bucharest pp.191-217.

Constantinescu D.R., Illston J.M.(1974). Direct methods of analysing the structural effects of linear creep of ageing concrete. Materials and Structures,RILEM. Vol.7 No.42 pp.395-401.

Constantinescu D.R., Illston J.M.(1975). Direct solutions to problems of time-dependent induced stresses in restrained concrete . Materials and Structures,RILEM. Vol.8 No.43 pp.11-17.

Courbon J.(1968). The effect of linear creep on the equilibrium of statically indeterminate structures of prestressed concrete (L'influence du fluage linéaire sur l'équilibre des systèmes

hyperstatiques en béton précontrainte). Annales de I.T.B.T.P. February No.242 pp.327-353.

Crainic L.N.(1972). Plastic design of reinforced concrete structures by assigning limit rotations. International Colloquium on Plastic Analysis,Iasi Sept.

Cranston W.B.(1972). Analysis and design of reinforced concrete columns. Cement and Concrete Association,London Publication 41 020 , 28 pp.

Croll J.G.A.,Walker A.C.(1972). Elements of structural stability. MacMillan, 200 pp.

Davies R.D.(1957). Some experiments on the applicability of the principle of superposition to the strains of concrete subjected to changes of stress,with particular reference to prestressed concrete. Mag.of Concrete Research,Vol.9 No.27 Nov. pp.161-172.

Dilger W.,Neville A.M.(1971). Creep buckling of long columns. The Structural Engineer,Vol.49 May pp.223-226.

Dischinger F.(1937). Research on the buckling safety of elastic deformation and creep of concrete in bridge arches (Untersuchungen über die Knicksicherheit die elastische Verformung und das Kriechen des Betons bei Bögenbrücken). Bauingenieur,Vol.18 Nos.33/34(pp.487-520) Nos.35/36(pp.539-552) Nos.39/40(pp.595-621).

Dishinger F.(1939). Elastic and plastic deformations of reinforced concrete structures with reference to bridge arches (Elastische and plastische Verformungen der Eisenbetontragwerke und insbesondere der Bögenbrücken). Bauingenieur,Vol.20 Nos.5/6 (pp.53-63) Nos.21/22(pp.286-294) Nos.31/32(pp.426-437) Nos. 47/48(pp.563-572).

Distefano J.N.(1960). Redistribution of stresses in a continuously supported beam due to creep. IABSE 6th Congress,Final reports Stockholm pp.417-427.

Distefano J.N.(1965). Creep buckling of slender columns. ASCE,Journal of Structural Division ST3 pp.127-150.

England G.L.,Illston J.M.(1965). Methods of computing stress in concrete from a history of measured strain. Civil Engineering and Public Works Review, April-June pp.2-8.

England G.L.(1966). Steady-state of stresses in concrete structures subjected to sustained temperature and loads. Nuclear Engineering and Design,North-Holland Publ.Company Vol.3 pp.54-65 and pp.246-255.

England G.L.(1967). Numerical creep analyses applied to concrete structures. Journal ACI,June pp.301-311.

England G.L.(1968). Time-dependent stresses in creep-elastic materials. A general method of calculation. Conference on Recent Advances in Stress Analysis, Royal Aeronautical Society.March pp.2-1..2-8

Erzen C.Z.(1956). An expression for creep and its application to prestressed concrete. Journal ACI,August pp.205-213.

Finsterwalter U.(1958). Results on creep and shrinkage measurements in prestressed structures (Ergebnisse von Kriech- und Schwindmessungen an Spannbetonbauwerken). Beton und Stahlbetonbau No.7 pp.136-144.

Fintel M., Khan F.(1969). Effects of column creep and shrinkage in tall structures. Prediction of inelastic column shortening. Journal ACI,Dec. pp.957-967.

Flügge W.(1975). Viscoelasticity. 2nd ed. Springer,194 pp.

Freudenthal A.M.(1956). Creep effects in the analysis of reinforced concrete structures. IABSE 5th Congress,Preliminary publications Lisbon pp.85-99.

Freudenthal A.M., Roll F.(1958). Creep and creep recovery of concrete under high compressive stress. Journal ACI,Proc.Vol.54 pp.1111-1142.

Furlong R.W.(1976). Guidelines for analysing column slenderness by a rational analysis of an elastic frame. Journal ACI,March pp.138-141.

Gamble B.R., Jordaan I.J.(1974). A direct method of viscoelastic analysis for ageing concrete. Materials and Structures. Vol.8 No.43 pp.37-43.

Ghali A., Neville A.M., Jha P.C.(1967). Effect of elastic and creep recoveries of concrete on loss of prestress. Journal ACI, Dec. pp.802-810.

Ghali A., Dilger W., Neville A.M.(1969). Time-dependent forces induced by settlement of supports in continuous reinforced concrete beams. Journal ACI,Nov. pp.907-915.

Gioncu V.(1974). Reinforced concrete thin shells.Special problems of analysis (Placi curbe subtiri de beton armat.Probleme speciale de calcul). Ed.Academiei RSRomania,Bucharest,436 pp.

Glainville W.H.(1930). The creep or flow of concrete under load. Building Research Technical Paper No.12,London H.M.S.O.

Glainville W.H., Thomas F.G.(1939). Further investigations on the creep or flow of concrete under load. Building Research Technical Paper No.21,London H.M.S.O.

Godden W.G.(1965). Numerical analysis of beam and column structures. Prentice-Hall Inc.,309 pp.

Goyal B.B., Jackson N.(1971). Slender concrete columns under sustained load. ASCE,Journal of Structural Division ST11 pp.2729-2750.

Gurfinkel G., Robinson A.(1967). Determination of the strain distribution and curvature in a reinforced concrete section subjected to bending moment and longitudinal load. Journal ACI,July pp.398-403

Gvozdev A.A.(1967). The creep of concrete (Le fluage du béton). Bulletin d'information CEB, No.64 Dec.

Habel A.(1961). Stresses induced by imposed strains in plain and reinforced concrete structures (Zwängungsspannungen nicht vorgespannter statisch unbestimmter Beton- und Stahlbeton-tragwerke). Die Bautechnik,No.6 pp.186-190.

Hangan M.D.(1938). The shrinkage of concrete and its effect on bond (Le retrait du béton et son influence sur l'adhérence). PhD Thesis,École Politechnique,Bucharest,100 pp.

Hangan M.D.(1965). On the question of the stability of gantry-columns (Beitrag zur Frage der Knickberechnung von Kranbahnstützen). Die Bautechnik,No.11 pp.386-388.

Hannant D.J.(1969). Creep and creep recovery of concrete subjected to multiaxial compressive stress. Journal ACI,May pp.391-394.

Hansen T., Mattock A.(1966). Influence of size and shape of member on the shrinkage and creep of concrete. Journal ACI,Febr. pp.267-288

Hatt W.K.(1907). Notes on the effect of time element in loading reinforced concrete beams. ASTM Proc. Vol.7 pp.421-433.

Hoff N.J.(1957). Buckling and stability. Journal of Royal Aeronautical Society, Jan. Vol.58 pp.3-51.

Hoff N.J.(1966). The analysis of structures based on the minimal principles and the principle of virtual displacements. 3rd print,493 pp.

Hutchinson J.W., Koiter W.T.(1971). Postbuckling theory. Applied Mech. Review, No.9 pp.1353-1366.

Illston J.M.(1965). The components of strain in concrete under sustained compressive stress. Mag.of Concrete Research Vol.17 No.50 March pp.21-28.

Illston J.M.(1965). The creep of concrete under uniaxial tension. Mag.of Concrete Research,Vol.17 No.51 June pp.77-84.

Illston J.M.(1968). Components of creep in mature concrete. Journal ACI,March pp.219-227.

Illston J.M., England G.L.(1970). Creep and shrinkage of concrete and their influence on structural behaviour.A review of methods of analysis. The Structural Engineer,Vol.48 July pp.283-292.

Illston J.M., Jordaan I.J.(1971). Three-dimensional creep measurements in young concrete. Materials and Structures,Vol.4 No.24 pp.371-377.

Illston J.M., Jordaan I.J.(1972). Creep prediction for concrete under multiaxial stress. Journal ACI,March pp.158-164.

Jordaan I.J., Illston J.M.(1969). The creep of sealed concrete under multiaxial compressive stress. Mag.of Concrete Research,Vol.21 No.69 Dec. pp.195-204.

Jordaan I.J., Illston J.M.(1971). Time-dependent strains in sealed concrete under systems of variable multiaxial sress. Mag.of Concrete Research,Vol.23 Nos.75-76 June-Sept. pp.79-88.

Jordaan I.J.(1974). Analysis of creep in concrete structures under general state of stress. IABSE Seminar on Concrete Structures subjected to Triaxial Stresses. Paper III-8,Rapports IABSE Vol.19

Kordina K.(1972). Behavior and design of slender concrete columns. ASCE-IABSE Int.Conference on Tall Building,Preprint Vol.III-23 Lehigh Univ.

Lempriere B.M.(1960). Comparison of ranges of applicability of predictions of creep buckling time. in Creep in Structures (ed.by N.J.Hoff) Colloquium IUTAM,Stanford Springer 1962 pp.291-307.

Leonhardt F.(1964) Prestressed concrete:design and construction. Wilhelm Ernst 2nd ed.,677 pp.

L'Hermite R.(1957). What do we know about the plastic deformation and the creep of concrete? (Que savons nous de la deformation plastique et du fluage de béton?). Annales de I.T.B.T.P. Vol.10 No.117 Sept. pp.778-809.

L'Hermite R.(1961). The deformations of concrete (Les déformations du béton). Cahiers de la Recherche Theorique et Experimentale sur les Materiaux et les Structures,Eyrolles.

MacGregor J.G., Breen J.E., Pfrang E.O.(1970). Design of slender concrete columns. Journal ACI,Jan. pp.6-28.

MacGregor J.G.(1974). Simple design procedures for concrete columns. Introductory report-Theme II. IABSE Symposium on Design and Safety of Reinforced Concrete Compression Members,Quebec pp.22-49.

Mamillan M.(1963). Report on the shrinkage and creep measurements at the prestressed bridge of Ponthierry (Compte rendu des mesures de retrait et de fluage effectuées sur le pont en béton précontrainte de Ponthierry). Annales de I.T.B.T.P., No.189 Sept. pp.895-917.

Manuel R.F., MacGregor J.G.(1967). Analysis of restrained reinforced concrete columns under sustained load. Journal ACI,Jan. pp.12-23

Martin I., MacGregor J.G., Pfrang E.O., Breen J.E.(1966). Critical review of the design of reinforced concrete columns. ACI Publication SP-13 pp.13-55.

Martin I.(1972). Reinforced concrete columns. ASCE-IABSE Int.Conference on Tall Buildings,Preprint. Vol.III-21 Lehigh Univ.

Mauch S.P., Holley M.J.(1963). Creep buckling of reinforced concrete columns. ASCE,Journal of Structural Division ST4 August

Mauch S.P.(1966). Effects of creep and shrinkage on the capacity of concrete columns. ACI Publication SP-13 pp.299-325.

McHenry D.(1943). A new aspect of creep in concrete and its application to design. ASTM Proceedings Vol.43 pp.1069-1087.

McMillan F.R.(1915). Shrinkage and time effects in reinforced concrete. Bulletin No.3 Univ.of Minnesota,41 pp.

NAG (1972). Library manual,ICL 1900 System. C05NAF Subroutine. May,8 pp. Nottingham Algoritms Group.

Nasser K., Neville A.M.(1967). Creep of old concrete at normal and elevated temperatures. Journal ACI,Febr. pp.97-102.

Neville A.M.(1970). Creep of concrete:plain,reinforced and prestressed. North-Holland Publ.Company,622 pp.

Neville A.M.(1973). Creep of concrete-Facts and problems in design. Buletinul Stiintific ICB,Bucharest Vol.16 No.2 pp.63-79.

Neville A.M.(1975). Properties of concrete. 2nd ed. Pitman Publ.,687 pp.

Odquist F.K.G.(1972). Creep stability of bars,plates and shells (Chapter 6 pp.199-242) in Stability,Study No.6, Solid Mechanics Division, Univ.of Waterloo.

Pfrang E.O., Siess C.P., Sozen M.A.(1964). Load-moment-curvature characteristics of reinforced concrete cross-sections. Journal ACI,July pp.763-778.

Pfrang E.O., Siess C.P.(1964). Behaviour of restrained reinforced concrete columns. ASCE,Journal of Structural Division ST5 pp.113-136.

Powell M.J.D.(1970). A hybrid method for non-linear equations. in Rabinowitz P.:Numerical Methods for Nonlinear Algebraic Equations, Gordon and Breach.

Prentis J.M., Ross A.D.(1948). Slender reinforced concrete columns. Concrete and Constructional Engineering,Sept.,12 pp.

Rabotnov Y.N., Shesterikov S.A.(1957). Creep stability of columns and plates. Journal of the Mechanics and Physics of Solids Vol.6 No.1 pp.27-35.

Rabotnov Y.N.(1969). Creep problems in structural members. North-Holland Publ.Company,822 pp.

Ramu P., Grenacher M., Baumann M., Thürlimann B.(1969). Investigation of pinned reinforced concrete columns under sustained load (Versuche an gelenkig gelagerten Stahlbetonstützen unter Dauerlast). Institut für Baustatik,Report No.6418-1 ETH Zürich May,86 pp.

Raphael J.M.(1953). The developments of stresses in Shasta Dam. ASCE, Transactions Vol.118 pp.289-309.

Reiner M.(1960). Lectures on theoretical rheology. North-Holland Publ. Company 3rd ed.,158 pp.

Roorda J.(1965). The buckling behaviour of imperfect structural systems. Journal of the Mechanics and Physics of Solids Vol.13 pp.267-280.

Ross A.D.(1943). Creep and shrinkage in plain,reinforced and prestressed concrete.A general method of calculation. Journal ICE Vol.21 No.1 pp.39-57.

Ross A.D.(1958). Creep of concrete under variable stress. Journal ACI, March pp.739-758.

Rüsch H.(1960). Researches toward a general flexural theory for structural concrete. Journal ACI,July pp.1-28.

Rüsch H., Jungwirth D., Hilsdorf H.(1973). Critical review of the approaches to consider the effects of creep and shrinkage on the behaviour of concrete structures (Kritische Sichtung der Verfahren zur Berücksichtigung der Einflüsse von Kriechen und Schwinden des Betons auf das Verhalten der Tragwerke). Beton und Stahlbetonbau No.3(pp.49-60),No.4(pp.76-86),No.6(pp.152-158).

Sewell M.J.(1965). The static perturbation technique in buckling problems. Journal of Mech. and Physics of Solids,Vol.13 pp.247-265.

STAS 10 107 (1975). The design and construction of plain,reinforced and prestressed concrete members (Constructii civile si industriale.Calculul si alcatuirea elementelor din beton,beton armat si beton precomprimat). Romanian Institute for Standards, Bucharest.

Supple W.J.(1967). Coupled branching configurations in the elastic buckling of symmetric structural systems. Int.Journal of Mechanical Science. Vol.9 pp.97-112.

Supple W.J.(1969). Initial post-buckling behaviour of a class of elastic structural systems. Int.Journal of Non-linear Mechanics Vol.4 pp.23-36.

Synge J.L., Griffith B.A.(1959). Principles of mechanics. McGraw Hill 3rd ed.

Thompson J.M.T.(1965). Discrete branching points in the general theory of elastic stability. Journal of Mech.and Physics of Solids Vol.13 pp.295-310.

Thompson J.M.T.(1969). A general theory for the equilibrium and stability of discrete conservative systems. Zeitschrift angew. Math.Physik Vol.20 pp.797-846.

Timoshenko S.P., Gere J.M.(1961). Theory of elastic stability (Chapter 7 pp.278-317) McGraw Hill,2nd ed.

Trost H.(1966). The stress-strain relationship of concrete and conclusions for reinforced and prestressed concrete structures (Spannungs-Dehnungsgesetz eines viskoelastishen Festkörpers wie Beton und Folgerungen für Stabtragwerke aus Stahlbeton und Spannbeton). Beton Herstellung Verwendung,Vol.16 No.6 pp.233-248

Trost H.(1967). The use of superposition principle in creep and relaxation problems for concrete and prestressed concrete (Auswirkungen des Superpositionsprinzips auf Kriech- und Relaxations Probleme bei Beton und Spannbeton). Beton und Stahlbetonbau No.10(pp.230-238),No.11(pp.261-268).

Warner R.F.(1974). Physical-mathematical models and theoretical considerations. Introductory report-Theme I. IABSE Symposium on Design and Safety of Reinforced Concrete Compression Members, Quebec pp.1-21.

Woolson I.H.(1905). Some remarkable tests indicating 'flow' of concrete under pressure. Engineering News,Vol.54 Nov. p.459.

Zerna W., Trost H.(1967). Rheological description of the concrete (Rheologische Beschreibungen des Werkstoffes Beton). Beton und Stahlbetonbau No.7 pp.165-170.

Zyczkowski M.(1960). Geometrically non-linear creep buckling of bars. in Creep of Structures (ed.by N.J.Hoff), Colloquium IUTAM, Stanford,Springer 1962, pp.307-326.